



Trinity College Dublin

Coláiste na Tríonóide, Baile Átha Cliath

The University of Dublin

DEPARTMENT OF CIVIL, STRUCTURAL AND ENVIRONMENTAL ENGINEERING

**POTENTIAL OF WASTE MATERIALS AS POZZOLANS AND THEIR INFLUENCE ON
THE QUALITY OF BUILDING MATERIALS**

by

Radson Lima Figueiredo

Supervisor: Dr. Sara Pavia

Thesis submitted to the University of Dublin, Trinity College for the degree of

Doctor of Philosophy

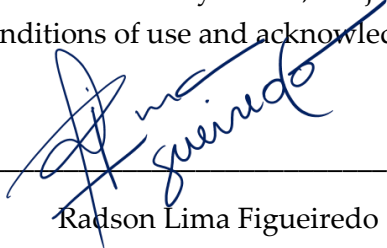
September 2019

This page intentionally left blank

DECLARATION

I declare that this thesis has not been submitted as an exercise for a degree at this or any other university and it is entirely my own work.

I agree to deposit this thesis in the University's open access institutional repository or allow the library to do so on my behalf, subject to Irish Copyright Legislation and Trinity College Library conditions of use and acknowledgement.

Author:  _____
Radson Lima Figueiredo

Date: 07/09/2019

This page intentionally left blank

ABSTRACT

This research investigates the properties of industrial and agricultural waste ashes to evaluate their potential as partial substitution for natural aggregates and cement; in an effort to make building materials more sustainable and recycle waste into construction. The partial replacement of limes/cements with waste would lower the embodied energy of building materials, their CO₂ emissions and the consumption of the non-renewable resources used to produce them. Thirteen ashes were investigated comprising sugarcane bagasse ashes and incinerator ashes. Properties including particle size distribution, specific surface area, chemical composition, mineralogy and amorphousness were investigated and related to the pozzolanic activity of lime: ash solutions. The formation of hydrates was monitored with Scanning Electron Microscopy coupled with Energy Dispersive X-Ray Spectroscopy (SEM-EDS).

The chemical and mechanical methods evidenced reactivity for the ashes and this was further evidenced with SEM, as hydrates appeared as early as 7 days (in sugarcane bagasse ash 1, incinerator bottom ash 1 and fly ash 1 pastes). The specific surface area and fineness of the ashes are comparable to traditional pozzolanic materials however, despite their reactivity, their amorphousness and silica content are low and their loss on ignition high.

The chemical and mechanical methods disagree on the reactivity rating. The chemical method overrates pozzolanic reactivity probably due to the aluminium content which is responsible for the quick consumption of Portlandite in solution. As a result, the incinerator bottom ashes, IBAs, with greater alumina content (11-15%) are rated chemically as the most reactive. However, according to the mechanical index, the sugarcane ashes (SCBA 2) are the most reactive. Taking into account all the properties measured, the assessment of reactivity by strength development (mechanical index) seems a better predictor of pozzolanic activity than the chemical test.

The seven most reactive ashes were selected for further investigation as partial Portland cement (PC) replacement in composites. Additionally, the 2 least reactive sugarcane bagasse ashes were investigated as sand substitution – sugarcane bagasse ash sand (SBAS 1 and 2). 27 ash composites were produced, with levels of cement/sand replacement of 5, 10 and 20%. The composites were investigated and the results compared with a PC control mix.

There are correlations among the composite properties. The ashes that caused a larger refinement of the pore structure and lower capillarity resisted frost action the best; general linear relationships exist between compressive strength and bulk density and a good correspondence exists within the thermal properties: all the ashes significantly lower the thermal conductivity of the cement composite (by c.30%) which agrees with the tendency of the ashes to reduce the density of the PC composites.

The porosity and capillarity of the composites reduced using ashes from the sugarcane industry, while incinerator ashes tend to increase porosity at high levels of replacement and increased capillarity and vapour permeability (FAs 1 and 2). The hygroscopic characteristics of their chlorides may enhance these effects.

As expected, the finest and most reactive ashes (SCBA 1, SCBA 2 and FA 3) with greater silica content and mechanical reactivity, used as cement replacement, lowered porosity, capillarity and vapour permeability the most. However, the coarse sugarcane ashes (SCBA 3 and 4) used as sand replacement – designated SBAS 1 and 2 - substantially lowered porosity and capillarity despite their poor reactivity and produced denser composites, likely due to their higher cement content.

All the ash composites reached significant compressive strength, only three mortars (IBA 1 20%, IBA 2 20% and FA 2 20%) did not attain the lower limit of 30 MPa at 28 days in EN 197-1, however, they still reached high strengths (24-29 MPa). The fly ashes significantly increase flexural strength surpassing the reference material. Some of the sugarcane bagasse ashes (1 and 4) and the fine incinerator bottom ashes (1 and 3) also exceeded the reference flexural strength but most ash composites reached c. 70% of the reference strength.

The ashes lowered the stiffness of the reference mortar, with the exception of FA 3 5%, which exceeded the reference elastic modulus by 18%. The ashes used as sand replacement increased mechanical resistance in compression, however maintaining plasticity.

Most composites produced with incinerator ashes have lower strengths however most comply with the lower strength requirement for PC mortars at 28 days in EN 197-1. Their durability is lower than the sugar ash composites probably due to their Cl and alkali content. The incinerator fly ashes FA 1 20% (with the highest strength loss at 26%) was the worst performer against salt attack probably due to their high Cl and alkali content.

The ash composites performed well against frost, at the end of freeze-thawing cycles no external damage was visually apparent however, their strength decreased likely due to the development of frost-induced microcracks.

The ash composites show outstanding thermal properties. The ashes lowered the thermal conductivity, specific heat and thermal mass of the PC. The bottom ashes were more effective at lowering thermal conductivity and providing better insulation properties. The lowering of the thermal conductivity by the ashes is interesting for material design, as it can lower a U-value of 3.44 to 2.11 W/m²K in a 300 mm wall of PC concrete, just by replacing 10% of the cement with IBA 2 (the ash with the lowest thermal conductivity 0.63 W/mK). In addition, using this ash, the standard U-value requirement of 0.21 W/m²K for a typical cavity wall can be reached with a block 40% thinner than the standard. The ashes also lower the thermal effusivity of the PC, sometimes substantially (e.g. FA 2 5% with a 29% reduction) which adds to the increased insulation ability of the ash composites.

The sugarcane ashes show great potential for PC and fine aggregate replacement in cement-based composites. The sugar ash composites have good resistance to frost and salt action, they reached the highest strengths and increased bulk density, lowering porosity, capillary suction and thermal conductivity while the water vapour ability is little changed. These combinations of properties have the potential to produce strong materials with a greater insulation ability and a lower moisture transport that enhance durability and water vapour properties adequate to maintain indoor air quality.

This page intentionally left blank

ACKNOWLEDGEMENTS

Firstly, I would like to thank my supervisor, Professor Sara Pavía, for all her support and guidance. Thank you for investing your time and knowledge throughout these years. I'm forever grateful.

A special thanks to Eoin Dunne, Michael Grimes and Kevin Ryan for their academic and technical support.

I would like to thank my friend Aderlânio for all his support throughout the years and his assistance with XRD analysis.

I also want to thank Matheus for all his support, patience and love. I love you.

I'm grateful for the friends that I had the opportunity to make during this period in Dublin.

A special thanks to the Brazilian National Counsel of Technological and Scientific Development (CNPq) – Ministry of Science, Technology, Innovations and Communications – for financing this investigation.

Lastly, I want to thank my parents for their example.

This page intentionally left blank

TABLE OF CONTENTS

Declaration	i
Abstract.....	iii
Acknowledgements	vii
Table of Contents.....	ix
List of Figures	xiii
List of Tables	xvii
Nomenclature, Abbreviations and Symbols.....	xxi
1 Introduction	1
1.1 Importance of Making Construction Sustainable and Manners in which Sustainability can be Increased.....	1
1.2 Research Novelty	5
1.3 Scope of this Research	6
2 Literature Review	7
2.1 SCMs and Pozzolans	7
2.1.1 Properties and Composition.....	7
2.1.2 Pozzolanic Activity	8
2.1.3 Effects of Pozzolans on the Properties of Portland Cement Composites.....	11
2.2 Ashes with Pozzolanic Potential.....	13
2.2.1 Waste Incineration	13
2.2.2 Sugarcane Industry	14
2.3 Reactivity of Ashes	15
2.3.1 Incinerator Bottom Ash (IBA).....	15
2.3.2 Sugarcane Bagasse Ash (SCBA) and Sugarcane Bagasse Ash Sand (SBAS).....	16
2.3.3 Fly Ashes (FA)	17
2.4 Effect of Ashes in the Properties of Composites.....	19
2.4.1 Porosity and Capillary Action.....	19
2.4.2 Water Vapour Permeability.....	23
2.4.3 Bulk and Real Densities.....	23
2.4.4 Resistance to freeze-thaw.....	24
2.4.5 Resistance to Salt Crystallisation	25

2.4.6	Thermal Properties.....	27
2.4.7	Strength of the Ash-Composites.....	28
3	Materials and Methods.....	33
3.1	Materials.....	33
3.1.1	Lime.....	33
3.1.2	Portland Cement.....	33
3.1.3	Ashes.....	34
3.1.4	Sand.....	34
3.2	Methods Phase 1: Properties of Ashes.....	35
3.2.1	Sample Preparation.....	35
3.2.2	Particle Size Distribution.....	36
3.2.3	Specific Surface Area (Brunauer–Emmett–Teller - BET).....	37
3.2.4	Chemical Composition by ICP-AES and Loss on Ignition (LOI).....	37
3.2.5	Scanning Electron Microscopy - Energy Dispersive Spectroscopy (SEM - EDS).....	37
3.2.6	X-Ray Diffraction (XRD).....	37
3.2.7	Chemical Reaction by Conductivity.....	38
3.2.8	Reactivity by Strength Development or Mechanical Method.....	39
3.3	Methods Phase 2: Properties of Ash-Composites.....	41
3.3.1	Mix Composition.....	41
3.3.2	Capillary Action.....	42
3.3.3	Porosity Accessible to Water, Bulk and Real densities.....	43
3.3.4	Thermal Conductivity.....	44
3.3.5	Specific Heat Capacity.....	46
3.3.6	Flexural Strength.....	48
3.3.7	Compressive Strength.....	48
3.3.8	Resistance to Salt Crystallisation.....	49
3.3.9	Resistance to Freeze-Thawing.....	50
3.3.10	Water Vapour Permeability.....	52
3.3.10.1	Change in mass of test assembly.....	53
3.3.10.2	Density of water vapour flow rate.....	53
3.3.10.3	Water vapour permeance.....	54
3.3.10.4	Water vapour resistance.....	54
3.3.10.5	Water vapour permeability.....	55

3.3.10.6	Water vapour diffusion resistance factor.....	55
3.3.11	Statistical analysis of the results.....	55
4	Results – Composition and Properties of the Ashes	57
4.1	Particle Size Distribution and Specific Surface Area	71
4.2	Chemical Composition and Mineral Composition	73
4.3	Microstructure of Ashes.....	79
4.4	Reactivity by Conductivity.....	85
4.5	Reactivity by Strength Development	87
4.6	Microstructure of the Pastes.....	90
5	Results – Properties of Ash-Composites.....	97
5.1	Bulk and Real Densities	98
5.2	Open Porosity.....	99
5.3	Capillary Action.....	100
5.4	Thermal Properties	105
5.4.1	Specific Heat Capacity.....	105
5.4.2	Thermal Conductivity, Thermal Mass and Diffusivity	106
5.5	Mechanical properties of the ash composites	110
5.5.1	Flexural Strength.....	110
5.5.2	Compressive Strength	111
5.5.3	Modulus of Elasticity.....	112
5.6	Resistance to Salt Crystallisation	114
5.7	Resistance to Damage by Frost	117
5.8	Water Vapour Permeability.....	119
6	Discussion.....	121
6.1	Composition, Properties and Reactivity of the Ashes	121
6.2	Properties of Ash-Composites	124
7	Conclusions	129
7.1	Final Remarks.....	132
7.2	Scope for further research.....	132
	References.....	133
	Appendix A Thermal Conductivity Test – Heat Flow and Specific Heat.....	152
	Appendix B Standard Force vs Strain – Modulus of Elasticity	170
	Appendix C Before and After of Specimens Subjected to Salt Crystallisation Test	189

Appendix D Change in mass for the selected time interval208
Appendix E Hydrated lime data sheet213
Appendix F Portland cement data sheet214
Appendix G Statistical Analysis.....216

LIST OF FIGURES

Figure 1-1: Clinker substitution evolution from companies from the CSI WBCS D (extract from Scrivener et al. (2016)).	2
Figure 2-1: Amorphous (left) and crystalline (right) silica structure (Patil, 2018).	9
Figure 2-2: Sugar/Ethanol plants and mapped sugarcane farming (extract from CONAB (2018)).	15
Figure 2-3: Schematic representation of the ball bearing effect (extract from Jiménez-Quero et al. (2013)).	18
Figure 2-4: Relative volumes of major compounds as a function of the degree of hydration estimated by a computer model for water/cement ratio = 0.50 (extract from Thomas (2013)).	19
Figure 2-5: Effect of age and fly ash on the pore size distribution of hardened cement paste as measured by the solvent absorption technique - Data from Thomas (1989) (extract from Thomas (2013)).	21
Figure 3-1: Particle size distribution of St. Astier sand compared with the standard CEN sand (extract from Chever et al. (2010)).	34
Figure 3-2: Incinerator bottom ashes (top), sugarcane bagasse ashes (middle) and fly ashes (bottom).	35
Figure 3-3: TEMA T100 Disc Mill (left) and Rotary Sample Divider laborette 27 (right).	36
Figure 3-4: Ash samples prepared for XRD analysis.	38
Figure 3-5: Sealed flasks for conductivity analysis.	38
Figure 3-6: Prismatic test specimens for strength development tests.	39
Figure 3-7: Water demand with respect to specific surface area.	40
Figure 3-8: Strength development test. 3-point bending (left) and compression (right).	41
Figure 3-9: Schematic drawing of the process used to determine the capillary action.	42
Figure 3-10: Polystyrene moulds produced for thermal conductivity tests.	45
Figure 3-11: Design of test rig.	45
Figure 3-12: Thermal conductivity test set-up.	46
Figure 3-13: Representative samples used for testing specific heat for IBA 1 and IBA 2.	47
Figure 3-14: Samples immersed in saturated MgSO ₄ solution.	49
Figure 3-15: Specimens allowed to drain after immersion period.	50
Figure 3-16: Samples maintained in oven for 24h after draining.	50
Figure 3-17: Specimens in polythene bags.	51
Figure 3-18: Water vapour assemblies in controlled chamber.	53

Figure 4-1: Particle size distribution of ashes. SCBAs – sugarcane bagasse (top left); FAs – fly ash (top right); IBAs – incinerator bottom ash fine fractions - (bottom left); and IBAs – incinerator bottom ash coarse fractions – (bottom right).	72
Figure 4-2: Percentage of particles larger than 45 and 75 μm	73
Figure 4-3: SEM micrograph of SCBA 1.	81
Figure 4-4: SEM micrograph of SCBA 2.	81
Figure 4-5: SEM micrograph of SCBA 3.	81
Figure 4-6: SEM micrograph of SCBA 4.	82
Figure 4-7: SEM micrograph of IBA 1.	82
Figure 4-8: SEM micrograph of IBA 2.	82
Figure 4-9: SEM micrograph of IBA 3.	83
Figure 4-10: SEM micrograph of FA 1.	83
Figure 4-11: SEM micrograph of FA 2.	83
Figure 4-12: SEM micrograph of FA 3.	84
Figure 4-13: Conductivity loss over-time.	86
Figure 4-14: Relationship between silica and alumina content and conductivity variation.	87
Figure 4-15: Specimen produced with IBA 2 – coarse after demoulding (at 72 hours).	89
Figure 4-16: Relationship between the chemical reactivity and the mechanical properties of the ashes.	90
Figure 4-17: Lime-SCBA 1 paste showing entangled needle-shaped particles typical of C-S-H, confirmed by EDS spectrum, and evident micro-porosity at 7 days.	92
Figure 4-18: Lime-SCBA 1 paste showing the porous structure with CASH phases identified by EDS at 7 days.	92
Figure 4-19: Porous character of Lime-SCBA 2 paste at 28 days with evident prismatic particles.	93
Figure 4-20: Lime-IBA 1 paste showing elevated micro porosity and eventual formation of needles at 7 days.	93
Figure 4-21: CASH identified in lime-IBA 1 paste at 28 days.	93
Figure 4-22: Lime-IBA 1 paste showing the morphology and composition of the paste during hydration at 28 days.	94
Figure 4-23: Lime-FA 1 paste with evident salt efflorescence.	94
Figure 4-24: Lime-FA 1 paste with efflorescence of salt crystals at 7 days.	94
Figure 4-25: Lime-FA 2 paste showing a particle covered with calcium aluminate silicate hydrate phase at 28 days.	95
Figure 4-26: Lime-FA 2 paste showing crystallised salt at 28 days.	95
Figure 5-1: Real and bulk densities of Portland cement:pozzolan mortars.	98

Figure 5-2: Open porosity available to water.	100
Figure 5-3: Water absorption by capillary action over time.	101
Figure 5-4: Relationship between open porosity and water intake due to capillary action.	102
Figure 5-5: Relationship between chlorine content and the water intake due to capillary action.	103
Figure 5-6: Water absorption coefficient of mortars with SCBA ashes in comparison with the reference specimens.	103
Figure 5-7: Water absorption coefficient of mortars with SBAS ashes in comparison with the reference specimens.	104
Figure 5-8: Water absorption coefficient of mortars with IBA ashes addition in comparison with the reference specimens.	104
Figure 5-9: Water absorption coefficient of mortars with FA ashes compared with the reference specimens.	104
Figure 5-10: Flexural strength of mortars.	110
Figure 5-11: Compressive strength of mortars at 28 days.	112
Figure 5-12: Relationship between real density and compressive strength.	112
Figure 5-13: Relationship between compressive strength and modulus of elasticity.	113
Figure 5-14: Mass change of mortars exposed to salt crystallisation resistance test.	115
Figure 5-15: Salt precipitated within IBA 1 specimens. IBA 1 10% (top) and IBA 1 20% (bottom).	116
Figure 5-16: Salt crystallisation within voids on prisms surfaces.	116
Figure 5-17: Compressive strength of mortars after salt exposure.	117
Figure 5-18: Comparison of compressive strength of mortars before and after freeze-thawing cycles.	119
Figure 6-1: Radar graphs of properties according to Table 6-3 values.	128
Figure A - 1: Heat flow for thermal conductivity test – reference.	152
Figure A - 2: Heat flow for thermal conductivity test – SCBA 1 5%.	153
Figure A - 3: Heat flow for thermal conductivity test – SCBA 1 10%.	154
Figure A - 4: Heat flow for thermal conductivity test – SCBA 1 20%.	155
Figure A - 5: Heat flow for thermal conductivity test – SBAS 2 5%.	156
Figure A - 6: Heat flow for thermal conductivity test – SBAS 2 10%.	157
Figure A - 7: Heat flow for thermal conductivity test – SBAS 2 20%.	158
Figure A - 8: Heat flow for thermal conductivity test – IBA 2 5%.	159
Figure A - 9: Heat flow for thermal conductivity test – IBA 2 10%.	160
Figure A - 10: Heat flow for thermal conductivity test – IBA 2 20%.	161

Figure A - 11: Heat flow for thermal conductivity test – FA 2 5%. 162

Figure A - 12: Heat flow for thermal conductivity test – FA 2 10%. 163

Figure A - 13: Heat flow for thermal conductivity test – FA 2 20%. 164

Figure B - 1: Compressive strength of reference mortar prisms..... 170

Figure B - 2: Compressive strength of SCBA 1 mortar prisms. 171

Figure B - 3: Compressive strength of SCBA 2 mortar prisms. 173

Figure B - 4: Compressive strength of SBAS 1 mortar prisms. 175

Figure B - 5: Compressive strength of SBAS 2 mortar prisms. 177

Figure B - 6: Compressive strength of IBA 1 mortar prisms. 179

Figure B - 7: Compressive strength of IBA 2 mortar prisms. 181

Figure B - 8: Compressive strength of FA 1 mortar prisms..... 183

Figure B - 9: Compressive strength of FA 2 mortar prisms..... 185

Figure B - 10: Compressive strength of FA 3 mortar prisms..... 187

Figure D - 1: Chamber’s temperature and relative humidity conditions during test..... 208

LIST OF TABLES

Table 1-1: Embodied energy and carbon coefficients of sand, cement and concretes (extract from Hammond et al. (2011)). RC – Reinforced concrete.	4
Table 2-1: Pores in cement paste.....	22
Table 3-1: Chemical composition of hydrated lime.	33
Table 3-2: Chemical composition of Portland Cement.	33
Table 3-3: Investigated ashes.....	34
Table 3-4: Pre-treatment of ashes.....	36
Table 3-5: Mix proportions for lime-ash mortars (lime: ash: aggregate: water).....	40
Table 3-6: Composition of mixes for ashes tested as pozzolans (Sand mass was constant, representing 75% of solid weight).....	41
Table 3-7: Composition of mixes for ashes testes as sand replacement (Portland cement mass was constant, representing 25% of solid weight).	42
Table 4-1: Ashes investigated on first stage of research.	57
Table 4-2: Properties of sugarcane bagasse ash 1.	58
Table 4-3: Properties of sugarcane bagasse ash 2.	59
Table 4-4: Properties of sugarcane bagasse ash 3.	60
Table 4-5: Properties of sugarcane bagasse ash 4.	61
Table 4-6: Properties of incinerator bottom ash 1-fine.....	62
Table 4-7: Properties of incinerator bottom ash 1-coarse.	63
Table 4-8: Properties of incinerator bottom ash 2-fine.....	64
Table 4-9: Properties of incinerator bottom ash 2-coarse.	65
Table 4-10: Properties of incinerator bottom ash 3-fine.....	66
Table 4-11: Properties of incinerator bottom ash 3-coarse.	67
Table 4-12: Properties of fly ash 1.....	68
Table 4-13: Properties of fly ash 2.....	69
Table 4-14: Properties of fly ash 3.....	70
Table 4-15: Cumulative particle sizes (μm).....	71
Table 4-16: Chemical analysis of SCBA 1-4 in comparison with SCBAs investigated by other authors.75	
Table 4-17: Chemical analysis of IBA 1-3 in comparison with IBAs investigated by other authors.	76

Table 4-18: Chemical analysis of FA 1-3 in comparison with FAs investigated by other authors.....	76
Table 4-19: SO ₃ , Na ₂ O contents, loss on ignition and sum of silica, alumina and iron components.	77
Table 4-20: Main mineral composition of ashes.....	79
Table 4-21: Level of amorphousness.	79
Table 4-22: Summary of the conductivity variation of lime/ash solutions.	87
Table 4-23: Mechanical properties, mechanical index and variations in strength.	89
Table 4-24: Chemical composition of C-S-H phases in the lime paste determined by SEM EDS.	91
Table 5-1: Number of specimens per test per level of replacement.	97
Table 5-2: Coefficient of water absorption C (in kg/m ² .min) – R ² in brackets (Reference = 0.25 (0.96)).	101
Table 5-3: Specific heat capacity of mortars in J/g°C (Reference cement composites average: 1.45 J/g°C).	105
Table 5-4: U-values of cavity walls including the reference and IBA 2 10% mixes, replacing the standard concrete blocks (thickness = 0.1 m; conductivity = 1.33 W/m K) -Technical Guidance Document L, Building Regulations 2017.	107
Table 5-5: Thermal properties of mortars.	109
Table 5-6: Modulus of elasticity.	114
Table 5-7: Strength and weight loss after freeze-thaw cycling.	118
Table 5-8: Water vapour resistance and permeability results.....	120
Table 6-1: Rating of ashes according to investigated properties.	123
Table 6-2: Points attributed to composites according to test results.....	124
Table 6-3: Rating of ash-composites and reference composite according to test results.....	127
Table A - 1: Thermal conductivity measurements – Reference mortar.	152
Table A - 2: Thermal conductivity measurements – SCBA 1 5% mortar.....	153
Table A - 3: Thermal conductivity measurements – SCBA 1 10% mortar.....	154
Table A - 4: Thermal conductivity measurements – SCBA 1 20% mortar.....	155
Table A - 5: Thermal conductivity measurements – SBAS 2 5% mortar.	156
Table A - 6: Thermal conductivity measurements – SBAS 2 10% mortar.	157
Table A - 7: Thermal conductivity measurements – SBAS 2 20% mortar.	158
Table A - 8: Thermal conductivity measurements – IBA 2 5% mortar.	159
Table A - 9: Thermal conductivity measurements – IBA 2 10% mortar.	160
Table A - 10: Thermal conductivity measurements – IBA 2 20% mortar.	161
Table A - 11: Thermal conductivity measurements – FA 2 5% mortar.....	162

Table A - 12: Thermal conductivity measurements – FA 2 10% mortar.....	163
Table A - 13: Thermal conductivity measurements – FA 2 20% mortar.....	164
Table A - 14: Determination of Specific Heat of samples.	165
Table B - 1: Compressive testing of reference mortar prisms.	170
Table B - 2: Compressive testing of SCBA 1 mortar prisms.....	172
Table B - 3: Compressive testing of SCBA 2 mortar prisms.....	174
Table B - 4: Compressive testing of SBAS 1 mortar prisms.	176
Table B - 5: Compressive testing of SBAS 2 mortar prisms.	178
Table B - 6: Compressive testing of IBA 1 mortar prisms.	180
Table B - 7: Compressive testing of IBA 2 mortar prisms.	182
Table B - 8: Compressive testing of FA 1 mortar prisms.....	184
Table B - 9: Compressive testing of FA 2 mortar prisms.....	186
Table B - 10: Compressive testing of FA 3 mortar prisms.....	188
Table C - 1: Before and after of reference specimens subjected salt crystallisation.	189
Table C - 2: Before and after of SCBA 1 mortar specimens subjected salt crystallisation.....	190
Table C - 3 Before and after of SCBA 2 mortar specimens subjected salt crystallisation.....	192
Table C - 4 Before and after of SBAS 1 mortar specimens subjected salt crystallisation.	194
Table C - 5 Before and after of SBAS 2 mortar specimens subjected salt crystallisation.	196
Table C - 6 Before and after of IBA 1 mortar specimens subjected salt crystallisation.	198
Table C - 7: Before and after of IBA 2 mortar specimens subjected salt crystallisation.	200
Table C - 8: Before and after of FA 1 mortar specimens subjected salt crystallisation.....	202
Table C - 9: Before and after of FA 2 mortar specimens subjected salt crystallisation.....	204
Table C - 10: Before and after of FA 3 mortar specimens subjected salt crystallisation.....	206
Table D - 1: Water vapour permeability test conditions and parameters.....	208
Table D - 2: Vapour Permeability Test - SCBA 1 and SCBA 2.....	209
Table D - 3: Vapour Permeability Test - SBAS 1 and SBAS 2.	210
Table D - 4: Vapour Permeability Test - IBA 1 and IBA 2.	211
Table D - 5: Vapour Permeability Test – FA 1, FA 2 and FA 3.	212

NOMENCLATURE, ABBREVIATIONS AND SYMBOLS

ABNT	Associação Brasileira de Normas Técnicas (Brazilian National Standards Organization)
BET	Brunauer–Emmett–Teller
Ca(OH) ₂	Calcium Hydroxide (Lime)
CaCO ₃	Calcium Carbonate
CaMg(CO ₃) ₂	Calcium Magnesium Carbonate
CaO	Calcium Oxide
C-A-S-H	Calcium Aluminate Silicate Hydrate
CEM I	Cement with up to 5% of minor additional constituents
CL	Calcium Lime
CO ₂	Carbon Dioxide
CSF	Condensed Silica Fume
C-S-H	Calcium Silicate Hydrate
Cu	Copper
DEF	Delayed Ettringite Formation
DL	Dolomitic Lime
EDX	Energy-Dispersive X-Ray
EN	European Standard
FA	Fly Ash
g	Gram
GGBS	Ground Granulated Blast Furnace Slag
GHP	Guarded hot plate
h	Hour
IBA	Incinerator Bottom Ash
kJ mol ⁻¹	Kilojoule per mole
kV	Kilovolt
LOI	Loss on Ignition
mA	Milliampere
MgO	Magnesium Oxide
mm	Millimetre
MOE	Modulus of Elasticity
MSWI	Municipal Solid Waste Incineration
NBR	Norma Brasileira – Brazilian Standard
NHL	Natural Hydraulic Lime
°	Degree
°C	Degree Celsius
OPC	Ordinary Portland Cement
PC	Portland Cement
PFA	Pulverised Fly Ash
RC	Reinforced Concrete
RH	Relative Humidity
RHA	Rice Husk Ash
s	Second
SBAS	Sugarcane Bagasse Ash Sand
SCBA	Sugarcane Bagasse Ash

SCM	Supplementary Cementing Material
SEM	Scanning Electron Microscopy
SEM/EDS	Scanning Electron Microscopy coupled with Energy Dispersive X-Ray Spectroscopy
SI	Sugarcane Industry
SP	São Paulo
TGA	Thermo-gravimetric Analysis
XRD	X-Ray Diffraction
XRF	X-Ray Fluorescence

This page intentionally left blank

1 INTRODUCTION

1.1 IMPORTANCE OF MAKING CONSTRUCTION SUSTAINABLE AND MANNERS IN WHICH SUSTAINABILITY CAN BE INCREASED

Sustainable development refers to ‘a development that meets the needs of the present without compromising the ability of future generations to meet their own needs’- United Nations Brundtland report (1987). The concept of sustainable development was introduced into construction by the International Council for Research and Innovation in Building and Construction (CIB) in 1994, with the aim of ‘creating and operating a healthy built environment based on resource efficiency and ecological design’ (Kibert, 2016). In addition, CIB formulated the seven Principles of Sustainable Construction as follows:

1. Reduce resource consumption (reduce);
2. Reuse resources (reuse);
3. Use recyclable resources (recycle);
4. Protect nature (nature);
5. Eliminate toxics (toxics);
6. Apply life-cycle costing (economics);
7. Focus on quality (quality).

Efforts towards increasing the sustainability of construction are essential for a global sustainable development. Most effort to date has concentrated on lowering the operational energy of buildings however, the sustainability of the constituent materials is also essential and has been less investigated.

Unfortunately, most of the materials currently used in construction are Portland cement (PC) based including shuttered concrete, cement blocks, bricks, pre-cast stone, pre-cast façade elements and other products. These are heavy on natural, unrenewable resource consumption, energy consumption and carbon emissions.

Cement is the largest manmade product on earth by mass, and it is the second most used substance in the world after water (Scrivener et al., 2016). Given the scale of the cement industry, the commitment of this sector is critical to contribute to the goal of the 2015 Paris Climate Change Agreement to limit global warming below 2 °C (UNFCCC, 2017).

According to a report by the Chatham House (Royal Institute of International Affairs), the cement industry accounts for around 8% of global CO₂ emissions (Lehne & Preston, 2018), being one of the main sources of CO₂ emissions by the Industrial Processes and Product Use

(IPPU) sector, (UNFCCC, 2016). Additionally, the global cement production is set to increase to over 5 billion tonnes a year over the next 30 years, representing more than 25% increase to current numbers. In contrast to this potential expansion, the global greenhouse gas emissions need to fall by around 50% to meet the Paris Agreement goal, which implies that the cement sector annual emissions will need to fall by at least 16 per cent by 2030 (Lehne & Preston, 2018).

In cement production, the thermal decomposition (calcination) of quarried minerals, i.e. the process for producing clinker, accounts for more than 50% of total CO₂ emissions on cement plants, while fuel combustion is responsible for 40% of total emissions. Depending on the type of combustion fuel, emissions can vary from 0.9 to 1 tons of CO₂ per tonne of clinker with heat demand of 3500 – 5000 MJ per ton of clinker (Deja et al., 2010). Additionally, it is projected that around 1.65 tons of limestone (1.5 to 1.8 tonnes) and 0.4 tons of clay are quarried for each tonne of cement produced. These materials are mined in large quarries, with typical outputs of up to, or over, 2.5 million tonnes per year (BGS, 2005).

Cement is essentially produced close to the site where it is used, as costs of transportation rapidly becomes uneconomic. However, these locally produced materials are subject to stringent, and sometimes unfitting, national and international standards, preventing modifications to any substantial extent to adapt them to local economic and environmental needs. This is a significant obstacle to maximising sustainability, as the adaptation of cement production to local raw materials and specific applications could greatly reduce environmental impact.

The level of Portland cement clinker substitution by supplementary cementitious materials (SCMs) in today's cement average around 20%, mainly fine limestone, granulated blast furnace-slags (GGBS) and fly ashes. Figure 1-1 shows the evolution of clinker substitutions, noticeably, the level of clinker replacement is levelling off, and the use of new sources of good quality SCMs is needed to change this picture to any significant extent (Scrivener et al., 2016). According to the 2018 Technology Roadmap, achieving an average global clinker substitution of 0.60 by 2050 has the potential to mitigate almost 0.2 gigatonnes (GT) of CO₂ in 2050 (Lehne & Preston, 2018).

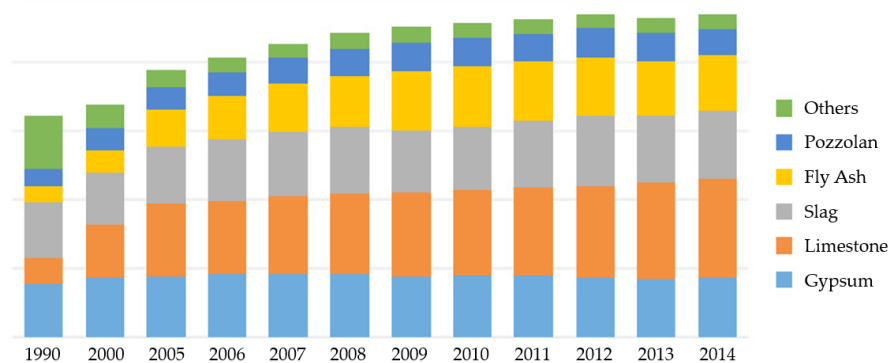


Figure 1-1: Clinker substitution evolution from companies from the CSI WBCS D (extract from Scrivener et al. (2016)).

In addition, the demand for construction aggregates will rise by c. 5% annually, to total approximately 51.7 billion tons in 2019 (Freedonia Group, 2018). As a result of this high demand, and due to the limited natural reserves and increasing carbon taxes, one of the main challenges of the cement/concrete industry today is to meet the current growing demand for aggregates and finding suitable alternatives (Kaur & Pavia, 2018).

This research aims at reducing some of the environmental impacts of the construction industry by replacing cement and aggregate in construction materials with waste ashes. This would lower the embodied energy and carbon emissions of materials and also the quarrying of non-renewable resources, consequently lowering energy demand which would further enhance sustainability.

In the last decades, an effort has been made to increase the sustainability of constructions. This implies to minimize the negative environmental impact of buildings in two different areas: their operational energy and the embodied energy of their material components. Most of the focus so far has been in reducing the operational energy of constructions, i.e. the energy required for cooling and heating of buildings. This is undeniably important, as the consumption of operational energy by buildings has the single largest impact on the environment (Shoubi et al., 2015). However, the embodied energy of construction materials can be substantial and is sometimes neglected (Koezjakov et al., 2018).

Embodied energy is probably the concept that best represents a material's sustainability as it encompasses all the energy input required for the material's life-cycle including raw material extraction, transport, manufacture, assembly, installation, disassembly, deconstruction and/or decomposition. As energy-input equals greenhouse gas emissions, the concept of embodied energy is essential to determine whether a material contributes to or mitigates global warming.

As mentioned, a common way to lower the embodied energy of a construction material is by using SCMs and / or pozzolans. SCMs are finely-divided-inorganic products used for making blended cements or as mineral additions in concrete. They reduce the clinker volume and modify or improve concrete properties in the fresh and hardened states (Khatib, 2016). According to the European standards (EN 206-2013+A1:2016) SCMs are divided in two categories: Type I – nearly inert addition; and Type II – pozzolanic or latent hydraulic addition (BSI, 2016b). Pozzolans are inorganic silicates and aluminates that react with calcium hydroxide, $\text{Ca}(\text{OH})_2$ produced during PC hydration to form additional hydraulic cements. In some instances, SCMs are reported to increase the material's strength, density and resistance to chemical attack.

Table 1-1 includes the embodied energy and carbon emission coefficients of aggregate and several types of cements and concretes, some including SCMs such as fly ash and GGBS.

As it can be seen from this table, the embodied energy of fly ash cements is from 4% to 33.1% lower (at 6% and 35% replacement levels respectively) than that of the pure cement (95% clinker) known as CEM I (5.5 MJ/kg). The use of GGBS also significantly lowers the embodied energy of cement, reaching up to 56% reduction at 80% replacement (CEM II/B). In this table,

the reduction of the embodied energy of concretes including SCMs as partial cement replacement is also evidenced.

Similarly, the significant reduction in the embodied carbon of cements and concretes, with fly ash and GGBS is also evidenced in the table. For example, replacing 35% of cement with fly ash lowers carbon emissions by 34%, representing less 0.32 kgCO₂/ kg of cement released into the environment versus the 0.93 kgCO₂/ kg emitted by the CEM I.

Table 1-1: Embodied energy and carbon coefficients of sand, cement and concretes (extract from Hammond et al. (2011)). RC – Reinforced concrete.

Material	Embodied energy (MJ/kg)			Embodied carbon (kgCO ₂ /kg)		
Sand	0.081			0.0048		
Cement						
Average CEM I Portland cement, 94% clinker	5.5			0.93		
6-20% Fly ash (CEM II/A-V)	5.28 to 4.51			0.88 (@ 6%) to 0.75 (@ 20%)		
21-35% Fly ash (CEM II/B-V)	4.45 to 3.68			0.74 to 0.61		
21-35% GGBS (CEM II/B-S)	4.77 to 4.21			0.76 to 0.64		
66-80% GGBS (CEM II/B)	2.96 to 2.4			0.37 to 0.25		
Concrete						
% Cement replacement – Fly Ash	0%	15%	30%	0%	15%	30%
General (6/8 MPa)	0.55	0.52	0.47	0.071	0.065	0.057
General (16/20 MPa)	0.81	0.75	0.68	0.115	0.105	0.093
RC 20/25 (20/25 MPa)	0.86	0.81	0.73	0.124	0.114	0.101
RC 40/50 (40/50 MPa)	1.17	1.10	0.99	0.176	0.164	0.146
% Cement replacement - Blast Furnace Slag	0%	25%	50%	0%	25%	50%
General 0 (6/8 MPa)	0.55	0.48	0.41	0.071	0.056	0.042
General 3 (16/20 MPa)	0.81	0.69	0.57	0.115	0.090	0.065
RC 20/25 (20/25 MPa)	0.86	0.74	0.62	0.124	0.097	0.072
RC 40/50 (40/50 MPa)	1.17	1.03	0.87	0.176	0.144	0.108

This investigation intends to contribute to these positive environmental impacts by furthering the use SCMs to include ashes from alternative industries, such as municipal solid waste incineration and sugarcane industries, that are not yet standardised into the SCM-blended cements.

Furthermore, considering the estimation of aggregate demand for 2019 at 51.7 billion tons (Freedonia Group, 2018) – this would account for 248.16 million tons of CO₂ emitted for the year. The replacement of 1/3rd of this natural aggregate with coarse waste ash would

considerably lower emissions to 165.44 million tons of CO₂; and the embodied energy would also reduce from 4.63 E+9 MJ to 3.08 E+9 MJ.

This research investigates the potential of waste ashes for use as pozzolans. As aforementioned, pozzolans and other SCMs are already widely used in construction. Most of the 27 members of the family of cements (EN 197-1 (2011)) include SCMs or pozzolans such as fly ash, slag, calcined clay, calcined shale and silica fume; and CEM I is the only cement product consisting mostly of clinker (calcium silicates). In 2006, the amount of CEM I in the CEMBUREAU (The European Cement Association) countries represented 28% of the total cement production, while blended cements (CEMs II, III, IV, V and others) corresponded to 72% (Cembureau, 2006). In 2011, the European cement industry used 47.8 million tons of alternative raw materials in PC or blended cements (Cembureau, 2014). It is estimated that the production of blended cements has a global potential for reducing CO₂ emission of at least 5% and up to 20% of the total cement-making CO₂ emissions (Worrell et al., 2001), not considering other sources of mineral additives or pozzolanic materials.

This research intends to contribute to the use of pozzolans in the cement industry. The use of pozzolanic materials directly addresses at least 3 of the Principles of Sustainable Construction (reduce, recycle and protect nature). In addition, some pozzolans have been reported to improve the service life of materials enhancing durability therefore, the project also studies the properties and durability of materials made with the waste ashes investigated.

1.2 RESEARCH NOVELTY

As aforementioned, replacing Portland cement and natural aggregate with waste ashes has the potential to significantly lower the embodied energy of construction materials which can be equivalent to years of operational energy and is sometimes neglected. This would also lower carbon emissions and quarrying of non-renewable resources, consequently lowering energy demand which would further enhance the sustainability of construction.

This work intends to increase the variety of pozzolans currently used by the cement industry by investigating the pozzolanic potential of ashes which result from industrial and agricultural activities and are dumped in landfills. Some SCMs / pozzolans used in construction today such as thermally activated clays and natural pozzolans are non-renewable and involve carbon emissions however, the ashes in this research are waste materials destined to landfill. In addition, very little work has been found on the use of sugarcane fly ash as cement replacement and on the use of sugarcane bagasse ash as fine aggregate replacement and its influence on properties such as thermal conductivity, water vapour permeability, porosity and densities (real and bulk). Furthermore, the durability of materials (resistance to frost attack and sulphate attack) made with incinerator and sugarcane bagasse ashes has not yet been investigated in detail, as shown in Section 3.2.

1.3 SCOPE OF THIS RESEARCH

The investigation intends to reduce the amount of raw material used in the manufacture of concrete (shales and carbonate rocks), reduce and recycle industrial and agricultural waste (incinerator and sugar-industry ashes) and reduce the energy consumption and CO₂ emissions of construction.

The objectives are as follows:

- Contribute to the knowledge on the properties of pozzolanic materials for building composites.
- Investigate the pozzolanic activity of waste ashes arising from industrial and agricultural activity and evaluate their potential to partially replace conventional binders.
- Measure the properties of waste ashes – including particle size (determined by laser diffraction), specific surface area (BET method), chemical (Inductively Coupled Plasma – Atomic Emission Spectroscopy (ICP-AES) analysis) and mineral composition and amorphousness (X-Ray Diffraction method) – and establish how these affect reactivity (pozzolanic activity).
- Design sustainable materials with different waste proportions and determine their performance by:
 - Assessing their microstructure and hydrate formation (SEM-EDS);
 - Evaluating their mechanical properties such as compressive strength (EN 196-1 (2016a)), flexural strength (EN 196-1 (2016a)) and elastic modulus (slope of the stress-strain relationship at origin);
 - Understanding their hygric and thermal behaviour by undertaking laboratory tests including porosity, density (RILEM 1980), capillary suction, thermal conductivity and specific heat capacity;
 - Estimating the material's durability by performing accelerated weathering cycles in laboratory, including freeze-thaw BS EN 15304 (2010b) and salt crystallisation cycling (RILEM 1980).

2 LITERATURE REVIEW

2.1 SCMS AND POZZOLANS

2.1.1 Properties and Composition

SCMs cover a variety of fine inorganic materials that can be blended into cements or added to concretes. These materials can be either virtually inert or active in enhancing composites' properties. Most SCMs are pozzolans. According to the building standards (ABNT, 2014; ASTM, 2003), pozzolans are siliceous and aluminous materials which, in themselves, possess little or no cementitious value but, in finely divided form, react chemically with calcium hydroxide in presence of moisture at ordinary temperature to form cementitious.

It has been known since antiquity that pozzolans can enhance the hardening, strength development and ultimate strength of hydrated-lime mortars (Ca(OH)_2 ; CL - Calcium lime). Pozzolans can enhance lime mortars while still preserving their physical and chemical compatibility with traditional and historic masonry (Aly & Pavia, 2015).

Important historic buildings rely on pozzolanic materials, evidencing the durability of lime-pozzolan mortars and concretes. Until the nineteenth century, lime-pozzolan mixes were the only hydraulic mortars capable of hardening in water and, at the same time, of resisting the attack of aggressive waters, including sea water, and sulphate and acid attack (Gutt & Nixon, 1979; Massazza, 1998).

Originally, the term 'pozzolan' referred to the glassy pyroclastic rocks found in the surroundings of Pozzuoli, Italy, used to enhance the properties of lime mortars. The term pozzolan includes a wide range of natural and artificial materials with very distinct characteristics in relation to chemical composition, mineralogical nature or geological origin, which prevents pozzolans to have more stringent classifications.

Natural pozzolans are materials of volcanic or sedimentary origin, and do not require any further treatment apart from grinding. Artificial pozzolans are materials originated as a result of chemical and/or structural modifications either by thermal treatment or as a by-product of industrial or agricultural activities.

Pozzolans, when heated, go through chemical and structural transformations, which may change their reactivity to lime. The positive effects caused by this process may be related to the loss of water in glassy or zeolitic phases as well as the destruction of the crystal structure in clay minerals; the negative effects are evidenced by the decrease in the specific surface area,

devitrification and crystallisation. The resulting effect, an increased or decreased pozzolanic activity, depends on the nature of the pozzolan, the temperature and the duration of heating (Massazza, 1998).

One of the main benefits of using pozzolans as SCMs is the improvement of the mechanical and chemical characteristics of mortars and concretes leading to an enhancement of durability. The reaction between the pozzolan and the $\text{Ca}(\text{OH})_2$ in excess produces calcium silicate hydrate (C-S-H), which reduces the porosity of the binder, positively affecting both fresh and hardened properties. The physical effects are associated with their influence on the packing characteristics of the mixture, which depend on size, shape and texture of the particles. The chemical effects are associated with their capability of providing siliceous/aluminous compounds (Cowper, 1998).

2.1.2 Pozzolanic Activity

Pozzolanic activity refers to all reactions developed when mixing pozzolans, calcium hydroxide and water. The products of these reactions are cementing hydrates, similar to those formed upon hydration of hydraulic binders, such as Portland cement and hydraulic lime. These reactions arise owing to the presence of active silica/alumina in the pozzolanic materials.

The ability of a pozzolanic material to combine lime depends on the amount of lime that a pozzolan can consume and the rate of the reaction. Both parameters depend on the nature of the pozzolan, and on the quality and quantity of its active phases. In fact, these two parameters cannot be split apart, however, understanding of the pozzolanic reaction suggests examining the two parameters separately (Massazza, 1998, 2002). In general, the amount of lime that a pozzolan can combine is determined by:

- the nature, composition and amount of active phases;
- the main active phase;
- the lime/pozzolan ratio of the mix;
- length of curing.

Whereas the reaction rate depends on:

- the specific surface area of the pozzolan;
- water/solid ratio;
- temperature.

In the cement industry, it is well known that fineness of cement determines reactivity and, as a result, compressive strength at early stages. Thus, it is preferable a fine particle size distribution to reach higher strength (Binici et al., 2007). Accordingly, fineness is one of the variables that affect pozzolan reactivity. It influences primarily the short-term activity of the pozzolanic reaction (Massazza, 1998). Grinding enhances fineness potentially lessening the negative effects of the crystalline phases on the reactivity of ashes (Cordeiro et al., 2016).

Additionally, the breaking of particles introduces imperfections, that function as active centres for reaction on the surface of the mineral particles (Cordeiro & Kurtis, 2017; Nakata et al., 1989).

Lime combination essentially depends upon the active silica content. It has been generally accepted that amorphous silica is the major responsible for the reaction with $\text{Ca}(\text{OH})_2$, while crystalline phases (quartz, andesite, leucite, feldspars, sanidine, mullite, magnetite) jeopardize the pozzolanic ability to combine lime (Cordeiro et al., 2016; Massazza, 1993). However, Walker and Pavia (2011) claim that the crystalline minerals in pozzolans can bind a considerable amount of lime. The authors proved this measuring the amount of lime combined by pozzolans; all with a significant crystalline fraction comprising silicoaluminates such as mullite – $3\text{Al}_2\text{O}_3\cdot 2\text{SiO}_2$; cordierite – $(\text{Mg,Fe})_2\text{Al}_4\text{Si}_5\text{O}_{18}$; illite – $(\text{K,H}_3\text{O})(\text{Al,Mg,Fe})_2(\text{Si,Al})_4\text{O}_{10}[(\text{OH})_2,(\text{H}_2\text{O})]$; paragonite – $\text{NaAl}_2(\text{Si}_3\text{Al})\text{O}_{10}(\text{OH})_2$; zeolite (gismondine) – $\text{CaAl}_2\text{Si}_2\text{O}_8\cdot 4(\text{H}_2\text{O})$; and feldspar (anorthite) – $\text{CaAlSi}_2\text{O}_8$; calcium/magnesium silicates such as wollastonite – CaSiO_3 and wadsleyite $\text{b-Mg}_2\text{SiO}_4$; metallic oxides/hydroxides (hematite Fe_2O_3 , tohdite $5\text{Al}_2\text{O}_3\cdot \text{H}_2\text{O}$ and aluminum oxide); and calcium sulphates (anhydrite and gypsum).

Figure 2-1 represents amorphous and crystalline silica structures. The lack of long-range order in the atoms of the amorphous structure reduces the stability of the silica facilitating the pozzolanic reaction. The crystalline phase possesses a long-range order, therefore a greater stability.

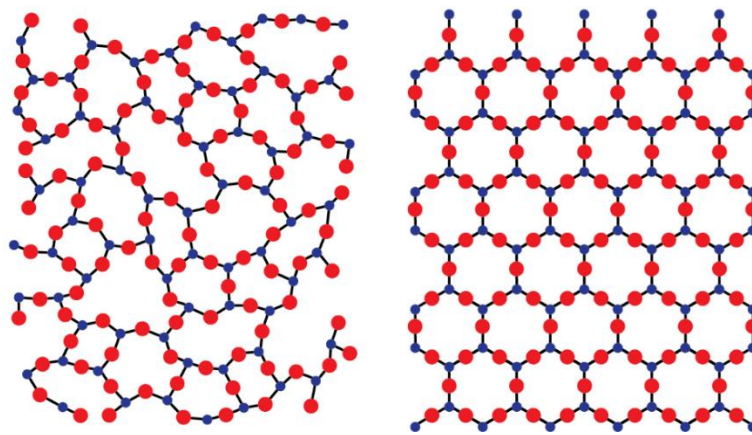


Figure 2-1: Amorphous (left) and crystalline (right) silica structure (Patil, 2018).

Also, there is a good relationship between the amount of combined lime and the quantity of active silica plus alumina ($\text{SiO}_2 + \text{Al}_2\text{O}_3$), since alumina also reacts with lime (Massazza, 2002). However, it is believed that alumina reacts later – except for the Al_2O_3 combined in calcium silicate hydrates (C-S-H) –, since it crystallises far from the pozzolan grains, in small holes and microcracks in the paste. Massazza attributes this to a smaller electric charge and oxygen content which make calcium aluminate hydrate diffuse more quickly and induce its precipitation far from the pozzolan grains (Massazza, 2002).

The rate of reaction depends on the specific surface area of the pozzolanic material, temperature and water/solid mix ratio. The specific surface area affects fundamentally the short-term activity of the pozzolan, that is, the greater the specific surface area, the higher the early pozzolanic activity (Massazza, 1998, 2002). Therefore, enhancing fineness – grinding - of a pozzolanic material will, consequently, favour lime combination, by enhancing the reactive surface area and increasing dissolution rate and solubility. Other means of enhancing the rate of pozzolanic reaction include firing, compacting and adding some chemicals. For instance, it has been found that the rate of lime combination increases in the presence of gypsum and other salts such as Na_2SO_4 and CaCl_2 , which have been found to accelerate the pozzolanic reaction and affect the strength development positively (Massazza, 2002).

The presence of alkalis K_2O and Na_2O can speed up the dissolution of amorphous silica due to the increase of pH in the pore solution, however high alkali content can adversely affect mortar durability due to the potential expansive alkali-silica reaction (ASR) (Cordeiro et al., 2016). The alkali-silica reaction occurs due to the presence of alkalis in the pore solution, reactive aggregates and moisture which react forming a gel (calcium-alkali-silicate-hydrate gel), which has the potential to absorb water causing expansion leading to cracking (Abbas et al., 2017). On the other hand, it has been reported that the pozzolanic reaction reduces ASR expansion due to the decrease of $\text{Ca}(\text{OH})_2$ and the production of hydration products with low calcium to silica ratio (Chappex & Scrivener, 2012; Monteiro et al., 1997; Wang & Gillott, 1991).

SO_3 content is an important factor for the transformation of monosulfate to ettringite, thus the greater the SO_3 content the greater the risk of delayed ettringite formation (DEF) (Horkoss et al., 2016). Taylor et al. (2001) explain that the expansion caused by SO_3 is favoured by high alkali content, however when the cement has low sulphate content the alkalis have no significant effect. Asamoto et al. (2017) state that cements containing high SO_3 proportions are more susceptible to DEF when exposed to high temperatures. The author also found that the addition of fly ash inhibited DEF and reduced the risk of expansion for limestone cements such as Portland limestone cement, even with high SO_3 content. At standard curing conditions, the studies conducted by Tosun (2006) revealed that no expansion or other symptoms of damage were developed in mortars prepared with fine cements at high SO_3 ratios.

The development of pozzolanic reaction is generally evaluated by measuring the depletion of free lime in the system or the rise in the silica + alumina soluble in acid. Owing to the wide heterogeneity of materials and the complex reactions occurring during hydration, a pozzolanic activity model cannot be designed, and only general trends are likely to be identified (Massazza, 1998). The reaction mechanism is complex and is likely to be the sum of topochemical reactions including dissolution and precipitation. It is only possible to suggest a simplified model based on examination and discussion of the results in this field. The main reactions include:

Calcium Hydroxide + Silica + Water → Calcium-Silicate-Hydrates (C-S-H);

Calcium Hydroxide + Alumina + Water → Calcium-Aluminate-Hydrates (CAH);

Calcium Hydroxide + Silica + Alumina + Water → Calcium-Aluminosilicate-Hydrates (CASH).

A simplified model can be explained as follows (Massazza, 2002):

- The liquid becomes saturated in $\text{Ca}(\text{OH})_2$ and the pH rises to over 12.7;
- The active phases in the pozzolans are attacked by the strong alkaline solution;
- The surfaces of groups are dissociated into SiOH^- and H^+ ;
- Grains are left negatively charged;
- Alkalis from the pozzolan dissolve in the liquid phase;
- Ca^{2+} is adsorbed on the surface of the grain – probably by electrostatic forces;
- Leaching of alkalis leave a thin, amorphous Si and Al rich layer on the glass surface;
- The unstable Si and Al layer gradually dissolves and combines Ca^{2+} .

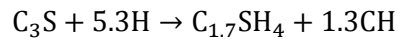
2.1.3 Effects of Pozzolans on the Properties of Portland Cement Composites

In a PC system, pozzolans react with the (calcium hydroxide – CH = portlandite) released upon hydration of the calcium silicates in the cement. PC hydration represents the sum of complex chemical reactions that occur when the calcium silicates (cement clinkers: C_3S , C_2S , C_3A and C_4AF) are mixed with water, producing cementitious products. These include C-S-H, CAH and C(A,F)SH. The dashes in C-S-H indicate that no particular composition is implied as CSH represents the specific composition $\text{CaO}\cdot\text{SiO}_2\cdot\text{H}_2\text{O}$. The term 'C-S-H gel' is sometimes used to distinguish the material formed in cement, C_3S or C_2S pastes, from other varieties of C-S-H (Taylor, 1997).

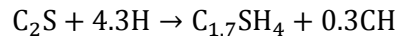
C_3S (alite) hydrates rapidly, typically 70% reacts in 28 days and virtually all in 1 year, and is responsible for initial set and early strength gain. The products formed from alite hydration are calcium hydroxide (CH) and a nearly amorphous calcium silicate hydrate having the properties of a rigid gel. C_2S behaves similarly, but the hydration is much slower, with around 30% of belite reacting in 28 days and 90% in a year. Also, much less CH is formed, and the hydrates are responsible for delayed strength gain. C_3A is also responsible for initial set and gives a small contribution to strength gain (Lea, 1970; Taylor, 1997).

PC hydration produces about 15% of its own volume of lime (CH) (Thomas & Jennings, 2018). The reactions showing the reaction of the main clinker phases and their products are as follows.

Silicate reactions:

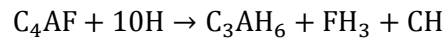
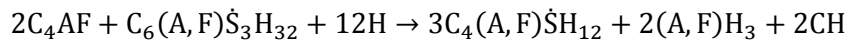
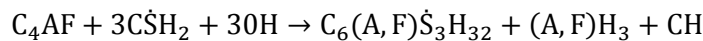
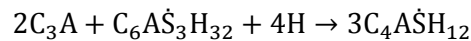
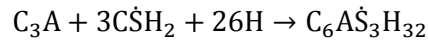
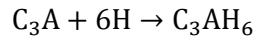


Equation 2-1: Alite hydration.



Equation 2-2: Belite hydration.

Aluminate and Ferrite reactions:



Pozzolans in the PC system react with the CH released upon calcium silicate hydration (Equation 2-1, Equation 2-2). Depending on the amount of pozzolan, the CH can be partially or entirely combined producing further calcium silicate and aluminate hydrate cements.

The CH consumption by the pozzolan affects the microstructure of the cement matrix. It has been reported that this enhances durability, mainly due to lowering the porosity and permeability of the paste which minimises the penetration of harmful substances that may be present in destructive environments such as sewage systems, acid sulphate soils and sea water (Meddah et al., 2014; Obe et al., 2017).

Pozzolans also positively influence the interfacial transition zone – the lowest strength zone where aggregate and bulk paste come together. This area is weakened due to the “wall” effect caused by water film around the aggregate, which leads to an area with higher porosity and water/cement ratio, ultimately unbalancing the stress distribution causing crack propagation (Maso, 1996). The transition zone consists mostly of calcium hydroxide and ettringite. Incorporating pozzolanic reactive materials strengthens this zone by reducing the amount of $Ca(OH)_2$, consequently lowering the width of the interfacial zone and reinforcing the microstructure around the aggregate (Scrivener et al., 1988; Zhang et al., 1996).

It has also been reported that pozzolans can enhance resistance to sulphate attack. In general, when PC mortars or concretes are subjected to sulphate attack, the excess CH and aluminate present in the mortar will react with H_2SO_4 producing low density and expansive gypsum and ettringite, leading to cracking and spalling (Arif et al., 2016). However, if the CH is combined with the pozzolan, these reactions would not take place, consequently increasing the durability of the materials (Chandra, 1996).

Walker and Pavia (2010) summarise the effect of pozzolans in PC composites as follows: the consumption of CH by the pozzolan results in a reduction in the number and size of

portlandite crystals both in the paste and at the aggregate interface which improves the microstructure of the paste by decreasing flaws, enhancing the homogeneity of the matrix (Massazza, 1998), and reinforcing the microstructure of the transition zone (Bentur & Cohen, 1987; Zhang et al., 1996). According to Walker and Pavia (2010), replacement of PC by pozzolans lowers early strength and improves the long term one as, initially, the pozzolan behaves as an inert material reducing the initial rate of strength gain. However, at greater ages, pozzolanic reaction begins and pozzolan cements attain the same or higher strengths than the parent PC.

2.2 ASHES WITH POZZOLANIC POTENTIAL

This research investigated ashes from two industrial sectors: waste incineration and the agricultural sugar industry. The ashes investigated were sourced from four sugarcane industries in Brazil and three waste incineration plants located in the Czech Republic, Portugal and Ireland.

2.2.1 Waste Incineration

The extraordinary increase in population and urbanisation of the past century has led the increase in solid waste generation. Solid waste is a major response to urbanisation and economic development. It is an output of a resource-intensive, consumer-based lifestyle, which is a great problem in the world. According to The World Bank Report (Hoornweg & Bhada-Tata, 2012) waste volumes are increasing faster than the rate of urbanisation and are expected to increase to 2.2 billion tonnes by 2025, indicating that the amount of waste generated per capita is critically escalating.

Historically, the disposal of solid waste in sanitary landfill has been the most widely used approach to manage waste in most countries. This method is often preferred because of its low investment, low running costs, low operation difficulty, simple management and high processing ability. Additionally, the methane released from the waste can be exploited as an electricity source. However, the disposal of waste in sanitary landfill has its downsides. In fact, some of the challenges faced by this method of waste management are the vast portions of land required, as well as the location of the land, which directly impacts the shipping costs and influences the values and use of land in the surrounding areas. Furthermore, the loss of resources by dumping valuable materials, due to poor or no segregation of recyclables and the undesirable fail in recovering the methane and treating the leachate, inherent to the decomposition chemistry of solid waste, will aggravate the environmental impacts of the system (Li et al., 2015).

An alternative to municipal solid waste management is incineration. It is one of the most effective methods, regarding mass and volume reduction. The input waste is burned, losing around 70% of its original mass and 90% of its volume. The process involves incineration;

energy recovery and air pollution control. The waste is fed into the furnace and exposed to high temperature and turbulence, to increase the burnout. The average incineration temperature is at least 850 °C, with a residence time of more than 2 seconds (Filipponi et al., 2003).

Incineration generates ash typically accounting for 1 – 30% by wet weight and 5-15% by volume of the wet municipal solid waste (Obe et al., 2017). The residue after burning can be broadly divided into bottom ash and fly ash. Bottom ashes correspond to approximately 80-90% of the total municipal solid waste incineration (MSWI) residues, and are usually composed of silica, alumina, calcium carbonate and lime (Chimeno et al., 1999; Pera et al., 1997). The fly ash accounts for 1-3% of the total municipal solid waste incineration residues and are usually high in chloride content and may contain heavy metals or organic compounds (Bertolini et al., 2004).

2.2.2 Sugarcane Industry

Sugarcane culture is key for production of essential commodities, such as sugar and ethanol. Brazil leads the world production of sugarcane. The 2017/18 harvesting reached 633.26 million tons, which represents a 3.6% decrease compared to the previous season due to irregular weather conditions in some growing areas and aging of sugarcane fields. The estimated productivity for the period was 72.734 kg/ha (CONAB, 2018). As shown on Figure 2-2, the state of São Paulo (SP) concentrates most of farming and sugar and alcohol industries. According to a report by CONAB (2018) on the total cultivated area in Brazil, it was revealed that the state of SP is responsible for around 52% of all the sugarcane processed in the country.

To reduce costs and become more efficient, the sugarcane industries burn the bagasse - which is the fibrous matter that remains after sugarcane is crushed to extract its juice - to generate steam and electricity to meet their demands. It is estimated that the electricity generated by burning bagasse and leaves may exceed the capacity of Brazil's largest hydroelectric plant, Itaipu (Sales & Lima, 2010). This practice has a sustainability side effect, as it reduces the dependence on the available energy matrix, reduces the demand for other wood sources to feed combustion boilers, reducing costs, and reduces the waste volume, by using the bagasse as a resource rather than dumping it as a waste. Though this practice reduces bagasse volume, it is not immune to producing a new material to be dealt with, the ash. It is estimated that each tonne of bagasse cogenerates 25 kg of residual ash. This shows that even though the burning of bagasse is advantageous in some economic and environmental respects, the disposal of the bagasse ash produced during burning is an important issue for the industries as, however reduced, there is still the need for areas to dump the ash (Bahurudeen et al., 2014).

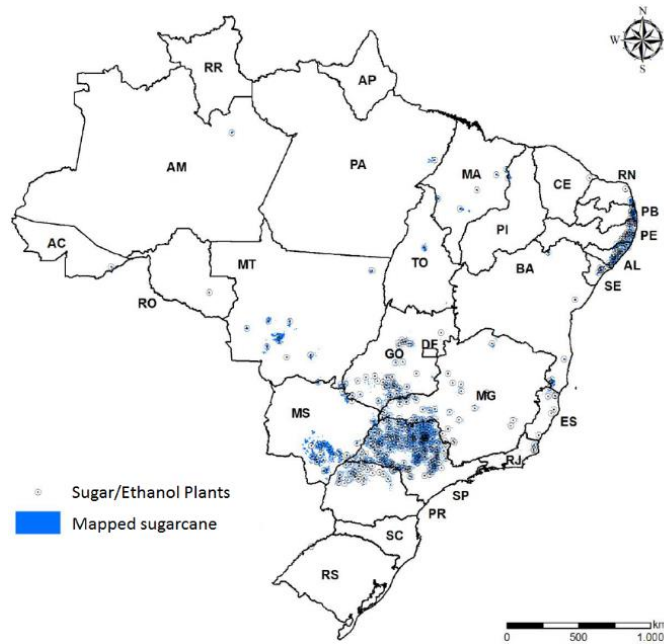


Figure 2-2: Sugar/Ethanol plants and mapped sugarcane farming (extract from CONAB (2018)).

2.3 REACTIVITY OF ASHES

2.3.1 Incinerator Bottom Ash (IBA)

The larger and heavier ash particles, which are removed from the bed of the incinerator, are known as incinerator bottom ashes (IBAs) (Siddique, 2010). As aforementioned, bottom ashes correspond to approximately 80-90% of the total municipal solid waste incineration (MSWI) residues, and are usually composed of silica, alumina, calcium carbonate, lime and iron oxide (Chimenes et al., 1999; Pera et al., 1997).

Approximately 90% of the bottom ash is known as grate ash. This is the ash fraction that remains on the stoker or grate at the completion of the combustion cycle, mainly composed of glass, ceramics, ferrous and nonferrous metals and minerals with small amounts of unburnt organic material (Siddique, 2010). Hence, the chemical characteristics suggest pozzolanic potential for ground IBAs.

Several authors have considered the use of bottom ash from MSWI in building materials (Bertolini et al., 2004; Filipponi et al., 2003; Lin et al., 2008; Müller & Rübner, 2006) however the results are contradictory. Filipponi et al. (2003) claim a low chemical reactivity for bottom ash and the need to enhance reactivity. In contrast, Lin et al. (2008) state that incinerator bottom ash is active when combined with PC and identified $\text{Ca}(\text{OH})_2$, CSH (tobermorite) and CAH (calcium aluminate hydrate) as the main hydration products in incinerator bottom ash - PC pastes. Jurič et al. (2006) studied the properties of bottom ash concrete concluding on a satisfactory quality for low strength requirements and the feasibility of IBA for use in PC concrete.

Bertolini et al. (2004) argument that the use of bottom ash did not lower workability of concrete and its fresh density was comparable with other concretes. The authors found that wet grinding avoid the evolution of hydrogen in the fresh concrete, as the reactions leading to hydrogen release begin at grinding process. However, they observed that concrete produced with dry ground bottom ash experienced remarkable expansion during setting. The authors explain that expansions occur due to the presence of metals in alkaline solution (such as the fresh concrete pore) that promote the cathodic process of hydrogen evolution, in the form of bubbles. They relate the event to the presence of traces of metallic aluminium in the bottom ash.

2.3.2 Sugarcane Bagasse Ash (SCBA) and Sugarcane Bagasse Ash Sand (SBAS)

Plants absorb silicon from soil solutions in the form of monosilicic acid (H_4SiO_4). According to the H_4SiO_4 incorporation mechanism - active, passive and rejective - plants are categorized as high-, intermediate- or non-accumulators, respectively (Takahashi et al., 1990). Sugarcane (*Saccharum officinarum*) is categorised as a high-accumulator, and plants in this category have a high silicon content that ranges from 1.0% to 10% of the dry weight (Tubaña & Heckman, 2015), a good quality with regard to reactivity.

As aforementioned, the fibrous matter that remains after the sugarcane is crushed to extract its juice is burned to generate steam and electricity and ash (SCBA) is produced. SCBA is composed predominantly of highly porous particles of various sizes formed by a silica skeleton from sugar cane and individual quartz particles (Cordeiro et al., 2016). The temperature reached by the ash can vary notably, from 850 °C reaching up to 1000 °C (Sales & Lima, 2010). The burning of the bagasse causes a reduction in mass, leaving approximately 0.3% of SCBA from the total amount of sugarcane processed (Cordeiro & Kurtis, 2017). Additionally, under controlled combustion, the bagasse ash produced in the boilers can be rich in reactive silica (Bahurudeen et al., 2014).

Sales and Lima (2010) state that the poor reactivity of sugarcane ashes is a barrier for the use of the material as mineral admixtures. The authors claim the lack of control over the combustion temperature of the bagasse and the cooling process result in ashes with no hydraulic properties.

In general, the use of SCBA as a SCM is of interest, especially in countries with shortage in supplementary cementitious materials traditionally used in combination with PC such as fly ash, blast-furnace slag and natural pozzolans. However, the presence of specific contaminants as well as the different burning conditions often leads to SCBAs with different chemical compositions (Cordeiro & Kurtis, 2017). Arif et al. (2016) highlights that differences in chemical composition affect the suitability of SCBAs for use as supplementary cementitious material, and for this reason, it is fundamental that individual sources are evaluated in terms of chemical and physical properties to determine the most suitable use of the resource.

In general, amorphous and crystalline silica (SiO_2) are the main components of SCBA. The crystalline portion is formed due to the crystallisation of the original hydrated silica ($\text{SiO}_2 \cdot n\text{H}_2\text{O}$), normally cristobalite, or contamination of SCBA with quartz from soil (sand) (Cordeiro & Kurtis, 2017). Cristobalite generation is normally attributed to non-controlled burning processes, usually associated with high temperatures (above 800°C) and/or long periods of burning, however, Cordeiro et al. (2016) observed the formation of cristobalite in a study where the temperature was controlled and maintained at 800°C in a laboratory furnace.

Additionally, a further contributor to crystalline silica (SiO_2) in SCBA is contamination with sand. This is relatively common as sand which adheres to the harvested cane stays attached even after the washing procedure. The quantity of sand adhered to the cane (up to 2 wt.% of the harvested cane) is considered insignificant by the industry to sugar-ethanol production (Cordeiro et al., 2008), however, after burning the bagasse, the sand amount reaches values higher than 50 wt.% due to the loss of organic matter (Cordeiro et al., 2016). The contamination of the sugarcane bagasse ash by sand can be further increased by the disposal of the ash in sandy areas. Once the ash is disposed in these areas its use as a pozzolanic material is compromised due to the level of contamination and difficulties in separating the materials. In order to give a use for the ashes with high levels of sand, it is proposed the use of the material as partial aggregate replacement, known as sugarcane bagasse ash sand (SBAS).

2.3.3 Fly Ashes (FA)

The use of fly ashes as pozzolans dates back to 1914, although the earliest comprehensive study of the material dates from 1937 (Halstead, 1986). Fly ashes (FAs) from power plants have been used in building materials for decades (Felekoğlu et al., 2009; Jiménez-Quero et al., 2013; Payá et al., 1995b; Sharma & Sivapullaiah, 2016; Siddique, 2004). Felekoğlu et al. (2009) stressed the importance of fineness to achieve a higher compressive strength, and noted that increasing fineness may also result in a higher water demand due to increasing specific surface area. Payá et al. (1995b) argue that the enhancement of compressive strength is mainly related to the content of fly ash particles under $10\ \mu\text{m}$. They also noted that a significant loss of flexural and compressive strengths is associated with the use of coarser fly ash fractions.

Power-plant FAs are mainly composed of SiO_2 , Al_2O_3 , Fe_2O_3 , and CaO with minor constituents such as MgO , Na_2O , K_2O , SO_3 , MnO and TiO_2 . According to their chemical composition, they are classified as silico-aluminous (having pozzolanic properties) or silico-calcareous, with hydraulic properties (Gutt & Nixon, 1979; Lea, 1970). Mostly composed of spherical particles, power-plant FAs also contain irregularly shaped particles of varying sizes depending on the sources (Gutt & Nixon, 1979; Ramezani-pour, 2014). Their spherical shape lessens the frictional forces of larger angular particles by filling in spaces, enhancing packing and reducing the yield stress (“ball bearing” effect, Figure 2-3) (Jiménez-Quero et al., 2013).

Furthermore, power-plant FAs have been reported to enhance the workability of pastes, reduce their water demand and heat evolution, therefore minimising expansion and cracking at early ages (Siddique, 2004). Jiménez-Quero et al. (2013) explored the rheological behaviour of cement pastes and mortars with sugarcane FA replacement, finding that pastes with 20% and 30% fly ash showed a smaller yield stress than a cement paste with superplasticizer (12 mL/kg of cement). They also noted that the use of superplasticizer on mortars with fly ash is not necessary, as there was a decrease of shear viscosity with the increase of shear rate.

Sugarcane FA is composed of particles of irregular shapes, different from the spherical shape typically found on fly ashes from coal combustion. Several studies have explored the adsorbent properties sugarcane fly ash on the removal and recovery of heavy metals and other hazard chemicals from aqueous solutions (Gupta & Ali, 2004; Gupta et al., 2003; Mall et al., 2005; Srivastava et al., 2006). However, the efficacy of sugarcane fly ash as a supplementary cementitious material has been investigated to a lesser extent, as seen in Section 2.4 Effect of ashes in the properties of composites.

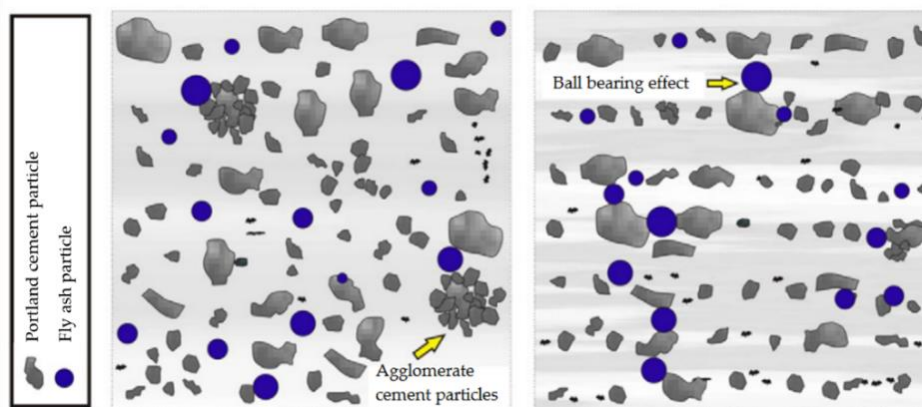


Figure 2-3: Schematic representation of the ball bearing effect (extract from Jiménez-Quero et al. (2013)).

Incinerator FAs are composed of particles with fairly smooth surfaces and eventual hollow spheres, as well as agglomerations of irregular shaped particles, also different from the spherical particles of power plant fly ashes (Chang & Wey, 2006), and correspond to c. 4% of the solid remnant after incineration of urban solid waste (López Zaldívar et al., 2015). The pozzolanic reactivity of incinerator fly ashes have been investigated to a lesser extent compared to incinerator bottom ashes. Some of the findings are described in Section 2.4.

2.4 EFFECT OF ASHES IN THE PROPERTIES OF COMPOSITES

2.4.1 Porosity and Capillary Action

The pore structure developed following hydration and pozzolanic reactions influences the permeability and mechanical resistance of concretes, mortars and pastes (Cordeiro, 2006) significantly affecting the performance of the materials in relation to water, frost, salt and chemical weathering, partially determining their durability (Pavia et al., 2006).

Porosity reduces with the decrease in water/cement ratio. Also, long curing times lower the volume of capillary pores as the pore system becomes less well connected and more tortuous. Pore interconnection rises permeability, likewise, if the pore system is disjointed, permeability is lessened, although porosity can remain the same (Kearsley & Wainwright, 2001; Neville, 1995). Refinements in the pore system lower permeability making the material more resistant to penetration of fluids and deleterious materials.

In a PC system, as water evaporates or is consumed by hydration, it is generally considered that the pores in the remaining space are of a size in which capillary effects occur (Thomas, 2013; Walker, 2013). Therefore, increasing the amount of mixing water can significantly increase the amount of capillary pores (Lea, 1970). Figure 2-4 presents the change in volume of the major PC compounds as a PC paste ($w/c = 0.5$) hydrates, and the space originally occupied by mixing water progressively fills up with cementing hydrates. Table 2-1 includes the origin of the different pores in a cement paste and their influence on the properties of the material.

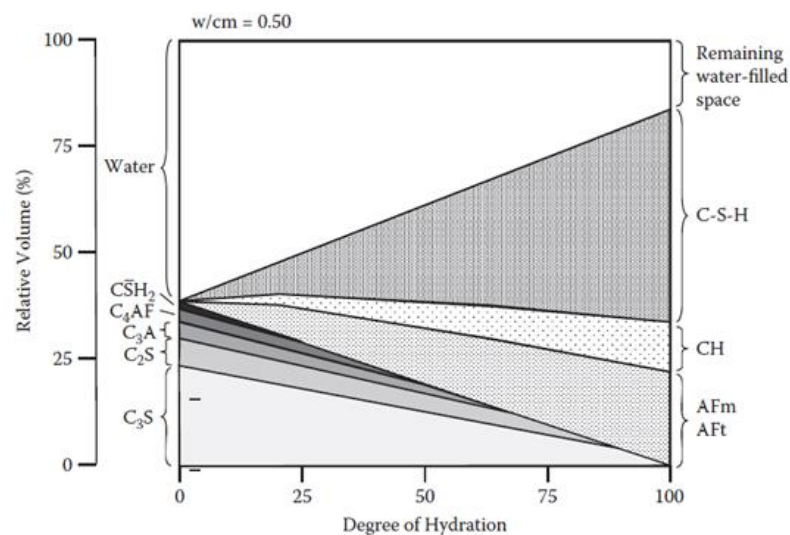


Figure 2-4: Relative volumes of major compounds as a function of the degree of hydration estimated by a computer model for water/cement ratio = 0.50 (extract from Thomas (2013)).

The absorption of water through capillary pores is the process by which moisture is carried through fine pores due to tension forces developed between the solid particles and the water

molecules (Taylor, 1997). Capillary suction relates to both mortar porosity and permeability and typically transfers the largest amount of water in a building material (Walker, 2013). It depends on factors such as the degree of saturation and environmental conditions and is the dominant mechanism for infiltration of chloride and sulphate ions in mortars, particularly near unsaturated surfaces (Martys & Ferraris, 1997). It has been determined that capillary forces transport liquid water within pores greater than 0.1 μm , with greater absorption rates in pores ranging from 1 μm to 1 mm (Benavente, 2011). This has been attributed to the lower flow resistance of the larger pores and the higher tractive forces of smaller pores (Aly & Pavia, 2016). An increase of capillary suction, porosity and bulk density rise permeability, enhancing salt, moisture and frost induced damage which undermine mortar durability (Pavia & Toomey, 2008).

Massazza (1998) summarises the effect of pozzolans on porosity/capillarity as follows: whatever the type of pozzolan, porosity decreases with time but it keeps higher than in the parent PC paste; it increases when increasing the FA content but lowers when rice husk ash (RHA) is increased. The author also states that pozzolans tend to lower capillarity and moisture movement through materials: after 28 days, the MCD (or critical pore size representing the larger fractions of interconnected pores) of a pozzolanic cement is lower than that of the parent PC. Other authors agree, stating that fly ash significantly reduced capillary sized- pores between 28 days and 1 year, with substantial shift from macropores to mesopores Figure 2-5. Pozzolanic hydrates can lower open porosity, capillary suction and water absorption as they imply the appearance of a greater number of small gel-pores and a reduction of the larger pores active to liquid moisture transport (Aly & Pavia, 2015). Pavia and Aly (2016) found that, in general, SCMs (RHA and GGBS) reduced the hygric properties of hydrated lime mortars and attributed this trend to the hydrates leading to a greater number of small gel pores and fewer larger pores active to moisture transport. However, the authors note that some SCMs (RHA) had little impact on the hygric properties of the composites because their high water demand increased porosity balancing the effect of their hydrates.

However, there are some discrepancies. For example, Chindaprasirt et al. (2005) reported that fly ash from power plants (20-40% cement replacement) increased the total porosity and capillary porosity of cement pastes at all ages (7, 28, 60 and 90 days). They also noted an increase of porosity and capillarity with growing ash replacement, this might be due to the higher water/cement ratio. The authors determined that finer fly ash significantly lowered porosity and capillarity compared with coarser fly ash. Massazza (1998) also noted a significant raise in porosity in fly ash concrete. Frías and Cabrera (2000) also noticed an increase of 16% in porosity owing to the replacement of cement by metakaolin. Their results show a gradual increase in the very fine pores (less than 100 Å) with age.

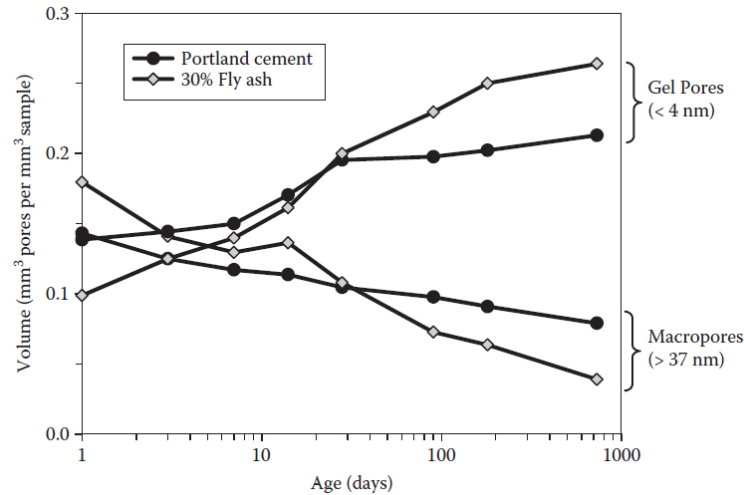


Figure 2-5: Effect of age and fly ash on the pore size distribution of hardened cement paste as measured by the solvent absorption technique - Data from Thomas (1989) (extract from Thomas (2013)).

In general, the addition of pozzolanic ashes tends to increase porosity at early ages, however, as the pozzolanic reaction evolves through time, the porosity tends to lower due to the formation of pozzolanic products. González-Fonteboa et al. (2017) found that the water absorption of CEM I with 10, 20 and 40% incinerator bottom ash replacement, was lower than the absorption of limestone filler mixes (CEM II/A-L and CEM II/B-L) but greater than the reference CEM I mix, however, at 40% replacement the water penetration was lower than reference which indicates the discontinuity of the pore system causing lower water penetration depth values. Lin et al. (2003) found that the replacement of cement by 10% incinerator fly ash slightly reduced the volume of capillary pore at ages from 1 day to 90 days. However, as the substitution level increased (20 and 40%) the capillary volume raised at early ages and gradually dropped to values comparable to the reference values at 90 days as the interspaces were gradually filled up due to the formation of pozzolanic products. Ganesan et al. (2007) reported that water absorption increased with sugarcane bagasse ash content at 28 days. They explain it is owed to the finer particles of the ash, compared to cement, and the hygroscopic nature of the ash. The authors also identified a considerable water absorption reduction (50%) after 90 days.

Table 2-1: Pores in cement paste.

Pore		Size	Role of water	Analysis	Origin		Importance	Properties influenced	
Gel Pores	Micropores (Interlayer)	Up to 0.5 nm	Structural water involved in bonding; Non-evaporable; Ionic/covalent bond	Gas adsorption-desorption; Thermal		< 2.6 nm Associated with C-S-H; Interparticle space between C-S-H sheets	Disjoining effects may occur during wetting and drying	Shrinkage, creep at all RH	Shrinkage, creep (< 11% RH)
	Micropores	0.5 nm to 2.5 nm	Strongly adsorbed water; No menisci form; Non-evaporable; Intermolecular interactions	Gas adsorption-desorption; MIP; IS	1 nm to 3 nm Interparticle space between C-S-H sheets			Shrinkage, creep at all RH	Shrinkage, creep (35-11% RH)
Capillary pores	Small (gel) capillaries	2.5 nm to 10 nm	Strong surface tension forces generated; Evaporable; Strong menisci	Gas adsorption-desorption; MIP; IS		2.6 nm to 50 nm Remnants of water-filled space; Smaller pores associated with C-S-H	Capillary effects create stress during drying	Shrinkage between 50% and 80% RH	Shrinkage (up to 50% RH)
	Medium capillaries	10 nm to 50 nm	Moderate surface tension forces generated; Evaporable; Moderate menisci	Gas adsorption-desorption; MIP; SEM	10 nm to 50 nm Capillary pores (low w/c)			Strength, permeability, shrinkage at high RH (> 80%)	Permeability, strength, shrinkage (high RH)
	Large capillaries	50 nm to 10 μ m	Behaves as bulk water; Evaporable	MIP; SEM; OM	3 μ m to 5 μ m Capillary pores (high w/c)	> 50 nm Remnants of water-filled space in fresh pastes	Control permeability and durability	Strength, permeability and diffusion	Permeability, strength, Mass transport
	Entrained air	0.1 mm to 1 mm	-	OM	50 μ m to 1 mm Entrained voids	> 5 μ m Air entrainment; entrapped air; inadequate consolidation or curing; excessive mix water	Limit strength	Strength	-
Reference			Mindess et al. (2003); Jennings et al. (2008).	Mehta (1986); Mindess et al. (2003).	Mehta (1986)	Barnes and Bensted (2002)	Barnes and Bensted (2002)	Mindess et al. (2003); Thomas (2013)	Jennings et al. (2008)

IS: Impedance Spectroscopy; MIP: Mercury Intrusion Porosimetry; OM: Optical Microscopy; SEM: Scanning Electron Microscopy

2.4.2 Water Vapour Permeability

Water vapour travels through a building material driven by differential vapour pressures, from a higher to a lower-pressure environment. Hence, the rate of transmission depends on the pressure differential and on the vapour permeability of the material. It is determined by the geometry of the pore structure and the air within the pore's moisture. In buildings, vapour usually travels from the interior to the exterior due to the high levels of water vapour produced within the building envelope (Walker, 2013; Walker & Pavia, 2015). Indirectly, this property reflects the microstructure of cementitious materials through their interaction with the water vapour (de Burgh et al., 2016). The interaction of vapour phases with solid phases within pores affects processes related to durability such as carbonation and chloride corrosion of reinforcement (de Burgh et al., 2016). Therefore, a reduced permeability would enhance durability. However, a reduced permeability can be detrimental when the material is not allowed to properly dry resulting in moisture accumulation.

The water vapour diffusion resistance factor (μ) measures the ratio of the resistance to moisture movement of the material to the resistance to moisture movement of the air, i.e. it is a dimensionless number describing how many times better a material or product is at resisting the passage of water vapour, compared with an equivalent thickness of air. Thus, the lower the value of μ the greater the moisture transfer. The water vapour permeability of lime based materials tends to be high. Walker and Pavia (2014) measured the water vapour permeability of lime-hemp concretes with the addition of different pozzolanic materials. The results showed relatively high permeabilities, with values ranging from 5.42 (metakaolin:lime binder) to 5.71 (GGBS:lime + water retainer).

It seems that water vapour permeability decreases with increasing pozzolanic content. According to (Massazza, 1998) the permeability of pozzolanic cement pastes decreases by increasing the pozzolan (natural, FAs, RHA etc) content and curing time, with some occasional deviations. However, this depends on the type of pozzolan and curing time; and the permeability of pozzolan-cement mortars at early ages is higher than that of the control PC. A reduction in permeability by pozzolans has also been reported by Vejmelková et al. (2012) in lime mortars with burnt shale and metakaolin as pozzolanic additions. The authors found an increase in the water vapour diffusion resistance of the pozzolanic materials with μ ranging from c. 20-23 versus the c. 14 value of the reference lime mix.

2.4.3 Bulk and Real Densities

Density informs on the degree of consolidation of a solid including grain packing and mechanical resistance (Pavia et al., 2006). Density and porosity are closely related and usually indirectly proportional. Thermal conductivity is also linked to density as it increases with increasing density. Expansion during setting or weathering after hardening can lower density.

It has been reported that the use of pozzolanic ashes lower the density of composites at early ages, however, it tends to increase with curing time (Chaipanich et al., 2010; Heikal et al., 2000). Esquinas et al. (2018) studied the use of non-conforming fly ash and observed that it tends to decrease the bulk and real densities of composites. The authors point out that bulk density shows a larger variation, owing to the influence of the accessible pores on bulk density, whereas porosity does not influence real density. However, other authors (Kristiawan & Murti, 2017) have observed an increase in the density due to fly ash pozzolanic reactions.

Bertolini et al. (2004) studied the use of MSWI ashes as mineral additions and also found that the addition of fly ash increased the 28-day density, whereas, the addition of incinerator bottom ash lowered the density of concretes. They found densities of 2450 kg/m³ for incinerator fly ash (30% replacement) and 2260 kg/m³ for incinerator bottom ashes (30% replacement). The author explains that an expansion during setting lowered the density of the specimen with bottom ash addition, which had a fresh density of 2400 kg/m³.

It is generally accepted that the particle size distribution and the chemical nature of supplementary cementitious materials influence density, hence, finer pozzolanic ashes and greater pozzolanic capacity will reduce porosity, consequently increasing density.

2.4.4 Resistance to freeze-thaw

The expansion of water caused by freezing (9% in volume) increases internal hydraulic pressures causing damage within porous structures (Barnes & Bensted, 2002). Hence, there is a close relationship between resistance to freezing and pore structure in construction materials. Pore characteristics such as volume, radius and size distribution determine the freezing point of the moisture contained within and the amount of ice formed (Cai & Liu, 1998). The resistance to freeze-thawing is the ability of the material to withstand strain caused by changes in volume as water solidifies, and the subsequent thawing upon heating. The transition of phases causes dimensional changes and internal stresses leading to failure (Cao & Chung, 2002; Eglinton, 2003).

The resistance of concrete to frost depends on the quality of the cement mortar and, to some extent, of the aggregate. It is known that the characteristics of the pore structure of a composite is of major importance. While larger pores are not considered detrimental, the finer pores (< 5 µm in diameter) if present in abundance, have most influence in reducing frost resistance of concrete, since they tend to retain water (Eglinton, 2003), hence, materials with either very high or very low porosity usually have good service record (Lawrence, 2003). For this reason, natural pozzolans, fly ashes and silica fume contained in blended cements do not worsen frost resistance, provided that concretes have a suitable entrained-air content, as microscopic air bubbles protects the concrete by providing accommodation to water being pushed forward by the ice in the process of being formed. However, the influence of pozzolanic ashes on the frost resistance of composites does depend on the replacement level. For instance, the use of fly ash

at high percentages ultimately decreases frost resistance, whereas when used within 15 - 40% limits it has no significant effect on the freezing and thawing resistance of concrete. Replacement of silica fume exceeding 15% also causes the resistance to frost attack to decrease (Massazza, 1998).

It should be noted, however, that owing to the slow initial hardening of pozzolanic cements, the frost exposure of pozzolanic blended cements should be somewhat delayed compared to that of Portland cement. Insufficient curing time often gives inferior results for blended cements. On the other hand, freeze-thaw tests carried out after long curing periods have shown that blended cements develop equivalent or higher resistance than that of Portland cements, provided that the composites have the same strength (Massazza, 1998).

Puertas et al. (2003) observed that slag mortars showed high stability against freeze-thawing cycles and a significant increase in flexural and compressive strengths after exposure. They evidenced that, under conditions of high humidity, the activated slag continues reacting and increasing the final strengths. In the same study, the reference cement mortar (CEM I) also increased compressive strength but experienced a decrease in flexural strength, possibly due to the increment of microcracks resulting from tensions originated as a consequence of the cycles.

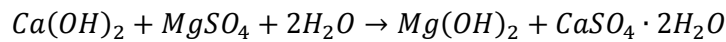
Bektas et al. (2009) replaced PC mortar aggregate with crushed brick at levels of 10 and 20 % by weight. They found that, as the quantity of crushed brick increased, the expansion caused by the freeze-thaw action lowered. They concluded that the inclusion of the highly porous crushed brick might have prevented freeze-thaw cracking by relieving the pressure caused by ice formation. Sabir (1997) studied the use of condensed silica fume (CSF) in concrete as cement replacement and found that at low water-binder ratios (0.25 – 0.3) and low cement replacement levels (5 – 10%) CSF has a beneficial effect on frost resistance. However, higher CSF contents (20 – 30%) showed detrimental effects over the range of water-binder ratios 0.35 – 0.55.

2.4.5 Resistance to Salt Crystallisation

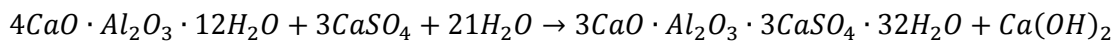
Composites are susceptible to weathering by salts, most commonly carbonates, chlorides, sulphates and nitrates. The crystallisation of salts within porous materials has been known for decades. Salt crystallization, differential thermal expansion and hydration/dehydration lead to stress accumulation and eventual fracturing and disruption (Winkler & Singer, 1972). Disruption occurs when the tensile strength of the composite is surpassed by the increasing of internal stress due to the replacement of the hydrates (or other original mineral components) for salts, which are compounds of larger volume (Massazza, 2002). The degradation is likely to happen first at the specimen's surface (spalling), affecting primarily the flexural strength of mortars and concretes (Vu et al., 2001). In addition, salts can react with calcium hydroxide – the most vulnerable product of cement hydration – and have a significant effect on C-S-H dissolution (Winkler, 2013a). Salt attack depends on the type and composition of the salt

involved. For example, the effect of sulphate attack depends on the cation associated with the sulphate ion. Calcium sulphate poses a lower threat while magnesium sulphate is more aggressive and cause a greater deleterious impact (Massazza, 2002).

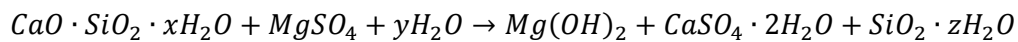
Magnesium sulphate ($MgSO_4$) attacks all cement compounds in the hardened paste, as explained in the reactions below. It first affects portlandite – $Ca(OH)_2$ – as follows (Massazza, 1998):



Then gypsum ($CaSO_4 \cdot 2H_2O$) can react with the calcium aluminate hydrate, producing expansive ettringite:



Finally, $MgSO_4$ also attacks calcium silicate hydrates as follows:



Although pozzolanic cements cannot prevent long-term failure, the addition of pozzolans has been found to improve the resistance of mortars to sulphate attack. Pozzolans react chemically with $Ca(OH)_2$, thereby lowering vulnerability by reducing $Ca(OH)_2$ content, which in turn drops the formation of gypsum while refining the pore structure, which lessens permeability and the intrusion of aggressive agents (Massazza, 1998). Moreover, the occurrence of C-S-H covering small calcium hydroxide crystals shields the particles against sulphate attack (Massazza, 1993). Therefore, pozzolanic cements can delay the decline in the performance of composites subjected to sulphate attack and improve their life expectancy.

Walker et al. (2014) tested lime-hemp concretes with different pozzolanic materials. The authors state that one-month exposure to sodium chloride does not damage the compressive strength of any concrete and no cracks were visible; and attributed these results to the high ductility of the pore walls accommodating expansive salt crystallisation pressures. They concluded that no significant change in durability was observed due to the existence of pozzolans in the concrete matrix.

Nehdi and Hayek (2005) tested resistance to salt exposure (by 9-month immersion in 10% Na_2SO_4 and 10% $MgSO_4$ solutions) of four different binders (100%PC, 92%PC - 8% silica fume, 75%PC - 25% fly ash and 75% PC - 25% blast furnace slag). They confirmed that the higher water/cement ratios showed the greatest expansion, with the greatest sulphate expansion observed in the PC mortar. The authors also observed that calcium-rich slag improved the resistance to surface attack by $MgSO_4$ probably due to the elevated pH, preventing the rapid attack and decalcification of C-S-H. It was also noted that expansion by Na_2SO_4 immersion was higher, however surface scaling and loss of mass only took place in the $MgSO_4$ solution.

2.4.6 Thermal Properties

The energy performance of materials in buildings is key for the design and evaluation of sustainability. Hence, it is essential to consider the ability of a construction materials to transfer heat. Conduction is one of the main heat transfer mechanism in building materials by which internal heating or cooling can be lost to the outside due to the presence of temperature gradient (Ä-zisik & Özışık, 1993). Understanding the thermal behaviour of materials favours the appropriate application of resources, minimising operating costs, carbon emissions and occupant discomfort. To improve thermal comfort and save energy, it is preferable to use low thermal conductivity materials, as these materials provide a level of thermal insulation. On the other hand, if a thermal stress reduction is needed, it is desirable the use of materials with higher thermal conductivity, as these have the ability to reduce temperature gradient, thus alleviating thermal stress in a structure (Xu & Chung, 2000b).

Thermal conductivity describes how quickly heat flows through a material from the hot side to the cold side under steady state conditions. It is not dependent on size or shape (McCarter & Tran, 1996) but is considered to be determined by factors such as temperature, moisture content and ageing (Gomes et al., 2017). However, it is the thermal diffusivity (rather than the thermal conductivity) that governs the speed of heat conduction because it describes how well a material spreads heat, taking into account both how quickly the heat can be conducted (thermal conductivity) and how quickly the material's temperature can change when heated (heat capacity). The higher the thermal diffusivity of a material, the higher the rate of temperature propagation. It is a measure of heat transport relative to energy storage and depends on the thermal conductivity, specific heat and density of the material (Carman & Nelson, 1921). High thermal diffusivity indicates high rate of temperature propagation, the heat transfer through the material will be fast and the amount of storage small. Hence, low thermal diffusivity means slower rate of heat transfer and large heat storage, therefore, a slow response to temperature variations similar to that of typical high thermal mass elements in construction, desirable for storing solar energy (Institute, 2002).

Effusivity is also a heat transfer property and dictates the interfacial temperature when two objects at different temperature touch. Therefore, it is important for thermal comfort in buildings (materials with low effusivity need less energy to warm up and warm wall surfaces highly increase comfort indexes) and it influences thermal stresses and strains due to heat conduction playing a key role in thermal fatigue and thermal shock. (Chabannes et al., 2015; Materion, 2018; Raut & Gomez, 2017). Thermal effusivity is given by $e = \sqrt{k\rho C_p}$, where k is the thermal conductivity, ρ is the material density and C_p is the heat capacity of the material under consideration.

Studies have demonstrated the lowering of the thermal conductivity of composites by pozzolans due to the higher porosity of the pozzolanic material and the porous character of the products of the pozzolanic reaction, mainly C-S-H gels. Černý et al. (2006) observed that partial substitution of lime by metakaolin in plasters reduced the thermal conductivity,

compared to reference lime plaster by almost 50%. Demirboğa and Gül (2003) studied the effects of silica fume and fly ash on the thermal conductivity of lightweight concrete and found that both pozzolans reduced thermal conductivity in relation to the reference composite. It was observed that fly ash reduced the thermal conductivity to a greater extent, (12% lower than reference at 30% replacement) while silica fume lowered it by 10% at the same level of substitution. The authors refer to the greater air content and lower density of the pozzolans driving the thermal conductivity down.

The ability of a material to store thermal energy is given by its specific heat capacity, or thermal capacity. It describes the amount of heat required to heat up 1 g of a material by 1 °C. Materials with a high specific heat have an increased ability to retain heat, desirable for energy conservation and insulation in buildings (Xu & Chung, 1999, 2000b) contributing to the thermal mass effect that delays heat transfer. The presence of moisture considerably increases specific heat: a variation in concrete's specific heat from 1.130 to 0.879 J/g.C has been reported at ages of 6 h and 7 days (Brown & Javaid, 1970).

It has been reported that pozzolans tend to increase the specific heat capacity of composites. Černý et al. (2006) observed that pozzolans, such as metakaolin, increased the specific heat capacity, from 0.970 J/g.C (reference lime plaster) to 1.020 J/g.C. Fu and Chung (1997) also observed an increase of 9% in specific heat by replacing cement with silica fume in cement pastes. They discuss that the effectiveness of silica fume in increasing specific heat is due to the interface between silica fume and the cement matrix, as silica fume itself is not high in specific heat. Xu and Chung (2000b) found that silica fume increased the specific heat of the mortar (from 0.642 to 0.705 J/g.C) and the paste (up to 0.788 J/g.C). This is attributed to the increase of mortar's density and decrease of the density of the cement paste. They also found the specific heat of PC mortar lowered by 13% due to the addition of sand (0.736 J/g.C vs 0.642 J/g.C), while the thermal conductivity increased by 9% (from 0.53 to 0.58 W/m.K). It is believed that the smaller interface area of the sand (larger particle size results in smaller interface) is responsible for the lower specific heat and higher thermal conductivity, as slippage at the interface contributes to the specific heat and the interface acts as a thermal barrier.

2.4.7 Strength of the Ash-Composites

The strength of composites is related to the amount of hydraulic set in the binder which in turn relates to durability (Pavia et al., 2006). It is the main property traditionally related to the cement quality (Binici et al., 2007). The transition zone determines strength because it is usually the weakest area in composites and limits ultimate strength (Barnes & Bensted, 2002) as hexagonal crystals of free lime or portlandite tend to crystallize here as PC progressively hydrates. Therefore, in cement composites, it is generally accepted that strength increases with the amount of combined lime however, there is no general relationship between strength development and lime combination, as not all combined lime hardens appreciably. For

example, clay rich materials combine lime however, their strength can only reach about one-third of the strength of materials with true pozzolanic reactivity (Massazza, 1998).

Replacing cement with pozzolans tends to lower the early strength of composites owed to the late pozzolanic reaction, however, at greater ages, pozzolanic cements can achieve the same or even higher strength than the corresponding reference PC (Massazza, 2002). As aforementioned, the strength development and ultimate strength largely depend on the pozzolan/lime and water/binder ratios, yet other factors such as grinding also influence strength development. Cordeiro et al. (2008) observed that the dilution effect – or decrease in compressive strength resulting from cement replacement by mineral admixtures such as limestone or pozzolans – lowers when increasing the ash fineness (SCBA).

It is known that the presence of certain compounds favour the lime-pozzolan reaction enhancing strength development. Gypsum for instance, enhances lime combination, as long as the sulphate content is kept to a limit of 7%, since higher levels can cause expansion and possibly cracking. Additionally, KOH, NaOH, Na₂SO₄ and CaCl₂ have also been reported to improve the strength of pozzolan mortars, whereas NaCl does not seem effective (Massazza, 2002).

The strength of composites is directly affected by the type of pozzolanic material used. This is owed to the variations on the physical, chemical and mineralogical properties of these materials, hence, different pozzolanic materials have different impact on composites (Massazza, 1998). The variations on the strength development caused by the use of different pozzolanic materials have been reported. For example, the addition of metakaolin has been reported to enhance the compressive strength of composites, whereas incinerator fly ashes and sugarcane bagasse ashes have been observed to lower the compressive strength in relation to their respective reference.

Poon et al. (2006) studied the mechanical properties of high-performance concrete with metakaolin (up to 20% replacement) and silica fume (up to 10%) as cement replacement. They found that the metakaolin enhanced the concrete strength further and the 10% metakaolin replacement resulted in the highest strength, 120.3 MPa at 90 days vs the 102.5 MPa of the control mix. The higher strength is credited to the higher rate of hydration in the metakaolin concrete.

Arenas-Piedrahita et al. (2016) studied the effects of sugarcane fly ash as a partial cement replacement (10% and 20%) and reported that there was a decrease on the compressive strength at 28 days, especially for mortars with 20% replacement, however, at 56 days, the compressive strength for both levels of replacement reached equal strength than the control.

According to Tang et al. (2016), the compressive strength of mortars with incinerator bottom ashes are lower than the reference mortar at all ages (up to 28 days) but the differences reduced as curing progressed. González-Fonteboa et al. (2017) observed that mixes of CEM I + 10% ground bottom ash lowered the early strength of composites, however, at 90 days the strength was comparable to that of the reference. At 20% replacement the strength was still slightly

lower at 90 days. Additionally, the authors compared the results with those of commercial cements with limestone and pointed out the much better mechanical activity (greater strength) of the mixes with bottom ash even at early ages.

The use of power plant fly ash has been reported to decrease the early strength of composites. Kiattikomol et al. (2001) studied fly ashes from 5 power plants and observed that the reference strength was reduced at all ages (up to 90 days). Mehta and Gjrrv (1982) reported that concretes containing power plant fly ash presented a significantly lower compressive strength at 3, 7 and 28 days, however, the strength of the concrete containing fly ash was similar to the control concrete. Tangpagasit et al. (2005) also detected a reduction in strength due to the addition of fly ash from power plant at ages from 3 to 90 days.

Similar to what has been reported for power plant fly ashes, incinerator fly ashes have also been reported to reduce reference strength of composites. Tang et al. (2016) reported that concretes made with incinerator fly ash achieved a 28-day strength (51.7 MPa) slightly lower than that of a concrete made with 30% coal fly ash replacement (53.4 MPa). Garcia-Lodeiro et al. (2016) found that matrices incorporating a blend of incinerator fly ash (17%) and bottom ash (83%) as Portland cement (CEM IV) replacement (60:40 cement:blend of ashes), alkali activated (5% mix of CaSO_4 and Na_2SO_4), achieved a compressive strength of 33 MPa at 28 days, still lower than that of reference.

Lin et al. (2003) observed that mortars with replacement of cement by 10% incinerator fly ash exhibited strength 1 – 2 MPa higher than that of reference mortar, after 60 and 90 days while mortars with 20% fly ash lowered the strength by 6 MPa.

Zareei et al. (2018) observed a decrease in compressive strength of concretes containing sugarcane bagasse ash. Replacement levels of 20 and 25% resulted in a reduction by 24 and 35% respectively. Similarly, Cordeiro and Kurtis (2017) showed reductions (up to 26%) in strength activity indexes of composites produced with bagasse ash as cement replacement. On the other hand, Ganesan et al. (2007) reported increase in strength of sugarcane bagasse ash blended cement mortars in replacement levels of 5, 10 and 15%. The greatest strength was achieved at 10% substitution, 20% higher than the reference.

It has been reported that pozzolans reduce flexural strength. Ghrici et al. (2007) observed a reduction on flexural strength of composites produced with natural pozzolan, from the Beni-Saf quarry in Algeria – type of pozzolan not mentioned – at cement 10, 20 and 30% replacement. The strengths varied between 6.6 and 8.3 MPa at 28 days and between 8.1 and 8.7 MPa at 90 days using natural pozzolan. Additionally, irregular particle shapes have a positive effect on flexural strength as they enhance the interlocking of particles (Tang et al., 2016).

Habeeb and Fayyadh (2009) investigated the effects of incorporating 20% of rice husk ash (RHA) as partial binder replacement in concrete at three different particle sizes. It was shown that the tensile strength of concrete increased systematically with increasing RHA fineness. The concrete produced with RHA possessing an average particle size of 11.5 μm achieved 5.2

MPa in flexural strength at 28 days, while the average particle sizes of 18.3 and 31.3 μm resulted in strengths equal to 5.0 and 4.9 MPa, respectively. The difference in the results are explained by the increased pozzolanic reaction and the packing ability of the finer RHA particles.

Tang et al. (2016) demonstrated that the loss in flexural strength of bottom ash mortars was not as significant as their compressive strength loss. Siddique (2004) observed that the flexural strength of concretes with high fly ash replacement (40 to 50%) were lower than the control mix at 7, 28, 91 and 365 days, however, the (15-25%) fly ash composites presented a continuous strength development beyond 91 days, while the control mix achieved its peak strength at 91 days, 5.5 MPa, and held the same strength at 365 days.

However, the use of RHA has been reported to increase the flexural strength of lime mortars. Pavia et al. (2014) observed an increase in flexural strength associated with the increase in RHA content. The authors also identified a decreasing rate of strength increase. While the 1:0.3 (CL90-S: RHA – lowest replacement level) mortar was 1.5 times stronger in flexion than the control lime mortar, the 1:3 (CL90-S: RHA – highest replacement level) was only 1.2 times stronger in flexion than the 1:2 (CL90-S: RHA) mortar. The increase in strength is attributed to the formation of hydrates, as a result of the pozzolanic reaction, and the reduction in water demand as the RHA content increases.

3 MATERIALS AND METHODS

3.1 MATERIALS

3.1.1 Lime

A hydrated lime (CL90-S) complying with EN 459-1 (2015) was used on this research. The product is produced by Clogrennane Lime and the data sheet is available in Appendix E.

Chemical composition:

Table 3-1: Chemical composition of hydrated lime.

	(%)		(%)
Ca(OH) ₂	92	Al ₂ O ₃	0.3
CaCO ₃	1.5	Fe ₂ O ₃	0.2
MgO	0.4	SO ₃	0.5
SiO ₂	1.4		

3.1.2 Portland Cement

An ordinary Portland cement (PC) CEM II/AL 32,5N was used on the second stage of this research. The cement complies with EN 197-1 (2011) and is produced by Irish Cement. The product data sheet is available in Appendix F. The chemical composition is shown in Table 3-2.

Table 3-2: Chemical composition of Portland Cement.

	(%)		(%)
SiO ₂	19	SO ₃	2.4
Al ₂ O ₃	4.9	K ₂ O	0.52
Fe ₂ O ₃	2.5	Na ₂ O	0.22
CaO	65.5	Cl	0.08
MgO	1.3	LOI	5.1
Cr (VI) - ppm	0.6		

3.1.3 Ashes

The ashes were sourced from Brazil, Portugal, Ireland and the Czech Republic. The type, origin and notation of the ashes are displayed in Table 3-3.

Table 3-3: Investigated ashes.

Type	Industry	Origin	Notation
Sugarcane bagasse ash	Sugarcane	Brazil	SCBA 1 SCBA 2 SCBA 3/ SBAS 1 SCBA 4/ SBAS 2
Incinerator bottom ash	MSWI	Portugal Ireland Czech Republic	IBA 1 IBA 2 IBA 3
Incinerator fly ash	MSWI	Portugal Czech Republic	FA 1 FA 2
Sugarcane fly ash	Sugarcane	Brazil	FA 3

MSWI – Municipal solid waste incineration.

3.1.4 Sand

A siliceous sand was used. The particle size distribution, determined by Chever et al. (2010) according to EN 812-103.1, establishes similarities in grading compared to the standard CEN reference sand in EN 196-1 (2005), as demonstrated in Figure 3-1. The sand consists of angular grains of medium sphericity, composed mainly of quartz, with lower amounts of feldspar and occasional amorphous silica.

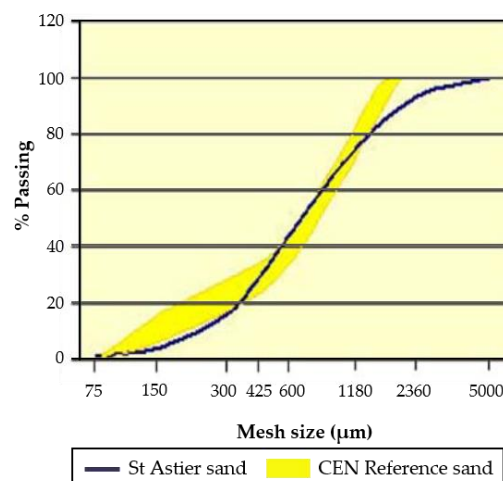


Figure 3-1: Particle size distribution of St. Astier sand compared with the standard CEN sand (extract from Chever et al. (2010)).

3.2 METHODS PHASE 1: PROPERTIES OF ASHES

3.2.1 Sample Preparation

The raw ashes required some level of pre-treatment, consisting of drying, sieving, and grinding, as shown in Table 3-4, in order to be used as a fine binder replacement. Figure 3-2 presents the ashes after initial sieve.

The ashes were oven dried at 105 °C for 24h to remove humidity. Once the material was dry sieving was performed with a 2 mm sieve to remove contamination, except IBAs. In this stage the incinerator bottom ashes were divided into fine (grains smaller than 1 mm) and coarse (from 1 mm to 3 mm).

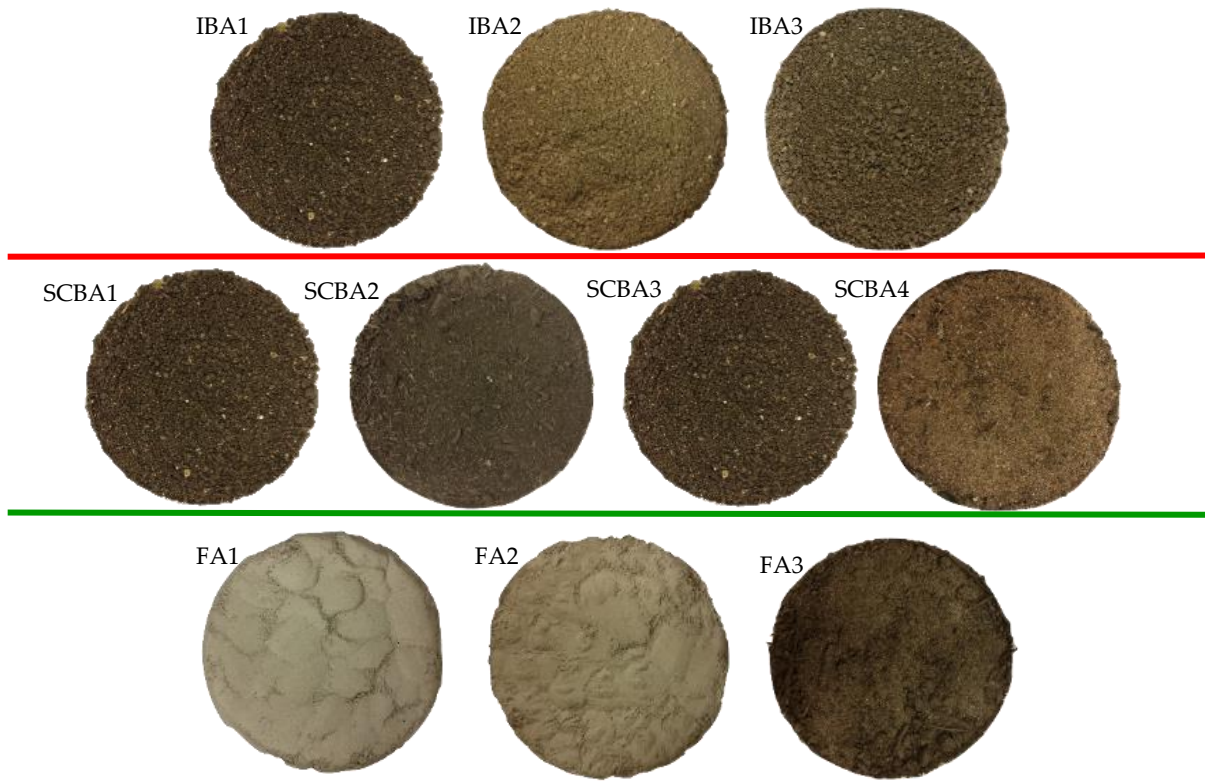


Figure 3-2: Incinerator bottom ashes (top), sugarcane bagasse ashes (middle) and fly ashes (bottom).

Table 3-4: Pre-treatment of ashes.

Material	Drying	Sieving	Grinding
SCBA 1	X	X	X
SCBA 2	X	X	X
SCBA 3	X	X	X
SCBA 4	X	X	X
IBA 1	X	X	X
IBA 2	X	X	X
IBA 3	X	X	X
FA 1	-	X	-
FA 2	-	X	-
FA 3	-	X	X

Grinding was performed to enhance the fineness of the ashes using a TEMA T100 Disc Mill (1000 RpM; max sample 150 g) shown in Figure 3-3. Homogenisation was ensured by subsampling with a Rotary Sample Divider laborette 27 to ensure representativity when small quantities were required for analysis (Figure 3-3).



Figure 3-3: TEMA T100 Disc Mill (left) and Rotary Sample Divider laborette 27 (right).

3.2.2 Particle Size Distribution

The particle size distribution was measured by laser diffraction using a Mastersizer 2000, composed of the Mastersizer 2000 unit; the Hydro 2000G wet dispersion and the Autosampler 2000 units. This method measures the angular distribution and intensity of the light by particles in suspension and utilises the Mie theory of diffraction in the prediction of laser particle size results.

Statistics were applied to understand the particle size distributions. The distribution width is defined to with three values on the x-axis, the D10, D50 and D90. The D50, the median, is defined as the diameter where half of the population lies below this value. Similarly, 90 percent of the distribution lies below D90, and 10 percent of the population lies below the D10.

3.2.3 Specific Surface Area (Brunauer–Emmett–Teller - BET)

The specific surface area of the ashes was determined with a Quantachrome Nova 4200e and the BET method which measures the specific surface area based on the physical adsorption of gas molecules on the ashes.

3.2.4 Chemical Composition by ICP-AES and Loss on Ignition (LOI)

The analysis of major oxides was performed by Inductively Coupled Plasma – Atomic Emission Spectroscopy (ICP-AES) analysis. A sample is added to lithium metaborate/lithium tetraborate flux (0.90 g), mixed well and fused in a furnace at 1000 °C. The resulting melt is then cooled and dissolved in 100 mL of 4% nitric acid/2% hydrochloric acid. This solution is then analysed by ICP-AES and the results are corrected for spectral inter-element interferences. Oxide concentration is calculated from the determined elemental concentration, and the result is reported in that format.

LOI was used to determine the unburnt carbon content by thermal decomposition furnace, where a prepared sample (1.0 g) is placed in an oven at 1000 °C for one hour, cooled and then weighed. The percent loss on ignition is calculated from the difference in weight.

3.2.5 Scanning Electron Microscopy - Energy Dispersive Spectroscopy (SEM - EDS)

The morphology of the ashes and the microstructure of the lime: ash pastes were determined with a scanning electron microscope (SEM), Tescan Mira XMU which revealed the surface topography, morphology and pore system. A backscattered electron (BE) signal detector was also used for observation and image acquisition. The formation of hydrate phases over time in the ash: lime pastes was also studied with the SEM-EDS.

3.2.6 X-Ray Diffraction (XRD)

The mineralogical composition and amorphous character of the pozzolans were analysed by XRD, using a Phillips PW1720 XRD with a PW1050/80 goniometer and a PW3313/20 Cu k-alpha anode tube at 40kV and 20mA. All measurements were taken from 3 to 60 degrees (2θ) at a step size of 0.02 degrees/second. Figure 3-4 shows the ash samples prepared for XRD testing. The diffractograms were also analysed with the software HighScore Plus for mineral phase identification.

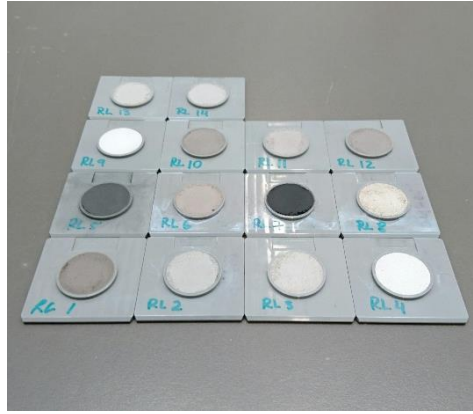


Figure 3-4: Ash samples prepared for XRD analysis.

3.2.7 Chemical Reaction by Conductivity

The reaction between the acid reactive components of the pozzolan (SiO_2 , Al_2O_3) and the calcium hydroxide reduces portlandite concentration in solution leading to a decrease in conductivity (Luxán et al., 1989).

The conductivity variation of a lime-ash suspension over time was measured to assess the ability of the ash to combine lime - $\text{Ca}(\text{OH})_2$ – and thus its reactivity. The study followed similar procedures carried out by Walker (2013) using a saturated solution of lime in distilled water (0.2 g of lime in 100 mL of water) followed by the addition of 1.6 g of pozzolan to the solution. The solutions were kept in sealed flasks to avoid water evaporation and carbonation, as shown in Figure 3-5. A thermostatic bath was used to maintain the flasks at constant temperature (20 °C). The loss in conductivity was then measured at intervals over 168 hours using a WTW Conductivity Meter ProfiLine Cond 197i.



Figure 3-5: Sealed flasks for conductivity analysis.

The conductivity loss (%) was calculated according to Equation 3-1.

$$C(\%) = \frac{C_i - C_t}{C_i} \times 100$$

Equation 3-1: Conductivity loss.

Where:

- C_i is the initial electrical conductivity, given by $\text{Ca}(\text{OH})_2$ suspension before the addition of the ash;
- C_t is the electrical conductivity ash and lime suspension measured through time intervals.

3.2.8 Reactivity by Strength Development or Mechanical Method

The reaction between pozzolanic materials and calcium hydroxide in the presence of moisture forms strength-developing calcium silicate and calcium aluminate hydrates. To assess the strength development prismatic test specimens were prepared and their strength development monitored over time (Figure 3-6). The mechanical method was undertaken according to EN 450-1 (2012). This measures reactivity by monitoring the compressive strength development of a lime: pozzolan mix in relation to a standard lime mix at constant water content over 28 days. The same method was applied to all ashes. The prismatic specimens sized 40 mm x 40 mm x 160 mm were subdivided into two groups of high and low water demand, as described in Table 3-5. The prisms were produced with a ratio by mass (lime: ash: aggregate: water) of 1:1:3:2 and 1:1:3:1.5, respectively. A fixed water content was not possible as the pozzolans have different water demand as explained below.



Figure 3-6: Prismatic test specimens for strength development tests.

Reference test specimens were produced with the ratio 2:3:2 (lime: sand: water). The specimens were demoulded after three days and cured for 28 days in a curing chamber at standard conditions of 20 °C and 60% of relative humidity.

Table 3-5: Mix proportions for lime-ash mortars (lime: ash: aggregate: water).

Proportion	Material
1:1:3:1.5	SCBA 3; SCBA 4; IBA 1; IBA 2; IBA 3; FA 1; FA 3
1:1:3:2	SCBA 1; SCBA 2; FA 2

The water content of lime:pozzolan prisms was determined based on studies of 9 pozzolanic materials of different nature conducted by Walker and Pavia (2011). It is known that the specific surface area plays a significant role on determining the water demand, and considering that, it was established a relationship between the specific surface area (x) and the water demand (y) for the pozzolans, fitting the results into the linear function ($y = 0.0598x + 0.0485$ (R-square = 0.907)). The result is illustrated on Figure 3-7.

The assessment of the compressive and flexural strengths were carried out in agreement with EN 459-2 (2010a) and EN 196-1 (2016a), using a Zwick loading machine (Figure 3-8).

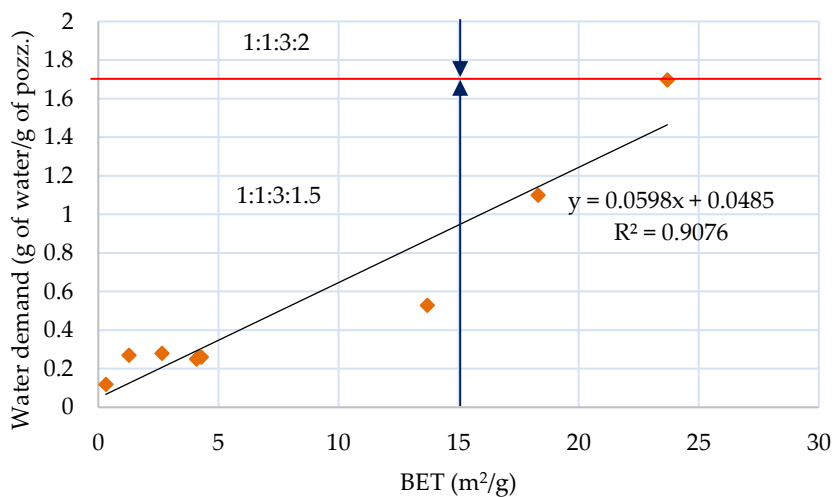


Figure 3-7: Water demand with respect to specific surface area.

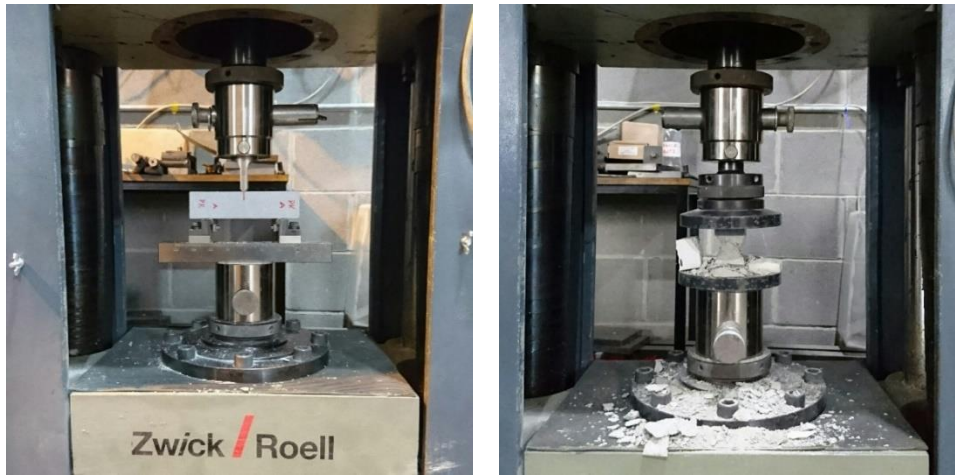


Figure 3-8: Strength development test. 3-point bending (left) and compression (right).

3.3 METHODS PHASE 2: PROPERTIES OF ASH-COMPOSITES

3.3.1 Mix Composition

Composites were prepared using ash as partial PC replacement or as partial aggregate replacement. Prisms, discs and blocks were casted as required by nature of the tests and the standards. The reference specimen consisted of 450 ± 2 g PC, $1,350 \pm 5$ g of sand and water/cement ratio of 0.5. The cement was substituted at levels of 5, 10 and 20%. The ashes tested as sand replacement followed the same percentage of replacement (5, 10 and 20%).

The composition of the mixes with PC replacement is set out in Table 3-6. The composition of the mixes with sugarcane bagasse ash sand appears in Table 3-7. The specimens were subjected to a series of tests as described in the following Sections.

Table 3-6: Composition of mixes for ashes tested as pozzolans (Sand mass was constant, representing 75% of solid weight).

Notation	% Cement	% Ash	Water/binder ratio
Ref.	25.00	0.00	0.50
SCBA 1 5%	23.75	1.25	0.54
SCBA 1 10%	22.50	2.50	0.54
SCBA 1 20%	20.00	5.00	0.54
SCBA 2 5%	23.75	1.25	0.54
SCBA 2 10%	22.50	2.50	0.54
SCBA 2 20%	20.00	5.00	0.54
IBA 1 5%	23.75	1.25	0.52
IBA 1 10%	22.50	2.50	0.52
IBA 1 20%	20.00	5.00	0.52
IBA 2 5%	23.75	1.25	0.52
IBA 2 10%	22.50	2.50	0.52

IBA 2 20%	20.00	5.00	0.52
FA 1 5%	23.75	1.25	0.54
FA 1 10%	22.50	2.50	0.54
FA 1 20%	20.00	5.00	0.54
FA 2 5%	23.75	1.25	0.54
FA 2 10%	22.50	2.50	0.54
FA 2 20%	20.00	5.00	0.54
FA 3 5%	23.75	1.25	0.52
FA 3 10%	22.50	2.50	0.52
FA 3 20%	20.00	5.00	0.52

Table 3-7: Composition of mixes for ashes testes as sand replacement (Portland cement mass was constant, representing 25% of solid weight).

Notation	% Sand	% Ash sand	Water/binder ratio
Ref.	75.00	0.00	0.50
SBAS 1 5%	71.25	3.75	0.52
SBAS 1 10%	67.50	7.50	0.52
SBAS 1 20%	60.00	15.00	0.52
SBAS 2 5%	71.25	3.75	0.52
SBAS 2 10%	67.50	7.50	0.52
SBAS 2 20%	60.00	15.00	0.52

3.3.2 Capillary Action

The capillary action tests were performed according to EN 1015-18 (2002) and EN 1925:1999 (1999). The specimens were dried to constant mass in a ventilated oven at a temperature of 65 °C. After reaching constant mass the bases of the samples were immersed in water to a depth of 3 ± 1 mm for the duration of the test, supported by a grill (Figure 3-9). A timing device was started in the moment of immersion. At time intervals of 1, 3, 5, 10, 15, 30, 60, 90, 180, 360 and 1440 minutes, each specimen was removed and weighed.

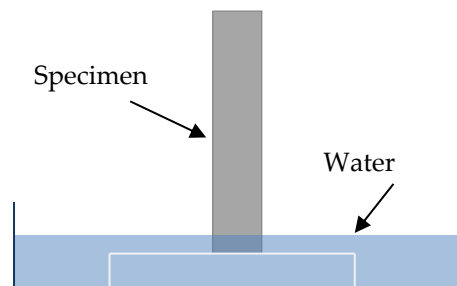


Figure 3-9: Schematic drawing of the process used to determine the capillary action.

The coefficient of water absorption due to capillary action was calculated according to BS EN 1925:1999 (1999) using Equation 3-2.

$$C = \frac{m_i - m_d}{A \times t_i}$$

Equation 3-2: Coefficient of water absorption due to capillary action.

Where:

- m_i is the mass of specimen after drying (g);
- m_d is the mass of the specimen in grams after soaking for time t (g);
- A is the gross area of the face of the specimen immersed in water (m²);
- t is the time of soaking (min);
- C is the coefficient of water absorption due to capillary action.

3.3.3 Porosity Accessible to Water, Bulk and Real densities

Porosity, bulk density and real density were assessed according to RILEM (1980). Tests I.1 and I.2. Porosity is a fundamental property which can have an influence on mortar durability. The porosity accessible to water was assessed. It reflects the ratio of the volume of the pores accessible to water to the bulk volume of the sample, expressed in per cent, calculated by means of Equation 3-3.

Bulk density (δ) (or apparent density) is the ratio of the mass to the bulk volume of the sample. It is expressed in kg/m³. Bulk density was calculated following Equation 3-4.

Real density (δ_r) (volume mass of the impermeable material) is the ratio of the mass to the impermeable volume of the sample, also expressed in kg/m³. Given by Equation 3-5.

$$P = \frac{M_3 - M_1}{M_3 - M_2} \times 100$$

Equation 3-3: Porosity accessible to water.

$$\delta = \frac{M_1}{M_3 - M_2} \times 10^3$$

Equation 3-4: Bulk density.

$$\delta_r = \frac{M_1}{M_1 - M_2} \times 10^3$$

Equation 3-5: Real density.

Where:

- M_1 is the mass of dried samples (g);
- M_2 is the mass of the specimen saturated with water under vacuum, weighed in water (g);
- M_3 is the mass of the sample saturated with water under vacuum, weighed in the air (g).

3.3.4 Thermal Conductivity

Thermal conductivity measures the ability of a material to transfer heat, which is influenced by its composition, porous structure, temperature of surroundings and direction of heat flow. The conductivity of the studied mortars was determined by a steady-state heat flow test, where the heat output is maintained constant throughout testing time.

A guarded hot plate (GHP) was used as heating source, in direct contact with the samples surface. The thermal conductivity of the samples was then determined by measuring the difference in temperature at different distances within the specimens. Thermocouples were positioned at known equivalent distances to record the variations in temperature. The conductivity was then calculated using Fourier's law of heat conduction (Equation 3-6).

$$k = \frac{Q \times L}{A \times \Delta t}$$

Equation 3-6: Fourier's law of heat conduction.

Where:

- Q is the heat flowing through the sample (W);
- L is the distance between thermocouples (m);
- A is the cross-Sectional area (m²);
- Δt is the temperature difference between thermocouples (°C).

For this test polystyrene moulds were produced. The internal dimensions of the moulds are 100 x 100 x 100 mm. K type thermocouples were positioned in the mould, fixed with fishing line, prior to mortar filling (Figure 3-10). This step lessens inaccuracies related to the positioning of thermocouples in hardened specimens. Three internal thermocouples were placed equidistantly, and two additional thermocouples were placed on the heating and exposed faces, fixed with tape. After curing, the base of the mould was removed, and the walls of the mould (25 mm thick) served as insulation box, to reduce heat losses to negligible levels.

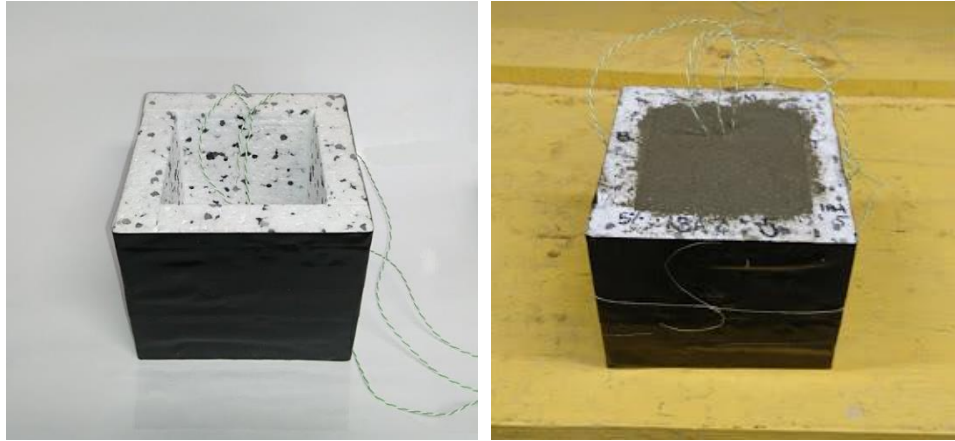


Figure 3-10: Polystyrene moulds produced for thermal conductivity tests.

A heating pad of 300 x 300 mm was used as a heat source. The heat pad is controlled by an ISO-tech power supply. The controller allows variation of the voltage across the circuit, which permits the control of the power supplied to the heating pad. A data logger was used to record the temperature at each thermocouple at one second interval, saved automatically to the computer. The rig design and the test set-up can be observed in Figure 3-11 and Figure 3-12 respectively.

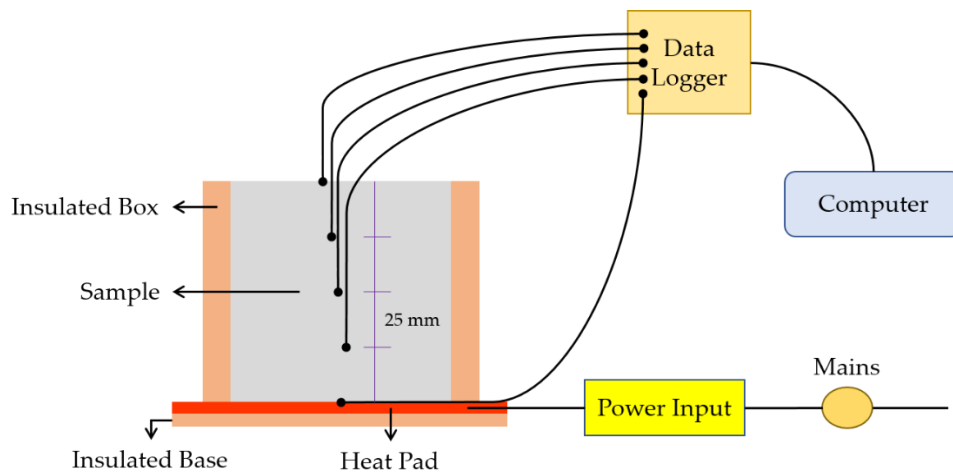


Figure 3-11: Design of test rig.



Figure 3-12: Thermal conductivity test set-up.

Thermal mass indicates the ability of the construction material to provide inertia against temperature changes. It is more adequate in climates where diurnal temperatures are high, as an efficient thermal mass material can absorb and store significant amounts of heat, thus balancing external temperature variations. The thermal mass of the ash materials, which is the product of the specific heat, density and thickness of the solid material were determined.

3.3.5 Specific Heat Capacity

The specific heat capacity of the materials was measured by means of the calorimetric method. This method measures the amount of heat energy transferred by a material for a given temperature change, specific heat and mass. Four representative samples, taken from the end of the prisms broken in compression, from each prism were used in this test (Figure 3-13). The samples were heated in boiling water and allowed reaching an equilibrium temperature. This allows the use of the temperature of the boiling water to represent the temperature of the material. The samples were then transferred directly to the insulated container filled with water of known mass and temperature. The rise in temperature of the water inside the container was measured until it reached the equilibrium point. The temperature rise was used to calculate the heat transferred, according to Equation 3-7.



Figure 3-13: Representative samples used for testing specific heat for IBA 1 and IBA 2.

$$Q = m \times c \times \Delta T$$

Equation 3-7: Energy heat.

Where:

- Q is the heat energy transferred (J);
- m mass of the liquid being heated (g);
- c is the specific heat capacity of the liquid (J/g°C);
- ΔT is the change in temperature of the liquid (°C).

Conferring to the law of conservation of energy the energy heat gained by the liquid is equal to the energy lost from the samples, thus, making possible the calculation of the specific heat capacity of the samples using Equation 3-8.

$$c_m = \frac{Q}{\Delta T_s \times m_s}$$

Equation 3-8: Specific heat capacity of tested samples.

Where:

- c_m is the specific heat capacity of the sample (J/g.C);
- ΔT_s is the change in temperature of the sample (°C);
- m_s mass of the material being cooled (g).

3.3.6 Flexural Strength

Series of nine prismatic mortar specimens of 40 x 40 x 160 mm were prepared with each pozzolanic ash, according to EN 196-1 (2005). The three-point bending method was used to determine the flexural strength of prisms, using a Zwick loading machine (Figure 3-8). The method was carried out in agreement with EN 196-1 (2016a). The prisms were placed in the apparatus with one side face on the supporting rollers and with its longitudinal axis normal to the supports. The load was applied vertically by means of the loading roller to the opposite side face of the prism and increased smoothly at the rate of 50 ± 10 N/s until fracture.

The flexural strength was calculated in megapascals from Equation 3-9.

$$R_f = \frac{1.5 \times F_f \times l}{b^3}$$

Equation 3-9: Flexural strength.

Where:

- R_f is the flexural strength (MPa);
- b is the side of the square Section of the prism (mm);
- F_f is the load applied to the middle of the prism at fracture (N);
- l is the distance between the supports (mm)

The result is the arithmetic mean of three individual results, each expressed at least to the nearest 0.1 MPa, obtained from a determination made on a set of three prisms.

3.3.7 Compressive Strength

The compressive strength testes were carried out on halves of the prisms broken in Section 3.3.6, using a Zwick loading machine (Figure 3-8).

The compression load increased smoothly at the rate of 2400 ± 200 N/s over the entire load application until fracture.

The compressive strength is calculated in megapascals from Equation 3-10.

$$R_c = \frac{F_c}{1600}$$

Equation 3-10: Compressive strength.

Where:

- R_c is the compressive strength (MPa);
 F_c is the maximum load at fracture (N);
1600 is the area of the platens or auxiliary plates (40 x 40 mm), (mm²).

The results are expressed as the arithmetic mean of the six individual results, each expressed at least to the nearest 0,1 MPa, obtained from the six determinations made on a set of three prisms. As expressed by the standard, if one result within the six individual results varies by more than $\pm 10\%$ from their mean, this result is to be discarded and calculated the arithmetic mean of the five remaining results.

3.3.8 Resistance to Salt Crystallisation

The salt exposure weathering test was undertaken according to BS 812-121 (1989).

The samples were immersed in a container holding the saturated solution of magnesium sulphate for a period of 17 h \pm 30 min (Figure 3-14). At the end of immersion period, the samples were removed and allowed draining for a period of 2 h \pm 15 min (Figure 3-15). The samples were then taken into an oven maintained at a temperature of 105 °C for 24 h (Figure 3-16). After the drying in oven period the samples were removed from the oven and allowed cooling to laboratory temperature for 5 h \pm 15 min. This completed 1 test cycle. Five cycles were completed for each specimen, each cycle taking 48 \pm 2h.

After the last cycle of the test the specimens were washed with water until the surfaces were free of magnesium sulphate. Followed by drying in oven, at 105 °C, to constant mass.

The results are reported in terms of loss of weight expressed as a percentage of initial dry weight. Photographic record of the final condition of specimens is available.

The compressive and flexural strengths of specimens subjected to salt exposure were assessed compared to reference test specimens tested for salt weathering.



Figure 3-14: Samples immersed in saturated MgSO₄ solution.



Figure 3-15: Specimens allowed to drain after immersion period.



Figure 3-16: Samples maintained in oven for 24h after draining.

3.3.9 Resistance to Freeze-Thawing

Resistance to freeze-thawing was tested according to BS EN 15304 (2010b) with adaptations in respect to specimen size and number of specimens. In order to attain adequate strength development, the specimens were cured in water for 28 days before exposed to the freeze-thaw cycles. After curing time, the specimens were dried in oven at 65 °C to constant weight. Prior to start the freeze-thawing cycles the specimens were immersed in water for 48 hours, followed by 24 hours of storage in polythene bags to allow water to equilibrate within the specimens and avoid moisture loss (Figure 3-17).

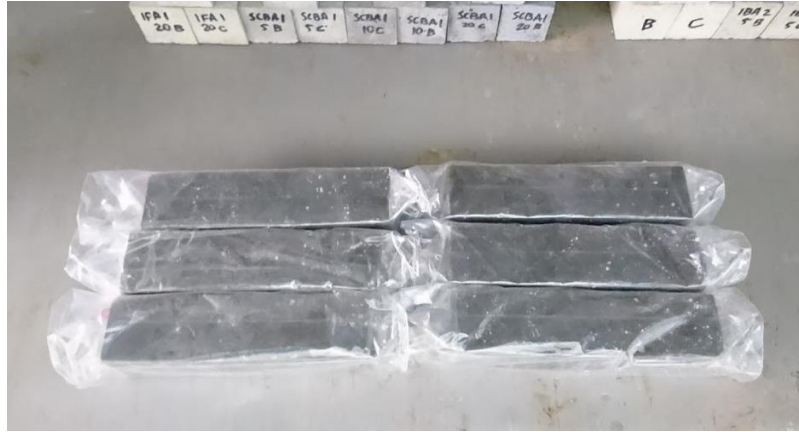


Figure 3-17: Specimens in polythene bags.

The samples were subjected to 15 freeze-thaw cycles, with freezing temperature of $-15\text{ }^{\circ}\text{C}$ and thawing at $20\text{ }^{\circ}\text{C}$ in a moisture chamber with $\text{RH} > 95\%$. The moisture content of the test specimens at the end of the freeze-thaw test were calculated in percent according to Equation 3-11.

$$\mu_{i,n}^m = 100 \times \frac{m_{i,n}^m}{m_{id,n}^m - 1}$$

Equation 3-11: Moisture content of specimen subjected to freeze-thaw.

Where:

- $\mu_{i,n}^m$ is the moisture content of the main test specimen (or tested specimen) at the end of the freeze-thaw test (%);
- $m_{i,n}^m$ is the measured moist mass of the main test specimen i immediately after completion of n freeze-thaw cycles (g);
- $m_{id,n}^m$ is the measured oven-dry mass of the main test specimen i immediately after completion of n freeze-thaw cycles (g).

The mass loss was calculated based on the loss in the oven-dry mass of the main test specimens. The equivalent oven-dry mass $m_{id,0}^m$ of the main test specimen i immediately after the removal from the polythene bag was calculated according to Equation 3-12.

$$m_{id,0}^m = m_{i,0}^m \times \frac{m_{id,n}^r}{m_{i,0}^r}$$

Equation 3-12: Equivalent oven-dry mass of test specimen.

Where:

- $m_{i,0}^m$ is the measured initial moist mass of the main test specimen (or tested specimen) i immediately after removal from polythene bag prior to commencing the freeze-thaw cycles (g);
- $m_{id,n}^r$ is the measured oven-dry mass of the reference test specimen (no cement replacement) i after completion of n freeze-thaw cycles (g);
- $m_{i,0}^r$ is the measured moist mass of the reference test specimen i immediately after removal from polythene bag (g).

The loss in oven-dry mass m_{iL} of the main test specimen i after number n of freeze-thaw cycles is calculated in percent according to Equation 3-13.

$$m_{iL} = 100 \times \left(1 - \frac{m_{id,n}^m}{m_{id,0}^m} \right)$$

Equation 3-13: Loss in oven-dry mass.

Where:

- $m_{id,0}^m$ is the equivalent dry mass of the considered main test specimen i immediately after removal from the polythene bag prior to commencing the freeze-thaw cycles (g), according to Equation 3-12;
- $m_{id,n}^m$ is the measured oven-dry mass of the considered main test specimen i after number n of freeze-thaw cycles (g);

3.3.10 Water Vapour Permeability

The tests were conducted in accordance with standards BS EN 12086 (2013) and BS EN ISO 12572 (2013), following a method based on cup tests for determining the water vapour permeability of building materials under isothermal conditions.

Three specimens were prepared for each mix. The specimens were sealed to the open side of test cups containing an aqueous salt solution (saturated salt solution in contact with a large content of undissolved salt) of Potassium Nitrate (KNO_3) – wet cup. The assemblies were then placed in a temperature and humidity-controlled test chamber (Figure 3-18). Because of the different partial vapour pressure between the test cups and the chamber, a vapour flow occurs through permeable specimens. Periodic weighing of the assemblies were made to determine the rate of water vapour transfer in the steady state.



Figure 3-18: Water vapour assemblies in controlled chamber.

3.3.10.1 Change in mass of test assembly

The change in mass for the selected time interval, $G_{1,2}$, in kilograms per second was calculated using the Equation 3-14 for each test specimen. G was then obtained as the mean of five successive determinations of $G_{1,2}$.

$$G_{1,2} = \frac{m_2 - m_1}{t_2 - t_1}$$

Equation 3-14: Change in mass of test assembly.

Where:

- $G_{1,2}$ is the change in mass per time for a single determination, in kg/s;
- m_1 is the mass of the test assembly at time t_1 , in kg;
- m_2 is the mass of the test assembly at time t_2 , in kg;
- t_1 and t_2 are the successive times of weighing, in s.

3.3.10.2 Density of water vapour flow rate

The water vapour transmission rate, also described as density of water vapour flow rate, g , in kilograms per square metre per seconds ($\text{kg}/(\text{s m}^2)$) was given by Equation 3-15.

$$g = \frac{G}{A}$$

Equation 3-15: Density of water vapour flow rate.

Where:

A is the exposed area (arithmetic mean of the free upper and free lower surface areas) of the test specimen, in m².

g – mass of water vapour transferred through the specimen per area and per time under specified conditions of temperature, humidity and thickness.

3.3.10.3 Water vapour permeance

The water vapour permeance, W , in kilograms per square metre per seconds per pascals (kg/(s.m².Pa)) was determined by Equation 3-16.

$$W = \frac{G}{A \times \Delta p_v}$$

Equation 3-16: Water vapour permeance.

Where:

Δp_v is the water vapour pressure difference in pascal and has a standard value, depending on the set of test condition¹ (=1210 Pa).

In other words, W is calculated as the density of the water vapour flow rate of the test specimen divided by the water vapour pressure difference between the two specimen faces during test.

3.3.10.4 Water vapour resistance

The water vapour resistance, Z , is the reciprocal of the water vapour permeance (Equation 3-17).

$$Z = \frac{1}{W}$$

Equation 3-17: Water vapour resistance.

¹ The conditions for the test fit into condition C (23-50/95) of the standard (BS EN 12086 (2013), Section 7.1, Table 1).

3.3.10.5 Water vapour permeability

The water vapour permeability, δ_{wv} , is the product of the water vapour permeance and the thickness of a homogeneous test specimen, in kilograms per metre per second per pascals, is given by Equation 3-18.

$$\delta_{wv} = W \times d$$

Equation 3-18: Water vapour permeability.

Where:

d is the test specimen thickness, in metres.

3.3.10.6 Water vapour diffusion resistance factor

The water vapour diffusion resistance factor, μ , was determined using Equation 3-19.

$$\mu = \frac{\delta_{air}}{\delta_{wv}}$$

Equation 3-19: Water vapour diffusion resistance factor.

Where:

δ_{air} is the water vapour permeability of air (depending on the mean barometric pressure during the test).

μ is calculated as the quotient of the water vapour permeability of air and the water vapour permeability of the material or the homogeneous product concerned; it indicates the relative magnitude of the water vapour resistance of the product and that of an equally thick layer of stationary air at the same temperature, i.e. the thickness of a motionless air layer which has the same water vapour resistance as the specimen.

3.3.11 Statistical analysis of the results

Statistical analysis were carried out using Minitab for the ash mortars in Chapter 6. The properties were evaluated with repetition tests (3 or more). The bar charts show lines that indicate +/- the standard deviation of the results. Analysis of variance (ANOVA) was undertaken on the results to determine significance, at a confidence level of 95% ($\alpha = 0.05$). Equal variances were assumed for all the analysis. The null hypothesis considered that all

means are equal, thus the alternative hypothesis considered that at least one mean is different. The different ash substitutions (groups) were compared against the control reference specimens using the Dunnett's Multiple Comparison. However, the results need to be used with caution as the number of samples within each group (less than 15) was not enough to determine normality.

4 RESULTS – COMPOSITION AND PROPERTIES OF THE ASHES

For the first stage 13 ashes were investigated in order to determine their pozzolanic activity and suitability as a building material. The ashes were divided into 3 categories, as shown in Table 4-1.

Table 4-1: Ashes investigated on first stage of research.

Sugarcane Bagasse Ashes	SCBA 1; SCBA 2; SCBA 3; and SCBA 4.
Incinerator Bottom Ashes	IBA 1 – fine; IBA 2 – fine; IBA 3 – fine; IBA 1 – coarse; IBA 2 – coarse; and IBA 3 coarse.
Incinerator Fly Ashes	FA 1; FA 2; and FA 3.

An overview of the studied properties for each individual ash is presented in the following pages. The tables include results for particle size distribution, chemical composition, SEM images, specific surface area, activity index (mechanical and chemical methods), mineralogy by XRD and additional information related to the ash origin.

The following Sections discuss these properties.

Table 4-2: Properties of sugarcane bagasse ash 1.

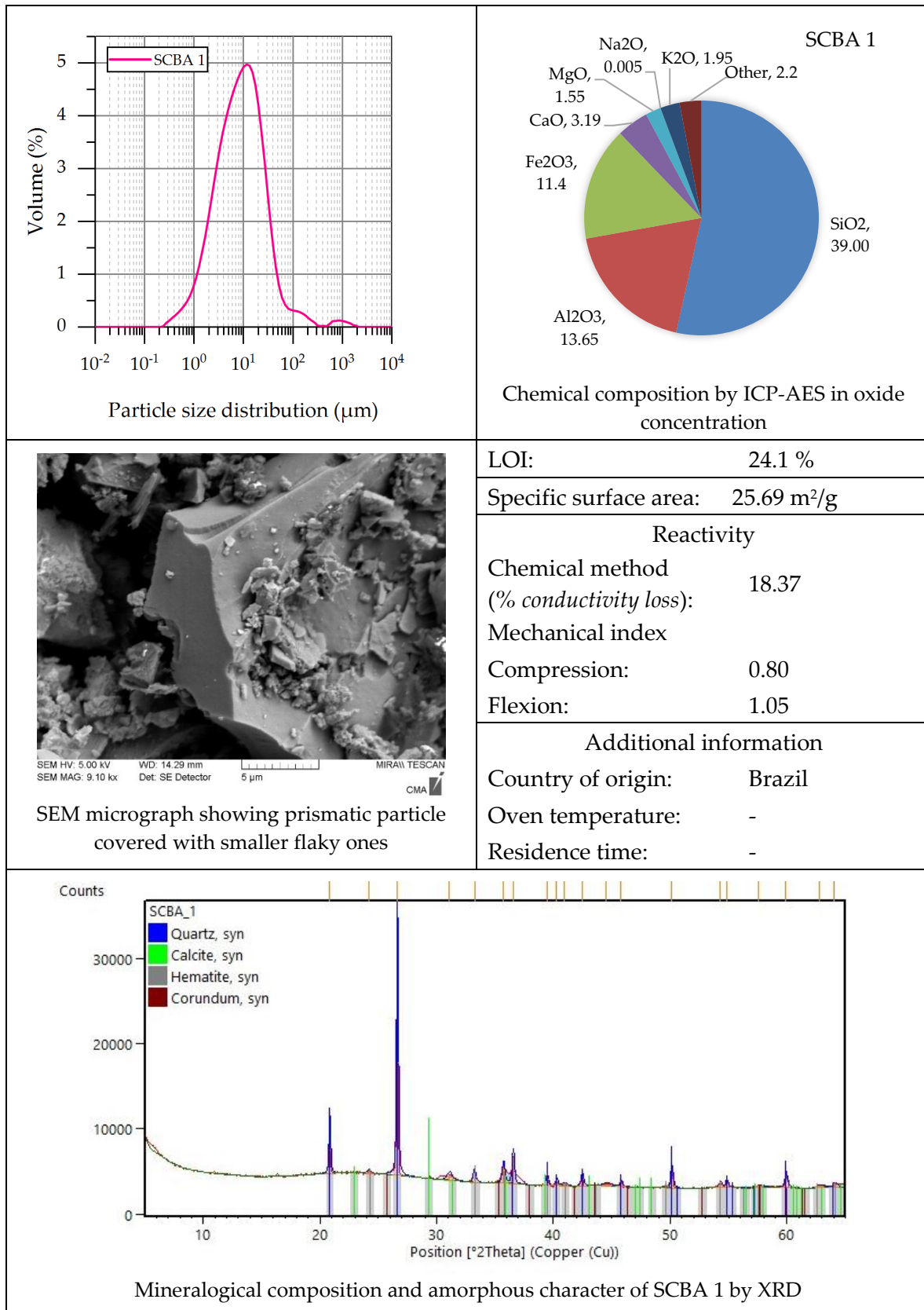


Table 4-3: Properties of sugarcane bagasse ash 2.

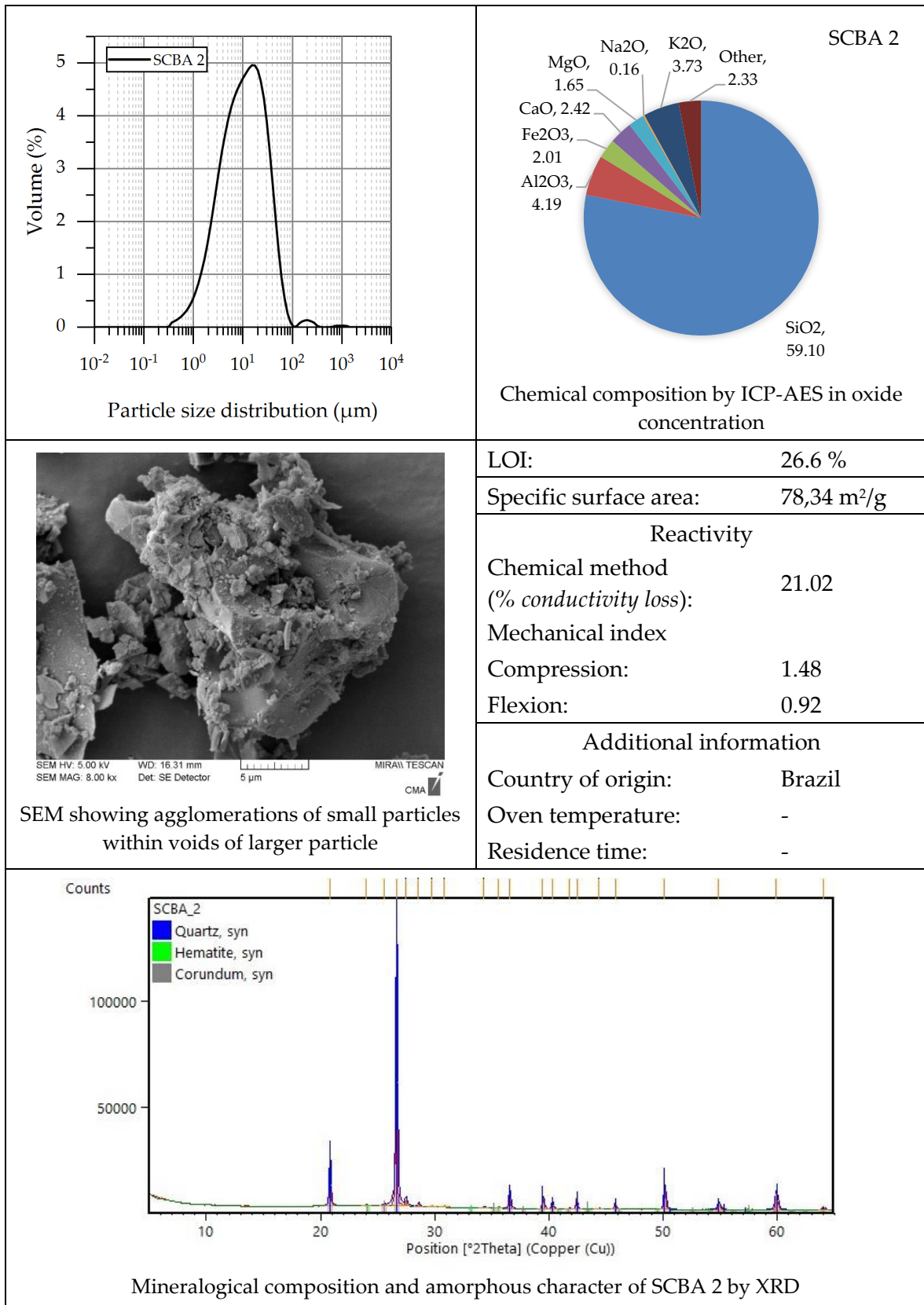


Table 4-4: Properties of sugarcane bagasse ash 3.

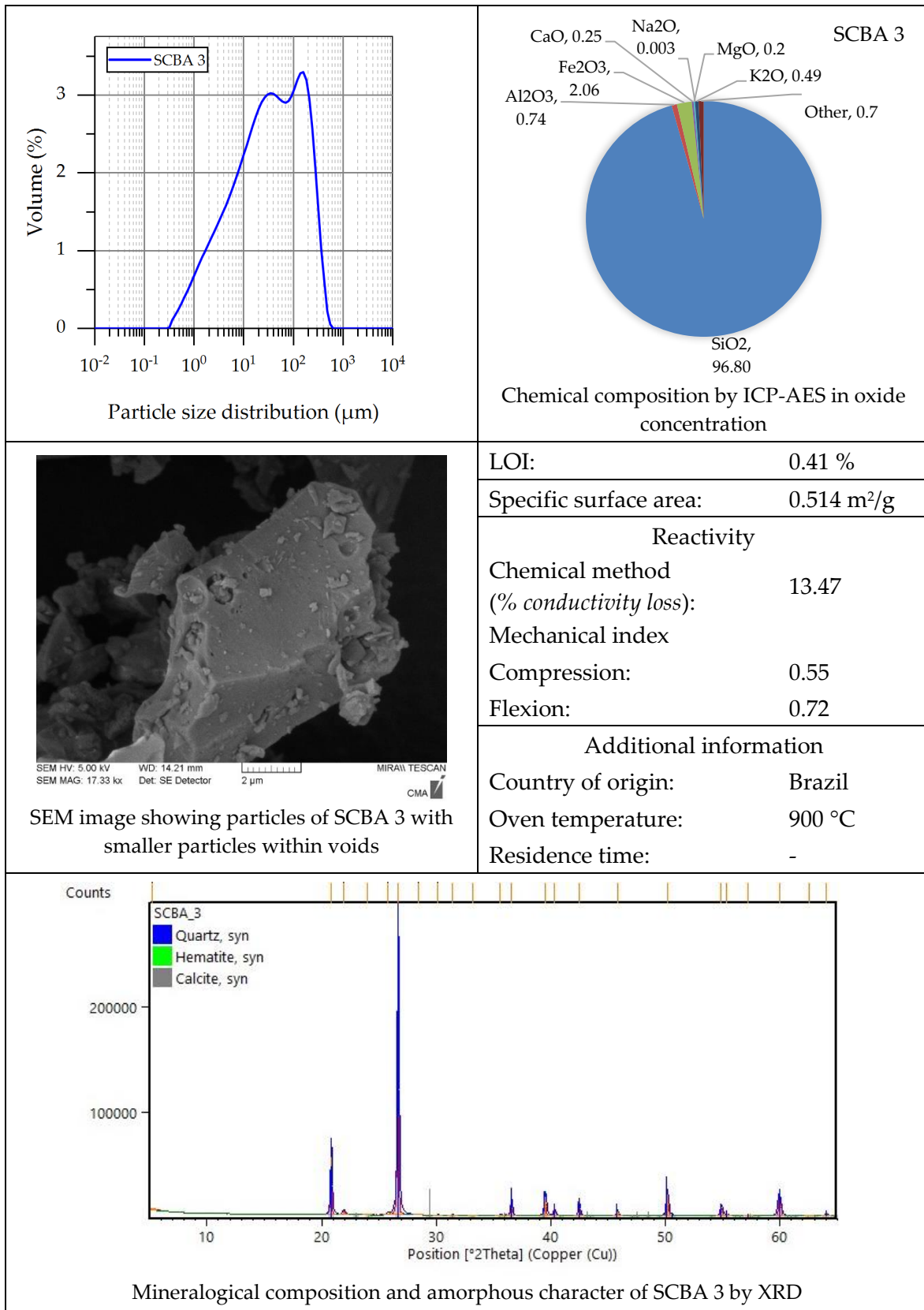


Table 4-5: Properties of sugarcane bagasse ash 4.

<p>Volume (%)</p> <p>Particle size distribution (µm)</p>	<p>SCBA 4</p> <p>Chemical composition by ICP-AES in oxide concentration</p>																						
<p>SEM showing particles with sharp and round edges with smaller particles attached</p>	<table border="1"> <tr> <td>LOI:</td> <td>0.31 %</td> </tr> <tr> <td>Specific surface area:</td> <td>2.19 m²/g</td> </tr> <tr> <td colspan="2" style="text-align: center;">Reactivity</td> </tr> <tr> <td>Chemical method (% conductivity loss):</td> <td>17.65</td> </tr> <tr> <td>Mechanical index</td> <td></td> </tr> <tr> <td>Compression:</td> <td>0.67</td> </tr> <tr> <td>Flexion:</td> <td>1.18</td> </tr> <tr> <td colspan="2" style="text-align: center;">Additional information</td> </tr> <tr> <td>Country of origin:</td> <td>Brazil</td> </tr> <tr> <td>Oven temperature:</td> <td>-</td> </tr> <tr> <td>Residence time:</td> <td>-</td> </tr> </table>	LOI:	0.31 %	Specific surface area:	2.19 m ² /g	Reactivity		Chemical method (% conductivity loss):	17.65	Mechanical index		Compression:	0.67	Flexion:	1.18	Additional information		Country of origin:	Brazil	Oven temperature:	-	Residence time:	-
LOI:	0.31 %																						
Specific surface area:	2.19 m ² /g																						
Reactivity																							
Chemical method (% conductivity loss):	17.65																						
Mechanical index																							
Compression:	0.67																						
Flexion:	1.18																						
Additional information																							
Country of origin:	Brazil																						
Oven temperature:	-																						
Residence time:	-																						
<p>Mineralogical composition and amorphous character of SCBA 4 by XRD</p>																							

Table 4-6: Properties of incinerator bottom ash 1-fine

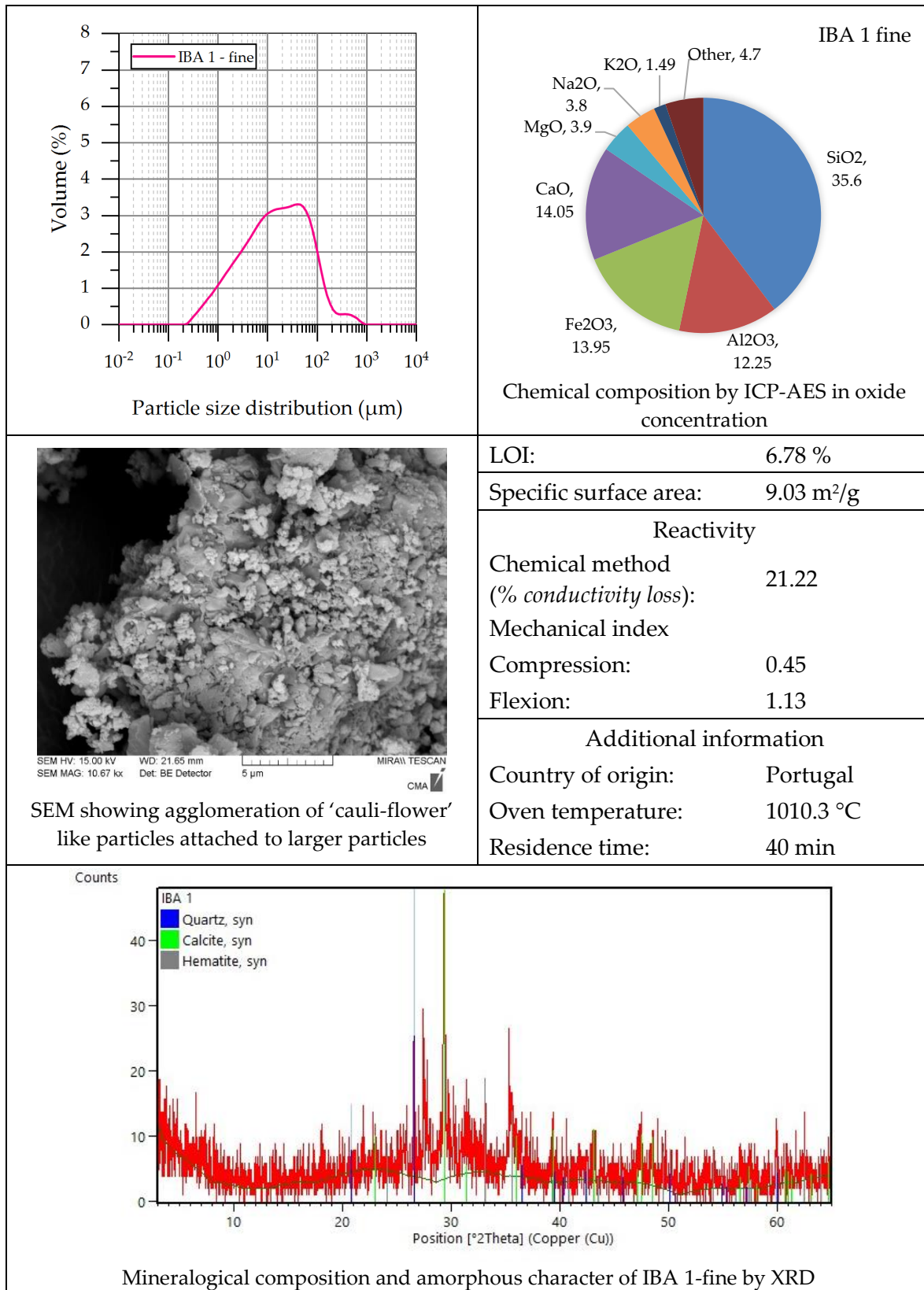


Table 4-7: Properties of incinerator bottom ash 1-coarse.

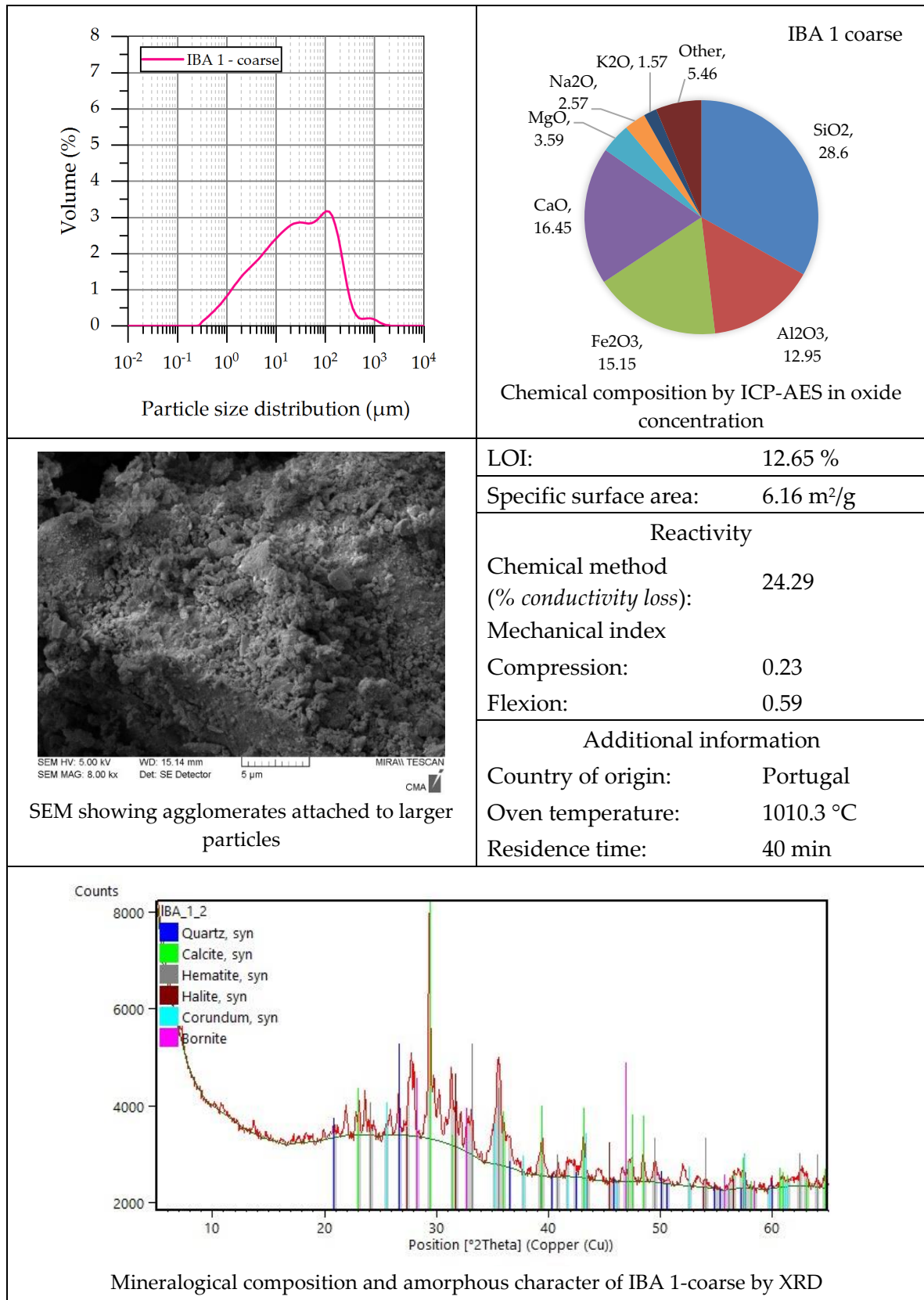


Table 4-8: Properties of incinerator bottom ash 2-fine.

<p>Volume (%)</p> <p>Particle size distribution (µm)</p>	<p>IBA 2 fine</p> <p>SiO₂, 31.9</p> <p>CaO, 19.1</p> <p>Al₂O₃, 15.75</p> <p>Fe₂O₃, 11</p> <p>MgO, 2.51</p> <p>Na₂O, K₂O, 0.98</p> <p>Other, 4.33</p> <p>Chemical composition by ICP-AES in oxide concentration</p>
<p>SEM image of agglomerates of irregular and prismatic shapes</p>	<p>LOI: 9.68 %</p> <p>Specific surface area: 9.67 m²/g</p> <p>Reactivity</p> <p>Chemical method (% conductivity loss): 27.55</p> <p>Mechanical index</p> <p>Compression: 0.68</p> <p>Flexion: 0.69</p> <p>Additional information</p> <p>Country of origin: Ireland</p> <p>Oven temperature: 1100 °C</p> <p>Residence time: -</p>
<p>Mineralogical composition and amorphous character of IBA 2-fine by XRD</p>	

Table 4-9: Properties of incinerator bottom ash 2-coarse.

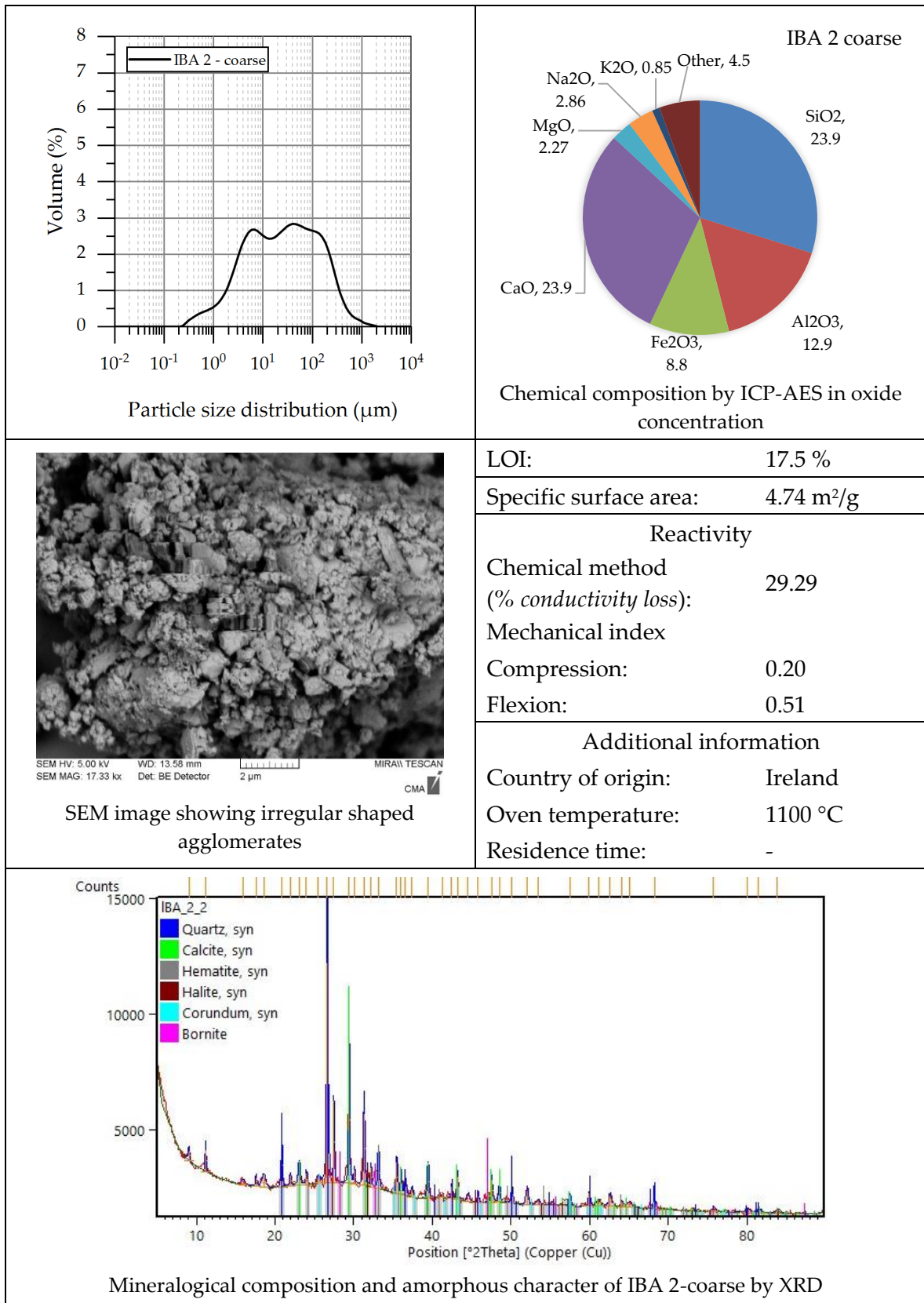


Table 4-10: Properties of incinerator bottom ash 3-fine.

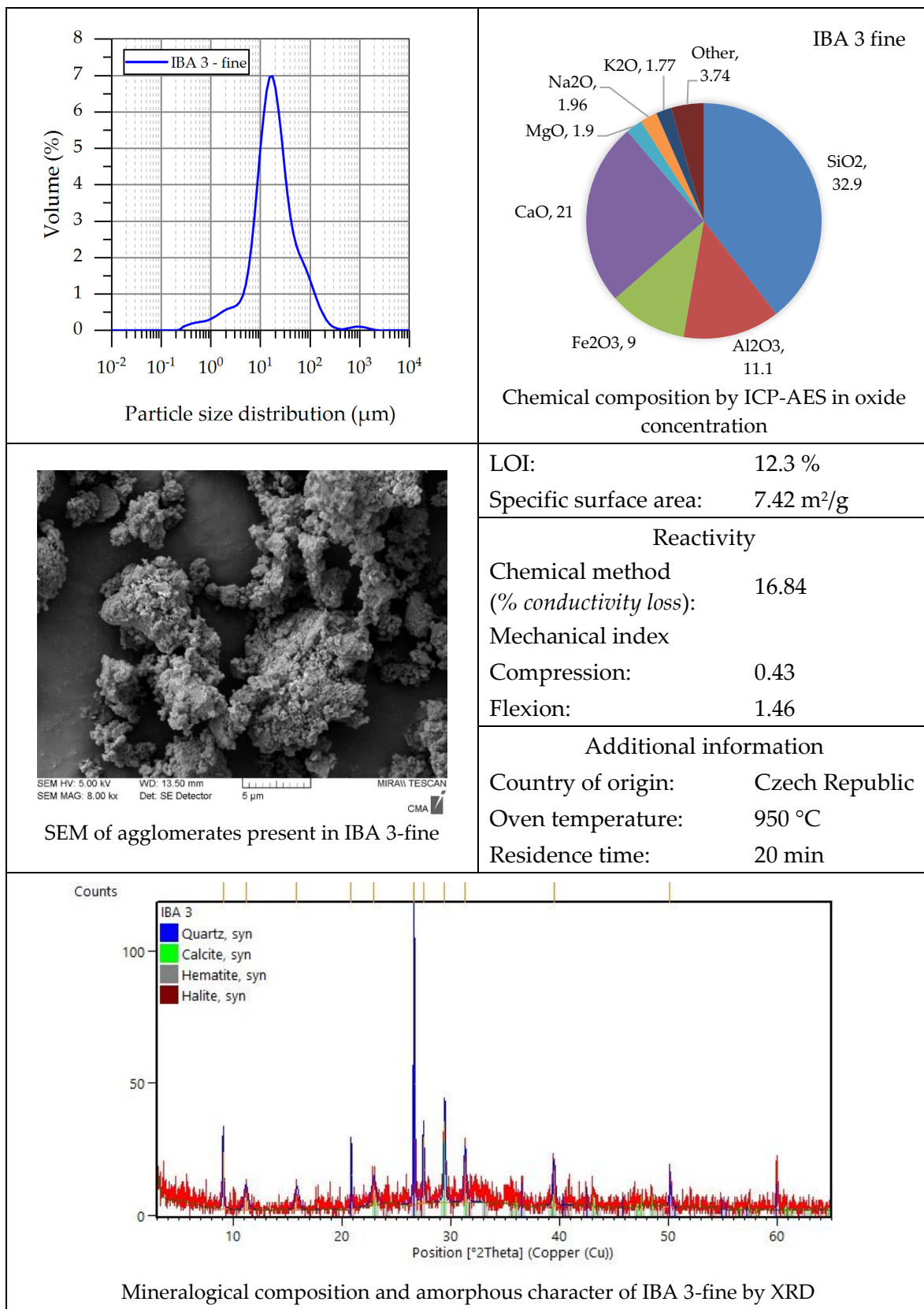


Table 4-11: Properties of incinerator bottom ash 3-coarse.

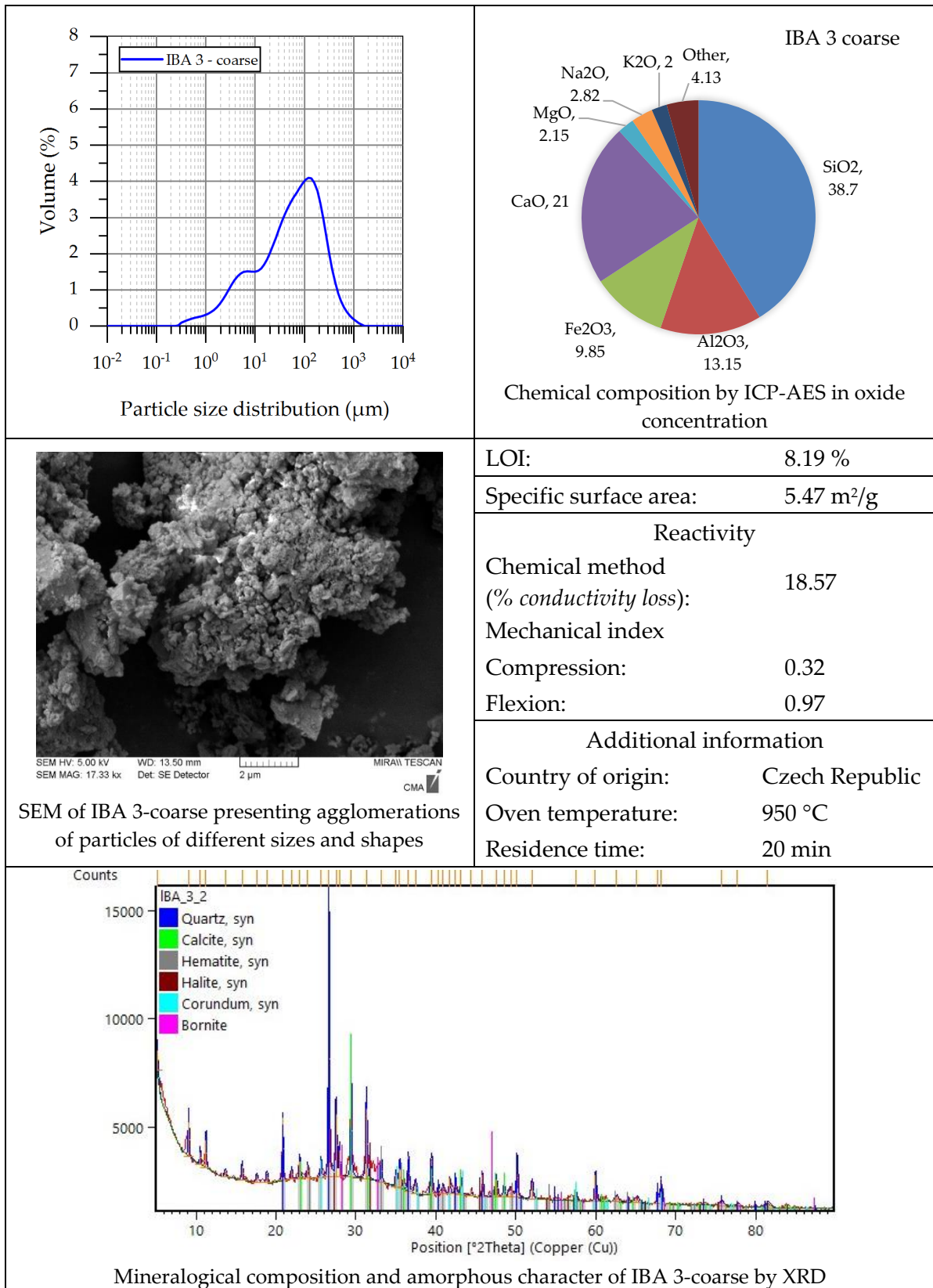


Table 4-12: Properties of fly ash 1.

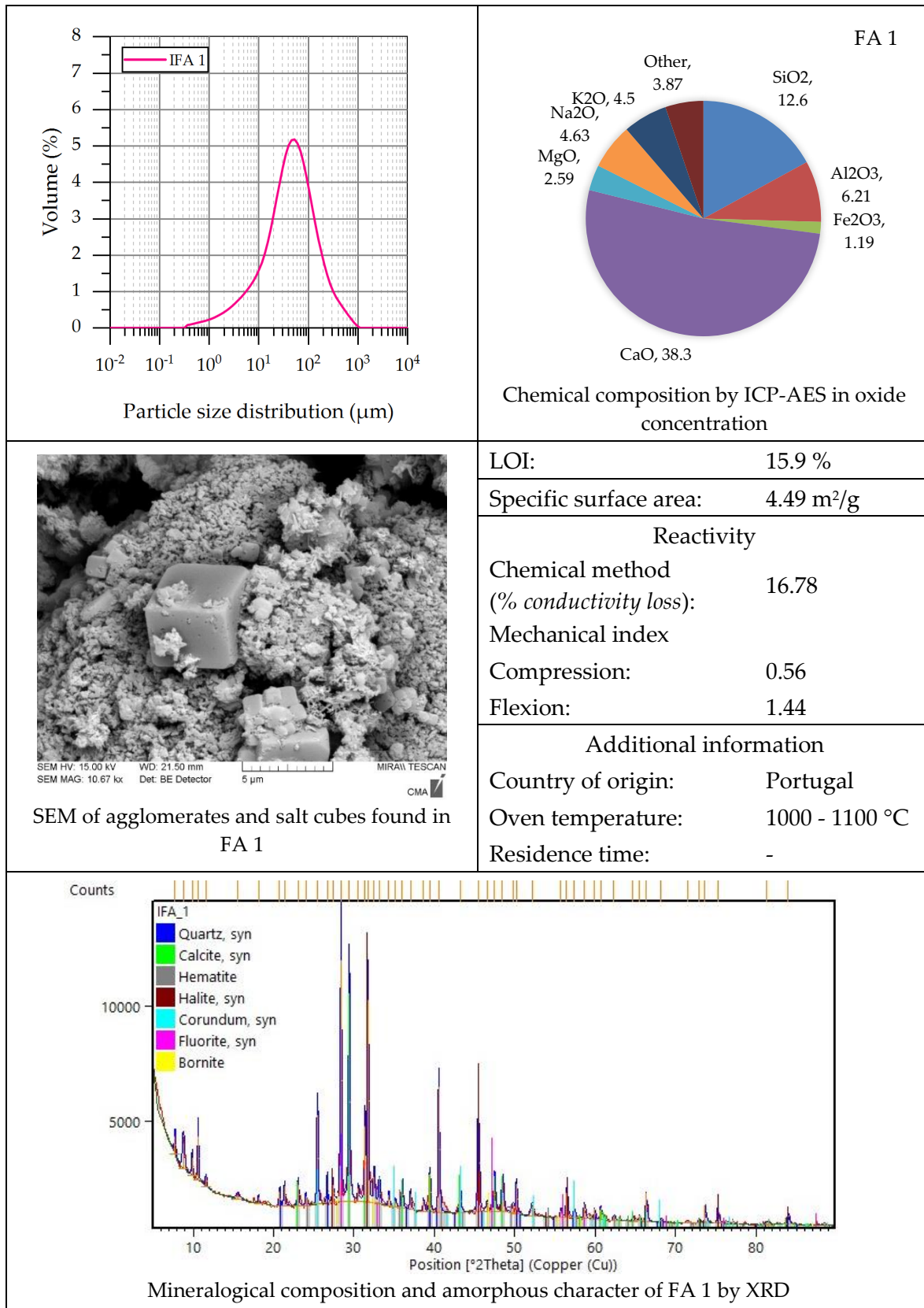


Table 4-13: Properties of fly ash 2.

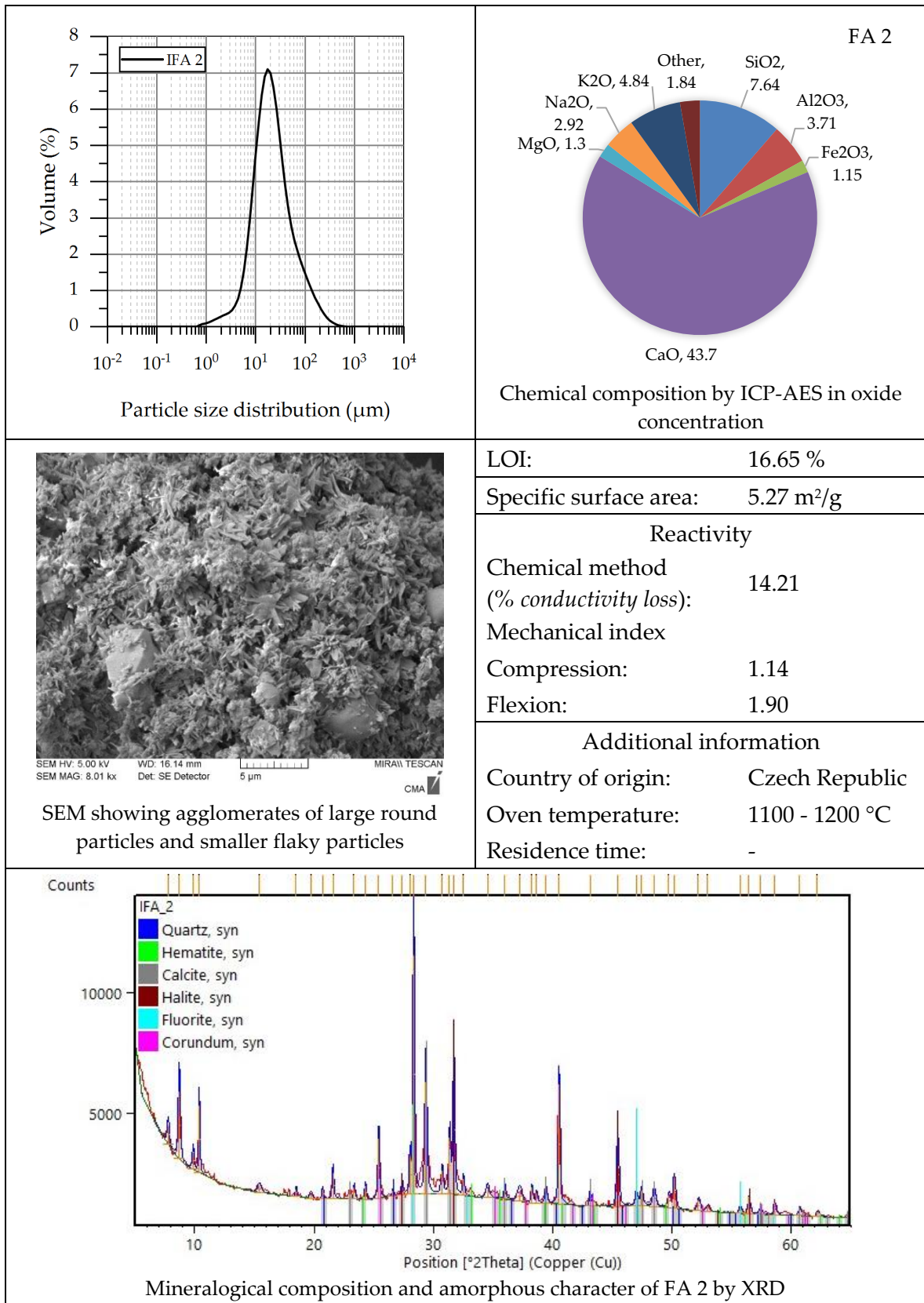
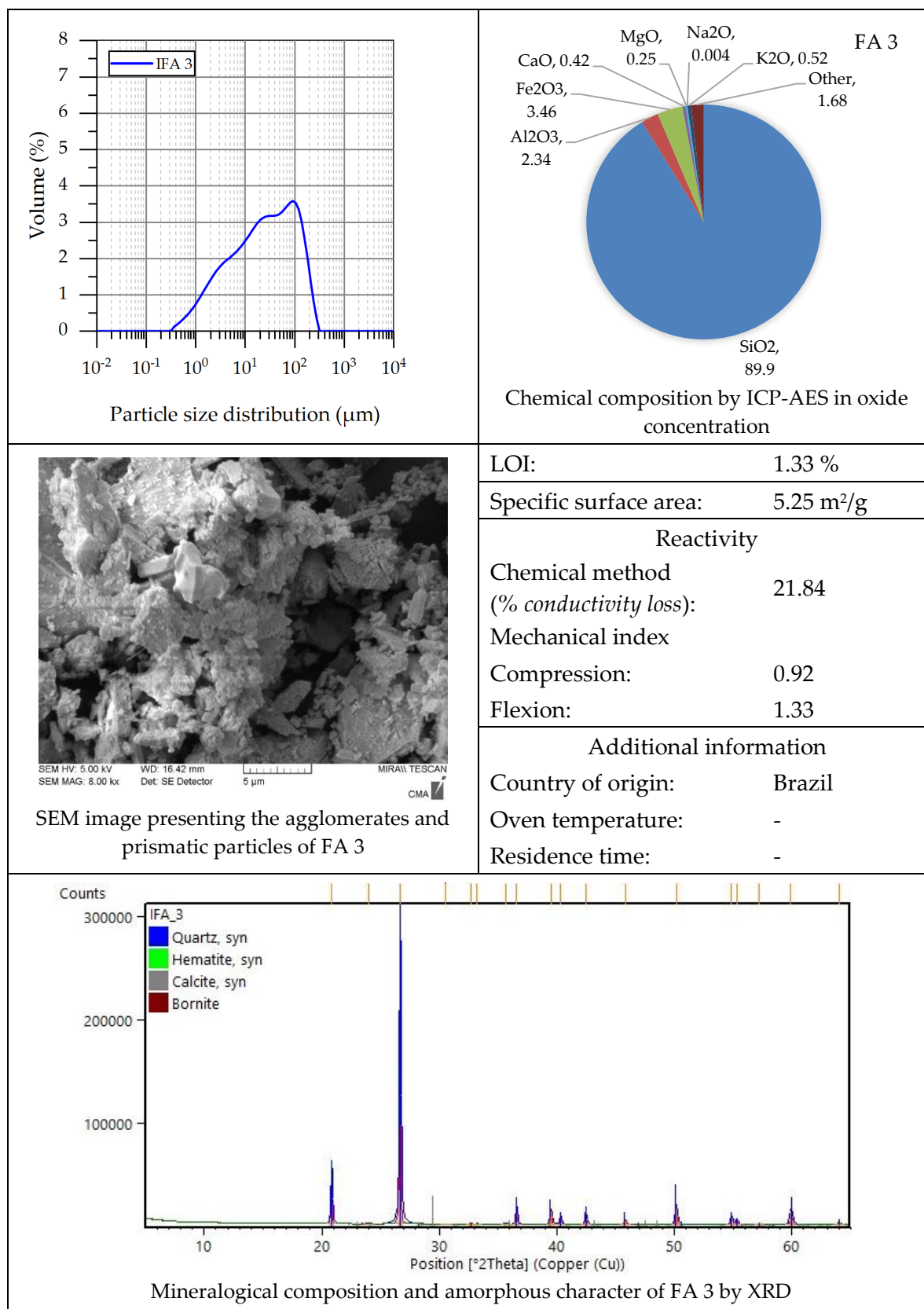


Table 4-14: Properties of fly ash 3.



4.1 PARTICLE SIZE DISTRIBUTION AND SPECIFIC SURFACE AREA

As seen in the background, fineness and specific surface area impact reactivity. In addition, unreacted fine pozzolanic particles can act as fillers and contribute to the micro-aggregate effect (Felekoğlu et al., 2009). Therefore, these properties are studied. Figure 4-1 shows the particle size distribution of the ashes in comparison with the hydrated lime (CL 90-S). In addition, Table 4-15 includes their specific surface areas measured with gas adsorption (BET) and the particle size distribution of the ashes as cumulative undersize particle size distributions (10 and 90% in volume - D10 and D90 - and D50 - median diameter).

The sugarcane ashes SCBA 1 and SCBA 2 are the finest (90% of the volume under 29 and 33 μm respectively, well under the lime value - D90%=57 μm) followed by bottom ashes IBA 1 and 3 fine (D90=64-82 μm) and the fly ash FA 2 (D90=68 μm).

Sugarcane ashes SCBA 1 and SCBA 2 are the finest and have the greatest specific surface areas. SCBA 1 contains a bigger fine fraction than SCBA 2 however the latter has a much greater specific surface area. These suggest that SCBA 2 is the most porous of the two ashes. Also, the specific surface area of SCBA 2 (78 m^2/g) is significantly higher than those typically reported in the literature for reactive pozzolanic materials (Walker & Pavia, 2011).

As expected, the finer ashes tend to show greater specific surface areas however, there are three notable exceptions: IBA 2 fine, IBA 1 coarse and IBA 3 coarse. These are amongst the coarsest ashes however, their specific surface areas are significant, ranging from c. 5 to 9 m^2/g indicating that these ashes are highly porous.

Table 4-15: Cumulative particle sizes (μm).

Material	D10	D50	D90	BET (m^2/g)
CL90-S	8.15	24.13	57.98	Not tested
SCBA 1	1.83	8.14	29.69	25.64
SCBA 2	2.29	9.88	33.03	78.34
SCBA 3	2.55	31.26	190.50	0.51
SCBA 4	2.39	28.13	154.65	2.20
IBA 1 - fine	1.50	14.26	82.96	9.04
IBA 2 - fine	1.42	18.28	167.31	9.68
IBA 3 - fine	5.09	16.53	64.23	7.42
IBA 1 - coarse	2.00	24.61	160.58	6.16
IBA 2 - coarse	2.46	23.67	187.20	4.74
IBA 3 - coarse	4.14	56.43	247.03	5.47
FA 1	6.74	42.19	167.70	4.50
FA 2	7.04	18.69	68.98	5.27
FA 3	2.16	22.88	120.53	5.26

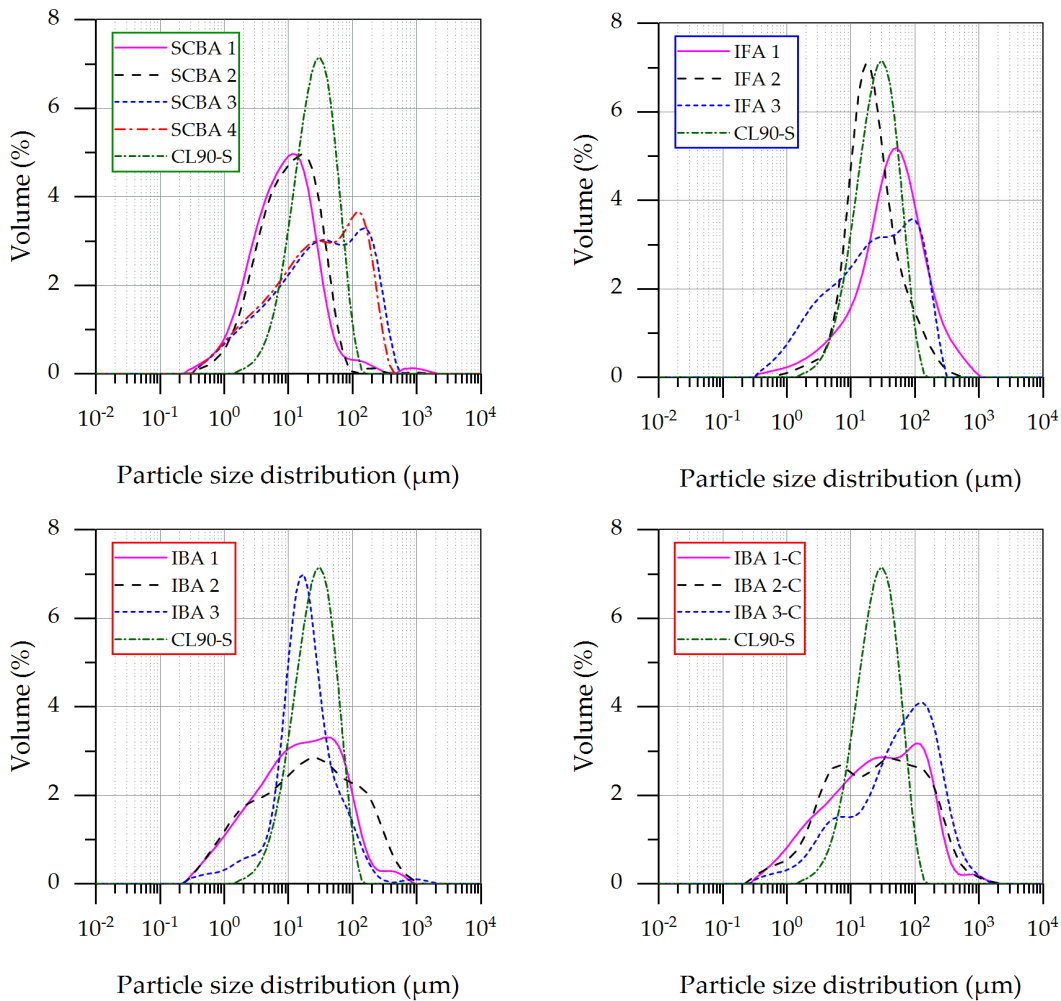


Figure 4-1: Particle size distribution of ashes. SCBAs – sugarcane bagasse (top left); FAs – fly ash (top right); IBAs – incinerator bottom ash fine fractions - (bottom left); and IBAs – incinerator bottom ash coarse fractions – (bottom right).

SCBA 3 and IBA 2 and 3 (coarse) are the coarsest ($D_{90}=187-247 \mu\text{m}$) however the IBAs show substantial specific surface areas of c. $5 \text{ m}^2/\text{g}$ which suggest that these ashes are highly porous. In contrast the SCBA 3 has the lowest specific surface area which combined with the coarse particles indicates a lower reactivity than the other ashes.

Apart from SCBA 3 and SCBA 4, all the ashes present significant specific surface areas, greater than reactive pozzolanic materials such as GGBS and pulverised fly ash (PFA) (2.65 and $4.09 \text{ m}^2/\text{g}$ respectively), rice husk ash (RHA) and microsilica ($13.7 \text{ m}^2/\text{g}$ and $26 \text{ m}^2/\text{g}$) (Walker & Pavia, 2011).

Most of the ashes (except for the SCBA 3, FA 1 and IBA 3-coarse) are finer than the lime (see D_{50} in Table 4-15). IBA 3-fine is the finest of the bottom ashes however, IBA 1-fine and IBA 2-fine contain more fine particles (see D_{10} in Table 4-15). As expected, the specific surface areas of the fine bottom ashes (IBAs) are greater than their parent coarse bottom ashes. The distribution peak for SCBAs 1 and 2 is around $15 \mu\text{m}$, comparable to values found by Frías et al. (2011) of $18 \mu\text{m}$.

To control the quality of cement, fineness is determined with the residues of standard sieves – 75 μm and 45 μm . It is commonly accepted that cement particles larger than 45 μm are difficult to hydrate and those larger than 75 μm seldom hydrate entirely (Mehta, 1986). Figure 4-2 presents the percentage of particles greater than 45 μm and 75 μm for each studied ash and the hydrated lime. It is noticed that SCBAs 1 and 2 present much lower quantities of particles greater than 45 μm and 75 μm , even lower than that of the hydrated lime. Additionally, IBA 3 – fine and IFA 2 have a lower number of particles larger than 45 μm compared to the hydrated lime, whereas, all the other ashes show a greater number of particles above the indicated limits when compared to that of the binder.

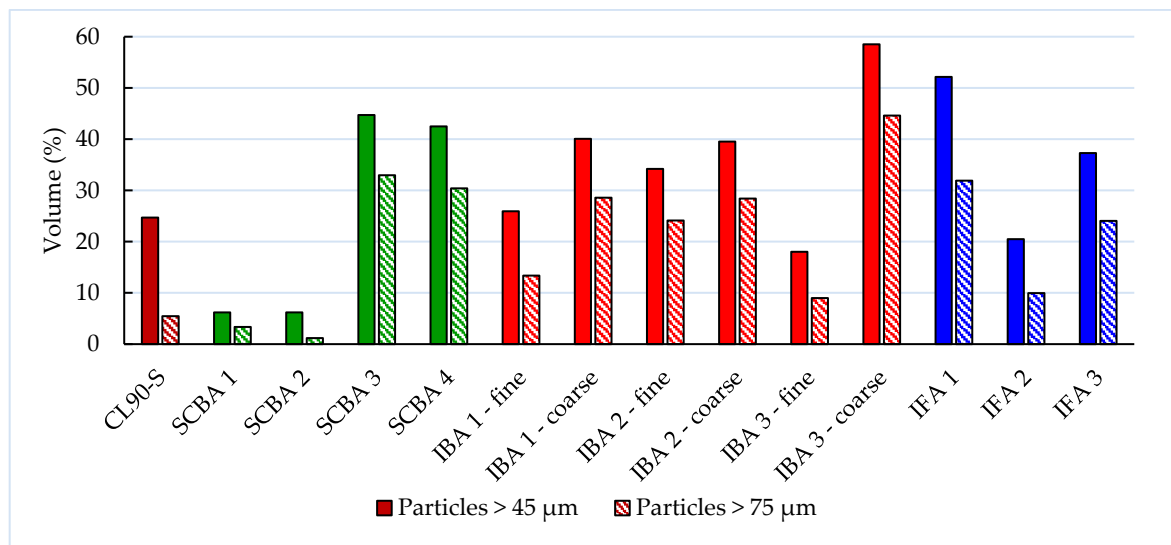


Figure 4-2: Percentage of particles larger than 45 and 75 μm .

4.2 CHEMICAL COMPOSITION AND MINERAL COMPOSITION

The chemical composition and loss on ignition (LOI) of the ashes are included in Table 4-16, Table 4-17 and Table 4-18, and compared with similar materials studied by other authors. The active silica content is the main responsible for the long-term pozzolanic reaction (Massazza, 1998). It is apparent from the results that the sugar fine ashes SCBA 3 and 4 and FA 3 are much more siliceous than the others (SiO_2 c.90% by mass). However, their high silica content is attributed to contamination by sand adhered to the sugarcane during production. Previous authors have reported high silica values due to sand contamination (Cordeiro & Kurtis, 2017; Cordeiro et al., 2008). This applies to all industrial plants as production is similar. However, there is a significant difference in the amount of SiO_2 in the ashes from the four providers in this research probably due to collection from the dumping sites, rather than the incineration chamber, increasing the amount of SiO_2 recorded.

The silica content of the ashes is in the low range when compared with the typical silica content of SCMs: the sugar ashes (non-contaminated) range from 39-59% while the incinerator ashes are even lower at 28-38 %, except for the fly ashes that are especially low at 7-12%.

All the sugar ashes have low calcium content (0-3%) however, the incinerator bottom ashes are high in Ca (14-24%) and the incinerator fly ashes are extremely high (38-47%). It is known that high-calcium fly ash has self-hardening properties, whereas low-calcium fly ash has little or no self-cementing properties.

The content in alumina is important as it partakes in the pozzolanic reaction with the formation of calcium aluminate silicate hydrate (C-A-S-H). Aluminium can replace silicon in the C-S-H structure. Once the ability of C-S-H to accommodate Al is exceeded, phases such as stratlingite may precipitate (Juenger & Siddique, 2015). The aluminium content in the ashes varies significantly: the incinerator bottom ashes are consistently high (11-15%) while the incinerator fly ashes are lower (3-6%) and the non-contaminated sugar ashes (SCBA 1-2) vary from 4-13% and the contaminated ones are very low at 0-1%.

The alkali content is also relevant as it can speed up the dissolution of amorphous silica favouring hydration however, they can later adversely affect durability due to alkali-silica reaction. The incinerator ashes (IBAs and fly ashes FA 1 and 2) have the highest alkali contents.

The chemical composition of FAs, Table 4-18, shows major differences in SiO₂ and CaO contents between the incineration fly ashes– FA 1 and FA 2 – and the sugarcane fly ash– FA 3. The high Ca in FAs 1 and 2 is credited to the practice of adding carbon followed by Ca(OH)₂.2H₂O into the hot flue for gas neutralisation. In contrast, FA 3 contains little CaO and high SiO₂. As discussed previously, the high SiO₂ content is due to sand contamination. These chemical characteristics classify FA 1 and FA 2 as silico-calcareous or high-calcium fly ash, and FA 3 as low calcium fly ash.

The LOI reveals the unburned residual carbon in the ash which increases water demand for a given consistency also affecting the air content (Bahurudeen et al., 2015a; Velandia et al., 2016), and can aggravate surface scaling of concrete under conditions of frost attack and de-icer usage (Jackson, 1998). Chusilp et al. (2009) and Ganesan et al. (2007) argue that LOI up to 10% does not significantly affect the compressive strength of concrete agreeing with the ASTM standard limit however, most ashes are over the LOI standard limits (Table 4-20). The contaminated sugar ashes (SCBA 3 and 4 and FA 3) present very low LOI. The results also evidence that the variation in the organic content of the incinerator ashes is significant: LOI varies from 6 to 17% which suggest an important variation in production temperatures.

The SCBA 1 and SCBA 2 ashes present high losses on ignition, whereas SCBA 3 and SCBA 4 have low losses (≤ 0.41). The high losses are comparable to other authors (Bahurudeen et al., 2014; Bahurudeen et al., 2015b) and low losses on ignition are also found in literature (Cordeiro et al., 2008; Payá et al., 2002; Wang et al., 2017). This suggests uncontrolled combustion during production.

Cordeiro et al. (2009) found that calcination at temperatures greater than 600 °C were sufficient to remove the carbon of sugarcane bagasse ashes. This suggests that there is a big difference in the production temperatures of the bagasse ashes in this study (LOI ranges from 24 to 0)

and that most did not reach 600 degrees (except for the SCBA 3 and 4). Nair et al. (2008) argument that a temperature range of 500 to 700 °C is optimum for reactive rice husk ash formation.

Table 4-16: Chemical analysis of SCBA 1-4 in comparison with SCBAs investigated by other authors.

	SCBAs (%)				Sales and Lima (2010)	Cordeiro et al. (2016)	Cordeiro and Kurtis (2017)	Ferreira et al. (2016)		
	1	2	3 ²	4 ³						
SiO ₂	39.00	59.10	96.80	93.40	62.7	93.5	96.2	70.5	80.8	66.8
Al ₂ O ₃	13.65	4.19	0.74	1.69	4.5	1.2	0.2	10.1	5.1	7.7
Fe ₂ O ₃	11.40	2.01	2.06	2.69	8.8	2.6	1.7	7.4	1.6	10.2
CaO	3.19	2.42	0.25	0.36	0.9	0.4	0.1	4.2	3.1	0.94
MgO	1.55	1.65	0.20	0.27	0.6	0.3	<0.1	-	-	0.49
K ₂ O	1.95	3.73	0.49	0.71	1.8	0.8	0.3	1.8	6.3	1.03
TiO ₂	0.90	0.78	0.45	0.97	3.1	0.5	0.2	0.3	0.3	-
P ₂ O ₅	1.16	1.25	0.15	0.16	0.7	0.2	0.1	1.1	0.8	-
SO ₃	0.213	0.81	0.02	0.03	0.2	<0.1	0.1	2.3	1.5	-
Na ₂ O	0.005	0.16	0.003	0.002	0.1	<0.1	-	-	-	<0.10
SrO	0.01	0.02	<0.01	<0.01	-	-	-	-	-	-
BaO	0.02	0.05	<0.01	<0.01	-	-	-	-	-	-
Cl	0.018	0.11	0.013	0.011	-	-	-	-	-	-
Cu	0.014	0.005	0.002	0.003	-	-	-	-	-	-
LOI	24.10	23.60	0.41	0.31	16.28	0.34	1.04	2.2	0.4	11.47

² SCBA 3 corresponds to SBAS 1 on the second stage of this research.

³ SCBA 4 corresponds to SBAS 2 on the second stage of this research.

The chemical composition of the bottom ashes are included in Table 4-17.

Table 4-17: Chemical analysis of IBA 1-3 in comparison with IBAs investigated by other authors.

	IBAs - fine (%)			IBAs - coarse			Wei et al. (2011)	Tang et al. (2015)	Wongsa et al. (2017)
	1	2	3	1	2	3			
SiO ₂	35.60	31.90	32.90	28.60	23.90	38.70	31.93	54.23	15.80
Al ₂ O ₃	12.25	15.75	11.10	12.95	12.90	13.15	16.65	7.86	0.90
Fe ₂ O ₃	13.95	11.00	9.00	15.15	8.80	9.85	5.97	13.83	4.20
CaO	14.05	19.10	21.00	16.45	23.90	21.00	33.40	13.45	38.1
MgO	3.90	2.51	1.90	3.59	2.27	2.15	3.33	1.81	3.50
K ₂ O	1.49	0.98	1.77	1.57	0.85	2.00	0.85	0.88	7.30
TiO ₂	1.93	2.03	1.61	2.09	2.05	1.75	1.45	0.84	0.30
P ₂ O ₅	2.41	1.79	1.56	2.99	1.97	1.76	0.02	0.79	1.70
SO ₃	-	-	-	0.83	2.17	3.31	0.40	1.28	1.50
Na ₂ O	3.80	4.08	1.96	2.57	2.86	2.82	2.53	2.81	0.20
SrO	0.04	0.05	0.04	0.04	0.05	0.05	-	-	0.10
BaO	0.11	0.17	0.20	0.11	0.16	0.26	-	-	0.10
Cl	0.296	0.478	0.726	0.424	0.813	0.615	1.08	0.26	0.50
Cu	0.505	0.444	0.242	0.208	0.475	0.207	0.23	0.38	-
LOI	6.78	9.68	12.30	12.65	17.50	8.19	-	3.0	23.00

Table 4-18: Chemical analysis of FA 1-3 in comparison with FAs investigated by other authors.

	FAs (%)			Funari et al. (2017) (MSWI)	Aubert et al. (2006) (MSWI)	Bahurudeen et al. (2015b) (SCI)
	1	2	3			
SiO ₂	12.6	7.64	89.9	9.48	21.10	59.32
Al ₂ O ₂	6.21	3.71	2.34	3.65	10.20	29.95
Fe ₂ O ₃	1.19	1.15	3.46	0.79	1.50	4.32
CaO	38.3	43.7	0.42	19.9	30.00	1.29
MgO	2.59	1.30	0.25	1.70	3.00	0.61
K ₂ O	4.50	4.84	0.52	3.76	1.20	1.44
TiO ₂	1.37	0.69	1.41	0.95	2.00	-
P ₂ O ₅	2.26	0.84	0.17	1.25	12.50	-
SO ₃	2.94	2.26	0.027	23.6	0.40	0.17
Na ₂ O	4.63	2.92	0.004	5.09	1.80	0.16
SrO	0.03	0.04	<0.1	-	-	-
BaO	0.09	0.10	0.01	-	-	-
Cl	>2.00	>2.00	0.013	12.80	0.10	-
Cu	0.042	0.052	0.004	0.07	0.171	-
LOI	15.9	16.65	1.33	15.20	8.70	-

MSWI – Municipal solid waste incineration; SCI – Sugarcane industry.

Table 4-19 presents the amounts of SO₃, available alkali as Na₂O, LOI and the sum of silica, alumina and iron phases in the ashes compared with ASTM and NBR standard requirements for: coal fly ash and calcined natural pozzolan; and pozzolanic materials. As it can be seen from the chemical composition results, all the ashes comply with the sulphur limits established by ASTM and NBR standards however, the alkalis in the incinerator ashes (IBAs and FA 1-2) are over the standard limits. The LOI in some of the sugar bagasse (SCBA 1-2) and incinerator ashes are also over the standard limits and so is the Σ (Si, Al, Fe) (%) in sugar ashes SCBA 3- 4 and FA 3.

As seen in the background, alkalis can favour hydration of amorphous silica however, they can affect durability in the presence of reactive aggregates and moisture, which form expansive calcium-alkali-silicate-hydrate gels. As aforementioned, SO₃ content is also important as the greater the SO₃ content the greater the risk of expansion by delayed ettringite formation (which is enhanced by high alkali content).

It is noticed that the fly ashes produced in the waste incineration plants (FA 1 and FA 2) have higher Cl, K₂O and SO₃ content than the other ashes. The sulphur and alkalis are important as explained above. In addition, chlorides are detrimental for the material's durability and can cause fracturing by expansion, leaching of portlandite and corrosion of embedded metal reinforcement, consequently reducing strength (Massazza, 1998, 2002). For these reasons, chloride content is one of the obstructive substances in recycling fly ash as building material.

Table 4-19: SO₃, Na₂O contents, loss on ignition and sum of silica, alumina and iron components.

	SO ₃ (%)	Na ₂ O (%)	LOI (%)	Σ (Si, Al, Fe) (%)
NBR 12635 (2014)	≤ 5	≤ 1.5	≤ 3	≥ 50
<u>ASTM C618 (2005)</u>	<u>≤ 4</u>	-	<u>≤ 10</u>	<u>> 70</u>
SCBA 1	0.213	0.005	24.10	64.05
SCBA 2	0.81	0.16	23.60	65.30
SCBA 3	0.02	0.003	0.41	99.60
SCBA 4	0.03	0.002	0.31	97.78
IBA 1 - fine	-	3.80	<u>6.78</u>	61.80
IBA 2 - fine	-	4.08	<u>9.68</u>	58.65
IBA 3 - fine	-	1.96	12.30	53.00
IBA 1 – coarse	0.83	2.57	12.65	56.70
IBA 2 - coarse	2.17	2.86	17.50	45.60
IBA 3 - coarse	3.31	2.82	<u>8.19</u>	61.70
FA 1	2.94	4.63	15.90	20.00
FA 2	2.26	2.92	16.65	12.50
FA 3	0.027	0.004	1.33	95.70

Numbers in bold are within the limits of the standard NBR 12635; Underlined numbers correspond to values within ASTM C618 limits. Non-formatted numbers do not comply with any of the standards.

As seen, the silica + alumina content usually shows a good correlation with the long-term pozzolanic activity. However, reactivity also depends on how these are combined (the minerals present), as some crystalline phases such as mullite, quartz and the iron oxides hematite and magnetite, have been reported to produce low reactivity.

The mineral composition of the ashes, determined by XRD, is presented in Table 4-20. All the ashes include quartz (SiO_2) and calcite (CaCO_3) as the main minerals, except for SCBA 2 with quartz only. Hematite (Fe_2O_3) was found in all ashes. There is a correlation between the chemical and the mineral composition, for example, all bottom ashes include significant Fe and hematite was found in all however, the correlation is loose as all IBAs contain similar high aluminium and corundum was only found in the coarse fractions.

The level of amorphousness (Table 4-21) was loosely categorised based on the analysis of the slopes of the base line and the background for the area between $2\theta=20-25^\circ$. According to the results, SCBA 1 and SCBA 2 are the most amorphous followed by the SCBA 3 and the coarse bottom ashes while the fine bottom ashes and the fly ashes are mostly crystalline.

The SiO_2 appears as quartz, the lack of high temperature phases such as cristobalite, usually associated with temperatures above 800°C and/or long periods of burning, suggests production temperatures in the medium to lower range. This agrees with the high LOI. It also agrees with the average incineration temperatures of 850°C and residence time of more than 2 seconds (Filipponi et al., 2003).

Additionally, in most fly ashes, most of the iron oxide (Fe_2O_3) is present as nonreactive hematite and magnetite. A small amount of iron is reported to have a deleterious effect on the pozzolanic activity of fly ashes (Ramezaniapour, 2014). Hence, iron oxide has to be separated from silica and alumina when considering chemical requirements and pozzolanic activity, as it does not effectively contribute to strength development. For these reasons the compressive strength generally has poor correlation with the sum of silica + alumina + iron oxides.

Small traces of the sulphide, bornite (Cu_5FeS_4), were detected in the coarse bottom ashes, and fly ashes 1 and 3 agreeing with the chemical analyses.

The aluminium appears in the form of corundum which is stable at high temperature. It has been reported that the presence of mullite and corundum result in a cement with greater heat resistance, alleviating problems associated with strength retrogression (Agapiou, 2017). In small quantities, the presence of corundum is not considered to significantly influence the long-term pozzolanic activity (Joshi, 1970).

Halite – NaCl – is present in most incinerator ashes except for IBA 1-2 fine. Halite can react with the aluminate phases, producing calcium chloroaluminates hydrate ($3\text{CaO}\cdot\text{Al}_2\text{O}_3\cdot\text{CaCl}_2\cdot 10\text{H}_2\text{O}$) (Frias et al., 2006) which reduce the aluminate phase affecting the formation of ettringite (Ubbriaco & Calabrese, 1998). When in high quantities, chloride salt interacts with C-S-H phases, and is incorporated to the C-S-H lattice, present in the interlayer space and chemisorbed on the surface of C-S-H. The ability of chloride to interact

with C-S-H phases has significant implications on durability. The presence of chloride causes the reduction of pore sizes due to the formation of the calcium chloride complexes. Furthermore, Cl⁻/OH⁻ ratio has been identified as a significant indicator for steel corrosion (Beaudoin et al., 1990).

Table 4-20: Main mineral composition of ashes.

Material	Main mineral composition	Minor minerals
SCBA 1	Quartz, calcite	Corundum, hematite
SCBA 2	Quartz	Corundum, hematite
SCBA 3	Quartz, calcite	Hematite
SCBA 4	Quartz, calcite	Corundum, hematite
IBA 1 - fine	Quartz, calcite	Hematite
IBA 2 - fine	Quartz, calcite	Hematite
IBA 3 - fine	Quartz, calcite	Hematite, halite
IBA 1 – coarse	Quartz, calcite, hematite	Corundum, halite
IBA 2 - coarse	Quartz, calcite, hematite	Corundum, halite, bornite
IBA 3 - coarse	Quartz, calcite, hematite	Corundum, halite, bornite
FA 1	Quartz, calcite, hematite	Fluorite, corundum, halite, bornite
FA 2	Quartz, calcite, hematite	Fluorite, corundum, halite
FA 3	Quartz, calcite	Bornite, hematite

Table 4-21: Level of amorphousness.

Material	Peak at ~ 20 (°2θ) (d-spacing ~ 4.26)	Rel. int. (%)	Slope base	Slope hump	Diff.	Level of amorphousness
SCBA 1	20.83	21.44	-37.052	-63.128	26.0759	S – I
SCBA 2	20.85	16.81	-36.039	-61.599	25.5598	S - I
SCBA 3	20.86	23.20	-28.228	-40.974	12.7460	S
SCBA 4	20.86	18.32	-0.002	-0.002	0.0003	MC
IBA 1 – fine	-	-	-0.027	-0.143	0.1167	MC
IBA 2 – fine	-	-	0.000	-0.046	0.0463	MC
IBA 3 – fine	-	-	0.016	-0.063	0.0791	MC
IBA 1 – coarse	21.95	19.06	-23.564	-35.150	11.5860	S
IBA 2 – coarse	20.83	19.88	-20.369	-30.741	10.3715	S
IBA 3 - coarse	20.83	27.04	-22.585	-34.517	11.9313	S
FA 1	20.74	6.04	-14.993	-19.161	4.1683	MC - S
FA 2	20.73	4.12	-16.512	-17.553	1.0417	MC
FA 3	20.86	18.66	-29.461	-35.136	5.6749	MC - S

MC – mostly crystalline; S – slightly amorphous; I – intermediate amorphousness.

4.3 MICROSTRUCTURE OF ASHES

The morphology and porosity of the ash particles is directly influenced by the processing and burning temperature and can influence reactivity. Under the SEM, they revealed a variety of

particles and clusters. The sugarcane bagasse ashes are a heterogeneous mixture of irregular, spherical, prismatic and flaky particles which agrees with other authors (Bahurudeen & Santhanam, 2015; Jagadesh et al., 2015; Payá et al., 2002; Sales & Lima, 2010).

At higher magnifications, porous particles were identified in SCBA 1 (Figure 4-3) and SCBA 2 (Figure 4-4) to a greater extent than in SCBA 3 (Figure 4-5) and SCBA 4 (Figure 4-6), agreeing with the specific surface area results. Furthermore, cavities in larger particles filled with smaller grains were observed in SCBA 1 and SCBA 2. It was noted, to a lesser extent, that some of the larger particles in SCBA 3 and SCBA 4 were also covered with fine needle shaped agglomerates, which increase specific surface area and build up porosity in the ashes. Even though the SCBA 3 and SCBA 4 ashes are less porous, porous particles were sporadically found as well as agglomerates of spherical particles mixed with finer flaky and elongated ones.

The uneven particle size distribution of the IBAs was further evidenced with the SEM images. Under the SEM, the bottom ashes were found to be composed of a heterogeneous mixture of particles of diverse, irregular shapes. They also include agglomerates of spherical particles agreeing with former authors (González-Fonteboa et al., 2017; Kurama & Kaya, 2008; Sathonsaowaphak et al., 2009; Tang et al., 2016; Wang et al., 2016). At high magnifications, it was noted that large particles are covered with fine, 'cauliflower-like' agglomerates which increase surface area and buildup porosity in the ashes. The SEM images of IBA 1, IBA 2 and IBA 3 are shown in Figure 4-7, Figure 4-8 and Figure 4-9 respectively.

Unlike the fly ashes from fossil fuel combustion which are typically spherical, the waste incinerator and sugarcane fly ashes consist of a mix of irregular and vitreous particles. Spherical hollow particles seldom appear, and most particles are very porous. The Scanning Electron Microscope (SEM) revealed that the incinerator ashes FA 1 and 2 (Figure 4-10 and Figure 4-11 respectively) consist of a heterogeneous mixture of irregularly shaped particles in clusters, cubes and needles. The qualitative composition and morphology of the cubic crystals further confirm the presence of halite (NaCl) – as seen in FA 1 (Figure 4-10). Agglomerates around larger particles building up porosity were also recorded agreeing with previous studies (Bayuseno & Schmahl, 2011; Felekoğlu et al., 2009; Payá et al., 1995a; Ramezani pour, 2014; Thipse et al., 2002). FA 3 (Figure 4-12) has less agglomerates than the other ashes.

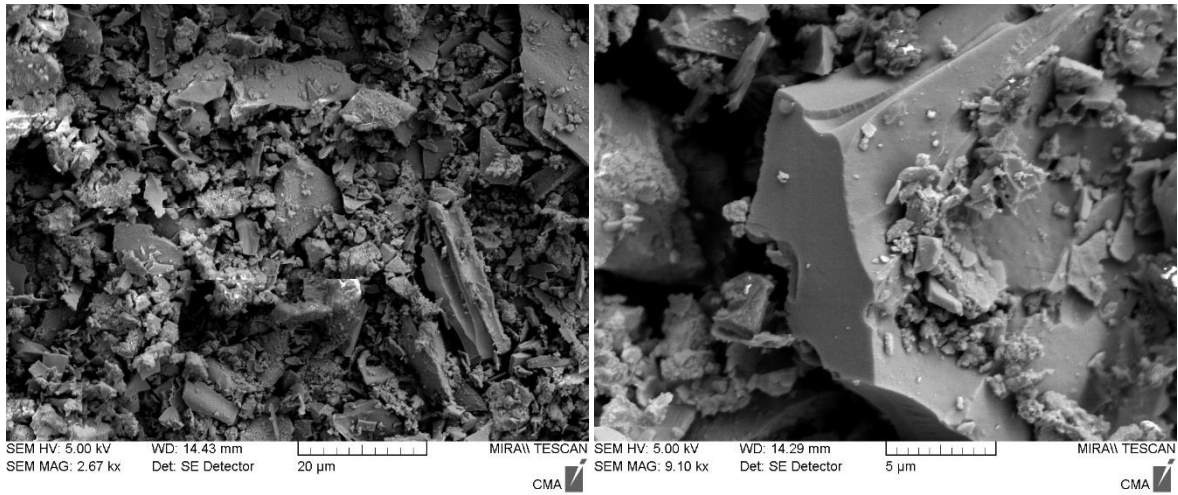


Figure 4-3: SEM micrograph of SCBA 1.

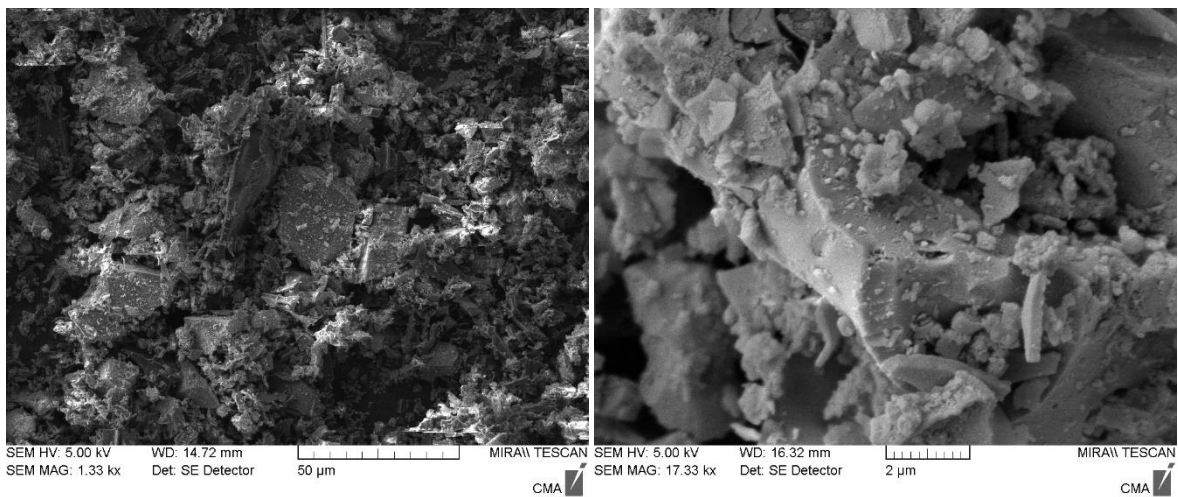


Figure 4-4: SEM micrograph of SCBA 2.

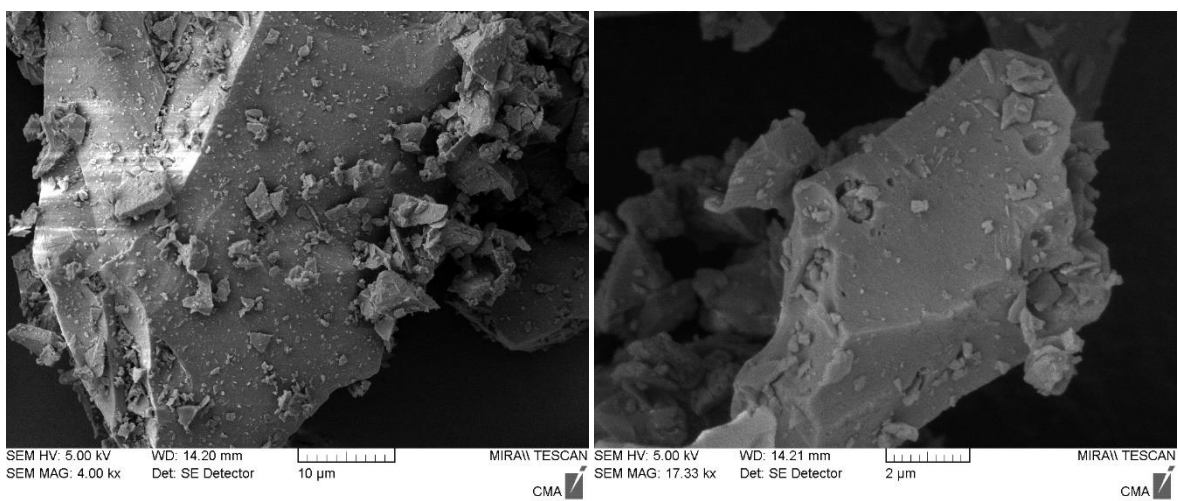


Figure 4-5: SEM micrograph of SCBA 3.

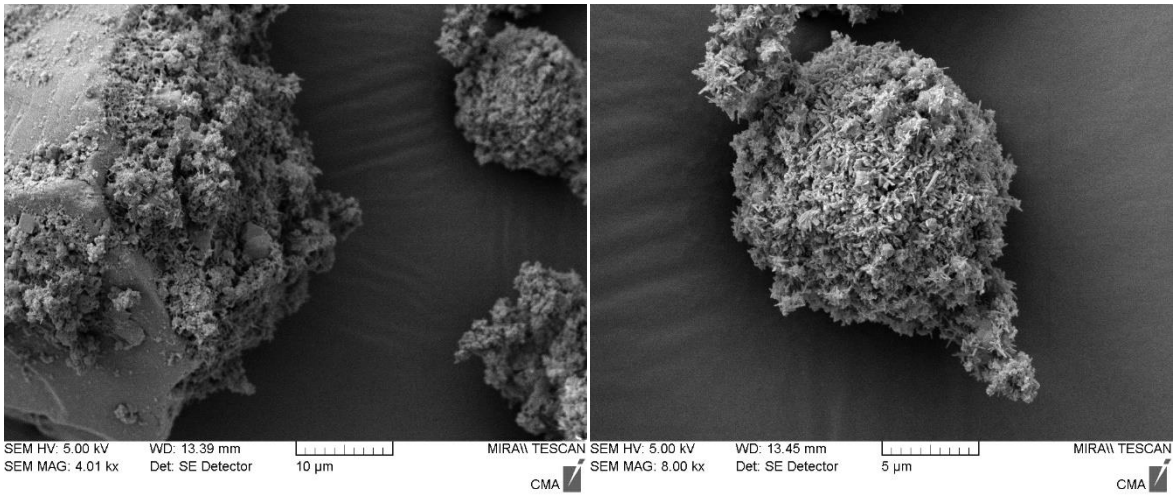


Figure 4-6: SEM micrograph of SCBA 4.

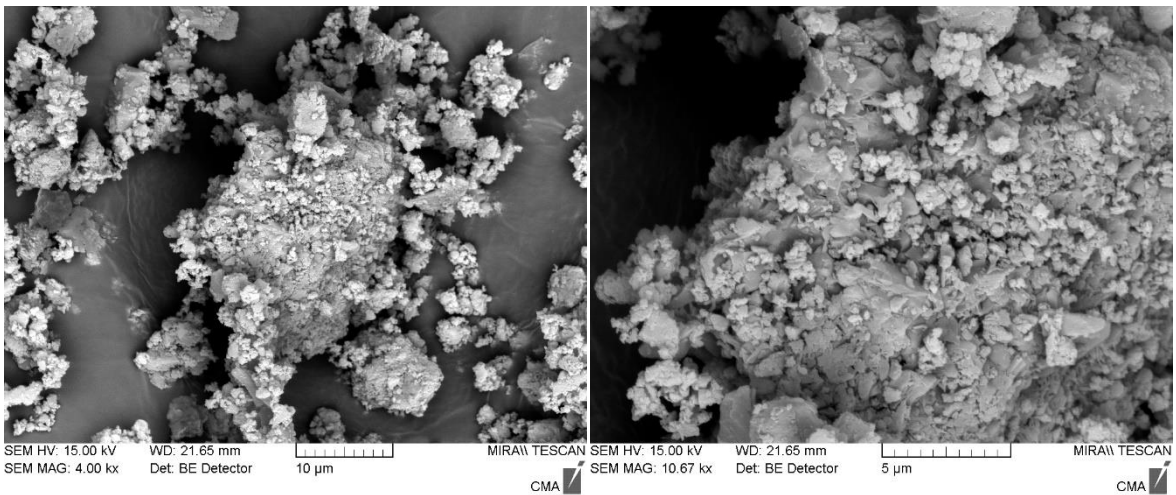


Figure 4-7: SEM micrograph of IBA 1.

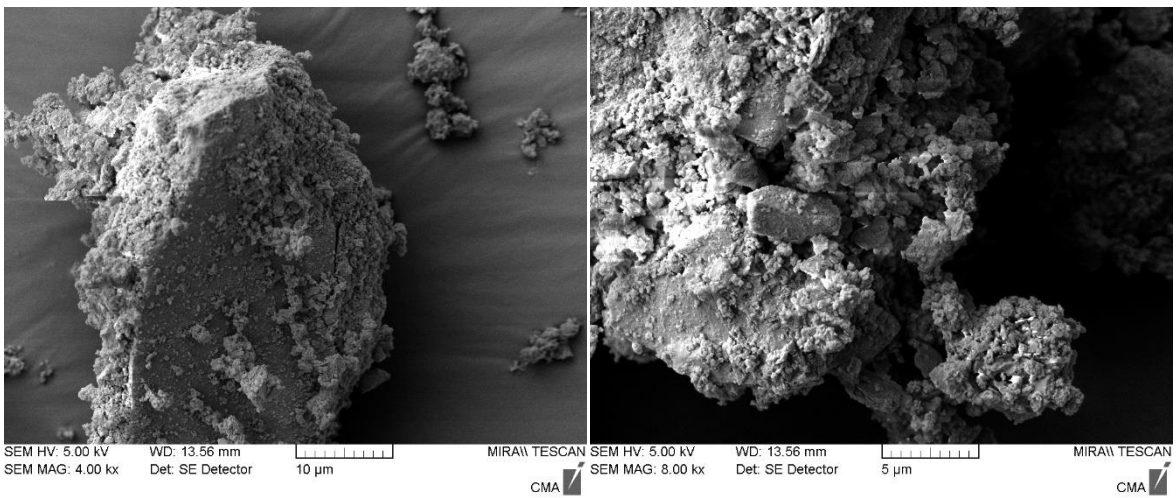


Figure 4-8: SEM micrograph of IBA 2.

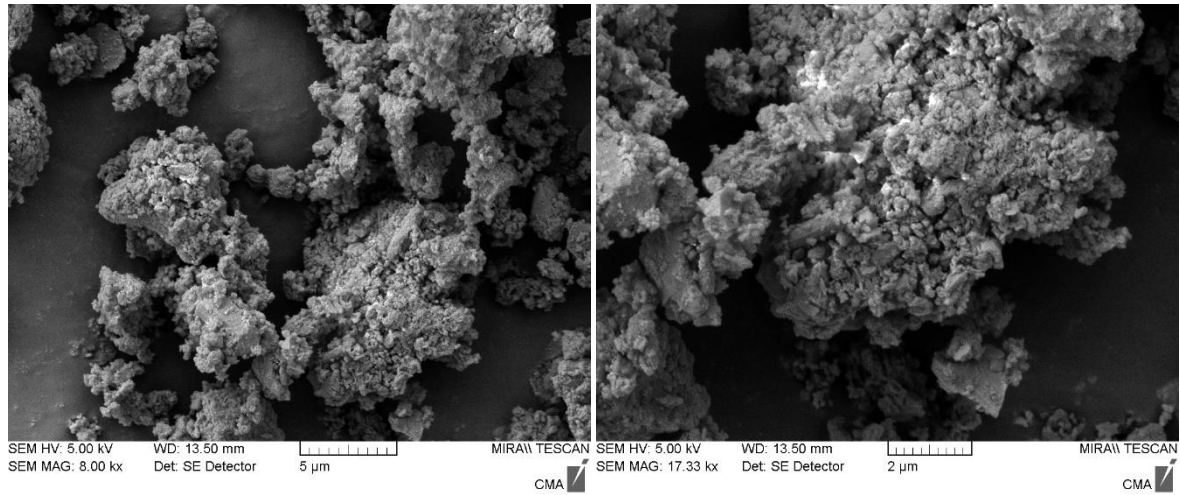


Figure 4-9: SEM micrograph of IBA 3.

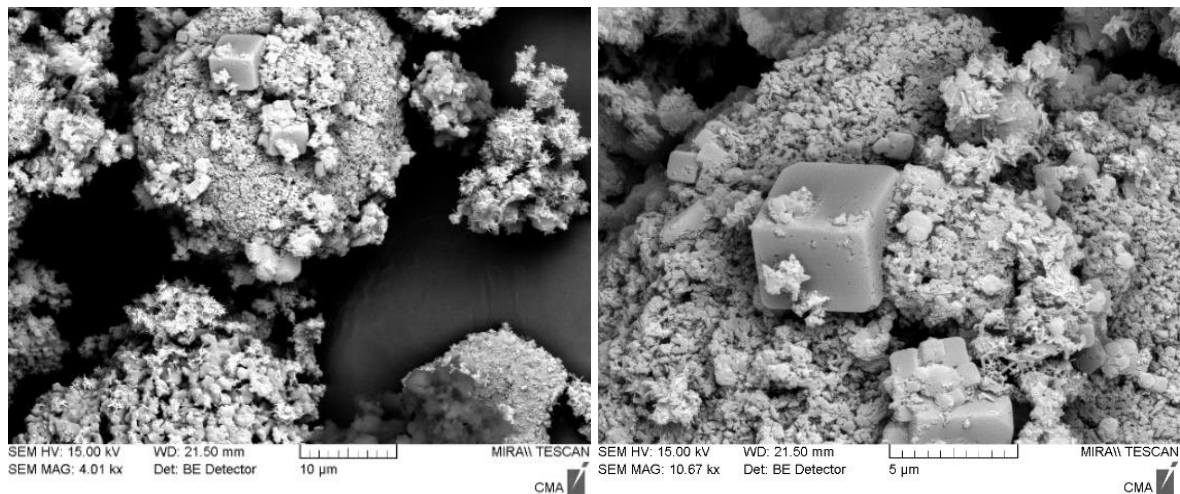


Figure 4-10: SEM micrograph of FA 1.

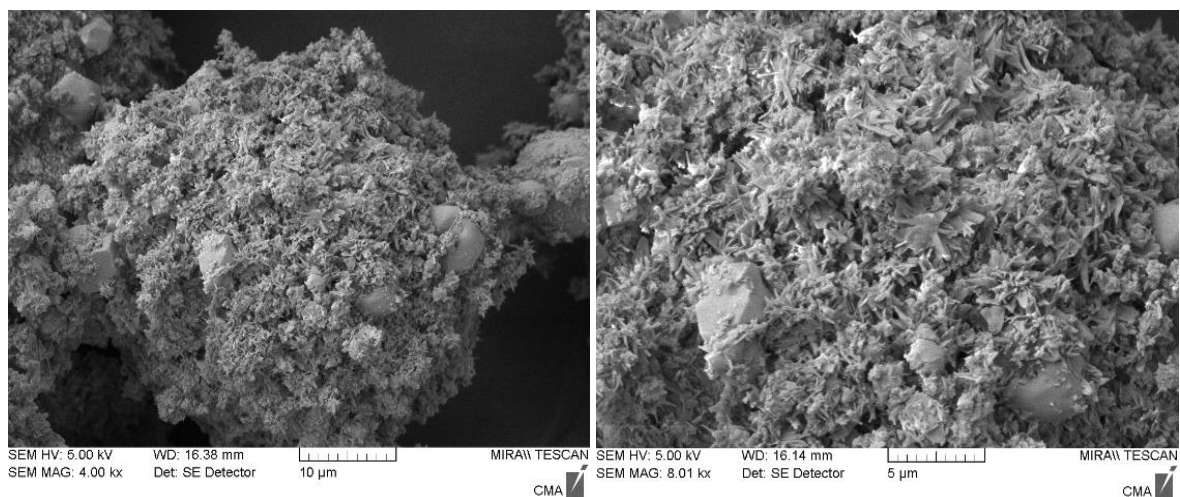


Figure 4-11: SEM micrograph of FA 2.

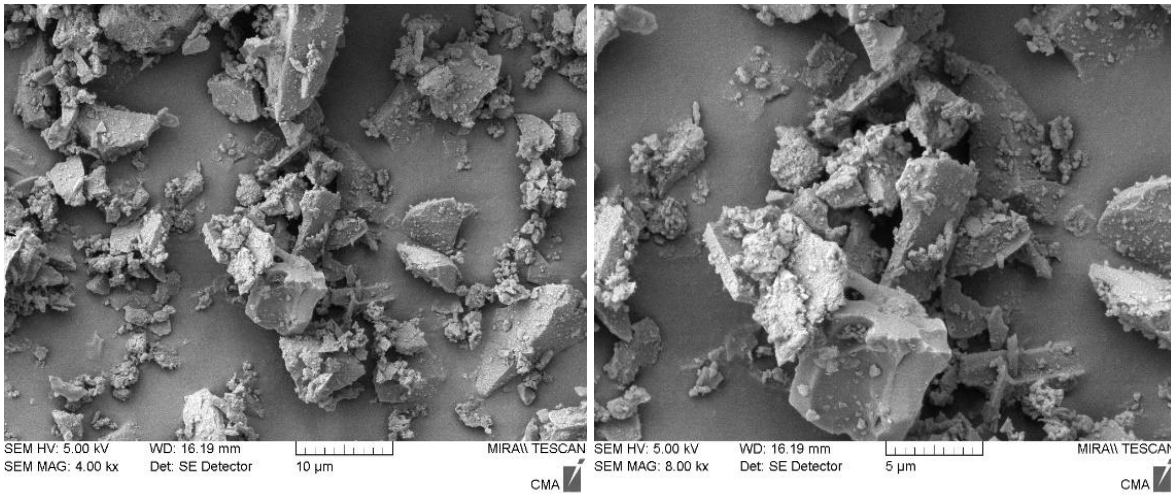


Figure 4-12: SEM micrograph of FA 3.

4.4 REACTIVITY BY CONDUCTIVITY

The conductivity test, performed on lime-ash solutions at 20 °C, demonstrated that all the ashes reacted with lime, causing gradual reduction in electrical conductivity over time. The ashes alone did not present any significant conductivity in water (except for FA 1 and 2) when compared to the lime alone (*Cl*) therefore, this parameter was negligible and not considered in the calculation of conductivity loss.

All the ashes show values ranging from 13 – 29 % conductivity loss. However, the incinerator bottom ashes (IBAs) tend to combine the most lime followed by the sugar ashes and finally the incinerator fly ashes.

The conductivity loss of the IBA 2 suspensions is notably superior suggesting the greatest reactivity: the other IBA ashes require at least 168 hours to cause reductions in conductivity comparable to the reduction caused by the IBA 2 in the first 24 hours. The conductivity test rates the IBAs in decreasing reactivity as follows: IBA 2, IBA 1 and IBA 3.

In the sugarcane ashes, the conductivity loss agrees with the expected reactivity based on the specific surface area rating SCBA 2 as the most reactive followed by SCBA 1 / SCBA 4 and SCBA 3. Among the fly ashes, sugarcane FA 3 achieves the highest loss in conductivity, followed by incinerator ashes FA 1 and FA 2.

The conductivity loss over-time in Figure 4-13, shows four phases agreeing with previous authors (McCarter & Tran, 1996; Walker, 2013). During the first 24 hours (Phase I) the curves show steep slopes whereby all solutions lose over 9.89% of their conductivity suggesting that the ashes combine lime at a faster rate. In the first stage, FA 1 and SCBA 3 were the least reactive, achieving losses of 9.81 and 9.90% respectively, while IBA 2-coarse presented the highest reactivity, achieving 21.12% loss, followed by IBA 2-fine (18.06% loss) in the first 24 hours. By the end of phase I, the fine and coarse IBA 3 ashes show the same conductivity while the other fines and their respective coarser fractions are well parted.

Between 24 and 48 hours (Phase II) the lesser steep curves indicate a drop in the reaction rate. FA 2 and SCBA 3 present a lower conductivity loss than the previous phase at 0.18 and 0.41% respectively. The other ashes show greater conductivity loss with IBA 2-coarse (3.16%) and IBA 2-fine (2.96%) being the greatest, followed by SCBA 2 and FA 3, each achieving 2.04% losses.

Phase III – between 48 and 96 hours – presents a significant reduction in chemical activity for the bottom ashes (conductivity drop under 1.5%), even a dormant period (in the case of ashes IBA 2-coarse and IBA 3 and 3-coarse) where the curves are flat. In this stage SCBA 3 further lowered the conductivity loss in 0.31%, indicating that for this proportion SCBA 3 is not able to consume solid calcium hydroxide present in the suspension, while SCBA 2 achieved the greatest loss for this period, of 3.98%, followed by FA 3, 2.55%.

The last phase (IV) shows a new increase on the reaction rate, evidenced by the steeper slopes in the curves after 96 hours. The final values for loss in conductivity are depicted in Table 4-22, which also shows the conductivity variation for the 7 days period and the slope of initial reactivity of all ashes.

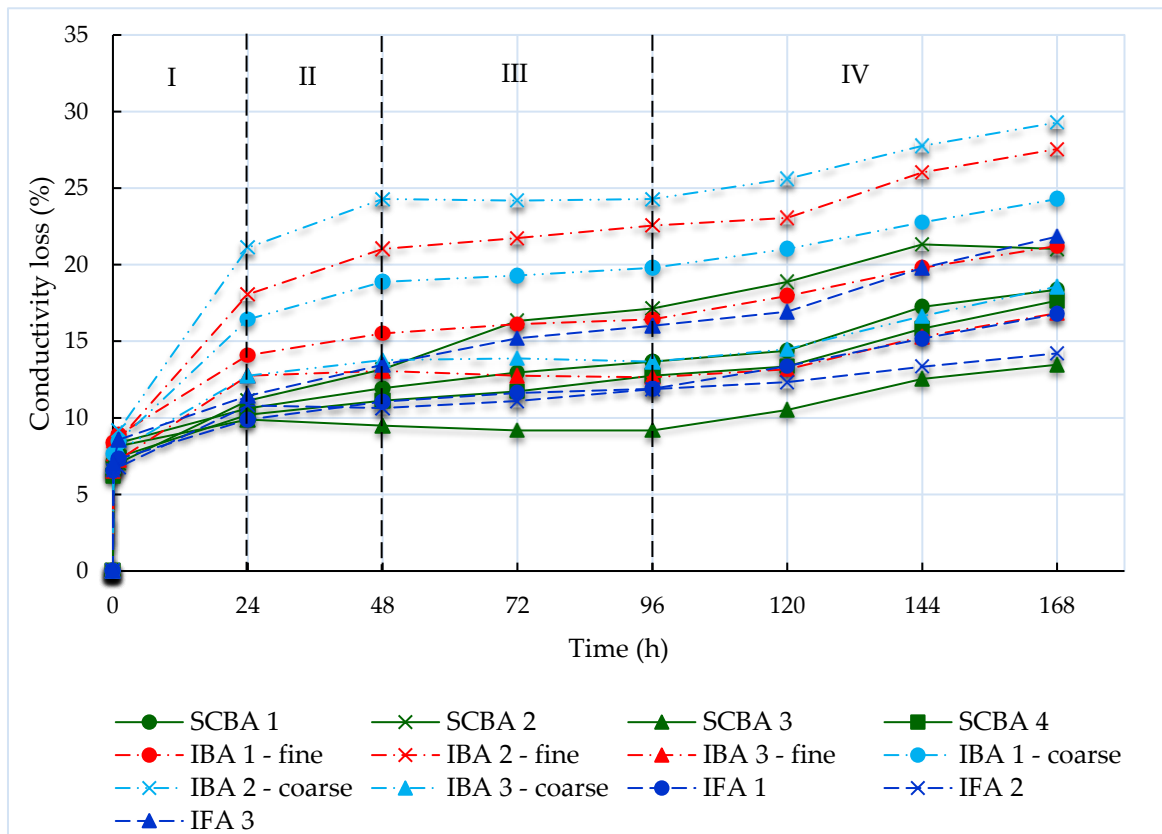


Figure 4-13: Conductivity loss over-time.

The alumina content is generally responsible for the quick consumption of CH (Tironi et al., 2013) which can explain the higher losses in conductivity experienced by the IBAs, as these ashes have greater amounts of alumina in their composition. Hence, the alumina content may overpower other variables in the lime: ash solution and consequently overestimate the prediction of pozzolanicity (Juenger & Siddique, 2015). In agreement, it is observed a general trend of increasing alumina content and increasing conductivity variation whereas there is a reduction in conductivity variation with the increase in silica content (Figure 4-14).

Table 4-22: Summary of the conductivity variation of lime/ash solutions.

Material	Initial conductivity (mS/cm)	Conductivity variation (mS/cm)	Loss in conductivity (%)	Initial activity of ash (slope of conductivity loss curve in 24h)
SCBA 1	9.8	1.80	18.37	0.44
SCBA 2	9.8	2.06	21.02	0.46
SCBA 3	9.8	1.32	13.47	0.41
SCBA 4	9.8	1.73	17.65	0.43
IBA 1-fine	9.8	2.08	21.22	0.59
IBA 2-fine	9.8	2.70	27.55	0.75
IBA 3-fine	9.8	1.65	16.84	0.53
IBA 1-coarse	9.8	2.38	24.29	0.68
IBA 2-coarse	9.8	2.87	29.29	0.88
IBA 3-coarse	9.8	1.82	18.57	0.53
FA 1	15.53	2.61	16.78	0.41
FA 2	17.08	2.43	14.21	0.45
FA 3	9.8	2.14	21.84	0.48

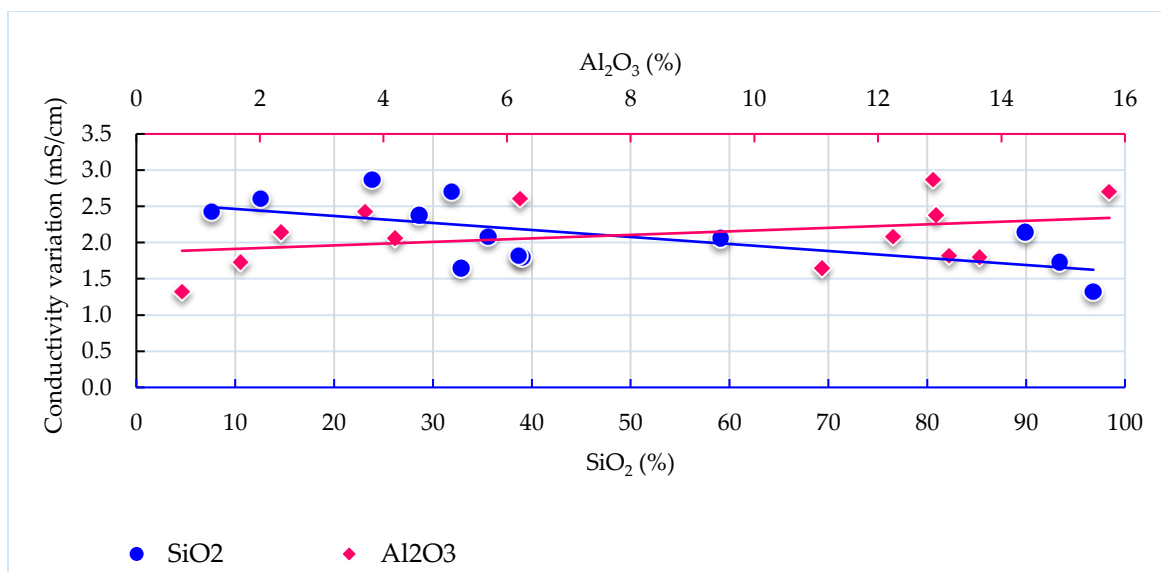


Figure 4-14: Relationship between silica and alumina content and conductivity variation.

4.5 REACTIVITY BY STRENGTH DEVELOPMENT

The mechanical tests further measured the pozzolanic activity of the ashes by monitoring strength development. Two mechanical indexes were calculated as the ratio of the flexural / compressive strength of the lime:ash mixes in relation to a standard lime mix (Table 4-23).

The mechanical indexes roughly agree however they partially differ when rating the reactivity of the ashes. According to the compressive strength, SCBA 2 is the most reactive

followed by FAs 2 and 3 and SCBA 1, the rest of the ashes are significantly lower and the coarse IBAs the lowest.

In contrast, the flexural strength rates the reactivity as follows: FA 2, IBA 3 fine, FA 1 and 3 are the most reactive followed by SCBA 4, IBA 1 fine and SCBA 1 with close values and all the others with lower reactivity.

The fly ashes greatly enhanced flexural strength: FA 2 nearly doubled the strength of the lime mix while FA 1 and FA 3 enhanced the flexural strength by 43 and 33% respectively. The fine bottom ashes IBAs 1 and 3 also improved flexural strength by 12 and 47% respectively. Sugarcane bagasse ashes SCBAs 1 and 4 surpassed the flexural strength of the reference test specimens, achieving indexes of 1.05 and 1.18 respectively. The coarse bottom ashes reached the lowest values.

The results compare well with those from previous authors. Moropoulou et al. (2005), using earth of milos and brick powder, attained results ranging from 0.34 to 0.38 MPa after 28 days and results of 0.41-0.62 MPa after 90 days. The flexural strength in this research ranges from 0.20 MPa (IBA 2-coarse) - to 0.74 MPa (FA 2) after 28 days. The pozzolanicity of brick dust was also assessed by Navrátilová and Rovnaníková (2016), showing similar results, with strength ranging from 0.58 to 0.62 MPa after 28 days.

SCBA 2 significantly raised compressive strength with a mechanical index of 1.48 (3.62 MPa), followed by FA 2, which achieved a compressive strength slightly superior than the reference (2.79 vs 2.45 MPa).

The fine bottom incinerator ashes nearly doubled the compressive strength of the coarse fractions. IBA 2-coarse presented the lowest compressive strength (0.50 MPa). Figure 4-15 shows the visual aspect of one IBA 2-coarse after demoulding.

The significant strength increase is probably due to the generation of pozzolanic cements and to the increase in nucleation sites for C-S-H precipitation. During hydration, pozzolan particles offer nucleation sites for the precipitation of C-S-H (Massazza, 1998).

It has been reported that high-calcium fly ashes lead to a more rapid strength gain as the large amounts of CaO, when released in solution, can react with the glass phase rendering these fly ashes as self-pozzolanic (Barnes & Bensted, 2002). This agrees with the results as the high calcium ash FA 2 produces the greatest compressive and flexural strengths. However, FA 3, with much lower Ca (0.42% vs 38-43%), has similar strengths than the other FAs. The higher alumina, SO₃, Cl and alkali content of the incinerator FAs (1 and 2) may be responsible for the lower strength.

Table 4-23: Mechanical properties, mechanical index and variations in strength.

Material	Compressive strength (MPa)	Flexural strength (MPa)	Mechanical index		Strength variation (%)	
			Compressive strength	Flexural strength	Compressive strength	Flexural strength
Reference	2.45	0.39	-	-	-	-
SCBA 1	1.95	0.41	0.80	1.05	-20.66	8.75
SCBA 2	3.62	0.36	1.48	0.92	47.46	-8.06
SCBA 3	1.35	0.28	0.55	0.72	-44.83	-28.05
SCBA 4	1.65	0.46	0.67	1.18	-32.95	16.83
IBA 1-fine	1.10	0.44	0.45	1.13	-55.08	12.07
IBA 2-fine	1.67	0.27	0.68	0.69	-31.83	-29.95
IBA 3-fine	1.05	0.57	0.43	1.46	-57.09	47.16
IBA 1-coarse	0.56	0.23	0.23	0.59	-77.23	-41.11
IBA 2-coarse	0.50	0.20	0.20	0.51	-79.64	-49.72
IBA 3-coarse	0.78	0.38	0.32	0.97	-68.14	-3.6
FA 1	1.36	0.56	0.56	1.44	-44.59	43.39
FA 2	2.79	0.74	1.14	1.90	13.78	89.98
FA 3	2.26	0.52	0.92	1.33	-7.78	33.71



Figure 4-15: Specimen produced with IBA 2 – coarse after demoulding (at 72 hours).

It is known that the strength of lime: pozzolan pastes increases as the pozzolans progressively combine lime however, as shown in Figure 4-16, there is no general correlation between the amount of combined lime and the development of strength. This is probably owed to the fact that conductivity measures early reactivity while the strength is measured at 28 days. Massazza (1998) explains that there is also a lack of correlation between the amount of combined lime and the strength development of PC: pozzolan pastes, as not all combined lime hardens substantially, and therefore do not contribute to strength development.

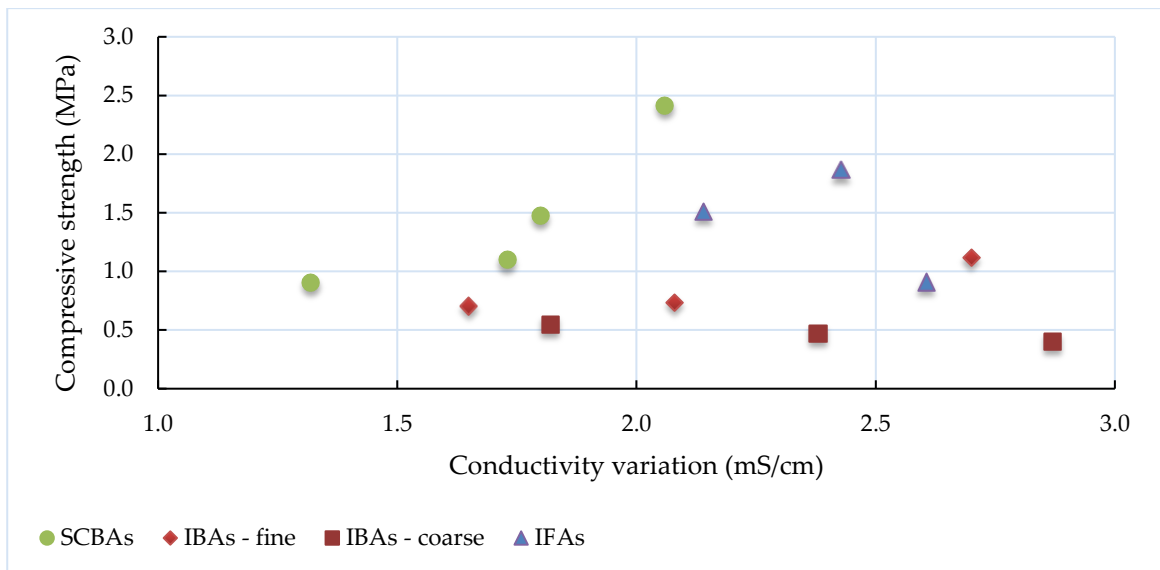


Figure 4-16: Relationship between the chemical reactivity and the mechanical properties of the ashes.

4.6 MICROSTRUCTURE OF THE PASTES

The analysis of the microstructure and the hydrate phases in the lime: ash pastes with SEM-EDS informed on the quality and presence of hydrates at 7 and 28 days. It is known that the reaction between hydrous silica and calcium hydroxide produces C-S-H. As this reaction has a varying stoichiometry, the calcium to silicate ratios of the C-S-H product also vary. It has been reported C-S-H with CaO/SiO₂ (C/S) ratios ranging from 0.6 to 2.0 (Souza et al., 2014; Stefanidou et al., 2017; Taylor, 1986, 1997; Taylor, 1950).

In the ashes studied, the EDS analysis suggests similar C-S-H as in previous studies (Table 4-24). Stefanidou et al. (2017) observed areas with identified C-S-H compounds of Ca/Si-Al ratio equal to 0.6 in natural pozzolan and lime pastes at 90 days. They also observed areas with high calcium contents (Ca/Si-Al ratio = 4) which function as nuclei for further development of hydrated calcium silicate compounds. Pereira et al. (2015) identified amorphous matrix of sugarcane straw ash and Portland cement mixes with molar ratios of Al/Si=0.63, Na/Si=1.34, Ca/Si=0.60 and K/Si=0.05. These ratios are similar to those found upon hydration of the lime:ash pastes in this study. And, as discussed by Stefanidou et al. (2017), potential areas for further C-S-H development were also observed.

The results also indicate the presence of calcium aluminate silicate hydrates at 7 and 28 days for different pastes, confirming the ability of the ashes to produce cementing materials in reaction with hydrated lime. Furthermore, it is noticed that the microstructure of the paste is composed of different structural areas.

Table 4-24: Chemical composition of C-S-H phases in the lime paste determined by SEM EDS.

Material	Ca	Si	C/S	Al	Mg	K	Fe	S	Na	Cl	Ref. Figure
SCBA 1 - 7 d (1)	14.72	11.6	1.3	1.1	0.3	0.14	0.33	1	-	-	Figure 4-17
SCBA 1 - 7 d (2)	12.16	9.15	1.3	0.8	0.1	0.16	0.28	0.2	-	-	Figure 4-17
SCBA 1 - 7 d (3)	11.57	20	0.6	0.9	0.1	0.26	0.33	-	-	-	Figure 4-17
SCBA 1 - 7 d	164.2	91.2	1.8	16	3.9	8.33	29.4	-	-	-	Figure 4-18
SCBA 2 - 28 d	2.5	4.22	0.6	0.1	0.1	0.33	-	-	-	0.06	Figure 4-19
IBA 1 - 7 d	173	60.9	2.8	16	2.8	5.44	13.1	-	3.8	-	Figure 4-20
IBA 1 - 28 d	30.45	106	0.3	10	3.1	4	3.2	0.6	2.3	-	Figure 4-21
IBA 1 - 28 d	49.67	47.8	1.0	1	0.4	0.49	11.9	0.5	0.8	-	Figure 4-22
FA 1 - 7 d	245.2	42.3	5.8	2.2	-	4.74	-	4.1	1.7	54.44	Figure 4-23
FA 2 - 28 d	18.83	23.2	0.8	8.1	1.2	-	-	0	1.1	0.2	Figure 4-25
FA 2 - 28 d	-	-	-	0.2	-	69.7	-	0.4	-	81.52	Figure 4-26

The most abundant C-S-H phases with needle-like morphology and significant crystallinity were earliest evidenced in SCBA 1 mixes (7 days), as shown in Figure 4-17. This agrees with Ríos-Parada et al. (2017) studying Mexican sugarcane bagasse ash. C-S-H and CASH were also evidenced early in the ashes with the highest flexural/compressive strengths: SCBA 1, IBA 1 and FA 2. However, the qualitative nature of the analyses did not allow to rate the ashes on the basis of the appearance of hydrates.

The porosities of the pastes are also evidenced. In Figure 4-18 and Figure 4-19 it is possible to observe the porous structure formed by the combined morphology of the solid phases. Throughout the images of the different materials used it is clear the high variability and complexity of the morphology of hydration products. Figure 4-21 shows the growth of ettringite needles within the pores. Also, it is apparent the presence of salts in the pastes produced with IBA 1 (Figure 4-22), FA 1 (Figure 4-23 and Figure 4-24) and FA 2 (Figure 4-26).

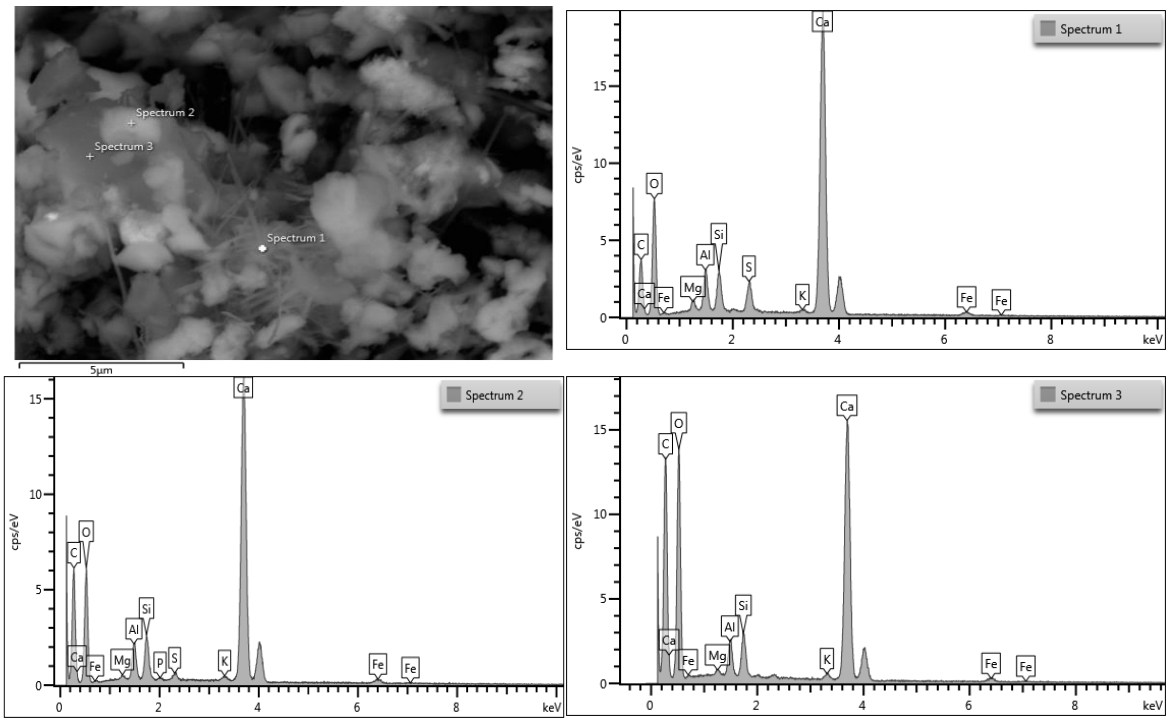


Figure 4-17: Lime-SCBA 1 paste showing entangled needle-shaped particles typical of C-S-H, confirmed by EDS spectrum, and evident micro-porosity at 7 days.

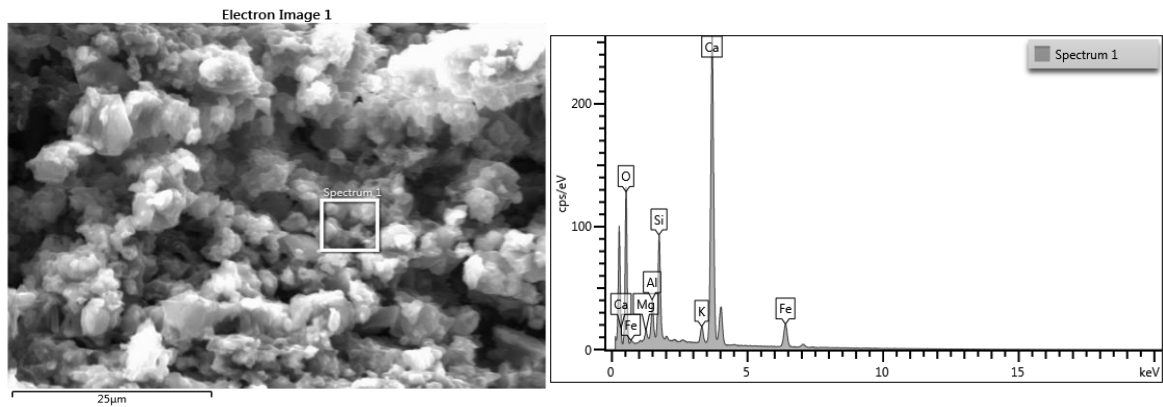


Figure 4-18: Lime-SCBA 1 paste showing the porous structure with CASH phases identified by EDS at 7 days.

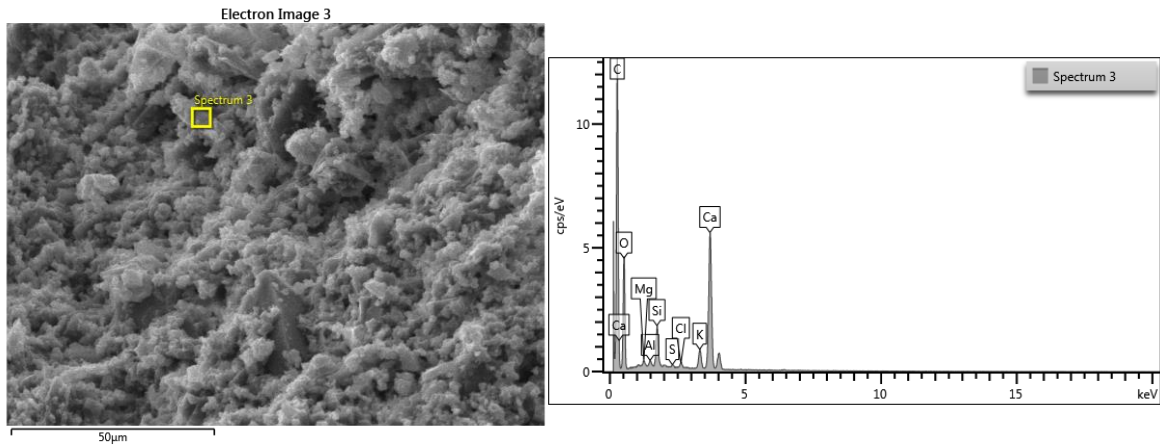


Figure 4-19: Porous character of Lime-SCBA 2 paste at 28 days with evident prismatic particles.

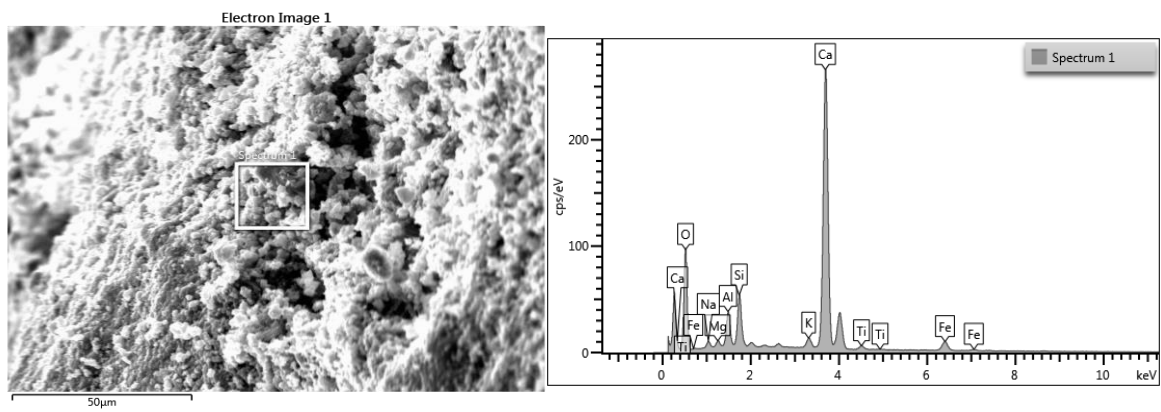


Figure 4-20: Lime-IBA 1 paste showing elevated micro porosity and eventual formation of needles at 7 days.

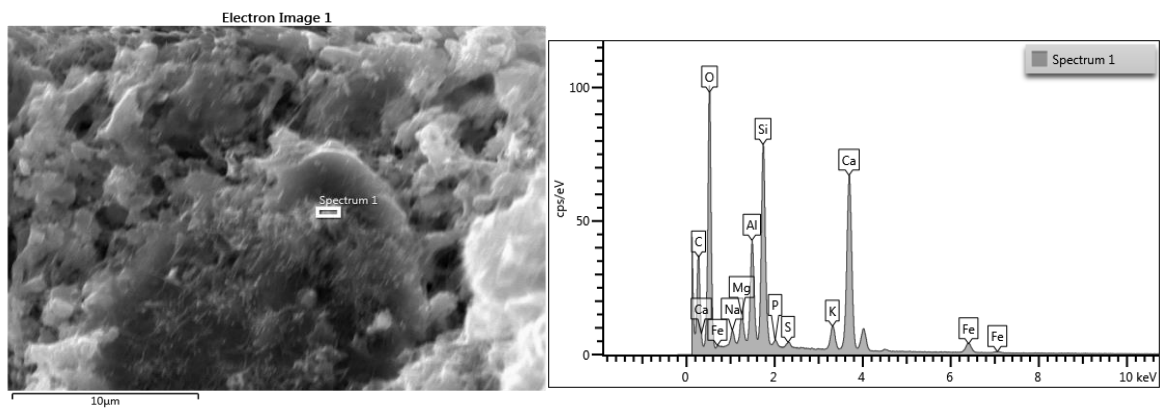


Figure 4-21: CASH identified in lime-IBA 1 paste at 28 days.

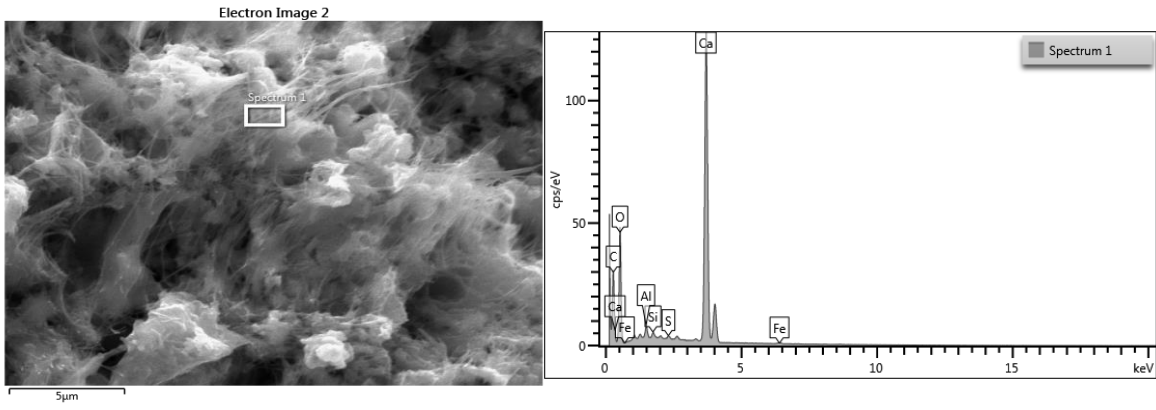


Figure 4-22: Lime-IBA 1 paste showing the morphology and composition of the paste during hydration at 28 days.

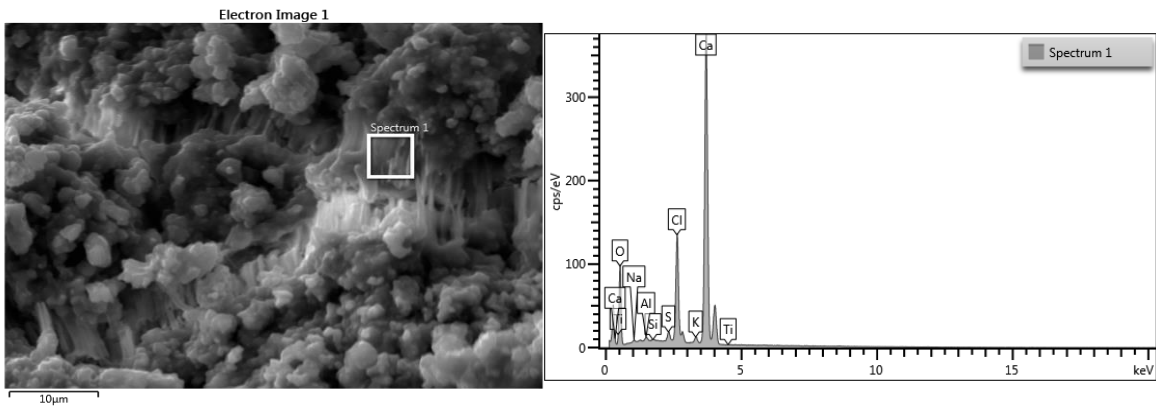


Figure 4-23: Lime-FA 1 paste with evident salt efflorescence.

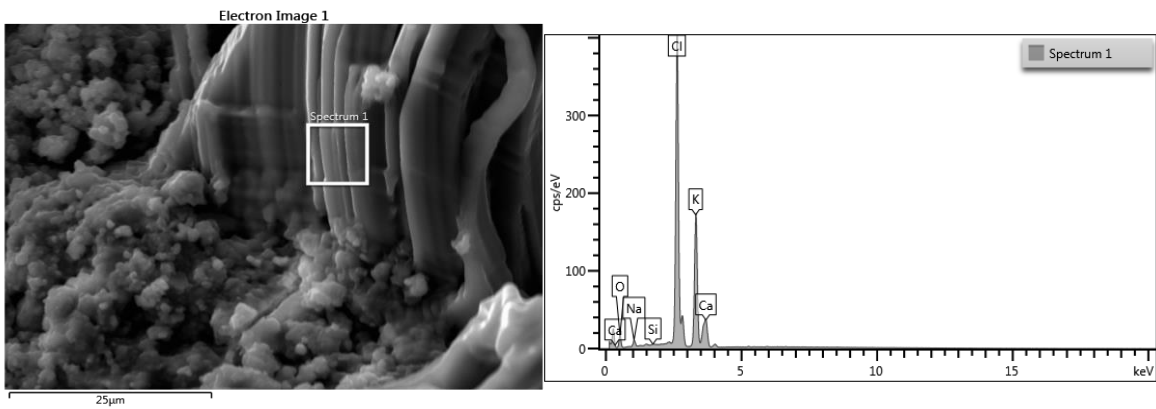


Figure 4-24: Lime-FA 1 paste with efflorescence of salt crystals at 7 days.

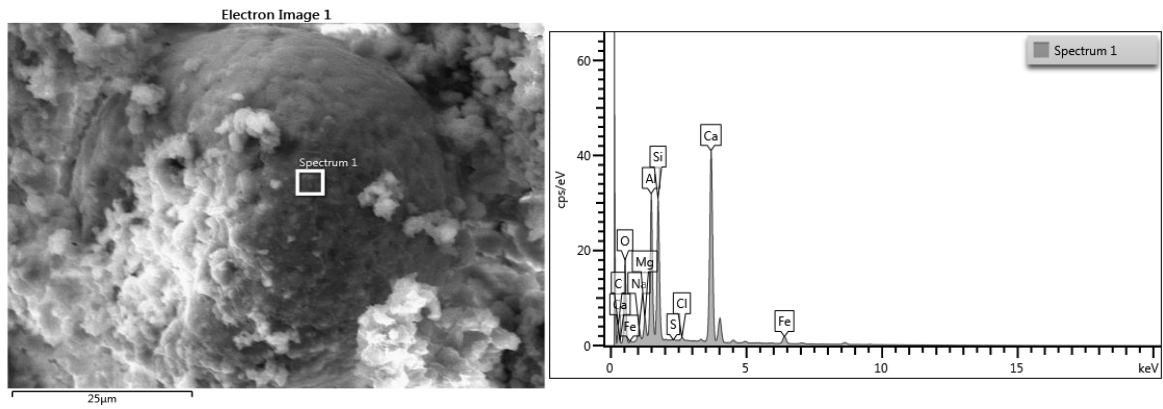


Figure 4-25: Lime-FA 2 paste showing a particle covered with calcium aluminate silicate hydrate phase at 28 days.

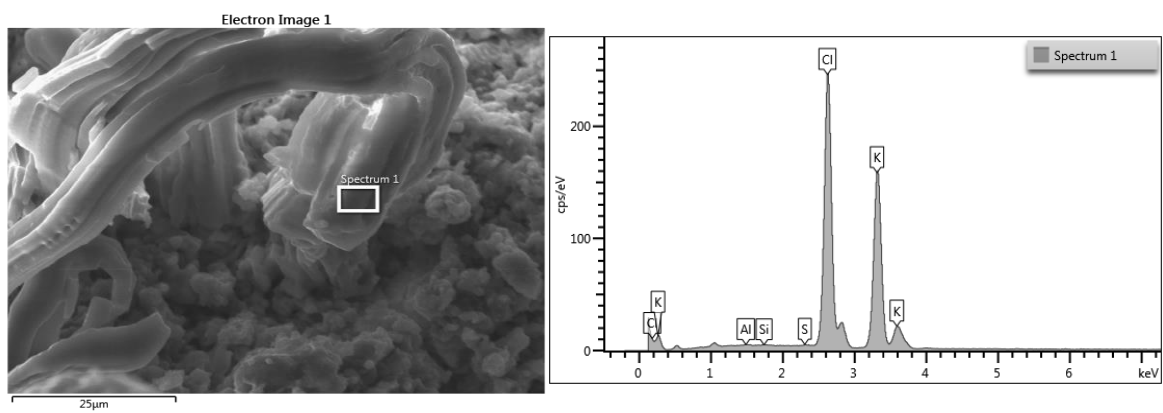


Figure 4-26: Lime-FA 2 paste showing crystallised salt at 28 days.

This page intentionally left blank

5 RESULTS – PROPERTIES OF ASH-COMPOSITES

On the second stage of the research, the best performers of stage one were selected for further investigation. The most reactive amongst the sugar and incinerator ashes (SCBA 1, SCBA 2, IBA 1 and IBA 2) were used as partial binder replacement to produce composites for construction. All 3 fly ashes were investigated on the second stage of research. The results are presented below.

Given the low strength results of the coarse incinerator bottom ashes, these materials were not considered for further investigation.

In addition, SCBA 3 and SCBA 4 were investigated as partial sand replacement in mortars and used as received with no particle size reduction. Hence, they received a new notation: SBAS (sugarcane bagasse ash sand) 1 and 2 respectively. According to Cordeiro and Kurtis (2017), the chemical composition and crystalline phases of ground and unprocessed SCBAs remain the same therefore, these properties are not altered by the grinding process and thus the properties of SCBA 3 and SCBA 4 in Section 4.2 are extrapolated to SBAS 1 and 2.

All the studied ashes were used as replacement at levels of 5%, 10% and 20%. For each of the replacement levels a number of specimens were produced, as detailed in Table 5-1.

Table 5-1: Number of specimens per test per level of replacement.

Tests	Number of Specimens
Reactivity by Conductivity	3
Reactivity by Strength Dev.	6
Capillary Action	3
Open Porosity	3
Bulk Density	3
Real Density	3
Thermal Conductivity	3
Specific Heat Capacity	4
Flexural Strength	3
Compressive Strength	3
Water Vapour Permeability	3
Durability	3
Resistance to Salt Crystallisation	3
Resistance to Freeze-thaw	3

5.1 BULK AND REAL DENSITIES

SBAS 1, SCBA 2, IBA 1, IBA 2, FA 1, FA 2 (at 10%) and FA 3 significantly reduce the real density of the reference PC mortar (0.05 level of significance) while the ashes present a slight, but not statistically significant, reduction.

The bulk density results show a smaller number of significant variations. The results show that samples produced with SBAS 1 (at 5 and 10%), SBAS 2 (at 5 and 20%), SCBA 2 (at 5 and 10%) and FA 3 (at 10%) significantly increase bulk density, whereas composites produced with IBA 1, IBA 2, FA 1 (at 10 and 20%) and FA 2 (at 10 and 20%) significantly reduce this property. The variations due to other ashes are not significant statistically.

Figure 5-1 presents the real and bulk densities of composites. From the results, it is evidenced that the incineration ashes (BAs and FAs 1 and 2) have greater differences between bulk and real densities, indicating that they possess a larger amount of voids. Particularly at higher levels of replacement. In contrast, the materials with sugarcane ashes (SBASs, SCBAs and FA 3) show denser structures, hence greater bulk densities and lower real densities, which reflect the microstructure enhancement caused by the ash. In particular, the sugarcane bagasse ash sand (SBAS 1) produces the densest structure with the smallest gap between densities, agreeing with the open porosity results in the previous Section. SBAS 1 at 10% replacement achieved a real density of 2231.33 kg/m³, representing a drop of 6.2% compared with the reference mix (2380.06 kg/m³), while the bulk density increased by 2.5%, and conferred the specimens the densest microstructure amongst all ashes.

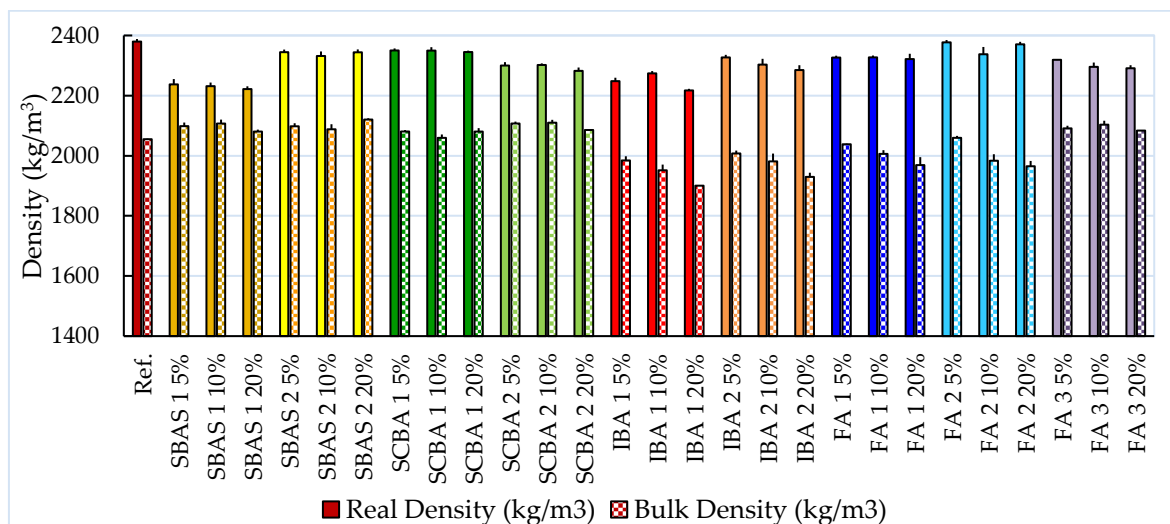


Figure 5-1: Real and bulk densities of Portland cement:pozzolan mortars.

It is observed that the mortars with bottom ashes (IBAs) generally achieve the lowest bulk density, ranging from 1900.4 to 2007.5 kg/m³. These values are similar to those found by Kim et al. (2012) in a study using fine bottom ash aggregates.

5.2 OPEN POROSITY

The values of porosity accessible to water (pores greater than 0.1 μm) are given in Figure 5-2. The porosities of the different mortars vary significantly from 5.6% (SBAS 1 10% sand replacement) to 17.1% (FA 2 20% binder replacement).

It was expected that the ashes would modify the pore structure of the composites, causing the segmentation of large pores and reducing porosity. This is the case for ash/sand composites SBAS 1 and 2 and cement/ash composites SCBA 1 and 2, FA 3 and IBA 1 5% which lowered the porosity of the reference mix. This can be related to the higher amount of particles greater than 45 μm (difficult to hydrate – see Section 4.1) of incinerator bottom ashes and fly ashes. Furthermore, the amorphousness of bottom ashes and incinerator fly ashes were lower compared to the other ashes, which confer lower reactivity.

As expected, the finest and most reactive ashes (SCBA 1 and SCBA 2) used as cement replacement lowered porosity the most, due to both the physical filler effect and the production of hydrates. However, coarse sugarcane ashes used as sand replacement SBAS 1 and 2 (SCBA 3 and 4 in Table 4-21) substantially lowered porosity despite their poor reactivity.

After this sand-ash, the next two ashes that significantly lower the porosity of the PC composites are SCBA 2 and FA 3. This agrees with the reactivity rating of the ashes as SCBA 2 is the finest, it has amorphous content and the greatest specific surface area; furthermore, it is rated as the most reactive (mechanical index) and amongst the most reactive chemically. Similarly, FA 3 was rated amongst the most reactive however, it is coarser, and has lower specific surface area and amorphousness.

On view of the above, there seems to be a mismatch between the properties of the ashes and the effect they cause in the composites. In addition, reactivity (hydrate production) seems to override the physical effect.

Increasing the amount of ash does not strongly impact the porosity except for the FAs. In particular FA 1 and 2 show a clear trend: an increase in porosity with increasing amounts of ashes in the composites (from 12 to 15% and 13 to 17% respectively). The IBAs also tend to increase the porosity as the ash content escalates (in IBA 1 and 2, c. 11 becomes 14% and 13 raises to 15% respectively) however, the porosity increment is lower. In contrast, in the other ashes, this tendency is either not so clear or reversed (i.e. increasing the amount of ash lowers the porosity of the composites e.g. FA 3 and SCBA 1).

Chindaprasirt and Rukzon (2008) found comparable results when studying pozzolanic materials including fly ash and rice husk ash at 10 and 20% replacements at 28 days. Their reference specimens achieved 13.7% porosity while their ash mortars ranged from 12.9 to 13.3%. Similarly, Pandey and Sharma (2000) found porosities ranging between 12 and 14% for PC mortars with pozzolanic materials, such as fly ash and granulated blast furnace slag.

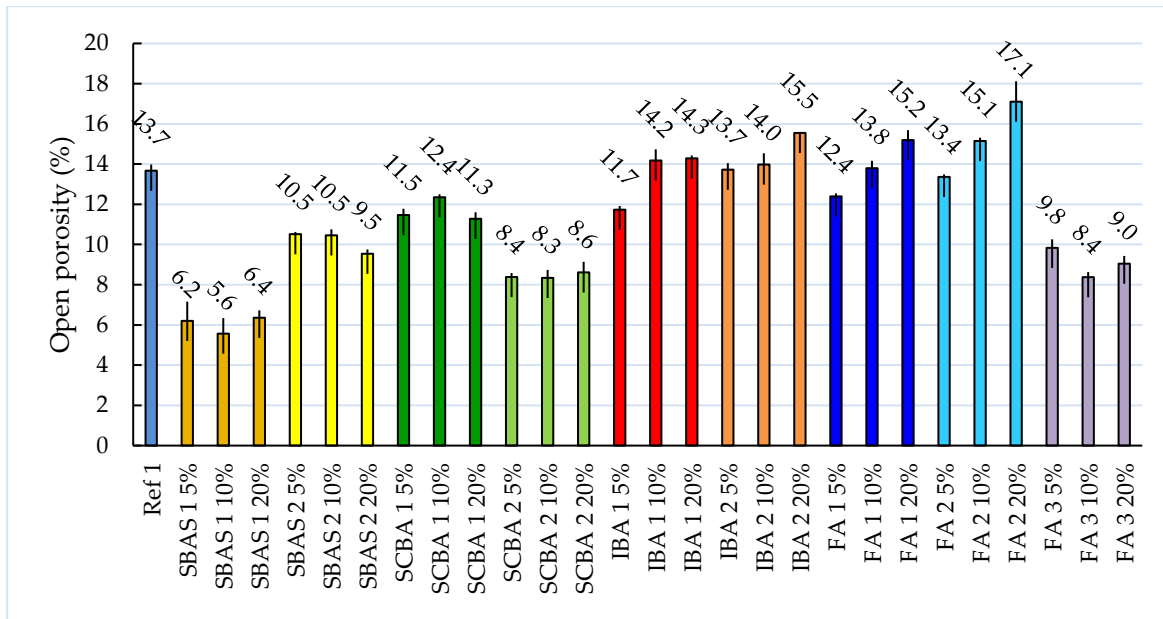


Figure 5-2: Open porosity available to water.

5.3 CAPILLARY ACTION

As reviewed in the background, there is no agreement on the effect of pozzolans and SCMs on hygric properties, with some authors reporting increase and others a decrease in moisture transport. The capillary uptake over time (Figure 5-3) and the coefficient of water absorption (Table 5-2) evidenced that only the incinerator fly ashes (FAs 1 and 2) increased the capillarity of the reference composite while the others tend to lower it: in particular the IBA 2 and the SBAS ashes, with approximately half the coefficient of the reference material. The IBA 2 presents the lowest water uptake by capillarity in the first 24 hours (4 – 5 g).

The capillary suction results mostly agree with the porosity results as most ashes (FA 3, SCBAs and the SBAS) lower both capillarity and porosity. The well-known fragmentation of the pore system typically triggered by pozzolans can be partially responsible for this.

The IBAs lower capillarity but they slightly raise porosity however not substantially. In contrast, the incinerator fly ashes (FAs 1 and 2) increased both capillarity and porosity.

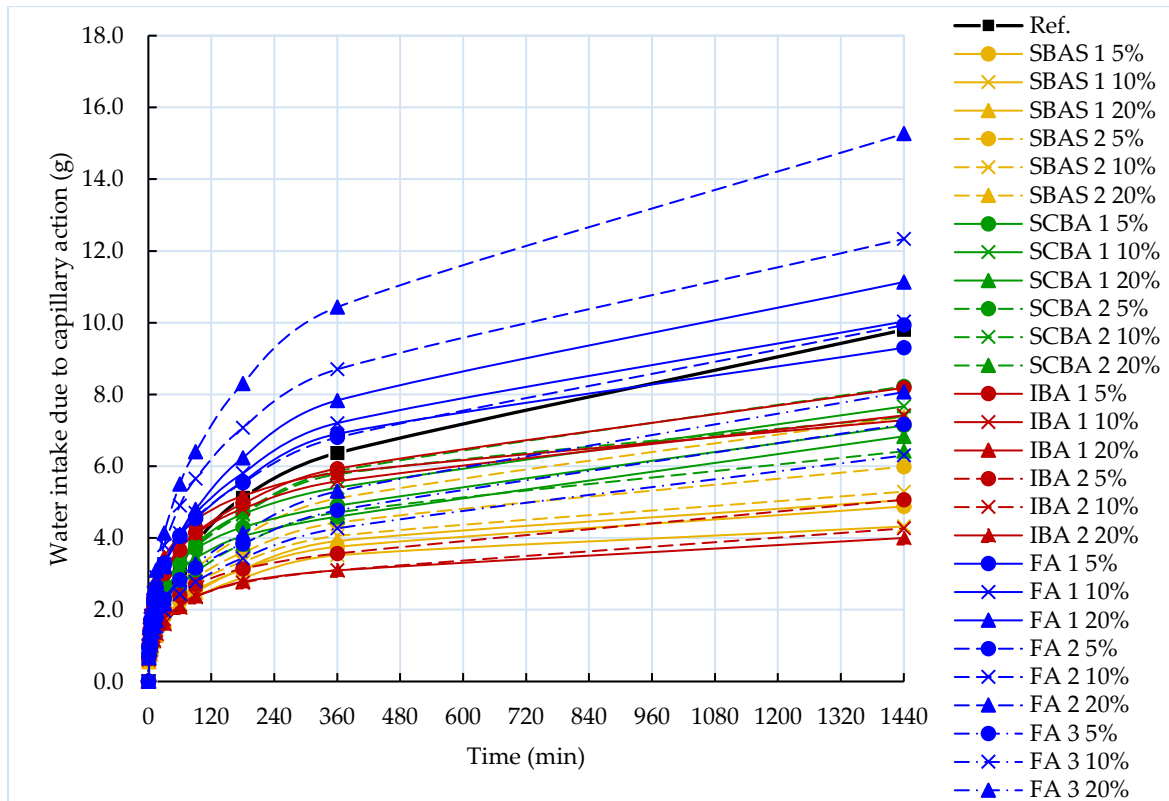


Figure 5-3: Water absorption by capillary action over time.

Figure 5-4 shows the relationship between capillary action and porosity. It is observed that, in most of the materials, capillary suction raises with increasing porosity up to a point (around 10-11% porosity), and decline past that point, evidencing that, as known, only certain pore spaces contribute to capillary suction, and increasing porosity or pore sizes of a composite reduces the tractive forces that transport moisture upwards in the material, reducing capillary action.

Table 5-2: Coefficient of water absorption C (in kg/(m².min)) – R² in brackets (Reference = 0.25 (0.96)).

Material	Replacement level		
	5%	10%	20%
SBAS 1	0.12 (0.91)	0.12 (0.88)	0.14 (0.91)
SBAS 2	0.15 (0.92)	0.14 (0.91)	0.18 (0.96)
SCBA 1	0.19 (0.91)	0.21 (0.92)	0.17 (0.92)
SCBA 2	0.20 (0.94)	0.21 (0.94)	0.16 (0.90)
IBA 1	0.20 (0.93)	0.18 (0.90)	0.20 (0.86)
IBA 2	0.13 (0.92)	0.11 (0.90)	0.12 (0.88)
FA 1	0.23 (0.92)	0.25 (0.94)	0.28 (0.95)
FA 2	0.24 (0.95)	0.32 (0.94)	0.38 (0.95)
FA 3	0.16 (0.96)	0.14 (0.96)	0.17 (0.97)

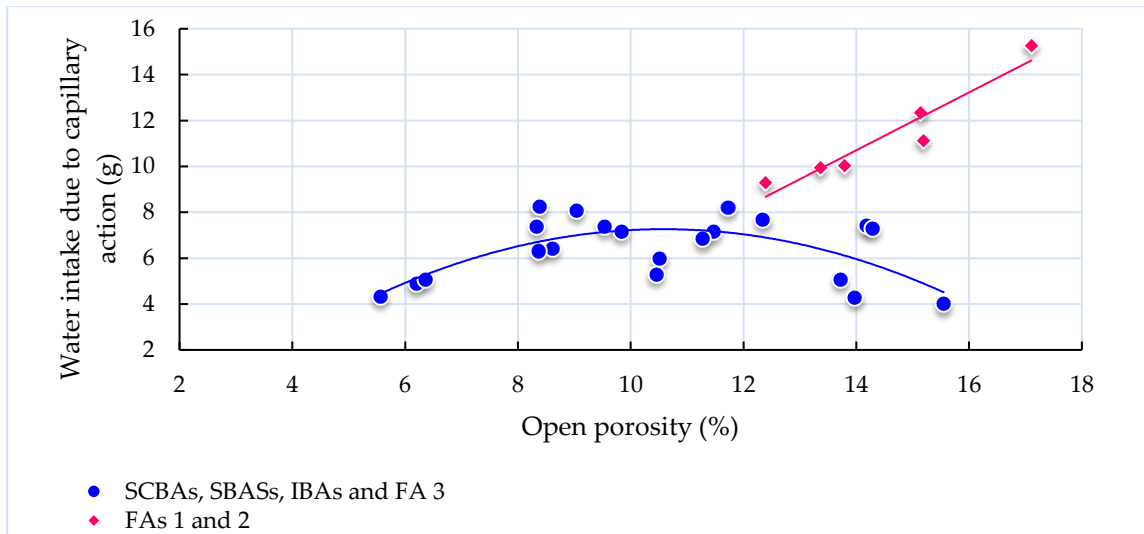


Figure 5-4: Relationship between open porosity and water intake due to capillary action.

The fly ash mortars have the highest capillarity, especially FA 2, which increases the coefficient of the reference material by 52% at 20% replacement. In the first 24 hours, the FA 2 takes up 55.7% more water by capillarity than the reference material. In addition, the capillarity of the incinerator fly ash materials increases as the amount of ash increases, a trend not found in the other ashes. Furthermore, fly ashes 1 and 2 behave in a different manner as capillarity and porosity show a linear relationship where both properties raise simultaneously.

These can be related to the chlorine content in the ashes, as salts crystallise at the open ends of capillary systems where outward-moving moisture is the vehicle of transport (Winkler, 2013b). There is a general relationship between the chlorine content and water intake in the ashes studied - Figure 5-5 (Pearson correlation = 0.808). This is likely due to the hygroscopic characteristics of chlorides increasing the water uptake and enhancing tractive forces of in small pores.

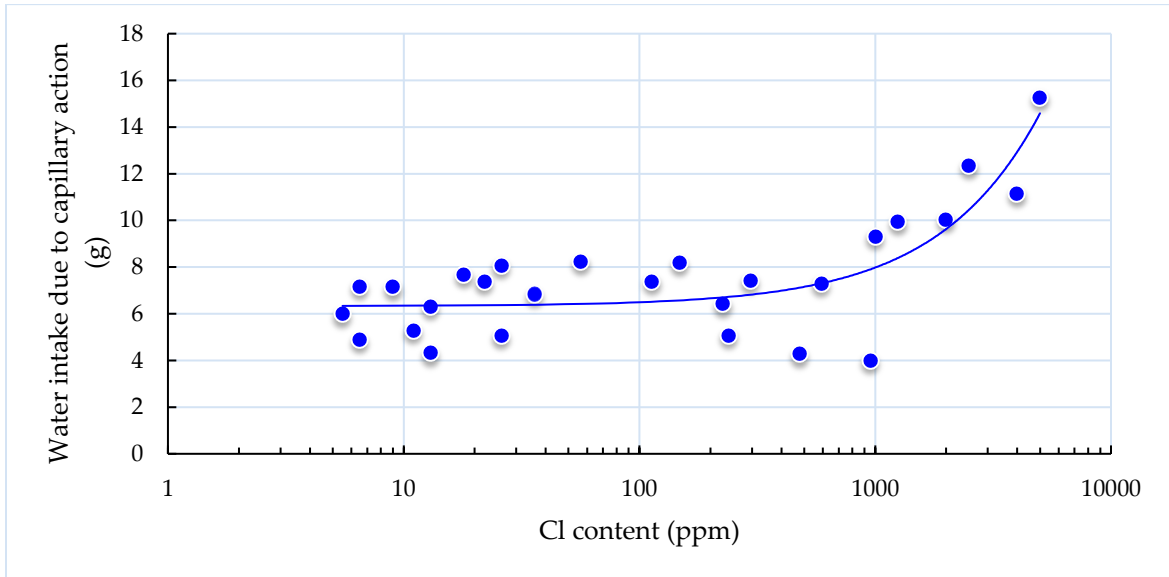


Figure 5-5: Relationship between chlorine content and the water intake due to capillary action.

As illustrated in Figure 5-6 – Figure 5-9, the water sorption coefficients clearly evidence that the incinerator fly ash materials (FA 1 and 2) absorb water more rapidly than the other composites which further supports the hygroscopicity of the materials.

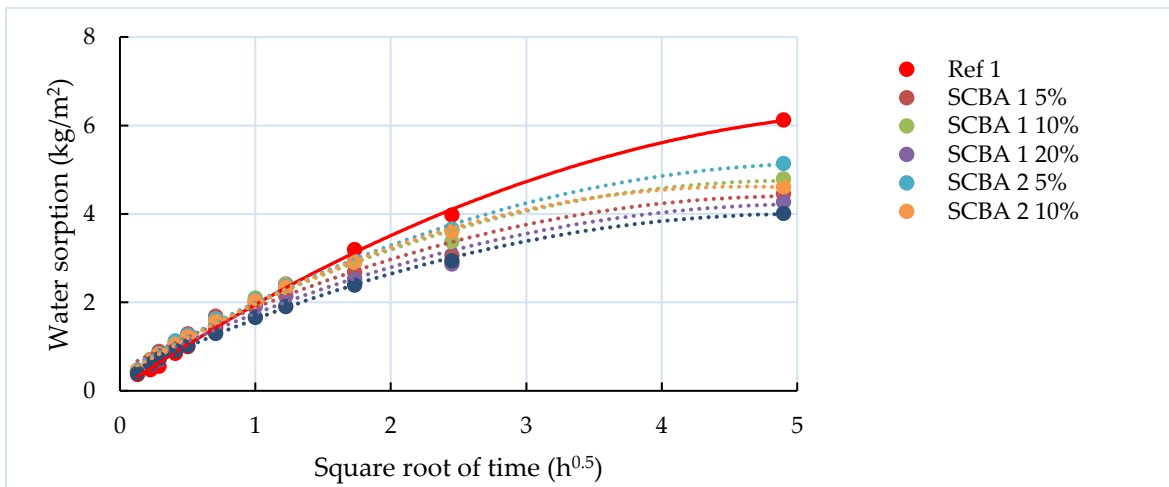


Figure 5-6: Water absorption coefficient of mortars with SCBA ashes in comparison with the reference specimens.

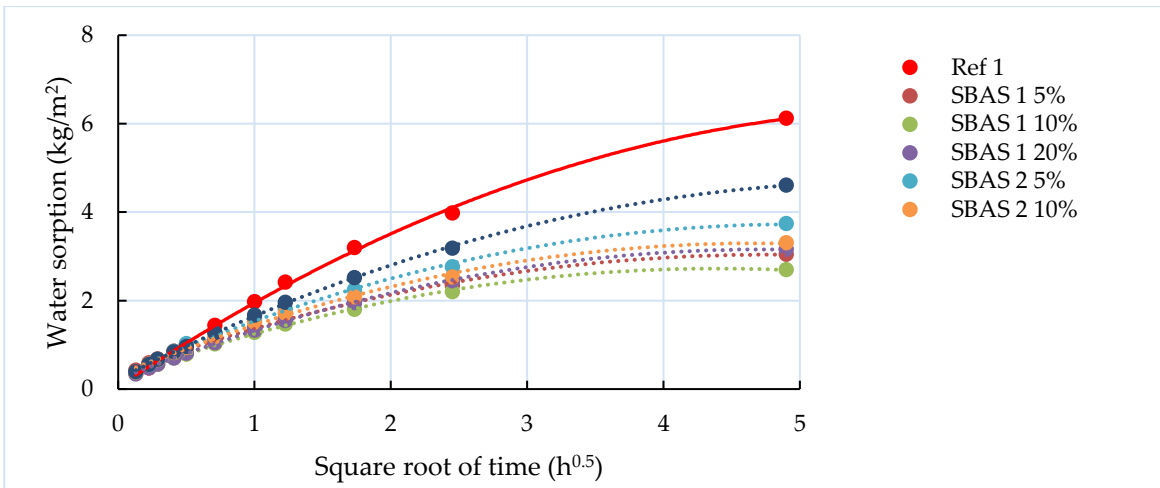


Figure 5-7: Water absorption coefficient of mortars with SBAS ashes in comparison with the reference specimens.

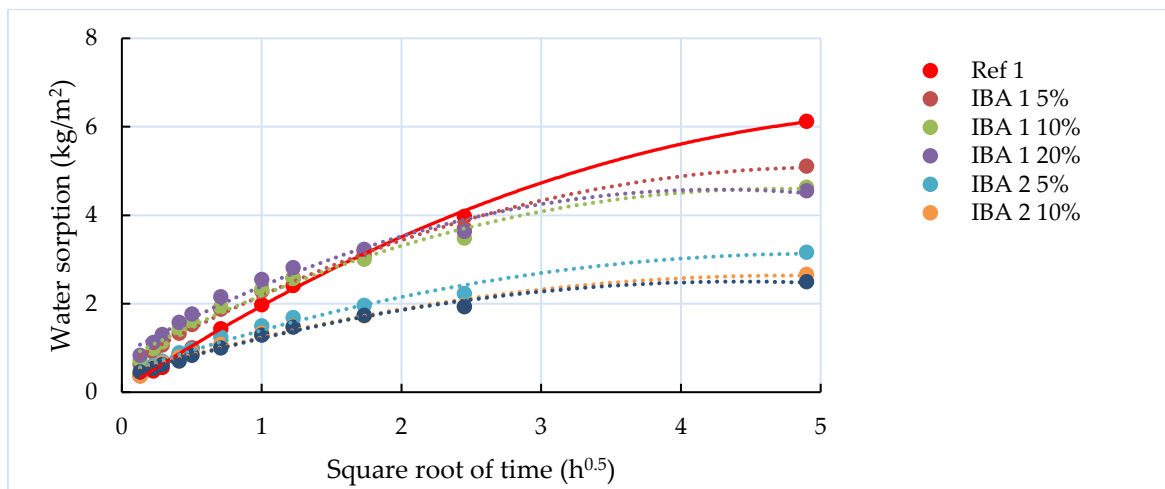


Figure 5-8: Water absorption coefficient of mortars with IBA ashes addition in comparison with the reference specimens.

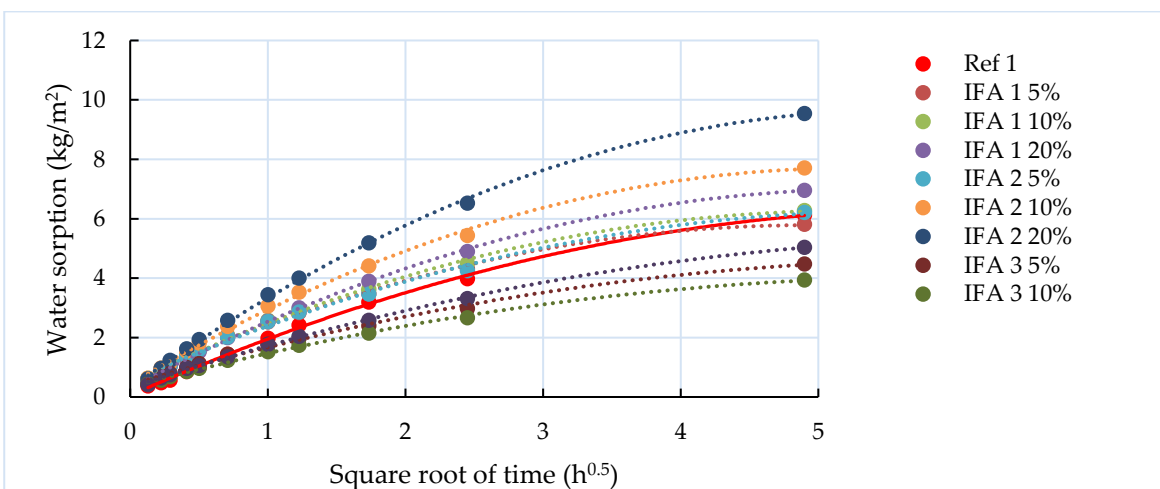


Figure 5-9: Water absorption coefficient of mortars with FA ashes compared with the reference specimens.

5.4 THERMAL PROPERTIES

5.4.1 Specific Heat Capacity

The specific heat capacity (amount of heat required per unit mass to change temperature by one degree) is significantly influenced by the moisture content in materials as well as their density and porosity.

The results (Table 5-3) evidenced that incorporating ashes lowers the specific heat capacity of cement composites however, the decline is not significant with the exception of ashes SCBA 1 and IBA 2 (at 20% replacement) which reached the lowest specific heat at 1.10 J/g°C - 24% lower than the reference composite (1.45 J/g°C).

These ashes are closely followed by the ash-sand mortars SBAS 1 and 2 which lowered the specific heat by 19-22%. In contrast, fly ash mortar FA 2 20% achieved the highest specific heat, however, still 9% lower than the reference cement mix. No statistically significant correlation was found to explain these results.

The results also show that increasing the ash content in the cement composites does not statistically significantly affect specific heat capacity. No consistent trend is evident as, with increasing ash content, some ashes slightly rise while others slightly decrease the heat capacity of the material.

The values measured here are typical of high density and high thermal mass materials such as concrete and rammed earth. The values are higher than those found by Xu and Chung (2000a), 0.782 J/g°C for mortars with 15% of silica fume as cement replacement and Vejmelková et al. (2012), who found values ranging from 0.904 to 0.962 J/g°C in lime mortars with clay shale.

Table 5-3: Specific heat capacity of mortars in J/g°C
(Reference cement composites average: 1.45 J/g°C).

Material	Replacement level		
	5%	10%	20%
SBAS 1	1.15	1.16	1.13
SBAS 2	1.12	1.15	1.17
SCBA 1	1.19	1.15	1.10
SCBA 2	1.25	1.22	1.25
IBA 1	1.14	1.18	1.16
IBA 2	1.18	1.16	1.10
FA 1	1.22	1.24	1.26
FA 2	1.2	1.30	1.32
FA 3	1.2	1.2	1.21

5.4.2 Thermal Conductivity, Thermal Mass and Diffusivity

The thermal conductivity was measured for each binder replacement level for one ash in each category. SCBA 2, SBAS 2, IBA 2 and FA 2 were selected on the basis of the material's availability, as some of the ashes were sourced overseas and were not easy to replace.

The detailed results are presented in Appendix A (Figure A - 1 to Figure A - 13). Despite the lack of gravel graded aggregate in the PC control material, the thermal conductivity (1.03 W/mK) is comparable to that of concretes of comparable density previously reported - 0.73 W/mK Corinaldesi et al. (2011); and 1.18 W/mK Demirboğa (2003).

As it can be seen from the thermal conductivity results in Table 5-5, all the ashes (either as cement or sand replacement) lowered the thermal conductivity of the cement composites. In fact, some ashes lowered over 30% of the reference conductivity. IBA 2 (10%) achieved the highest reduction at 39% while SCBA 2 (5%) lowered conductivity by 34% and SCBA 2 (20%), FA 2 (at 5 and 10% replacement) and IBA 2 (5%) reduced thermal conductivity by 31-32%. The greatest reduction experienced by IBA 2 can be explained by the lower density of the composite combined with a porosity, allowing greater air content (which possesses lower conductivity) within the composite, while the remaining ashes did not change significantly the densities.

The reduction in thermal conductivity agrees with the tendency of the ashes to reduce the density of the composites.

Aydın and Baradan (2007) explain that reductions in conductivity can also be related to the amorphous structure of minerals, as crystalline silica possesses conductivity around 15 times greater than the amorphous form.

There is a general relation between conductivity and porosity. The composites with the highest porosities, such as IBA 2 and FA 2, lower conductivity the furthest while the SBAS 2 materials (10% sand substitution by ash) with the lowest open porosity displayed the highest conductivity at 0.97 W/mK. This trend is explained by the much lower thermal conductivity of air (0.026 W/mK), more abundant in the composites with greater porosity.

A typical 300 mm thick wall of shuttered cement concrete construction of standard density 2380.06 kg/m³ has a U value of 3.44 W/m²K. By replacing 10% of the cement with IBA 2 (the ash with the lowest thermal conductivity 0.63 W/mK) the U value would significantly improve to 2.11 W/m²K.

According to the building regulations (Ireland, 2017) the standard requirement for the U-value of walls is 0.21 W/m²K. Considering a standard masonry cavity wall (Diagram A1- Technical Guidance Document L (Ireland, 2017)) of this U-value, it is possible to calculate the thickness of the composite block for the reference PC composite and the IBA 2 (10%) composite. The results (Table 5-4) evidence that the use of IBA 2 10% drops the block thickness by 40% which implies a significant economy of material.

Table 5-4: U-values of cavity walls including the reference and IBA 2 10% mixes, replacing the standard concrete blocks (thickness = 0.1 m; conductivity = 1.33 W/m K) -Technical Guidance Document L, Building Regulations 2017.

Layer surface	Thickness (m)	Conductivity (W/mK)	Resistance (m ² K/W)
External surface	-	-	0.04
External render	0.019	1	0.019
Reference	0.1	1.03	0.097
Air cavity	-	-	0.18
Insulation	0.1	0.023	4.348
Reference	0.1	1.03	0.097
Plaster (lightweight)	0.013	0.018	0.072
Internal surface	-	-	0.13
Total Resistance			4.983
U-value (W/m²K)			0.2007
U-value of construction = 1 / 4.983 = 0.20 W/m ² K			
Layer surface	Thickness (m)	Conductivity (W/mK)	Resistance (m ² K/W)
External surface	-	-	0.04
External render	0.019	1	0.019
IBA 2 10%	0.06	0.63	0.095
Air cavity	-	-	0.18
Insulation	0.1	0.023	4.348
IBA 2 10%	0.06	0.63	0.095
Plaster (lightweight)	0.013	0.018	0.072
Internal surface	-	-	0.13
Total Resistance			4.979
U-value (W/m²K)			0.2008
U-value of construction = 1 / 4.979 = 0.20 W/m ² K			

The conductivity of mortars with SCBA and FA ashes ranges between 0.68 and 0.78 W/mK, lower than the values found by Chousidis et al. (2016) with conductivities of 0.98 and 0.95 W/mK for concretes with 5 and 10% fly ash replacement respectively. However, the results are higher than those found by Xu and Chung (2000b) (using 15% silica fume replacement) achieving thermal conductivity of 0.54 W/mK, and higher than the results acquired by Aydın and Baradan (2007) when using fly ash as binder replacement at 20, 40 and 60% levels. The authors found values ranging from 0.52 W/mK (60% replacement) to 0.66 W/mK (20% replacement).

The thermal diffusivity indicates the ability of a material to respond to temperature variations. It is determined by the thermal conductivity, density and specific heat of the material. According to the results, the ashes generally lowered the thermal diffusivity of composites (Table 5-5). However, SBAS 2 10 and 20% increased diffusivity of the control composite, up to

23% (SBAS 2 10%), this is most probably due to the denser structure of SBAS, as discussed in Section 5.1, which gives the material a relatively high thermal conductivity in relation to its specific heat. IBA 2 20% also slightly increased conductivity due to its lower specific heat.

Thermal effusivity - ability of a material to exchange heat with its surroundings (surface property) - decreased with the incorporation of ashes. FA 2 5% presented the greatest reduction, 29% smaller than reference ($2796.98 \text{ J/m}^2\cdot\text{K}\cdot\text{s}^{0.5}$). While SBAS 2 10% caused the smallest drop, 10% lower than reference. This property is often analysed for materials with insulation properties, with much lower thermal effusivity, e.g. the thermal effusivity of hemp concrete of $231 \text{ J/m}^2\cdot\text{K}\cdot\text{s}^{0.5}$ (Maalouf et al., 2014) or lime-hemp concrete of $241.33 \text{ J/m}^2\cdot\text{K}\cdot\text{s}^{0.5}$ (Walker & Pavia, 2015).

The results for thermal mass (amount of heat that can be stored in a material) range between 251.05 and 279.25 $\text{kJ/m}^2\text{K}$, values 27 and 18% lower than those of the reference composite ($344.09 \text{ kJ/m}^2\text{K}$). As expected, the values are typical of high density materials with high thermal conductivity, substantially higher than those displayed by insulating materials such as aerogel ($12.25 \text{ kJ/m}^2\text{K}$), PIR foil ($12.44 \text{ kJ/m}^2\text{K}$) and lime plaster ($62.89 \text{ kJ/m}^2\text{K}$), Walker and Pavia (2015).

Table 5-5: Thermal properties of mortars.

Material	Thickness (m)	Thermal conductivity (k - W/(m.C))	Specific heat (J/g.C)	Density (kg/m ³)	Thermal mass (kJ/m ² .C)	Diffusivity (m ² /s (E-04))	Effusivity (Wm ⁻² C ⁻¹ s ^{-0.5})
	<i>L</i>	<i>k</i>	<i>C</i>	ρ	$L \times C \times \rho$	$k/(C \times \rho)$	$\sqrt{(k \times \rho \times C_p)}$
Ref.	0.1	1.03	1.45	2380.06	344.09	3.00	2796.98
SBAS 2 5%	0.1	0.76	1.12	2344.38	261.62	2.92	2286.80
SBAS 2 10%	0.1	0.97	1.15	2331.72	267.31	3.69	2634.65
SBAS 2 20%	0.1	0.84	1.17	2343.92	273.25	3.09	2510.74
SCBA 2 5%	0.1	0.68	1.19	2350.09	279.25	2.43	2298.81
SCBA 2 10%	0.1	0.78	1.15	2349.58	270.04	2.90	2389.39
SCBA 2 20%	0.1	0.70	1.10	2344.79	257.78	2.73	2161.98
IBA 2 5%	0.1	0.71	1.18	2326.87	273.95	2.57	2300.59
IBA 2 10%	0.1	0.63	1.16	2303.03	267.65	2.37	2131.42
IBA 2 20%	0.1	0.79	1.10	2284.87	251.05	3.15	2400.43
FA 2 5%	0.1	0.70	1.12	2377.07	265.27	2.64	1973.81
FA 2 10%	0.1	0.70	1.15	2337.44	267.96	2.61	2012.15
FA 2 20%	0.1	0.76	1.17	2370.44	276.32	2.75	2125.05

5.5 MECHANICAL PROPERTIES OF THE ASH COMPOSITES

5.5.1 Flexural Strength

The 28-day flexural strength of mortars produced with ash replacement of sand and cement are shown in Figure 5-10. Deboucha et al. (2017) found flexural strengths of around 8MPa for PC replacement levels of 10 and 20% by natural pozzolan. This roughly agrees with the results, especially for IBA 2 and FAs at 5%.

As it can be seen from the results, the SBAS 2 (5%) materials attained the highest flexural strength (10.02 MPa) closely followed by the reference test specimen (9.88 MPa). Most mortars achieved around or over 70% of the reference strength except for SCBA 2 20%, IBA 1 20% and FA 2 20% with slightly lower strength.

In the lime pastes (Table 4-23) the fly ashes (from the sugar and incinerator industries: FA 1, 2 and 3) reached outstanding flexural strengths. However, in the cement composites, it is the SCBA 4 ash (used to make the SBAS 2) that reaches the greatest flexural strength. This result may have been influenced by the presence of additional amorphous silica in the ash/sand combined with the absence of the dilution effect, as the cement content was not reduced.

The flexural strength usually lowers as the amount of ash replacement increases however, there are small inconsistencies for SCBA 1 and IBA 1 which present higher strength at 10% replacement followed by 5% and finally 20%. The sand-ash materials– SBAS 1 and SBAS 2 -, on the other hand, have lower flexural strength at 10% replacement.

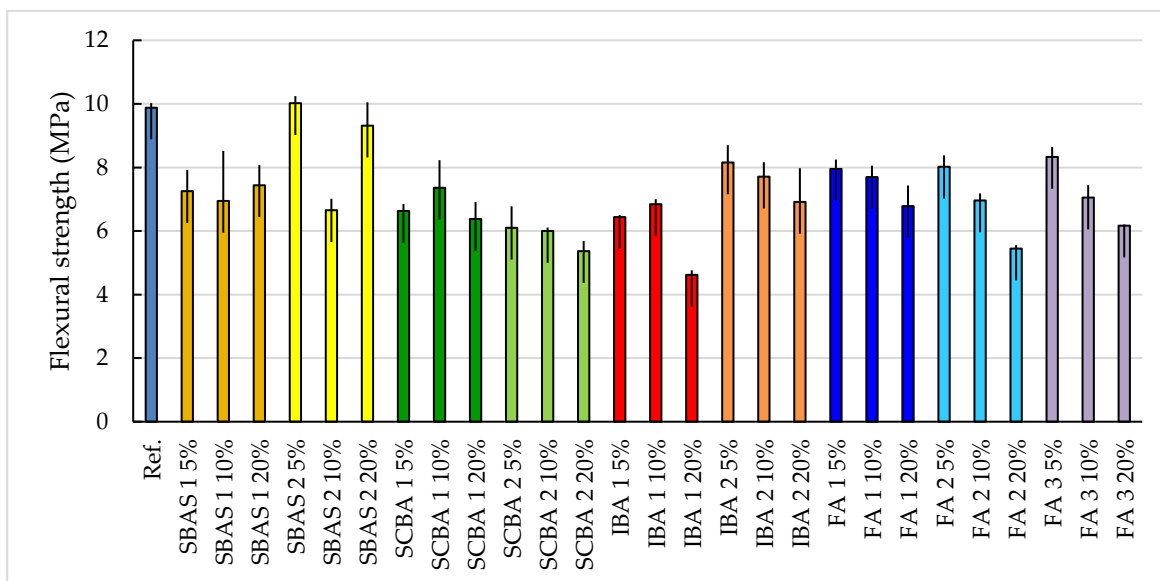


Figure 5-10: Flexural strength of mortars.

Wongkeo et al. (2012), investigating bottom ash in lightweight concrete, observed that the increase in flexural strength was related to the increase in bulk density of the concrete. The same relationship is true for the flexural strength of bottom ash composites, however, no general relationship between density and flexural strength occur for the other ashes. Additionally, irregular shaped particles with lower pozzolanic activity, as observed in the ashes (see Section 4.3), act as filler in mortar matrix enhancing the interlocking between aggregate and paste contributing to flexural strength (Tang et al., 2016), which further supports the bottom ash results.

The reduction in flexural strength in incinerator fly ash composites can also be caused by the presence of salts, as seen in Section 4.6, however, the strength produced by fly ashes at 5% replacement level was superior than the strength of sugarcane fly ashes, which showed more hydrates (calcium silicate hydrates and calcium silicates aluminates hydrates) in pastes (see Section 4.6).

5.5.2 Compressive Strength

The ash composites reached significant strength, only three mortars (IBA 1 20%, IBA 2 20% and FA 2 20%) did not attain the lower limit of 30 MPa at 28 days in EN 197-1 (2011) for strength class 32.5 - lowest in the standard - however, they still reached high strengths (24.4, 29.5 and 29.1 MPa respectively). This limit value is represented by the red line in Figure 5-11.

The SCBA, SBAS and FA ashes achieved strengths over 30 MPa at all replacement levels. In particular, SBAS 2 attained higher strength than the reference PC material at all substitution levels, which shows the enhancement of packing of composites with this fine aggregate.

The loss in compressive strength experienced by mortars with bottom ash are higher than other reported in the literature. Li et al. (2012) report a 19% strength loss compared to the reference at 20% replacement while Figure 5-11 evidences losses of 46% and 35% for IBA 1 and 2 at 20% replacement. The reduced strength is also a result of the dilution effect caused by higher cement replacement (Wild et al., 1996).

A general linear relationship exists between compressive strength and real density ($y = 0.0873x - 139.25$ ($R^2 = 0.57$)) in which the increase of density is accompanied by a more or less proportional increase in mechanical strength. This relationship is presented in Figure 5-12.

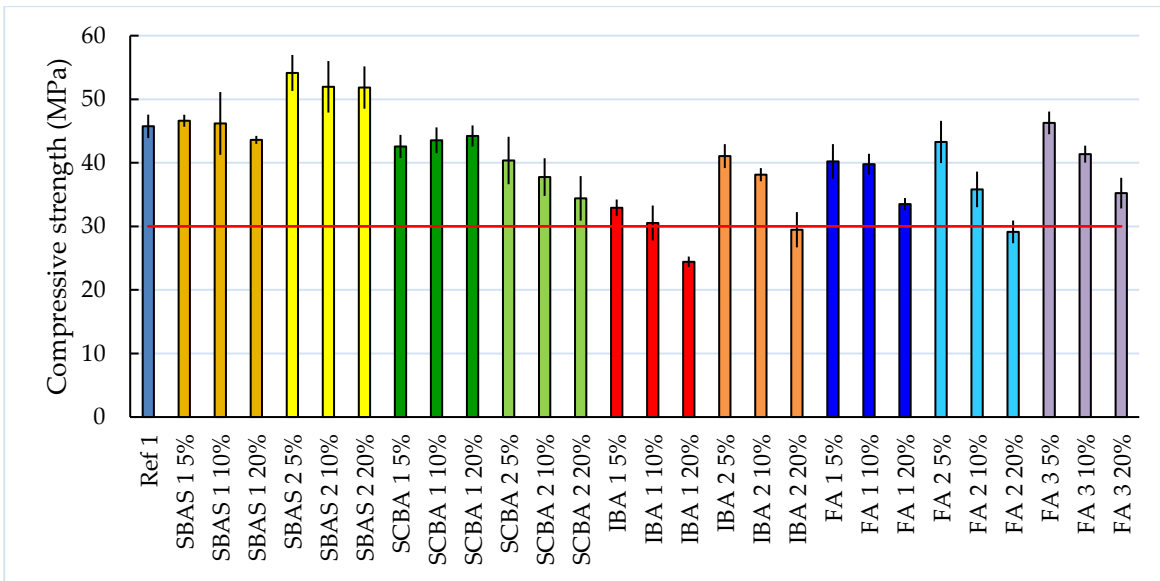


Figure 5-11: Compressive strength of mortars at 28 days.

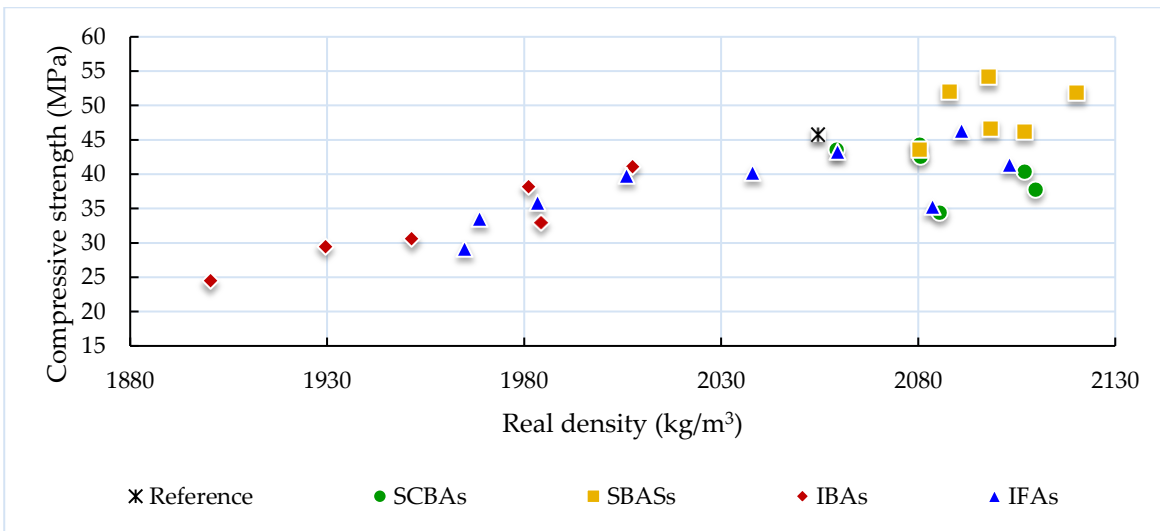


Figure 5-12: Relationship between real density and compressive strength.

5.5.3 Modulus of Elasticity

The modulus of elasticity (MOE) describes the stiffness of a solid material. When subjected to mechanical deformation, a material stores energy either elastically or dissipates it plastically. This process is summarized in stress-strain curves. The static modulus of elasticity is defined as the slope of the stress-strain relationship at origin. The MOE at failure (Table 5-6) was calculated based on the maximum stress and strain. The stress-strain curves are presented in Appendix B. It is observed that increased compressive strength implies an increase in toughness, with the compressive strength and the MOE showing a good correlation ($\rho = 0.901$) (see Figure 5-13).

The addition of ashes lowered the MOE in relation to the reference mortar, with the exception of FA 3 5%, which exceeded the reference MOE by 1.8%. Sata et al. (2007) also found a positive relationship between compressive strength and MOE of concrete with traditional pozzolanic materials – fly ash and rice husk ash. Though some SBASs mixes reached greater compressive strength, the reference mortar still presented a higher modulus of elasticity, this differs from what was observed by Siddique (2003) when using fly ash as sand replacement in concrete. The author found that the MOE of concretes produced with 10 – 50% fine aggregate replacement were higher than the control mix and continued to increase with the increase in fly ash content, which is also different from what was observed on the results of sand replacement by SBASs, which do not show a particular trend with respect to level of replacement. Therefore, the SBAS ashes increase the mechanical resistance in compression, however maintaining a level of plasticity as they increase the compressive strength of the reference material while keeping its MOE lower.

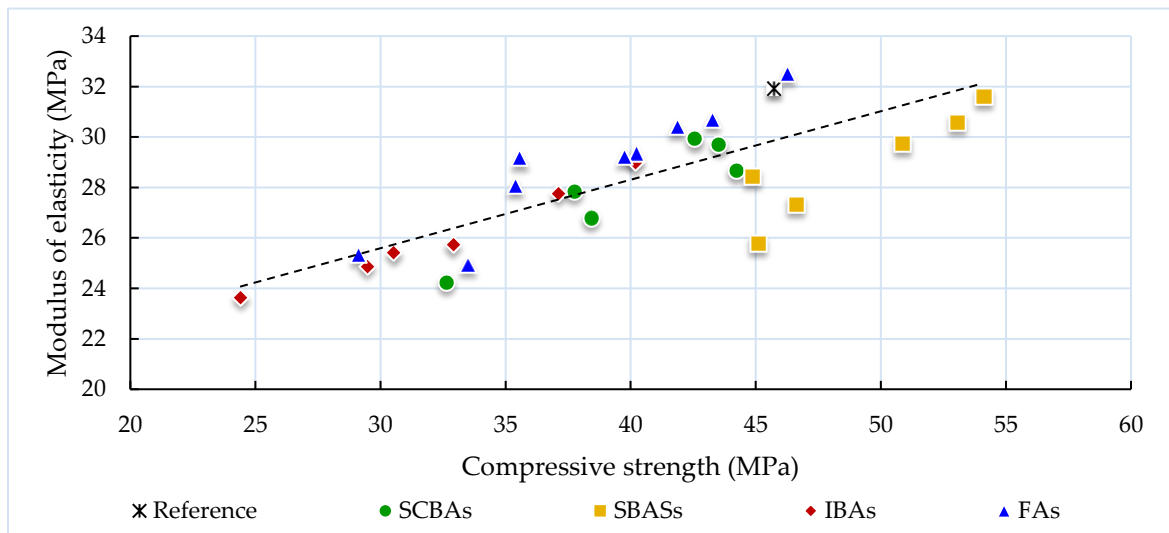


Figure 5-13: Relationship between compressive strength and modulus of elasticity.

Table 5-6: Modulus of elasticity.

Material	Force (N)	Strain)	MOE (MPa)
Reference	73173.52	1.43	31.91
SBAS 1 5%	74587.39	1.76	27.33
SBAS 1 10%	72170.41	1.76	25.76
SBAS 1 20%	71807.48	1.59	28.42
SBAS 2 5%	86618.32	1.72	31.59
SBAS 2 10%	81390.88	1.71	29.72
SBAS 2 20%	84908.67	1.74	30.58
SCBA 1 5%	68105.71	1.43	29.92
SCBA 1 10%	69662.02	1.47	29.68
SCBA 1 20%	70759.06	1.54	28.66
SCBA 2 5%	61488.12	1.45	26.78
SCBA 2 10%	60410.89	1.35	27.85
SCBA 2 20%	52237.08	1.35	24.24
IBA 1 5%	52673.41	1.29	25.71
IBA 1 10%	48852.08	1.20	25.39
IBA 1 20%	39076.47	1.03	23.63
IBA 2 5%	64289.58	1.39	28.98
IBA 2 10%	59397.18	1.34	27.77
IBA 2 20%	47153.75	1.19	24.87
FA 1 5%	64351.92	1.37	29.36
FA 1 10%	63649.96	1.36	29.22
FA 1 20%	53602.88	1.35	24.94
FA 2 5%	69245.53	1.41	30.70
FA 2 10%	56932.82	1.22	29.17
FA 2 20%	46609.42	1.15	25.34
FA 3 5%	74045.92	1.42	32.51
FA 3 10%	67004.36	1.38	30.40
FA 3 20%	56633.43	1.26	28.07

5.6 RESISTANCE TO SALT CRYSTALLISATION

The resistance of the ash materials to damage by salt crystallisation was evaluated using magnesium sulphate which, as stated by Massazza (1998), is capable of producing the strongest damage, forming compounds such as ettringite and gypsum causing expansion leading to fracturing.

As it can be seen from the results, most of the ashes improved the resistance of PC composites to damage by salt crystallization (Figure 5-14). The progress of deterioration of each specimen was monitored closely. Detailed photographs of each tested specimen are available in Appendix C. Moreover, the weight variation, expressed as a percentage of the initial dry

weight was calculated according to RILEM (1980) and is presented in Figure 5-14. It was observed that the reference specimens had the highest mass loss, losing 2.7% of their weight. These were followed by the mortars produced with SCBA 1 at 20% binder replacement with a much lower weight loss at 0.31%. SCBA 1 10% presented the smallest variation in mass, losing 0.03% in weight.

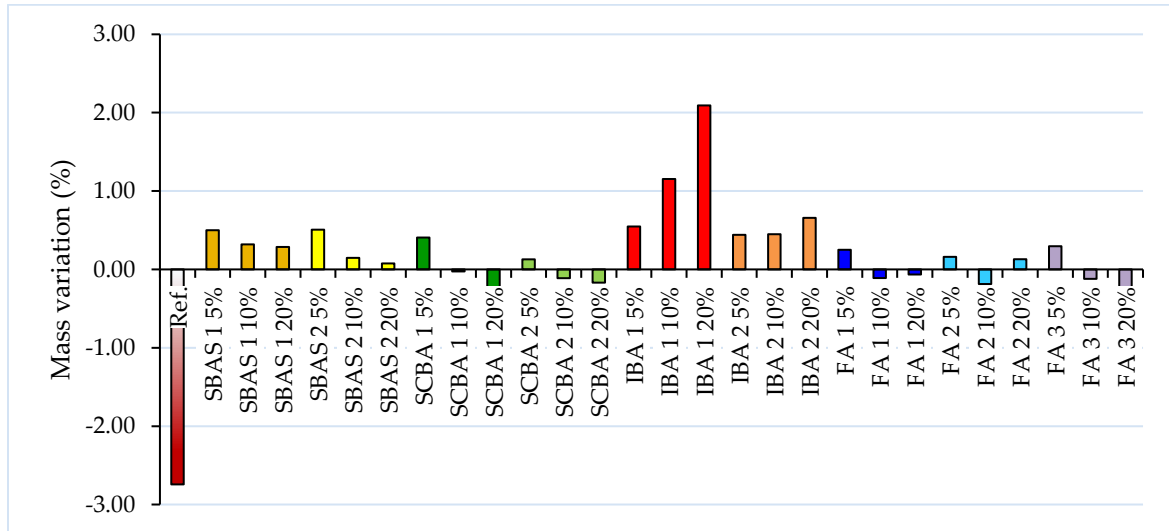


Figure 5-14: Mass change of mortars exposed to salt crystallisation resistance test.

Weight increase due to salt attack in construction materials with pozzolans has been observed by previous authors (Khatib & Wild, 1998; Torii & Kawamura, 1994; Walker, 2013). Most of the ash mortars increased weight. IBA 1 20% shows the largest mass increase (2.09%) followed by IBA 1 10% and IBA 1 5%, with increases of 1.15 and 0.55% respectively. The crystallisation of salt within the pore structure, which caused the greatest mass increase in IBA 1, is further evidenced in Figure 5-15. Specimens that presented cavities on their surfaces favoured the attachment of salt (Figure 5-16). This was observed in specimens produced with SCBAs 1 and 2, SBAS 2, IBAs 1 and 2 and FAs 2 and 3 (see Appendix C).

In order to evaluate the impact of salt exposure on the mechanical resistance of the materials, the prisms were subjected to compressive strength testing following cycling. The results are shown in comparison with their 28-day strength. The results, Figure 5-17, show that the reference mortar lost 1.7% of its original strength, while the FA 1 20% materials presented the highest loss, 26.49%, a significant reduction that caused strength to decrease to a value lower than that of the lower limit strength of 30 MPa, indicating a reduced sulphate resistance at higher substitution levels. Moreover, as observed in Section 5.3 FA 1 20% presented the highest water intake due to capillary action, which makes this composite prone to intrusion of deleterious compounds.

Following the highest reduction caused by FA 1 20%, other composites also experienced significant strength reduction, and presented strength below what is recommended by

standard. These composites are: FA 2 20%, IBA 1 20% and IBA 2 20%. As observed previously in Section 4.2, these ashes have a considerable amount of alkalis favouring expansion by alkali silica reaction, which offers more sites for incorporation of salts.



Figure 5-15: Salt precipitated within IBA 1 specimens. IBA 1 10% (top) and IBA 1 20% (bottom).

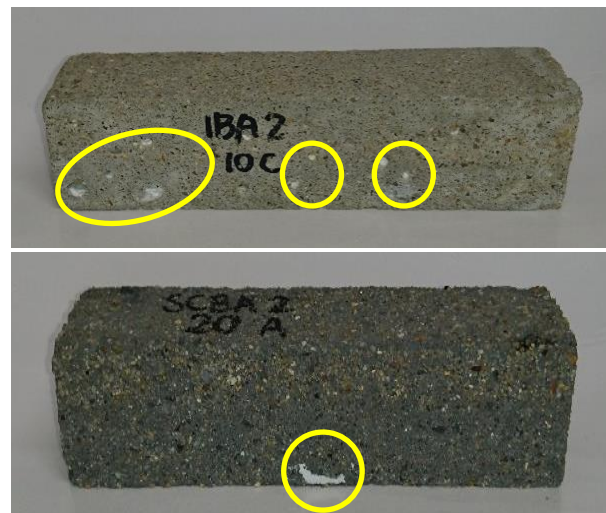


Figure 5-16: Salt crystallisation within voids on prisms surfaces.

On the other hand, the FA 1 5% material increased the compressive strength by 8.52%. An increase in compressive strength of specimens after the salt exposure was also experienced by other mortars. SCBA 2 20% increased strength by 22.4%. Suggesting that further hydration took place with the water supplied by the solution. Binici et al. (2007) have reported similar results using both natural and artificial pozzolans, stating that blended cements perform better in sulphate environment by enhancing the chemical resistance of concrete.

Interestingly, all IBA 1 mortars (with the highest gains in mass) improved compressive strength after salt exposure, suggesting not only a good accommodation of stress imposed by the salt on the pore structure but also an improvement on the composite's density.

In relation to mortars with sand replacement, it was observed that in all cases, the strength decreased when compared with the 28-day strength, revealing a low sulphate resistance. No significant correlation was found between mass change and strength after salt test.

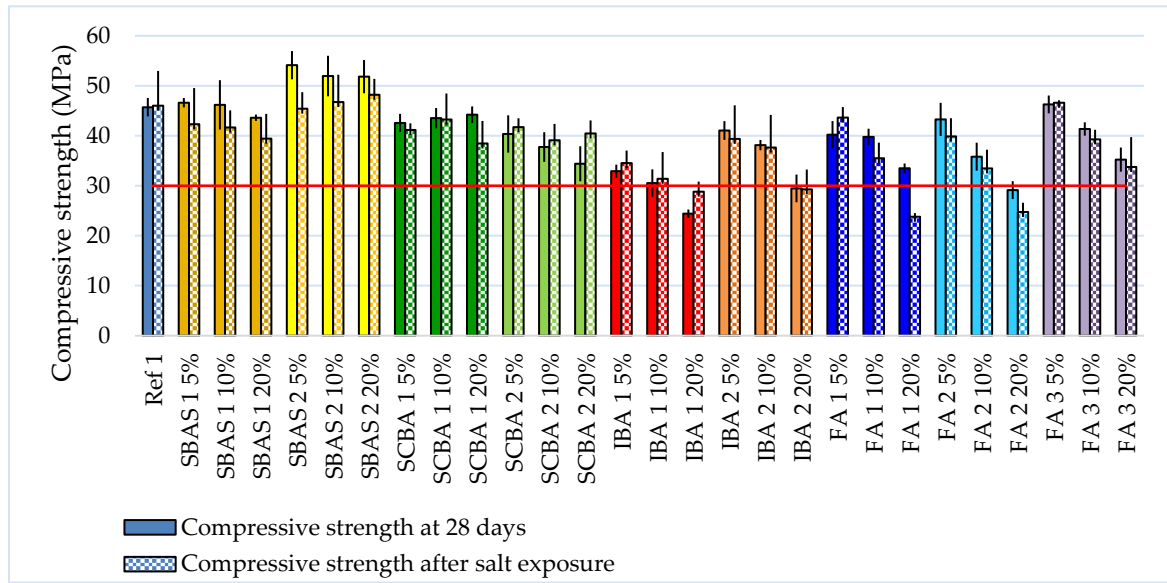


Figure 5-17: Compressive strength of mortars after salt exposure.

5.7 RESISTANCE TO DAMAGE BY FROST

The freeze-thaw test was performed to compare the durability of the different mixes with respect to damage by frost. At the end of freeze-thawing cycles no external damage was visually apparent on the specimens, and the evaluation of strength and weight variations were used to assess durability. The results are depicted in Table 5-7. Most materials lost weight after drying following freeze-thaw cycles, with the exception of SBAS 1 (10% and 20%) and SBAS 2 5% that slightly increased weight, while reference specimens remained close to zero. The increase in weight is likely owing to further hydration due to the excess water.

Contrary to the observations upon salt crystallisation test, where most mortars increased strength following cycling, the strength decreased for all of the ash materials after freeze-thaw cycling, as shown in Figure 5-18. Most ash materials, except for the IBA 2 20% that only lost 10.24% strength, lost more strength than the reference mix (13.64% strength loss) after frost cycling. Therefore, despite the possible occurrence of further hydration during cycling, the strength loss caused by freeze-thawing cycles is significant.

Table 5-7: Strength and weight loss after freeze-thaw cycling.

Material		Strength loss following freeze-thaw cycling (%)	Weight loss after freeze-thaw cycling (%)
Reference		13.64	0.00
SBAS 1	5%	33.90	1.48
	10%	18.94	-0.80
	20%	24.14	-0.12
SBAS 2	5%	34.03	-0.79
	10%	44.22	1.77
	20%	21.63	1.19
SCBA 1	5%	37.65	0.64
	10%	23.32	0.75
	20%	27.81	1.30
SCBA 2	5%	45.07	0.95
	10%	32.73	1.25
	20%	23.23	1.57
IBA 1	5%	22.87	1.03
	10%	40.01	0.72
	20%	18.71	0.45
IBA 2	5%	48.15	0.90
	10%	42.26	0.52
	20%	10.24	0.36
FA 1	5%	17.28	0.73
	10%	24.24	0.85
	20%	41.45	1.49
FA 2	5%	26.89	0.50
	10%	28.39	1.06
	20%	22.97	1.70
FA 3	5%	31.44	0.22
	10%	24.23	0.52
	20%	18.53	0.56

The overall results show that ashes that presented better refinement of the pore structure (see Section 5.2) achieved better resistance to frost attack, especially those produced with ash sand SBAS 1 and 2. The results also align with the capillary action results (see Section 5.3), where composites with lower water absorption presented the best compressive strength after freeze-thaw cycles.

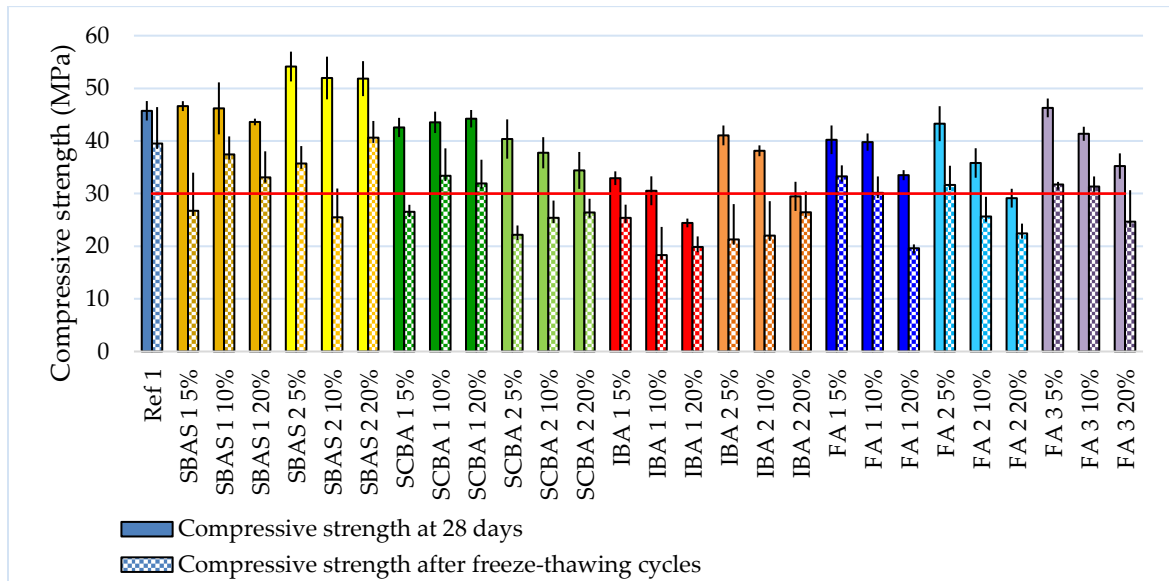


Figure 5-18: Comparison of compressive strength of mortars before and after freeze-thawing cycles.

5.8 WATER VAPOUR PERMEABILITY

The water vapour resistance factor and water vapour permeability of each material are included in Table 5-8. The change in mass of the test cups and the test conditions can be found in Appendix D. The water vapour resistance factors (μ) of all ash materials are lower than the reference mix therefore the ashes increase the passage of water vapour through the composites. The changes in permeability produced by the different ashes are significant therefore, adding ashes to cement composites would increase their water vapour permeability, facilitating water transfer and potentially lessening problems caused by accumulation of moisture.

High moisture content adversely affect building thermal performance and can cause considerable damage to human health, as water condensation within building materials can lead to mould growth and bacteria (Lief & Trechsel, 1982). It has been shown that the presence of moisture influences the thermal conductivity of building materials, as the air, which has a thermal conductivity of approx. $0.026 \text{ W/m}^\circ\text{C}$, is replaced by water, with a thermal conductivity 23 times higher ($0.6 \text{ W/m}^\circ\text{C}$), resulting on the overall increase of thermal conductivity of the material (Bal et al., 2013; Belkharchouche & Chaker, 2016; Khedari et al., 2005; Taoukil et al., 2013).

The sugarcane ash materials (both with bagasse ashes and fly ash) have the lowest permeability. Likewise, mixes with sand replacement by sugarcane bagasse ash also show lower vapour permeability than the incinerator ashes (both bottom and fly ashes).

Overall, FA 3 presented the highest μ values, whereas FA 1 have the lowest μ values. These results contrast well with the results on open porosity, where FA 1 20% holds one of the highest open porosity (15.2%) while FA 3 10% has a much lower porosity (8.4%). Accordingly, the

composites that presented lower capillary action (with the exception of IBA 2 fine) attained better diffusion resistance to vapour permeability.

It is known that the early permeability of PC pastes is lower than that of pozzolanic cement pastes, however, the permeability of pozzolanic pastes tends to lower as the curing time increases due to the segmentation and lowering of the interconnection between pores caused by the pozzolanic reaction (Lea, 1970). Therefore, despite a higher porosity of pozzolanic cements, the C-S-H formed by pozzolanic activity is enough to block thinner connecting channels or reduce their span (Massazza, 1998), explaining the lack in correlation between porosity and permeability.

Table 5-8: Water vapour resistance and permeability results.

Material		δ_{wv}	μ
Reference		6.29265E-13	234.90
SBAS 1	5%	3.27218E-12	59.23
	10%	3.84551E-12	50.40
	20%	4.05526E-12	47.79
SBAS 2	5%	3.49592E-12	55.44
	10%	3.21624E-12	60.26
	20%	3.28616E-12	58.97
SCBA 1	5%	2.51706E-12	76.99
	10%	2.23739E-12	86.62
	20%	1.46828E-12	131.99
SCBA 2	5%	3.27218E-12	59.23
	10%	1.95771E-12	98.99
	20%	2.69885E-12	71.81
IBA 1	5%	5.45363E-12	35.54
	10%	5.7333E-12	33.80
	20%	6.43249E-12	30.13
IBA 2	5%	7.13167E-12	27.17
	10%	6.99183E-12	27.72
	20%	7.76093E-12	24.97
FA 1	5%	6.71216E-12	28.87
	10%	9.50889E-12	20.38
	20%	1.07674E-11	18.00
FA 2	5%	5.87314E-12	33.00
	10%	6.08289E-12	31.86
	20%	6.62826E-12	29.24
FA 3	5%	1.81788E-12	106.61
	10%	1.35642E-12	142.88
	20%	1.67804E-12	115.49

δ_{wv} – water vapour permeability (kg/m.s.Pa); μ – water vapour diffusion resistance factor.

6 DISCUSSION

6.1 COMPOSITION, PROPERTIES AND REACTIVITY OF THE ASHES

The results evidenced reactivity for all the ashes however, in general, a poor correlation exists between the properties measured. The specific surface area, amorphousness and fineness determine the reactivity (mechanical index) of the sugarcane ashes however, for most of the ashes, a poor correlation exists: for example, fly ashes (2-3) have high mechanical indices and yet they are crystalline, coarser and with lower specific surface area than other ashes.

Furthermore, there is no correlation between the chemical and mechanical reactivity: the IBAs combine more lime faster and yet their mechanical indices are amongst the lowest. This agrees with Massazza (1998) and is likely due to not all combined lime hardening satisfactorily.

This work also evidences that amorphousness is not essential for reactivity agreeing with previous studies claiming that crystalline minerals in pozzolans can bind a considerable amount of lime (Walker and Pavia 2010). Most ashes (except for SCBA 1 and 2) are mostly crystalline or slightly amorphous however, despite their crystallinity the incinerator bottom ashes (IBAs) combine the most lime by conductivity (mainly IBA 2). Similarly, the fly ashes are mostly crystalline and yet they combine significant lime and reach high early strengths.

The LOI does not seem to impact reactivity greatly as the LOI of most ashes is over the ASTM standard limit of 10% and yet most are reactive. The SCBA 1 and SCBA 2 ashes were as most reactive by most tests, present high losses on ignition, whereas SCBA 3 and SCBA 4 have low losses (≤ 0.41) and yet low reactivity.

The results demonstrate the impact of the alumina content on early reactivity. It was evidenced that the alumina content is responsible for the quick consumption of CH through the higher losses in conductivity experienced by the IBAs, with greater alumina content (11-15%). A general trend of increasing alumina content and increasing conductivity variation is observed. The alumina is supposed to partake in hydration and pozzolanic reaction with the formation of C-A-S-H and replacement of Al with Si in the C-S-H structure. However, there is no correspondence between the Al content and the strength development as the IBAs (with greatest Al content) generally reached lower strengths than the other ashes.

There is a good correlation between the Si content and the reactivity by strength except for FA 2 which has the 2nd highest mechanical index and lowest Si. The silica seems to determine reactivity more than the Ca content. This was clear in the fly ashes where the reactivity tests evidenced that the low-Ca FA 3 (with only 0.42% CaO however much greater silica content

than the others - 90 vs 7-12%) combines more lime chemically in solution and faster than the other FAs and furthermore, it reached similar or superior compressive strength than the others (2.26 vs 1.36-2.79 MPa).

The alkali content can speed up the dissolution of amorphous silica favouring hydration. However, there is no strong correlation between this and reactivity. The incinerator ashes (IBAs and fly ashes FAs 1 and 2) have the highest alkali contents while sugar cane ashes are very low in alkalis complying with the ASTM and NBR standard requirements and yet, these are the most reactive so the relationship between reactivity and alkali content seems to be inverse.

No clear relationship was found between the sulphate content and the reactivity of the ashes although the most reactive ashes (SCBAs 1 and 2) are low in sulphur. Gypsum is supposed to enhance lime combination however this is inconsistent. For example, IBA 2-3, considerably higher in sulphur than the others (2-3%), do not show high reactivity by strength while FA 2-3, with high sulphur also have the 2nd and 3rd highest mechanical indices. All the ashes are under the ASTM /NBR standard sulphate limits to avoid expansion.

The non-contaminated sugarcane bagasse ashes (SCBAs 1 and 2) with the highest fineness, specific surface, amorphousness and Si content, are among the most reactive: their mechanical indices are among the highest, but they combine little lime and slowly in solution.

The IBAs combine abundant lime in solution fast however their mechanical indices are among the lowest whereas most of the fly ashes display great mechanical indices.

The fly ashes significantly increase flexural strength surpassing the reference material. Some of the sugarcane bagasse ashes (1 and 4) and the fine incinerator bottom ashes (1 and 3) also exceeded the reference flexural strength. Incinerator fly ashes contain significant chloride (halite) c.2% that can be detrimental to durability while the Cl content of the bottom ashes are very low.

Table 6-1: Rating of ashes according to investigated properties.

Material	Fineness (in terms of D-90)	Specific surface area (descending order)	Si content (descending order)	Ca content (descending order)	Al content (descending order)	LOI (ascending order)	Amorphousness (descending order)	Conductivity (% loss - chemical reactivity)	Compressive strength (index - mechanical reactivity)
SCBA 1	1	2	3	9	2	13	1	8	4
	Highest	High	Moderate	Low	High	Highest	Highest	Low-mod.	Mod.-high
SCBA 2	2	1	2	10	9	12	2	6	1
	High	Highest	Mod-high	Low	Low-mod.	High	High	Moderate	Highest
SCBA 3	12	13	Not applicable	13	13	2	3	13	8
	Low	Lowest	Not applicable	Lowest	Lowest	Low	Moderate	Lowest	Moderate
SCBA 4	7	12	Not applicable	12	12	1	13	9	6
	Low-mod.	Low	Not applicable	Low	Low	Lowest	Lowest	Low-mod.	Moderate
IBA 1 - fine	5	4	5	8	6	4	10	5	9
	Mod.-high	Low-mod.	Moderate	Low-mod.	High	Low-mod.	Low	Moderate	Low-mod.
IBA 2 - fine	9	3	7	6	1	6	12	2	5
	Low-mod.	Low-mod.	Low-mod.	Moderate	Highest	Moderate	Low	High	Moderate
IBA 3 - fine	3	5	6	4	7	7	11	10	10
	Mod.-high	Low-mod.	Low-mod.	Moderate	Mod-high	Moderate	Low	Low-mod.	Low-mod.
IBA 1 - coarse	8	6	8	7	4	8	5	3	12
	Low-mod.	Low-mod.	Low-mod.	Low-mod.	High	Moderate	Moderate	Mod.-high	Low
IBA 2 - coarse	11	10	9	3	5	11	6	1	13
	Low	Low	Low-mod.	Moderate	High	Mod.-high	Low-mod.	Highest	Lowest
IBA 3 - coarse	13	7	4	5	3	5	4	7	11
	Lowest	Low-mod.	Moderate	Moderate	High	Low-mod.	Moderate	Low-mod.	Low-mod.
FA 1	10	11	10	2	8	9	8	11	7
	Low-mod.	Low	Low	High	Moderate	Mod.-high	Low	Low-mod.	Moderate
FA 2	4	8	11	1	10	10	9	12	2
	Mod.-high	Low-mod.	Lowest	Highest	Low-moderate	Mod-high	Low	Low	High
FA 3	6	9	1	11	11	3	7	4	3
	Moderate	Low-mod.	Highest	Low	Low	Low	Low-mod.	Moderate	Mod.high

6.2 PROPERTIES OF ASH-COMPOSITES

In order to rate the general effect of the ashes, the composites were positioned between 1 and 28 (27 ash-composites + reference), according to the results of each test (for each test a different position) - Table 6-2 -. Then, each composite was rated between 1 and 10 to reflect their position (e.g. the MOE of composite SBAS 2 10% was positioned in 8th place and received 7.6 points).

Table 6-2: Points attributed to composites according to test results.

Position	1	2	3	4	...	26	27	28
Points	10	9.66	9.33	9.0	...	1.66	1.33	1

The arithmetic mean of the three replacements (5, 10 and 20%) is reported for each ash. According to the results the composites were classified as: low (1 - 3.2); low to moderate (3.2 - 3.5); moderate (3.5 - 6.5); moderate-high (6.5 – 6.8); and high (> 6.8). The results are shown in Table 6-3. However, as these do not reflect each replacement level, some notes are added. Radar graphs (Figure 6-1) give an overview of the effect of the ashes in the properties of the composites.

The sugarcane ashes show great potential for PC and fine aggregate replacement in cement-based composites. The sugar ash composites have good resistance to frost and salt action, they reached the highest strengths and increased bulk density, lowering porosity, capillary suction and thermal conductivity while the water vapour ability is little changed. These combinations of properties have the potential to produce strong materials with a greater insulation ability and a lower moisture transport that enhance durability and water vapour properties adequate to maintain indoor air quality.

The ash composites generally resist well to salt attack, with many increasing strength after salt exposure probably due to further hydration. The ashes that performed worse on salt attack were the incinerator fly ashes FA 1 20% (with the highest strength loss at 26%) probably due to their high Cl and alkali content.

At the end of freeze-thawing cycles no external damage was visually apparent on the specimens, however, the strength decreased for all of the ash materials after freeze-thaw cycling. Therefore, despite the possible occurrence of further hydration during cycling, the strength loss caused by frost is significant, likely due to the development of frost-induced microcracks.

The ash composites reached significant compressive strength, only three mortars (IBA 1 20%, IBA 2 20% and FA 2 20%) did not attain the lower limit of 30 MPa at 28 days in EN 197-1 (2011) for strength class 32.5 however, they still reached high strengths (24-29 MPa). The SCBA, SBAS and FAs 1 and 3 achieved strengths over 30 MPa at all replacement levels. In particular, SBAS 2 attained higher strength than the reference PC material at all substitution levels probably due to the replacement of the sand with the ash rather than the cement.

Most composites produced with incinerator ashes have lower strengths however most comply with the lower strength requirement for PC mortars at 28 days in EN 197-1. Their durability is lower than the sugar ash composites probably due to their Cl and alkali content.

In most cases, the most reactive ashes produced the strongest composites however, the SBAS 2 composites fabricated with the lower reactivity sugarcane ash (SCBA 4) as sand replacement surpassed the compressive and flexural strengths of the most reactive ashes probably due to their higher cement content. The SBAS 2 (5%) materials attained the highest flexural strength (10.02 MPa) but most ash composites reached around or over 70% of the reference strength except for SCBA 2 20%, IBA 1 20% and FA 2 20% with slightly lower strength.

The ashes lowered the stiffness of the reference mortar, with the exception of FA 3 5%, which exceeded the reference MOE by 1.8%. The ashes used as sand replacement increased the mechanical resistance in compression, however maintaining a level of plasticity as they keep their MOE lower than the reference PC.

As expected, the finest and most reactive ashes (SCBA 1, SCBA 2 and FA 3) with greater silica content and mechanical reactivity, used as cement replacement, lowered porosity and capillarity the most due to the fragmentation of the pore system and the production of hydrates. However, the coarse sugarcane ashes (SCBA 3 and 4) used as sand replacement - SBAS 1 and 2 - substantially lowered porosity and capillarity despite their poor reactivity and produces denser composites likely due to their higher cement content. Incinerator ashes - IBAs and FAs 1 and 2 - increase vapour permeability facilitating water transfer and potentially lessening problems caused by accumulation of moisture. Most ashes lower both capillarity and porosity. However, there are exceptions such as the incinerator fly ashes (FAs 1 and 2) that increased both capillarity and porosity. This is likely due to the hygroscopic characteristics of chlorides increasing the water uptake and enhancing tractive forces of in small pores.

In general, there is a correlation between the properties measured. The ashes that caused a larger refinement of the pore structure and lower capillary action presented the best compressive strength after freeze-thaw cycles. A general linear relationship also exists between compressive strength and bulk density in which the increase of density is accompanied by a more or less proportional increase in mechanical strength. A good correspondence also exists with the thermal properties. All the ashes significantly lower the thermal conductivity of the cement composite (by c.30%). This agrees with the tendency of the ashes to reduce the density of the PC composites (SBAS 1, SCBA 2, IBA 1, IBA 2 – at 5 and 20% -, FA 1 – at 5 and 10% - and FA 3 significantly reduce the real density of the reference) and also agree with the porosity results, as the composites with the highest porosities, such as IBA 2 and FA 2, lowered thermal conductivity the furthest.

The lowering of the thermal conductivity by the ashes is interesting for material design, as it can lower a U-value of 3.44 to 2.11 W/m²K in a 300 mm wall of PC concrete, just by replacing 10% of the cement with IBA 2 (the ash with the lowest thermal conductivity 0.63 W/mK). In

addition, using this ash, the standard U-value requirement of 0.21 W/m²K for a typical cavity wall can be reached with a block 40% thinner than the standard.

The ashes also lower the thermal effusivity of the PC, sometimes substantially (e.g. FA 2 5% with a 29% reduction) which adds to the increased insulation ability of the ash composites. The ashes lower the specific heat capacity of cement composites however, the decline is not significant with the exception of ashes SCBA 1 and IBA 2 (at 20% replacement) and SBAS 1 and 2 which lowered the specific heat by 19-22%.

Table 6-3: Rating of ash-composites and reference composite according to test results.

Material	Open porosity (in terms of pore refinement)	Real density (highest to lowest density)	Lowering of capillary action	Vapour permeability (in terms of diffusion resistance)	Thermal conductivity (highest to lowest)	MOE (highest to lowest)	Compressive strength (highest to lowest)	Flexural strength (highest to lowest)	Salt attack resistance (in terms of compressive strength)	Frost attack resistance (in terms of compressive strength)
Ref	6 4.0 - Moderate	6 4.7 - Moderate	9 2.7 - Low	1 10.0 - Highest	1 10.0 - Highest	1 9.7 - Highest	2 9.0 - High	1 9.7 - Highest	2 8.0 - High	1 9.7 - Highest
SBAS 1	1 9.7 - Highest	3 7.8 - High	2 9.0 - High	6 5.7 - Moderate	Not tested	7 4.2 - Moderate	4 6.9 - Moderate-high	5 6.2 - Moderate	4 6.3 - Moderate	2 7.8 - High
SBAS 2	4 6.8 - High	2 8.4 - High	3 7.0 - High	5 6.2 - Moderate	2 9.1 - High	2 8.6 - High	1 9.7 - Highest	2 7.8 - High	1 9.3 - Highest	2 7.8 - High
SCBA 1	5 5.6 - Moderate	5 5.7 - Moderate	4 5.8 - Moderate	3 8.3 - High	Not tested	4 7.0 - High	3 7.2 - High	8 4.4 - Moderate	3 6.7 - Mod-high	4 7.3 - High
SCBA 2	2 8.4 - High	1 8.7 - Highest	6 5.1 - Moderate	4 7.3 - High	4 7.4 - High	9 3.2 - Low	7 4.3 - Moderate	10 1.9 - Lowest	6 5.9 - Moderate	8 3.9 - Moderate
IBA 1	7 3.4 - Low-mod	10 2 - Lowest	7 4.7 - Moderate	7 4.1 - Moderate	Not tested	10 2.2 - Lowest	10 1.78 - Low	9 3.0 - Low	2 2.4 - Low	10 2.1 - Lowest
IBA 2	10 2.7 - Lowest	9 2.7 - Low	1 9.3 - Highest	9 2.0 - Lowest	3 7.6 - High	8 4.0 - Moderate	9 3.7 - Low-mod	3 7.1 - High	8 4.1 - Moderate	9 3.2 - Low-mod
FA 1	8 3.2 - Low-mod	7 3.4 - Low-mod	10 2.2 - Lowest	10 1.7 - Low	Not tested	6 5.2 - Moderate	6 4.6 - Moderate	4 6.5 - Mod-high	7 4.6 - Moderate	6 5.3 - Moderate
FA 2	9 2.4 - Low	7 3.4 - Low-mod	7 4.7 - Moderate	8 3.6 - Low-mod	5 7.2 - High	5 5.9 - Moderate	8 4.1 - Moderate	7 5.2 - Moderate	9 3.3 - Low-mod	7 4.9 - Moderate
FA 3	3 7.8 - High	4 7.67 - High	4 5.8 - Moderate	2 9.1 - High	Not tested	3 7.8 - High	5 6.1 - Moderate	6 5.9 - Moderate	5 6.0 - Moderate	5 5.8 - Moderate
Notes	Ref > IBA 1 (10, 20); IBA 2 (5, 10, 20); FA 1 (10, 20); FA 2 (10, 20)	Ref > IBA 1 (5, 10, 20); IBA 2 (5, 10, 20); FA 1 (5, 10, 20); FA 2 (10, 20)	Ref > FA 1(10, 20); FA 2 (5, 10, 20)	Ref - highest water vapour diffusion resistance factor	Ref - highest thermal conductivity	Ref < FA 3 (5)	Ref < SBAS 2 (5, 10, 20)	Ref < SBAS 2 (5)	Ref < SBAS 2 (5, 10, 20); SCBA 1 (10); FA 1 (5); FA 3 (5)	Ref < SBAS 2 (20)

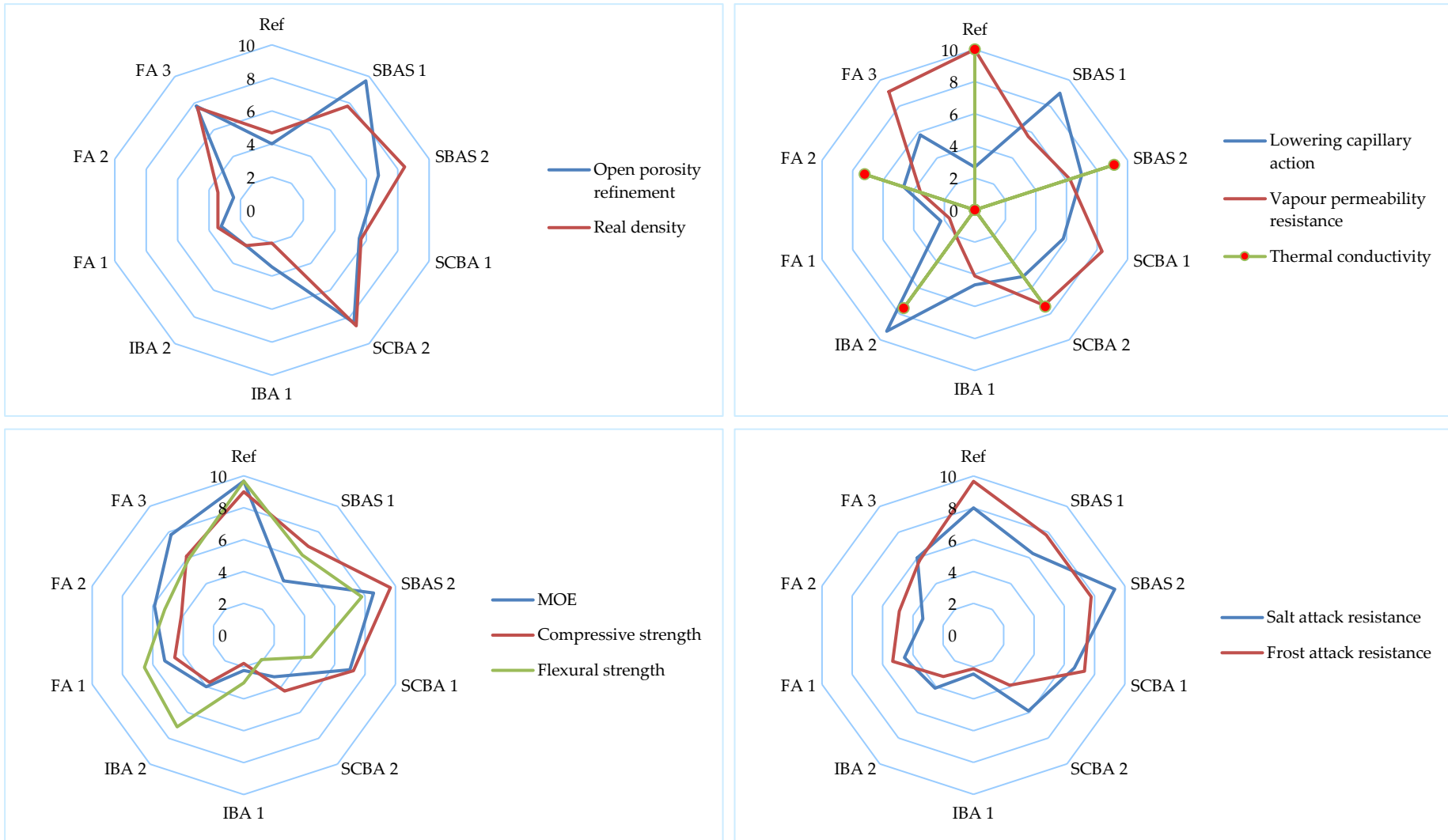


Figure 6-1: Radar graphs of properties according to Table 6-3 values.

7 CONCLUSIONS

This research examined the pozzolanic activity of industrial waste ashes. Thirteen ashes were investigated to determine their suitability for use as partial binder replacement in composites. An experimental programme was undertaken to investigate the properties, considered to significantly impact the reactivity of pozzolanic materials. Physical properties (including particle size distribution and specific surface area), chemical composition, mineralogy and amorphousness of the ashes were examined. Reactivity was investigated chemically, by measuring the conductivity of lime:ash solutions through time, and mechanically, by evaluating the strength development of lime:ash composites.

Specific surface area and particle size distribution results demonstrated properties comparable to traditional pozzolanic materials. However, the amorphousness and silica content of the ashes are low. Despite these deficiencies, both the chemical and mechanical methods evidenced the reactivity of the ashes. The reactivity of the ashes was further evidenced with SEM as hydrates appeared as early as 7 days in pastes produced with sugarcane bagasse ash 1, incinerator bottom ash 1 and fly ash 1.

The chemical and mechanical methods disagree on the rating of the reactivity. This is due to the Al content which is responsible for the quick consumption of CH in solution and therefore overrates pozzolanic reactivity. As a result, the incinerator bottom ashes, IBAs, with greater alumina content (11-15%) and thus higher losses in conductivity were rated chemically as the most reactive. However, according to the mechanical index, sugarcane ash 2 (SCBA 2) is the most reactive. From the above, there seems to be a lack of correlation between the amount of combined lime and the strength development; and the assessment of reactivity by strength development is a better predictor of pozzolanic activity than the electrical conductivity test.

It is also noted that incinerator ashes should be analysed or cleaned prior to use due to contamination by salt (especially NaCl), however, they have significant potential to develop strength, increase the modulus of elasticity and resist salt attack.

This work also evidences that a high amorphousness and a low LOI are not essential for reactivity: most ashes are crystalline and their LOI is over the ASTM standard limit of 10% and yet they are reactive. Al is supposed to partake in hydration and pozzolanic reaction however, there is no correspondence between the Al content and the strength development (the IBAs, with greatest Al content, generally reached lower strengths). There is a good correlation between the Si content and the reactivity by strength except for FA 2 which has the 2nd highest mechanical index and lowest Si. Contrary to what was expected, the relationship between

reactivity and alkali content seems to be inverse: sugar cane ashes are very low in alkalis and they are the most reactive.

Based on the investigation of the ashes, 27 composites were produced with the best performers and the results were compared with a PC control mix. In general, there is a correlation between the composite properties. The ashes that caused a larger refinement of the pore structure and lower capillary action resisted frost action the best (highest strength after freeze-thaw cycles). A general linear relationship also exists between compressive strength and real density. A good correspondence also exists within the thermal properties. All the ashes significantly lower the thermal conductivity of the cement composite (by c.30%). This agrees with the tendency of the ashes to reduce the density of the PC composites (SBAS 1, SCBA 2, IBA 1, IBA 2 – at 5 and 20%-, FA 1 –at 5 and 10%- and FA 3 significantly reduce the real density of the reference) and also agree with the porosity results, as the composites with the highest porosities, such as IBA 2 and FA 2, lowered thermal conductivity the furthest.

The porosity of composites was refined using ashes from the sugarcane industry, while ashes from municipal solid waste incineration tend to increase porosity at high levels of replacement. The ashes generally reduced the differences between real and bulk densities (amount of voids) enhancing the microstructure.

As expected, the finest and most reactive ashes (SCBA 1, SCBA 2 and FA 3) with greater silica content and mechanical reactivity, used as cement replacement, lowered porosity, capillarity and vapour permeability the most due to the fragmentation of the pore system and the production of hydrates. However, the coarse sugarcane ashes (SCBA 3 and 4) used as sand replacement - SBAS 1 and 2 - substantially lowered porosity and capillarity despite their poor reactivity and produced denser composites likely due to their higher cement content. Most ashes lower both capillarity and porosity. However, there are exceptions such as the incinerator fly ashes (FAs 1 and 2) that increased both capillarity and porosity. This is likely due to the hygroscopic characteristics of chlorides increasing the water uptake and enhancing tractive forces of small pores.

Incinerator ashes - IBAs and FAs 1 and 2 – increase vapour permeability facilitating water transfer and potentially lessening problems caused by accumulation of moisture.

The ash composites reached significant compressive strength, only three mortars (IBA 1 20%, IBA 2 20% and FA 2 20%) did not attain the lower limit of 30 MPa at 28 days in EN 197-1, however, they still reached high strengths (24-29 MPa). The SCBA, SBAS and FA ashes achieved strengths over 30 MPa at all replacement levels. The use of sugarcane ash as sand replacement (SBAS 2) produced the strongest composites which surpassed the compressive and flexural strengths of the most reactive ashes probably due to their higher cement content.

The fly ashes significantly increase flexural strength surpassing the reference material. Some of the sugarcane bagasse ashes (1 and 4) and the fine incinerator bottom ashes (1 and 3) also exceeded the reference flexural strength. The SBAS 2 (5%) materials attained the highest flexural strength (10.02 MPa) but most ash composites reached around or over 70% of the

reference strength except for SCBA 2 20%, IBA 1 20% and FA 2 20% with slightly lower strength.

The ashes lowered the stiffness of the reference mortar, with the exception of FA 3 5%, which exceeded the reference MOE by 18%. The ashes used as sand replacement increased the mechanical resistance in compression, however maintaining a level of plasticity as they keep their MOE lower than the reference PC.

Most composites produced with incinerator ashes have lower strengths however most comply with the lower strength requirement for PC mortars at 28 days in EN 197-1. Their durability is lower than the sugar ash composites probably due to their Cl and alkali content. The incinerator fly ashes FA 1 20% (with the highest strength loss at 26%) performed worse on salt attack probably due to their high Cl and alkali content. At the end of freeze-thawing cycles no external damage was visually apparent however, the strength decreased. Therefore, despite the possible occurrence of further hydration during cycling, the strength loss caused by frost is significant likely due to the development of frost-induced microcracks.

The incorporation of ashes lowered the thermal conductivity, specific heat and thermal mass of composites. The bottom ashes were more effective at lowering thermal conductivity and providing better insulation properties. The lowering of the thermal conductivity by the ashes is interesting for material design, as it can lower a U-value of 3.44 to 2.11 W/m²K in a 300 mm wall of PC concrete, just by replacing 10% of the cement with IBA 2 (the ash with the lowest thermal conductivity 0.63 W/mK). In addition, using this ash, the standard U-value requirement of 0.21 W/m²K for a typical cavity wall can be reached with a block 40% thinner than the standard.

The ashes also lower the thermal effusivity of the PC, sometimes substantially (e.g. FA 2 5% with a 29% reduction) which adds to the increased insulation ability of the ash composites. The ashes lower the specific heat capacity of cement composites however, the decline is not significant with the exception of ashes SCBA 1 and IBA 2 (at 20% replacement) and SBAS 1 and 2 which lowered the specific heat by 19-22%.

The sugarcane ashes show great potential for PC and fine aggregate replacement in cement-based composites. The sugar ash composites have good resistance to frost and salt action, they reached the highest strengths and increased bulk density, lowering porosity, capillary suction and thermal conductivity while the water vapour ability is little changed. These combinations of properties have the potential to produce strong materials with a greater insulation ability and a lower moisture transport that enhance durability and water vapour properties adequate to maintain indoor air quality.

7.1 FINAL REMARKS

This investigation presents an approach to dealing with the existing problems of waste production and conservation of natural resources, encouraging the use of waste ashes as partial binder replacement and supporting the transition of materials from residues to valuable resources.

The main objectives of this research were met as summarised below. This research:

- Strengthens and contributes to the knowledge on the properties pozzolanic materials for building composites;
- Investigated the pozzolanic activity of industrial and agricultural waste ashes and evaluated their potential to partially replace conventional binders;
- Measured physical, chemical and mineralogical properties of waste and their effect on reactivity;
- Determined their performance by monitoring their microstructure, morphology and hydrate formation;
- Designed sustainable composites with different waste proportions;
- Assessed their mechanical, hygric and thermal properties;
- Evaluated their endurance to salt crystallisation and frost damage.

7.2 SCOPE FOR FURTHER RESEARCH

The incorporation of industrial waste ashes into building materials shows a great potential to reduce the negative impacts of construction. Potential areas for further research have been considered, as follows:

- Optimise the process in which the ashes are produced by applying higher temperature rates and controlled cooling.
- Examine the best practices of the rice industry in relation to the burning and production of rice husk ash with high pozzolanic value aiming at adapting and optimising the production of reactive sugarcane bagasse ashes.
- Map industries that produce waste ashes with pozzolanic potential and cement manufacturers to analyse the cost-benefit of implementing the use of the ashes on the production of blended cements.
- Assess the behaviour of pozzolanic concrete as recycled coarse aggregate for mass and reinforced concrete with strength no greater than 40 MPa.

REFERENCES

- Ãzisik, M. N., & Özisik, M. N. (1993). *Heat conduction*: John Wiley & Sons.
- Abbas, S., Kazmi, S. M. S., & Munir, M. J. (2017). Potential of rice husk ash for mitigating the alkali-silica reaction in mortar bars incorporating reactive aggregates. *Construction and Building Materials*, 132, 61-70. doi:<https://doi.org/10.1016/j.conbuildmat.2016.11.126>
- ABNT. (2014). ABNT NBR 12653:2014 Pozzolanic materials - Requirements. In (3rd ed., Vol. ABNT NBR 12653:2014, pp. 10). Rio de Janeiro - RJ.
- Agapiou, K. (2017). High-Alumina Refractory Aluminosilicate Pozzolan in Well Cementing. In: Google Patents.
- Aly, M., & Pavia, S. (2015). *Properties of hydrated lime mortars with pozzolans*. Paper presented at the III International Congress on Construction and Building Research, Universidad Politécnica de Madrid. Escuela Técnica Superior de Edificación.
- Aly, M., & Pavia, S. (2016, May 24-27). *Effect of limestone aggregate on the properties of natural hydraulic lime mortar (NHL 5)*. Paper presented at the Congreso Euro-Americano REHABEND 2016 Patología de la Construcción, Tecnología de la Rehabilitación y Gestión del Patrimonio, Burgos, Spain.
- Arenas-Piedrahita, J. C., Montes-García, P., Mendoza-Rangel, J. M., López Calvo, H. Z., Valdez-Tamez, P. L., & Martínez-Reyes, J. (2016). Mechanical and durability properties of mortars prepared with untreated sugarcane bagasse ash and untreated fly ash. *Construction and Building Materials*, 105(Supplement C), 69-81. doi:<https://doi.org/10.1016/j.conbuildmat.2015.12.047>
- Arif, E., Clark, M. W., & Lake, N. (2016). Sugar cane bagasse ash from a high efficiency co-generation boiler: Applications in cement and mortar production. *Construction and Building Materials*, 128, 287-297. doi:<http://dx.doi.org/10.1016/j.conbuildmat.2016.10.091>
- Asamoto, S., Murano, K., Kurashige, I., & Nanayakkara, A. (2017). Effect of carbonate ions on delayed ettringite formation. *Construction and Building Materials*, 147, 221-226. doi:<https://doi.org/10.1016/j.conbuildmat.2017.04.107>
- ASTM. (2003). C125 Standard terminology relating to concrete and concrete aggregates. *Annual Book of ASTM Standards*, 4.
- ASTM. (2005). C618 Standard specification for coal fly ash and raw or calcined natural pozzolan for use as a mineral admixture in concrete. In. Philadelphia: Annual Book of ASTM Standards.

- Aubert, J., Husson, B., & Sarramone, N. (2006). Utilization of municipal solid waste incineration (MSWI) fly ash in blended cement: Part 1: Processing and characterization of MSWI fly ash. *Journal of Hazardous Materials*, 136(3), 624-631. doi:<https://doi.org/10.1016/j.jhazmat.2005.12.041>
- Aydın, S., & Baradan, B. (2007). Effect of pumice and fly ash incorporation on high temperature resistance of cement based mortars. *Cement and Concrete Research*, 37(6), 988-995. doi:<https://doi.org/10.1016/j.cemconres.2007.02.005>
- Bahurudeen, A., Kanraj, D., Gokul Dev, V., & Santhanam, M. (2015a). Performance evaluation of sugarcane bagasse ash blended cement in concrete. *Cement and Concrete Composites*, 59, 77-88. doi:<http://dx.doi.org/10.1016/j.cemconcomp.2015.03.004>
- Bahurudeen, A., Marckson, A. V., Kishore, A., & Santhanam, M. (2014). Development of sugarcane bagasse ash based Portland pozzolana cement and evaluation of compatibility with superplasticizers. *Construction and Building Materials*, 68, 465-475. doi:<http://dx.doi.org/10.1016/j.conbuildmat.2014.07.013>
- Bahurudeen, A., & Santhanam, M. (2015). Influence of different processing methods on the pozzolanic performance of sugarcane bagasse ash. *Cement and Concrete Composites*, 56, 32-45. doi:<http://dx.doi.org/10.1016/j.cemconcomp.2014.11.002>
- Bahurudeen, A., Wani, K., Basit, M. A., & Santhanam, M. (2015b). Assesment of pozzolanic performance of sugarcane bagasse ash. *Journal of Materials in Civil Engineering*, 28(2), 04015095. doi:[https://doi.org/10.1061/\(ASCE\)MT.1943-5533.0001361](https://doi.org/10.1061/(ASCE)MT.1943-5533.0001361)
- Bal, H., Jannot, Y., Gaye, S., & Demeurie, F. (2013). Measurement and modelisation of the thermal conductivity of a wet composite porous medium: Laterite based bricks with millet waste additive. *Construction and Building Materials*, 41, 586-593. doi:<https://doi.org/10.1016/j.conbuildmat.2012.12.032>
- Barnes, P., & Bensted, J. (2002). *Structure and performance of cements*: CRC Press.
- Bayuseno, A. P., & Schmahl, W. W. (2011). Characterization of MSWI fly ash through mineralogy and water extraction. *Resources, Conservation and Recycling*, 55(5), 524-534. doi:<http://dx.doi.org/10.1016/j.resconrec.2011.01.002>
- Beaudoin, J. J., Ramachandran, V. S., & Feldman, R. F. (1990). Interaction of chloride and C₃S_H. *Cement and Concrete Research*, 20(6), 875-883. doi:[https://doi.org/10.1016/0008-8846\(90\)90049-4](https://doi.org/10.1016/0008-8846(90)90049-4)
- Bektas, F., Wang, K., & Ceylan, H. (2009). Effects of crushed clay brick aggregate on mortar durability. *Construction and Building Materials*, 23(5), 1909-1914. doi:<https://doi.org/10.1016/j.conbuildmat.2008.09.006>
- Belkharouché, D., & Chaker, A. (2016). Effects of moisture on thermal conductivity of the lightened construction material. *International Journal of Hydrogen Energy*, 41(17), 7119-7125. doi:<https://doi.org/10.1016/j.ijhydene.2016.01.160>

- Benavente, D. (2011). Why pore size is important in the deterioration of porous stones used in the built heritage.
- Bentur, A., & Cohen, M. D. (1987). Effect of condensed silica fume on the microstructure of the interfacial zone in Portland cement mortars. *Journal of the American Ceramic Society*, 70(10), 738-743. doi:<https://doi.org/10.1111/j.1151-2916.1987.tb04873.x>
- Bertolini, L., Carsana, M., Cassago, D., Quadrio Curzio, A., & Collepardi, M. (2004). MSWI ashes as mineral additions in concrete. *Cement and Concrete Research*, 34(10), 1899-1906. doi:<http://dx.doi.org/10.1016/j.cemconres.2004.02.001>
- BGS, B. G. S. (2005). *Mineral Profile - Cement Raw Materials*. Retrieved from <https://www.bgs.ac.uk/downloads/start.cfm?id=1408>.
- Binici, H., Aksogan, O., Cagatay, I. H., Tokyay, M., & Emsen, E. (2007). The effect of particle size distribution on the properties of blended cements incorporating GGBFS and natural pozzolan (NP). *Powder Technology*, 177(3), 140-147. doi:<https://doi.org/10.1016/j.powtec.2007.03.033>
- Brown, T., & Javid, M. (1970). The thermal conductivity of fresh concrete. *Matériaux et Construction*, 3(6), 411-416. doi:<https://doi.org/10.1007/BF02478765>
- Brundtland, G., Khalid, M., Agnelli, S., Al-Athel, S., Chidzero, B., Fadika, L., . . . de Botero, M. M. (1987). Our common future.
- BSI. (1989). BS 812-121:1989 Testin aggregates - Part 121: Method for determination of soundness. In (pp. 12): BSI Standards Publication.
- BSI. (1999). BS EN 1925:1999 Natural stone test methods -Determination of water absorption coefficient by capillarity. In (Vol. BS EN 1925:1999, pp. 10): BSI Standards Publication.
- BSI. (2002). BS EN 1015-18:2002 Methods of test for mortar for masonry - Part 18: Determination of water absorption coefficient due to capillary action of hardened mortar. In (Vol. BS EN 1015-18:2002, pp. 12): BSI Standards Publication.
- BSI. (2005). BS EN 196-1:2005 Methods of Testing Cement. In (Vol. BS EN 196-1:2005, pp. 36): BSI Standards Limited.
- BSI. (2010a). BS EN 459-2:2010 Building Lime. Test Methods. In (Vol. BS EN 459-2:2010, pp. 68): BSI Standards Limited.
- BSI. (2010b). BS EN 15304:2010 Determination of the freeze-thaw resistance of autoclaved aerated concrete. In (pp. 22): BSI Standards Publication.
- BSI. (2011). BS EN 197-1:2011 Cement. Composition, specifications and conformity criteria for common cements. In (Vol. BS EN 197-1:2011, pp. 50): BSI Standards Limited.

- BSI. (2012). BS EN 450-1:2012 Fly ash for concrete. Definition, specifications and conformity criteria. In (Vol. BS EN 450-1:2012, pp. 34).
- BSI. (2013). BS EN 12086:2013 Thermal insulating products for building applications – Determination of water vapour transmission properties. In (Vol. BS EN 12086:2013, pp. 22): BSI Standards Publication.
- BSI. (2015). BS EN 459-1:2015 Building lime. Definitions, specifications and conformity criteria. In (Vol. BS EN 459-1:2015, pp. 56): BSI Standards Limited 2015.
- BSI. (2016a). BS EN 196-1: 2016 Methods of testing cement. Part 1: Determination of strength.
- BSI. (2016b). BS EN 206:213+A1:2016 Concrete - Specification, performance, production and conformity. In (Vol. BS EN 206:213+A1:2016, pp. 108): BSI Standards Limited 2016.
- Cai, H., & Liu, X. (1998). Freeze-thaw durability of concrete: ice formation process in pores. *Cement and Concrete Research*, 28(9), 1281-1287. doi:[https://doi.org/10.1016/S0008-8846\(98\)00103-3](https://doi.org/10.1016/S0008-8846(98)00103-3)
- Cao, J., & Chung, D. (2002). Damage evolution during freeze–thaw cycling of cement mortar, studied by electrical resistivity measurement. *Cement and Concrete Research*, 32(10), 1657-1661. doi:[https://doi.org/10.1016/S0008-8846\(02\)00856-6](https://doi.org/10.1016/S0008-8846(02)00856-6)
- Carman, A. P., & Nelson, R. A. (1921). *Thermal conductivity and diffusivity of concrete*. Retrieved from
- Cembureau, T. E. C. A. (2006). Key facts: Cement industry contributes to waste management. In Brussels, Belgium.
- Cembureau, T. E. C. A. (2014). The role of cement in the 2050 low carbon economy. In.
- Černý, R., Kunca, A., Tydlitát, V., Drchalová, J., & Rovnaníková, P. (2006). Effect of pozzolanic admixtures on mechanical, thermal and hygric properties of lime plasters. *Construction and Building Materials*, 20(10), 849-857. doi:<https://doi.org/10.1016/j.conbuildmat.2005.07.002>
- Chabannes, M., Nozahic, V., & Amziane, S. (2015). Design and multi-physical properties of a new insulating concrete using sunflower stem aggregates and eco-friendly binders. *Materials and Structures*, 48(6), 1815-1829. doi:<https://doi.org/10.1617/s11527-014-0276-9>
- Chaipanich, A., Nochaiya, T., Wongkeo, W., & Torkittikul, P. (2010). Compressive strength and microstructure of carbon nanotubes–fly ash cement composites. *Materials Science and Engineering: A*, 527(4), 1063-1067. doi:<https://doi.org/10.1016/j.msea.2009.09.039>
- Chandra, S. (1996). *Waste materials used in concrete manufacturing*: Elsevier.

- Chang, F.-Y., & Wey, M.-Y. (2006). Comparison of the characteristics of bottom and fly ashes generated from various incineration processes. *Journal of Hazardous Materials*, 138(3), 594-603. doi:<https://doi.org/10.1016/j.jhazmat.2006.05.099>
- Chappex, T., & Scrivener, K. L. (2012). The influence of aluminium on the dissolution of amorphous silica and its relation to alkali silica reaction. *Cement and Concrete Research*, 42(12), 1645-1649. doi:<https://doi.org/10.1016/j.cemconres.2012.09.009>
- Chever, L., Pavia, S., & Howard, R. (2010). Physical properties of magnesian lime mortars. *Materials and Structures*, 43(1-2), 283-296. doi:<https://doi.org/10.1617/s11527-009-9488-9>
- Chimenos, J. M., Segarra, M., Fernández, M. A., & Espiell, F. (1999). Characterization of the bottom ash in municipal solid waste incinerator. *Journal of Hazardous Materials*, 64(3), 211-222. doi:[http://dx.doi.org/10.1016/S0304-3894\(98\)00246-5](http://dx.doi.org/10.1016/S0304-3894(98)00246-5)
- Chindaprasirt, P., Jaturapitakkul, C., & Sinsiri, T. (2005). Effect of fly ash fineness on compressive strength and pore size of blended cement paste. *Cement and Concrete Composites*, 27(4), 425-428. doi:<https://doi.org/10.1016/j.cemconcomp.2004.07.003>
- Chindaprasirt, P., & Rukzon, S. (2008). Strength, porosity and corrosion resistance of ternary blend Portland cement, rice husk ash and fly ash mortar. *Construction and Building Materials*, 22(8), 1601-1606. doi:<https://doi.org/10.1016/j.conbuildmat.2007.06.010>
- Chousidis, N., Ioannou, I., Rakanta, E., Koutsodontis, C., & Batis, G. (2016). Effect of fly ash chemical composition on the reinforcement corrosion, thermal diffusion and strength of blended cement concretes. *Construction and Building Materials*, 126, 86-97. doi:<https://doi.org/10.1016/j.conbuildmat.2016.09.024>
- Chusilp, N., Jaturapitakkul, C., & Kiattikomol, K. (2009). Utilization of bagasse ash as a pozzolanic material in concrete. *Construction and Building Materials*, 23(11), 3352-3358. doi:<https://doi.org/10.1016/j.conbuildmat.2009.06.030>
- CONAB, C. N. d. A. (2018). Acompanhamento da Safra Brasileira de Cana de Açúcar: Safra 2017/2018. [Follow-up of the Brazilian Sugarcane Harvest: 2017/2018 Harvest]. (Fourth survey).
- Cordeiro, G. C. (2006). *Utilização das cinzas ultrafinas do bagaço de cana de açúcar e da casca de arroz como aditivos minerais em concretos*. Tese Doutorado. Ciências em Engenharia Civil. Universidade Federal do Rio de Janeiro, Rio de Janeiro, RJ,
- Cordeiro, G. C., & Kurtis, K. E. (2017). Effect of mechanical processing on sugar cane bagasse ash pozzolanicity. *Cement and Concrete Research*, 97, 41-49. doi:<http://dx.doi.org/10.1016/j.cemconres.2017.03.008>
- Cordeiro, G. C., Tavares, L. M., & Toledo Filho, R. D. (2016). Improved pozzolanic activity of sugar cane bagasse ash by selective grinding and classification.

- Cement and Concrete Research*, 89, 269-275.
doi:<http://dx.doi.org/10.1016/j.cemconres.2016.08.020>
- Cordeiro, G. C., Toledo Filho, R. D., & Fairbairn, E. M. R. (2009). Effect of calcination temperature on the pozzolanic activity of sugar cane bagasse ash. *Construction and Building Materials*, 23(10), 3301-3303.
doi:<https://doi.org/10.1016/j.conbuildmat.2009.02.013>
- Cordeiro, G. C., Toledo Filho, R. D., Tavares, L. M., & Fairbairn, E. M. R. (2008). Pozzolanic activity and filler effect of sugar cane bagasse ash in Portland cement and lime mortars. *Cement and Concrete Composites*, 30(5), 410-418.
doi:<http://dx.doi.org/10.1016/j.cemconcomp.2008.01.001>
- Corinaldesi, V., Mazzoli, A., & Moriconi, G. (2011). Mechanical behaviour and thermal conductivity of mortars containing waste rubber particles. *Materials & Design*, 32(3), 1646-1650. doi:<https://doi.org/10.1016/j.matdes.2010.10.013>
- Cowper, A. D. (1998). *Lime and lime mortars*: Donhead Publishing.
- de Burgh, J. M., Foster, S. J., & Valipour, H. R. (2016). Prediction of water vapour sorption isotherms and microstructure of hardened Portland cement pastes. *Cement and Concrete Research*, 81, 134-150. doi:10.1016/j.cemconres.2015.11.009
- Deboucha, W., Leklou, N., Khelidj, A., & Oudjit, M. N. (2017). Natural pozzolana addition effect on compressive strength and capillary water absorption of Mortar. *Energy Procedia*, 139, 689-695.
doi:<https://doi.org/10.1016/j.egypro.2017.11.273>
- Deja, J., Uliasz-Bochenczyk, A., & Mokrzycki, E. (2010). CO₂ emissions from Polish cement industry. *International Journal of Greenhouse Gas Control*, 4(4), 583-588.
doi:<https://doi.org/10.1016/j.ijggc.2010.02.002>
- Demirboğa, R. (2003). Influence of mineral admixtures on thermal conductivity and compressive strength of mortar. *Energy and Buildings*, 35(2), 189-192.
doi:[https://doi.org/10.1016/S0378-7788\(02\)00052-X](https://doi.org/10.1016/S0378-7788(02)00052-X)
- Demirboğa, R., & Gül, R. (2003). The effects of expanded perlite aggregate, silica fume and fly ash on the thermal conductivity of lightweight concrete. *Cement and Concrete Research*, 33(5), 723-727. doi:[https://doi.org/10.1016/S0008-8846\(02\)01032-3](https://doi.org/10.1016/S0008-8846(02)01032-3)
- Eglinton, M. (2003). Resistance of Concrete to Destructive Agencies. *Lea's chemistry of cement and concrete*, 299-342.
- Esquinas, A. R., Álvarez, J. I., Jiménez, J. R., & Fernández, J. M. (2018). Durability of self-compacting concrete made from non-conforming fly ash from coal-fired power plants. *Construction and Building Materials*, 189, 993-1006.
doi:<https://doi.org/10.1016/j.conbuildmat.2018.09.056>

- Felekoğlu, B., Türkel, S., & Kalyoncu, H. (2009). Optimization of fineness to maximize the strength activity of high-calcium ground fly ash – Portland cement composites. *Construction and Building Materials*, 23(5), 2053-2061. doi:<http://dx.doi.org/10.1016/j.conbuildmat.2008.08.024>
- Ferreira, R. T. L., Nunes, F., Bezerra, A. C. d. S., Figueiredo, R. B., Cetlin, P. R., & de Aguiar, M. T. P. (2016). *Influence of Reburning on the Pozzolanicity of Sugar-Cane Bagasse Ashes with Different Characteristics*. Paper presented at the Materials Science Forum.
- Filipponi, P., Poletti, A., Pomi, R., & Sirini, P. (2003). Physical and mechanical properties of cement-based products containing incineration bottom ash. *Waste Management*, 23(2), 145-156. doi:[http://dx.doi.org/10.1016/S0956-053X\(02\)00041-7](http://dx.doi.org/10.1016/S0956-053X(02)00041-7)
- Freedonia Group, T. (2018). World Construction Aggregates to Reach 51.7 Billion Metric Tons. Retrieved from <https://www.prnewswire.com/news-releases/the-freedonia-group-world-construction-aggregates-to-reach-517-billion-metric-tons-300241261.html>
- Frías, M., & Cabrera, J. (2000). Pore size distribution and degree of hydration of metakaolin–cement pastes. *Cement and Concrete Research*, 30(4), 561-569. doi:[https://doi.org/10.1016/S0008-8846\(00\)00203-9](https://doi.org/10.1016/S0008-8846(00)00203-9)
- Frias, M., de Rojas, M. I. S., Santamaría, J., & Rodríguez, C. (2006). Recycling of silicomanganese slag as pozzolanic material in Portland cements: basic and engineering properties. *Cement and Concrete Research*, 36(3), 487-491. doi:<https://doi.org/10.1016/j.cemconres.2005.06.014>
- Frías, M., Villar, E., & Savastano, H. (2011). Brazilian sugar cane bagasse ashes from the cogeneration industry as active pozzolans for cement manufacture. *Cement and Concrete Composites*, 33(4), 490-496. doi:<http://dx.doi.org/10.1016/j.cemconcomp.2011.02.003>
- Fu, X., & Chung, D. D. L. (1997). Effects of silica fume, latex, methylcellulose, and carbon fibers on the thermal conductivity and specific heat of cement paste. *Cement and Concrete Research*, 27(12), 1799-1804. doi:[https://doi.org/10.1016/S0008-8846\(97\)00174-9](https://doi.org/10.1016/S0008-8846(97)00174-9)
- Funari, V., Mäkinen, J., Salminen, J., Braga, R., Dinelli, E., & Revitzer, H. (2017). Metal removal from Municipal Solid Waste Incineration fly ash: A comparison between chemical leaching and bioleaching. *Waste Management*, 60, 397-406. doi:<https://doi.org/10.1016/j.wasman.2016.07.025>
- Ganesan, K., Rajagopal, K., & Thangavel, K. (2007). Evaluation of bagasse ash as supplementary cementitious material. *Cement and Concrete Composites*, 29(6), 515-524. doi:<https://doi.org/10.1016/j.cemconcomp.2007.03.001>

- Garcia-Lodeiro, I., Carcelen-Taboada, V., Fernández-Jiménez, A., & Palomo, A. (2016). Manufacture of hybrid cements with fly ash and bottom ash from a municipal solid waste incinerator. *Construction and Building Materials*, 105, 218-226. doi:<http://dx.doi.org/10.1016/j.conbuildmat.2015.12.079>
- Ghrici, M., Kenai, S., & Said-Mansour, M. (2007). Mechanical properties and durability of mortar and concrete containing natural pozzolana and limestone blended cements. *Cement and Concrete Composites*, 29(7), 542-549. doi:<https://doi.org/10.1016/j.cemconcomp.2007.04.009>
- Gomes, M. G., Flores-Colen, I., Manga, L. M., Soares, A., & de Brito, J. (2017). The influence of moisture content on the thermal conductivity of external thermal mortars. *Construction and Building Materials*, 135, 279-286. doi:<https://doi.org/10.1016/j.conbuildmat.2016.12.166>
- González-Fonteboa, B., Carro-López, D., de Brito, J., Martínez-Abella, F., Seara-Paz, S., & Gutiérrez-Mainar, S. (2017). Comparison of ground bottom ash and limestone as additions in blended cements. *Materials and Structures*, 50(1), 84. doi:<https://doi.org/10.1617/s11527-016-0954-x>
- Gupta, V. K., & Ali, I. (2004). Removal of lead and chromium from wastewater using bagasse fly ash—a sugar industry waste. *Journal of Colloid and Interface Science*, 271(2), 321-328. doi:<https://doi.org/10.1016/j.jcis.2003.11.007>
- Gupta, V. K., Jain, C. K., Ali, I., Sharma, M., & Saini, V. K. (2003). Removal of cadmium and nickel from wastewater using bagasse fly ash—a sugar industry waste. *Water Research*, 37(16), 4038-4044. doi:[https://doi.org/10.1016/S0043-1354\(03\)00292-6](https://doi.org/10.1016/S0043-1354(03)00292-6)
- Gutt, W., & Nixon, P. (1979). Use of waste products in the construction industry. Analysis of the RILEM Symposium by correspondence. *Materiaux & Constructions/Materials & Structures*(70).
- Habeeb, G. A., & Fayyadh, M. (2009). Rice husk ash concrete: the effect of RHA average particle size on mechanical properties and drying shrinkage. *Australian Journal of Basic and Applied Sciences*, 3(3), 1616-1622.
- Halstead, W. (1986). Use of Fly Ash in Concrete. *National Cooperative Highway Research Project*.
- Hammond, G., Jones, C., Lowrie, E. F., & Tse, P. (2011). Embodied carbon. *The inventory of carbon and energy (ICE)*.
- Heikal, M., El-Didamony, H., & Morsy, M. S. (2000). Limestone-filled pozzolanic cement. *Cement and Concrete Research*, 30(11), 1827-1834. doi:[https://doi.org/10.1016/S0008-8846\(00\)00402-6](https://doi.org/10.1016/S0008-8846(00)00402-6)
- Hoorweg, D., & Bhada-Tata, P. (2012). What a waste: a global review of solid waste management.

- Horkoss, S., Escadeillas, G., Rizk, T., & Lteif, R. (2016). The effect of the source of cement SO₃ on the expansion of mortars. *Case Studies in Construction Materials*, 4, 62-72. doi:<https://doi.org/10.1016/j.cscm.2015.12.004>
- Institute, A. C. (2002). *Guide to Thermal Properties of Concrete and Masonry Systems*, ACI 122R-02.
- Ireland, G. o. (2017). *Technical Guidance Document L - Buildings other than Dwellings*. Dublin: Stationery Office.
- Jackson, P. J. (1998). Portland cement: classification and manufacture. *Lea's chemistry of cement and concrete*, 4, 25-94.
- Jagadesh, P., Ramachandramurthy, A., Murugesan, R., & Sarayu, K. (2015). Micro-analytical studies on sugar cane bagasse ash. *Sadhana*, 40(5), 1629-1638. doi:<https://doi.org/10.1007/s12046-015-0390-6>
- Jennings, H. M., Bullard, J. W., Thomas, J. J., Andrade, J. E., Chen, J. J., & Scherer, G. W. (2008). Characterization and modeling of pores and surfaces in cement paste. *Journal of Advanced Concrete Technology*, 6(1), 5-29. doi:<https://doi.org/10.3151/jact.6.5>
- Jiménez-Quero, V. G., León-Martínez, F. M., Montes-García, P., Gaona-Tiburcio, C., & Chacón-Nava, J. G. (2013). Influence of sugar-cane bagasse ash and fly ash on the rheological behavior of cement pastes and mortars. *Construction and Building Materials*, 40(Supplement C), 691-701. doi:<https://doi.org/10.1016/j.conbuildmat.2012.11.023>
- Joshi, R. C. (1970). Pozzolanic reactions in synthetic fly ashes.
- Juenger, M. C. G., & Siddique, R. (2015). Recent advances in understanding the role of supplementary cementitious materials in concrete. *Cement and Concrete Research*, 78, Part A, 71-80. doi:<http://dx.doi.org/10.1016/j.cemconres.2015.03.018>
- Jurič, B., Hanžič, L., Ilić, R., & Samec, N. (2006). Utilization of municipal solid waste bottom ash and recycled aggregate in concrete. *Waste Management*, 26(12), 1436-1442. doi:<http://dx.doi.org/10.1016/j.wasman.2005.10.016>
- Kaur, G., & Pavia, S. (2018). Recycled plastic waste in cementitious composites. High Performance cementitious composites. *In press*.
- Kearsley, E. P., & Wainwright, P. J. (2001). Porosity and permeability of foamed concrete. *Cement and Concrete Research*, 31(5), 805-812. doi:[https://doi.org/10.1016/S0008-8846\(01\)00490-2](https://doi.org/10.1016/S0008-8846(01)00490-2)
- Khatib, J. (2016). *Sustainability of construction materials*: Woodhead Publishing.
- Khatib, J., & Wild, S. (1998). Sulphate resistance of metakaolin mortar. *Cement and Concrete Research*, 28(1), 83-92. doi:[https://doi.org/10.1016/S0008-8846\(97\)00210-X](https://doi.org/10.1016/S0008-8846(97)00210-X)

- Khedari, J., Watsanasathaporn, P., & Hirunlabh, J. (2005). Development of fibre-based soil–cement block with low thermal conductivity. *Cement and Concrete Composites*, 27(1), 111-116. doi:<https://doi.org/10.1016/j.cemconcomp.2004.02.042>
- Kiattikomol, K., Jaturapitakkul, C., Songpiriyakij, S., & Chutubtim, S. (2001). A study of ground coarse fly ashes with different finenesses from various sources as pozzolanic materials. *Cement and Concrete Composites*, 23(4–5), 335-343. doi:[http://dx.doi.org/10.1016/S0958-9465\(01\)00016-6](http://dx.doi.org/10.1016/S0958-9465(01)00016-6)
- Kibert, C. J. (2016). *Sustainable construction: green building design and delivery*: John Wiley & Sons.
- Kim, H.-K., Jeon, J., & Lee, H.-K. (2012). Flow, water absorption, and mechanical characteristics of normal-and high-strength mortar incorporating fine bottom ash aggregates. *Construction and Building Materials*, 26(1), 249-256. doi:<https://doi.org/10.1016/j.conbuildmat.2011.06.019>
- Koezjakov, A., Urge-Vorsatz, D., Crijns-Graus, W., & van den Broek, M. (2018). The relationship between operational energy demand and embodied energy in Dutch residential buildings. *Energy and Buildings*, 165, 233-245. doi:<https://doi.org/10.1016/j.enbuild.2018.01.036>
- Kristiawan, S., & Murti, G. (2017). *Porosity of Self-Compacting Concrete (SCC) incorporating high volume fly ash*. Paper presented at the IOP Conference Series: Materials Science and Engineering.
- Kurama, H., & Kaya, M. (2008). Usage of coal combustion bottom ash in concrete mixture. *Construction and Building Materials*, 22(9), 1922-1928. doi:<http://dx.doi.org/10.1016/j.conbuildmat.2007.07.008>
- Lawrence, C. D. (2003). Physicochemical and Mechanical Properties of Portland Cements. In *Lea's chemistry of cement and concrete* (pp. 343-419).
- Lea, F. (1970). *The Chemistry of Cement and Concrete*. 3rd edn, E. Arnold, London.
- Lehne, J., & Preston, F. (2018). Making Concrete Change, Innovation in Low-carbon Cement and Concrete. *Chatham House Report, Energy Environment and Resources Department: London, UK*, 1-66.
- Li, X.-G., Lv, Y., Ma, B.-G., Chen, Q.-B., Yin, X.-B., & Jian, S.-W. (2012). Utilization of municipal solid waste incineration bottom ash in blended cement. *Journal of cleaner production*, 32, 96-100. doi:<http://dx.doi.org/10.1016/j.jclepro.2012.03.038>
- Li, Y., Zhao, X., Li, Y., & Li, X. (2015). Waste incineration industry and development policies in China. *Waste Management*, 46(Supplement C), 234-241. doi:<https://doi.org/10.1016/j.wasman.2015.08.008>
- Lieff, M., & Trechsel, H. R. (1982). *Moisture migration in buildings* (Vol. 779): ASTM International.

- Lin, K., Chang, W., & Lin, D. (2008). Pozzolanic characteristics of pulverized incinerator bottom ash slag. *Construction and Building Materials*, 22(3), 324-329. doi:<https://doi.org/10.1016/j.conbuildmat.2006.08.012>
- Lin, K. L., Wang, K. S., Tzeng, B. Y., & Lin, C. Y. (2003). The reuse of municipal solid waste incinerator fly ash slag as a cement substitute. *Resources, Conservation and Recycling*, 39(4), 315-324. doi:[https://doi.org/10.1016/S0921-3449\(02\)00172-6](https://doi.org/10.1016/S0921-3449(02)00172-6)
- López Zaldívar, Ó., Mayor Lobo, P. L., Fernández Martínez, F., & Hernández Olivares, F. (2015). Improved cement mortars by addition of carbonated fly ash from solid waste incineration. *Materiales de Construcción*, 65(319), e062. doi:<https://doi.org/10.3989/mc.2015.07114>
- Luxán, M. d., Madruga, F., & Saavedra, J. (1989). Rapid evaluation of pozzolanic activity of natural products by conductivity measurement. *Cement and Concrete Research*, 19(1), 63-68. doi:[https://doi.org/10.1016/0008-8846\(89\)90066-5](https://doi.org/10.1016/0008-8846(89)90066-5)
- Maalouf, C., Le, A. D. T., Umurirwa, S. B., Lachi, M., & Douzane, O. (2014). Study of hygrothermal behaviour of a hemp concrete building envelope under summer conditions in France. *Energy and Buildings*, 77, 48-57. doi:<https://doi.org/10.1016/j.enbuild.2014.03.040>
- Mall, I. D., Srivastava, V. C., Agarwal, N. K., & Mishra, I. M. (2005). Adsorptive removal of malachite green dye from aqueous solution by bagasse fly ash and activated carbon-kinetic study and equilibrium isotherm analyses. *Colloids and Surfaces A: Physicochemical and Engineering Aspects*, 264(1), 17-28. doi:<https://doi.org/10.1016/j.colsurfa.2005.03.027>
- Martys, N. S., & Ferraris, C. F. (1997). Capillary transport in mortars and concrete. *Cement and Concrete Research*, 27(5), 747-760. doi:[https://doi.org/10.1016/S0008-8846\(97\)00052-5](https://doi.org/10.1016/S0008-8846(97)00052-5)
- Maso, J. C. (1996). *Interfacial Transition Zone in Concrete*. Retrieved from E&FN Spon, London:
- Massazza, F. (1993). Pozzolanic cements. *Cement and Concrete Composites*, 15(4), 185-214. doi:[https://doi.org/10.1016/0958-9465\(93\)90023-3](https://doi.org/10.1016/0958-9465(93)90023-3)
- Massazza, F. (1998). Pozzolana and pozzolanic cements. *Lea's chemistry of cement and concrete*, 471-632.
- Massazza, F. (2002). Properties and applications of natural pozzolanas. *Structure and Performance of Cements*, 326-352.
- Materion. (2018). Thermal Diffusivity and Effusivity [Press release]. Retrieved from <https://materion.com/-/media/files/alloy/newsletters/technical-tidbits/issue-no-111-thermal-diffusivity-and-effusivity.pdf>

- McCarter, W. J., & Tran, D. (1996). Monitoring pozzolanic activity by direct activation with calcium hydroxide. *Construction and Building Materials*, 10(3), 179-184. doi:[http://dx.doi.org/10.1016/0950-0618\(95\)00089-5](http://dx.doi.org/10.1016/0950-0618(95)00089-5)
- Meddah, M. S., Lmbachiya, M. C., & Dhir, R. K. (2014). Potential use of binary and composite limestone cements in concrete production. *Construction and Building Materials*, 58, 193-205. doi:<https://doi.org/10.1016/j.conbuildmat.2013.12.012>
- Mehta, P. K. (1986). *Concrete. Structure, properties and materials*.
- Mehta, P. K., & Gjrv, O. E. (1982). Properties of portland cement concrete containing fly ash and condensed silica-fume. *Cement and Concrete Research*, 12(5), 587-595. doi:[https://doi.org/10.1016/0008-8846\(82\)90019-9](https://doi.org/10.1016/0008-8846(82)90019-9)
- Mindess, S., Young, J. F., & Darwin, D. (2003). *Concrete, 2003*. Prentice Hall, Upper Saddle River, NJ.
- Monteiro, P., Wang, K., Sposito, G., Dos Santos, M., & de Andrade, W. P. (1997). Influence of mineral admixtures on the alkali-aggregate reaction. *Cement and Concrete Research*, 27(12), 1899-1909. doi:[https://doi.org/10.1016/S0008-8846\(97\)00206-8](https://doi.org/10.1016/S0008-8846(97)00206-8)
- Moropoulou, A., Bakolas, A., Moundoulas, P., Aggelakopoulou, E., & Anagnostopoulou, S. (2005). Strength development and lime reaction in mortars for repairing historic masonries. *Cement and Concrete Composites*, 27(2), 289-294. doi:<https://doi.org/10.1016/j.cemconcomp.2004.02.017>
- Mller, U., & Rbner, K. (2006). The microstructure of concrete made with municipal waste incinerator bottom ash as an aggregate component. *Cement and Concrete Research*, 36(8), 1434-1443. doi:<http://dx.doi.org/10.1016/j.cemconres.2006.03.023>
- Nair, D. G., Fraaij, A., Klaassen, A. A., & Kentgens, A. P. (2008). A structural investigation relating to the pozzolanic activity of rice husk ashes. *Cement and Concrete Research*, 38(6), 861-869. doi:<https://doi.org/10.1016/j.cemconres.2007.10.004>
- Nakata, Y., Suzuki, M., Okutani, T., Kikuchi, M., & Akiyama, T. (1989). Preparation and properties of SiO₂ from rice hulls. *Journal of the Ceramic Society of Japan*, 97(1128), 842-849. doi:<https://doi.org/10.2109/jcersj.97.842>
- Navrtilov, E., & Rovnankov, P. (2016). Pozzolanic properties of brick powders and their effect on the properties of modified lime mortars. *Construction and Building Materials*, 120, 530-539. doi:<https://doi.org/10.1016/j.conbuildmat.2016.05.062>
- Nehdi, M., & Hayek, M. (2005). Behavior of blended cement mortars exposed to sulfate solutions cycling in relative humidity. *Cement and Concrete Research*, 35(4), 731-742. doi:<https://doi.org/10.1016/j.cemconres.2004.05.032>
- Neville, A. M. (1995). *Properties of Concrete (Fourth Ed.)*. Essex, England: Longman Group Limited.

- Obe, R. K. D., de Brito, J., Lynn, C. J., & Silva, R. V. (2017). *Sustainable Construction Materials: Municipal Incinerated Bottom Ash*: Woodhead Publishing.
- Pandey, S., & Sharma, R. (2000). The influence of mineral additives on the strength and porosity of OPC mortar. *Cement and Concrete Research*, 30(1), 19-23. doi:[https://doi.org/10.1016/S0008-8846\(99\)00180-5](https://doi.org/10.1016/S0008-8846(99)00180-5)
- Patil, D. (2018). Types of Solids - The Solid State of Matter. Retrieved from <https://hemantmore.org.in/foundation/science/chemistry/solid-state/9330/>
- Pavia, S., & Aly, M. (2016). Influence of aggregate and supplementary cementitious materials on the properties of hydrated lime (CL90s) mortars. *Materiales de Construcción*, 66(324), 104. doi:<https://doi.org/10.3989/mc.2016.01716>
- Pavia, S., Fitzgerald, B., & Treacy, E. (2006). *An assessment of lime mortars for masonry repair*. Paper presented at the Concrete Research in Ireland Colloquium, University College Dublin, Dublin.
- Pavia, S., & Toomey, B. (2008). Influence of the aggregate quality on the physical properties of natural feebly-hydraulic lime mortars. *Materials and Structures*, 41(3), 559-569. doi:<https://doi.org/10.1617/s11527-007-9267-4>
- Pavia, S., Walker, R., Veale, P., & Wood, A. (2014). Impact of the properties and reactivity of rice husk ash on lime mortar properties. *Journal of Materials in Civil Engineering*, 26(9), 04014066. doi:[https://doi.org/10.1061/\(ASCE\)MT.1943-5533.0000967](https://doi.org/10.1061/(ASCE)MT.1943-5533.0000967)
- Payá, J., Monzó, J., Borrachero, M. V., Díaz-Pinzón, L., & Ordóñez, L. M. (2002). Sugarcane bagasse ash (SCBA): studies on its properties for reusing in concrete production. *Journal of Chemical Technology and Biotechnology*, 77(3), 321-325. doi:<https://doi.org/10.1002/jctb.549>
- Payá, J., Monzó, J., Borrachero, M. V., & Peris-Mora, E. (1995a). Mechanical treatment of fly ashes. Part I: Physico-chemical characterization of ground fly ashes. *Cement and Concrete Research*, 25(7), 1469-1479. doi:10.1016/0008-8846(95)00141-X
- Payá, J., Monzó, J., Peris-Mora, E., Borrachero, M. V., Tercero, R., & Pinillos, C. (1995b). Early-strength development of portland cement mortars containing air classified fly ashes. *Cement and Concrete Research*, 25(2), 449-456. doi:[https://doi.org/10.1016/0008-8846\(95\)00031-3](https://doi.org/10.1016/0008-8846(95)00031-3)
- Pera, J., Coutaz, L., Ambroise, J., & Chababbet, M. (1997). Use of incinerator bottom ash in concrete. *Cement and Concrete Research*, 27(1), 1-5. doi:[http://dx.doi.org/10.1016/S0008-8846\(96\)00193-7](http://dx.doi.org/10.1016/S0008-8846(96)00193-7)
- Pereira, A., Akasaki, J. L., Melges, J. L., Tashima, M. M., Soriano, L., Borrachero, M. V., . . . Payá, J. (2015). Mechanical and durability properties of alkali-activated mortar based on sugarcane bagasse ash and blast furnace slag. *Ceramics*

- International*, 41(10), 13012-13024.
doi:<https://doi.org/10.1016/j.ceramint.2015.07.001>
- Poon, C.-S., Kou, S., & Lam, L. (2006). Compressive strength, chloride diffusivity and pore structure of high performance metakaolin and silica fume concrete. *Construction and Building Materials*, 20(10), 858-865.
doi:<https://doi.org/10.1016/j.conbuildmat.2005.07.001>
- Puertas, F., Amat, T., Fernández-Jiménez, A., & Vázquez, T. (2003). Mechanical and durable behaviour of alkaline cement mortars reinforced with polypropylene fibres. *Cement and Concrete Research*, 33(12), 2031-2036.
doi:[https://doi.org/10.1016/S0008-8846\(03\)00222-9](https://doi.org/10.1016/S0008-8846(03)00222-9)
- Ramezani pour, A. A. (2014). Fly ash. In *Cement replacement materials* (pp. 47-156): Springer.
- Raut, A. N., & Gomez, C. P. (2017). *Performance Evaluation of Newly Developed Sustainable Blocks for Affordable Housing in Malaysia*. Paper presented at the MATEC Web of Conferences.
- RILEM. (1980). Recommended tests to measure the deterioration of stone and to assess the effectiveness of treatment methods: Commission 25-PEM Protection et erosion des Monuments. *Materiaux et Constructions*, 216-220.
- Ríos-Parada, V., Jiménez-Quero, V. G., Valdez-Tamez, P. L., & Montes-García, P. (2017). Characterization and use of an untreated Mexican sugarcane bagasse ash as supplementary material for the preparation of ternary concretes. *Construction and Building Materials*, 157, 83-95.
doi:<https://doi.org/10.1016/j.conbuildmat.2017.09.060>
- Sabir, B. B. (1997). Mechanical properties and frost resistance of silica fume concrete. *Cement and Concrete Composites*, 19(4), 285-294.
doi:[https://doi.org/10.1016/S0958-9465\(97\)00020-6](https://doi.org/10.1016/S0958-9465(97)00020-6)
- Sales, A., & Lima, S. A. (2010). Use of Brazilian sugarcane bagasse ash in concrete as sand replacement. *Waste Management*, 30(6), 1114-1122.
doi:<http://dx.doi.org/10.1016/j.wasman.2010.01.026>
- Sata, V., Jaturapitakkul, C., & Kiattikomol, K. (2007). Influence of pozzolan from various by-product materials on mechanical properties of high-strength concrete. *Construction and Building Materials*, 21(7), 1589-1598.
doi:<https://doi.org/10.1016/j.conbuildmat.2005.09.011>
- Sathonsaowaphak, A., Chindaprasirt, P., & Pimraksa, K. (2009). Workability and strength of lignite bottom ash geopolymer mortar. *Journal of Hazardous Materials*, 168(1), 44-50. doi:<http://dx.doi.org/10.1016/j.jhazmat.2009.01.120>
- Scrivener, K. L., Bentur, A., & Pratt, P. (1988). Quantitative characterization of the transition zone in high strength concretes. *advances in Cement Research*, 1(4), 230-237. doi:<https://doi.org/10.1680/adcr.1988.1.4.230>

- Scrivener, K. L., John, V. M., & Gartner, E. M. (2016). Eco-efficient cements: Potential economically viable solutions for a low-CO₂ cement-based materials industry. *Cement and Concrete Research*. doi:<https://doi.org/10.1016/j.cemconres.2018.03.015>
- Sharma, A. K., & Sivapullaiah, P. V. (2016). Strength development in fly ash and slag mixtures with lime. *Proceedings of the Institution of Civil Engineers: Ground Improvement*, 169(3), 194-205. doi:10.1680/jgrim.14.00024
- Shoubi, M. V., Shoubi, M. V., Bagchi, A., & Barough, A. S. (2015). Reducing the operational energy demand in buildings using building information modeling tools and sustainability approaches. *Ain Shams Engineering Journal*, 6(1), 41-55. doi:<https://doi.org/10.1016/j.asej.2014.09.006>
- Siddique, R. (2003). Effect of fine aggregate replacement with Class F fly ash on the mechanical properties of concrete. *Cement and Concrete Research*, 33(4), 539-547. doi:[https://doi.org/10.1016/S0008-8846\(02\)01000-1](https://doi.org/10.1016/S0008-8846(02)01000-1)
- Siddique, R. (2004). Performance characteristics of high-volume Class F fly ash concrete. *Cement and Concrete Research*, 34(3), 487-493. doi:<https://doi.org/10.1016/j.cemconres.2003.09.002>
- Siddique, R. (2010). Use of municipal solid waste ash in concrete. *Resources, Conservation and Recycling*, 55(2), 83-91. doi:<https://doi.org/10.1016/j.resconrec.2010.10.003>
- Souza, L. M. S. d., Fairbairn, E. d. M. R., Toledo Filho, R. D., & Cordeiro, G. C. (2014). Influence of initial CaO/SiO₂ ratio on the hydration of rice husk ash-Ca (OH)₂ and sugar cane bagasse ash-Ca (OH)₂ pastes. *Química Nova*, 37(10), 1600-1605. doi:<http://dx.doi.org/10.5935/0100-4042.20140258>
- Srivastava, V. C., Mall, I. D., & Mishra, I. M. (2006). Equilibrium modelling of single and binary adsorption of cadmium and nickel onto bagasse fly ash. *Chemical Engineering Journal*, 117(1), 79-91. doi:<https://doi.org/10.1016/j.cej.2005.11.021>
- Stefanidou, M., Tsardaka, E.-C., & Pavlidou, E. (2017). Influence of nano-silica and nano-alumina in lime-pozzolan and lime-metakaolin binders. *Materials Today: Proceedings*, 4(7), 6908-6922. doi:<https://doi.org/10.1016/j.matpr.2017.07.020>
- Takahashi, E., Ma, J., & Miyake, Y. (1990). The possibility of silicon as an essential element for higher plants. *Comments on Agricultural and Food Chemistry*, 2(2), 99-102.
- Tang, P., Florea, M. V. A., Spiesz, P., & Brouwers, H. J. H. (2015). Characteristics and application potential of municipal solid waste incineration (MSWI) bottom ashes from two waste-to-energy plants. *Construction and Building Materials*, 83, 77-94. doi:<http://dx.doi.org/10.1016/j.conbuildmat.2015.02.033>
- Tang, P., Florea, M. V. A., Spiesz, P., & Brouwers, H. J. H. (2016). Application of thermally activated municipal solid waste incineration (MSWI) bottom ash

- finer as binder substitute. *Cement and Concrete Composites*, 70, 194-205. doi:<http://dx.doi.org/10.1016/j.cemconcomp.2016.03.015>
- Tangpagasit, J., Cheerarot, R., Jaturapitakkul, C., & Kiattikomol, K. (2005). Packing effect and pozzolanic reaction of fly ash in mortar. *Cement and Concrete Research*, 35(6), 1145-1151. doi:<https://doi.org/10.1016/j.cemconres.2004.09.030>
- Taoukil, D., El bouardi, A., Sick, F., Mimet, A., Ezbakhe, H., & Ajzoul, T. (2013). Moisture content influence on the thermal conductivity and diffusivity of wood-concrete composite. *Construction and Building Materials*, 48, 104-115. doi:<https://doi.org/10.1016/j.conbuildmat.2013.06.067>
- Taylor, H., Famy, C., & Scrivener, K. (2001). Delayed ettringite formation. *Cement and Concrete Research*, 31(5), 683-693. doi:[https://doi.org/10.1016/S0008-8846\(01\)00466-5](https://doi.org/10.1016/S0008-8846(01)00466-5)
- Taylor, H. F. (1986). Proposed structure for calcium silicate hydrate gel. *Journal of the American Ceramic Society*, 69(6), 464-467. doi:<https://doi.org/10.1111/j.1151-2916.1986.tb07446.x>
- Taylor, H. F. (1997). *Cement chemistry*: Thomas Telford.
- Taylor, H. W. (1950). 726. Hydrated calcium silicates. Part I. Compound formation at ordinary temperatures. *Journal of the Chemical Society (Resumed)*, 3682-3690.
- Thipse, S. S., Schoenitz, M., & Dreizin, E. L. (2002). Morphology and composition of the fly ash particles produced in incineration of municipal solid waste. *Fuel Processing Technology*, 75(3), 173-184. doi:[http://dx.doi.org/10.1016/S0378-3820\(02\)00007-3](http://dx.doi.org/10.1016/S0378-3820(02)00007-3)
- Thomas, J. J., & Jennings, H. M. (2018, 14/08/2018). The science of concrete. Retrieved from <http://iti.northwestern.edu/cement/index.html>
- Thomas, M. (1989). The effect of curing on the hydration and pore structure of hardened cement paste containing pulverized fuel ash. *advances in Cement Research*, 2(8), 181-188. doi:<https://doi.org/10.1680/adcr.1989.2.8.181>
- Thomas, M. (2013). *Supplementary cementing materials in concrete*: CRC press.
- Tironi, A., Trezza, M. A., Scian, A. N., & Irassar, E. F. (2013). Assessment of pozzolanic activity of different calcined clays. *Cement and Concrete Composites*, 37, 319-327. doi:<https://doi.org/10.1016/j.cemconcomp.2013.01.002>
- Torii, K., & Kawamura, M. (1994). Effects of fly ash and silica fume on the resistance of mortar to sulfuric acid and sulfate attack. *Cement and Concrete Research*, 24(2), 361-370. doi:[https://doi.org/10.1016/0008-8846\(94\)90063-9](https://doi.org/10.1016/0008-8846(94)90063-9)
- Tosun, K. (2006). Effect of SO₃ content and fineness on the rate of delayed ettringite formation in heat cured Portland cement mortars. *Cement and Concrete Composites*, 28(9), 761-772. doi:<https://doi.org/10.1016/j.cemconcomp.2006.06.003>

- Tubaña, B. S., & Heckman, J. R. (2015). Silicon in soils and plants. In *Silicon and Plant Diseases* (pp. 7-51): Springer.
- Ubbriaco, P., & Calabrese, D. (1998). Solidification and stabilization of cement paste containing fly ash from municipal solid waste. *Thermochimica acta*, 321(1-2), 143-150. doi:[https://doi.org/10.1016/S0040-6031\(98\)00453-5](https://doi.org/10.1016/S0040-6031(98)00453-5)
- UNFCCC. (2016). *Industrial Processes and Product Use (IPPU)*. Retrieved from https://unfccc.int/files/national_reports/non-annex_i_natcom/cge/application/pdf/ippu_ps_lesotho_2016.pdf.
- UNFCCC. (2017). Bigger Climate Action Emerging in Cement Industry. Retrieved from <https://unfccc.int/news/bigger-climate-action-emerging-in-cement-industry>
- Vejmelková, E., Keppert, M., Rovnaníková, P., Keršner, Z., & Černý, R. (2012). Application of burnt clay shale as pozzolan addition to lime mortar. *Cement and Concrete Composites*, 34(4), 486-492. doi:<http://dx.doi.org/10.1016/j.cemconcomp.2012.01.001>
- Velandia, D. F., Lynsdale, C. J., Provis, J. L., Ramirez, F., & Gomez, A. C. (2016). Evaluation of activated high volume fly ash systems using Na₂SO₄, lime and quicklime in mortars with high loss on ignition fly ashes. *Construction and Building Materials*, 128, 248-255. doi:<https://doi.org/10.1016/j.conbuildmat.2016.10.076>
- Vu, D., Stroeven, P., & Bui, V. (2001). Strength and durability aspects of calcined kaolin-blended Portland cement mortar and concrete. *Cement and Concrete Composites*, 23(6), 471-478. doi:[https://doi.org/10.1016/S0958-9465\(00\)00091-3](https://doi.org/10.1016/S0958-9465(00)00091-3)
- Walker, R. (2013). *A Study of the Properties of Lime-Hemp Concrete with Pozzolans*. (Doctor of Philosophy), Trinity College Dublin, Dublin Ireland.
- Walker, R., & Pavia, S. (2010). *Effect of pozzolan properties on the properties of building composites*. Paper presented at the BCRI Bridge Infrastructure Concrete Research, University College Cork.
- Walker, R., & Pavia, S. (2011). Physical properties and reactivity of pozzolans, and their influence on the properties of lime-pozzolan pastes. *Materials and Structures*, 44(6), 1139-1150. doi:<https://doi.org/10.1617/s11527-010-9689-2>
- Walker, R., & Pavia, S. (2014). Moisture transfer and thermal properties of hemp-lime concretes. *Construction and Building Materials*. doi:<https://doi.org/10.1016/j.conbuildmat.2014.04.081>
- Walker, R., & Pavia, S. (2015). Thermal performance of a selection of insulation materials suitable for historic buildings. *Building and environment*, 94, 155-165. doi:<https://doi.org/10.1016/j.buildenv.2015.07.033>

- Walker, R., Pavia, S., & Mitchell, R. (2014). Mechanical properties and durability of hemp-lime concretes. *Construction and Building Materials*, 61, 340-348. doi:<https://doi.org/10.1016/j.conbuildmat.2014.02.065>
- Wang, H., & Gillott, J. (1991). Mechanism of alkali-silica reaction and the significance of calcium hydroxide. *Cement and Concrete Research*, 21(4), 647-654. doi:[https://doi.org/10.1016/0008-8846\(91\)90115-X](https://doi.org/10.1016/0008-8846(91)90115-X)
- Wang, I. F., Lee, C. H., & Lu, C. K. (2017). *Compressive Strength and High-Temperature Residual Strength of Cement Specimens Containing Bagasse Ash*. Paper presented at the Key Engineering Materials.
- Wang, Y., Huang, L., & Lau, R. (2016). Conversion of municipal solid waste incineration bottom ash to sorbent material for pollutants removal from water. *Journal of the Taiwan Institute of Chemical Engineers*, 60, 275-286. doi:<http://dx.doi.org/10.1016/j.jtice.2015.10.013>
- Wei, Y., Shimaoka, T., Saffarzadeh, A., & Takahashi, F. (2011). Mineralogical characterization of municipal solid waste incineration bottom ash with an emphasis on heavy metal-bearing phases. *Journal of Hazardous Materials*, 187(1-3), 534-543. doi:<http://dx.doi.org/10.1016/j.jhazmat.2011.01.070>
- Wild, S., Khatib, J. M., & Jones, A. (1996). Relative strength, pozzolanic activity and cement hydration in superplasticised metakaolin concrete. *Cement and Concrete Research*, 26(10), 1537-1544. doi:[https://doi.org/10.1016/0008-8846\(96\)00148-2](https://doi.org/10.1016/0008-8846(96)00148-2)
- Winkler, E. (2013a). *Stone in architecture: properties, durability*: Springer Science & Business Media.
- Winkler, E. M. (2013b). *Stone: properties, durability in man's environment* (Vol. 4): Springer Science & Business Media.
- Winkler, E. M., & Singer, P. C. (1972). Crystallization pressure of salts in stone and concrete. *Bulletin of the Geological Society of America*, 83(11), 3509-3514. doi:10.1130/0016-7606(1972)83[3509:CPOSIS]2.0.CO;2
- Wongkeo, W., Thongsanitgarn, P., Pimraksa, K., & Chaipanich, A. (2012). Compressive strength, flexural strength and thermal conductivity of autoclaved concrete block made using bottom ash as cement replacement materials. *Materials & Design*, 35, 434-439. doi:<https://doi.org/10.1016/j.matdes.2011.08.046>
- Wongsa, A., Boonserm, K., Waisurasingha, C., Sata, V., & Chindaprasirt, P. (2017). Use of municipal solid waste incinerator (MSWI) bottom ash in high calcium fly ash geopolymer matrix. *Journal of cleaner production*, 148, 49-59. doi:<https://doi.org/10.1016/j.jclepro.2017.01.147>
- Worrell, E., Price, L., Martin, N., Hendriks, C., & Meida, L. O. (2001). Carbon dioxide emissions from the global cement industry. *Annual review of energy and the environment*, 26(1), 303-329.

- Xu, Y., & Chung, D. D. L. (1999). Increasing the specific heat of cement paste by admixture surface treatments. *Cement and Concrete Research*, 29(7), 1117-1121. doi:[https://doi.org/10.1016/S0008-8846\(99\)00080-0](https://doi.org/10.1016/S0008-8846(99)00080-0)
- Xu, Y., & Chung, D. D. L. (2000a). Cement of high specific heat and high thermal conductivity, obtained by using silane and silica fume as admixtures. *Cement and Concrete Research*, 30(7), 1175-1178. doi:[https://doi.org/10.1016/S0008-8846\(00\)00296-9](https://doi.org/10.1016/S0008-8846(00)00296-9)
- Xu, Y., & Chung, D. D. L. (2000b). Effect of sand addition on the specific heat and thermal conductivity of cement. *Cement and Concrete Research*, 30(1), 59-61. doi:[https://doi.org/10.1016/S0008-8846\(99\)00206-9](https://doi.org/10.1016/S0008-8846(99)00206-9)
- Zareei, S. A., Ameri, F., & Bahrami, N. (2018). Microstructure, strength, and durability of eco-friendly concretes containing sugarcane bagasse ash. *Construction and Building Materials*, 184, 258-268. doi:<https://doi.org/10.1016/j.conbuildmat.2018.06.153>
- Zhang, M. H., Lastra, R., & Malhotra, V. M. (1996). Rice-husk ash paste and concrete: Some aspects of hydration and the microstructure of the interfacial zone between the aggregate and paste. *Cement and Concrete Research*, 26(6), 963-977. doi:[https://doi.org/10.1016/0008-8846\(96\)00061-0](https://doi.org/10.1016/0008-8846(96)00061-0)

This page intentionally left blank

Appendix A THERMAL CONDUCTIVITY TEST – HEAT FLOW AND SPECIFIC HEAT

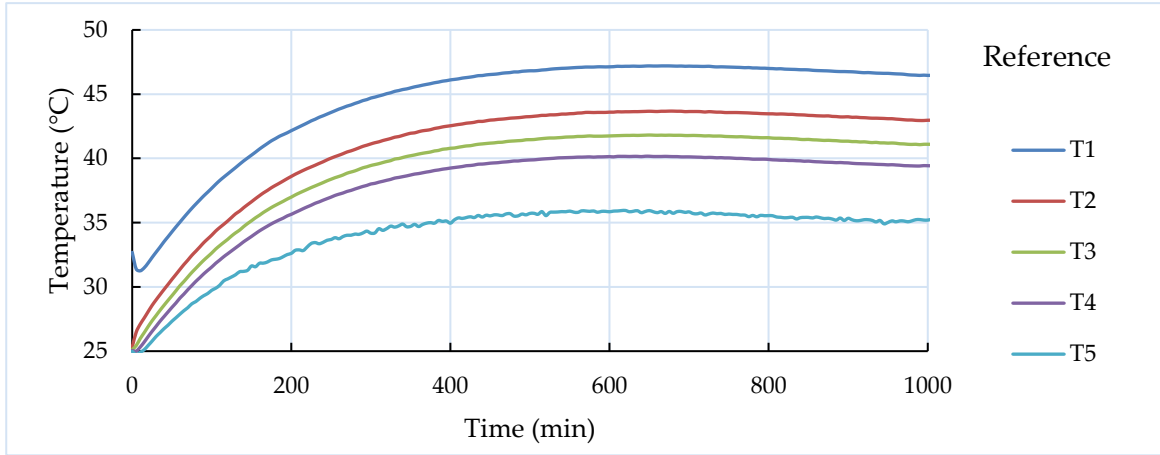


Figure A - 1: Heat flow for thermal conductivity test – reference.

Table A - 1: Thermal conductivity measurements – Reference mortar.

Reference					
Time (min)	T1	T2	T3	T4	T5
501-600	47.01	43.46	41.64	40.04	35.82
601-700	47.18	43.65	41.79	40.15	35.86
701-800	47.11	43.58	41.71	40.03	35.64
801-900	46.88	43.36	41.47	39.78	35.38
901-1000	46.61	43.09	41.20	39.51	35.15
Δt	T1 - T2	T2 - T3	T3 - T4	T4 - T5	
501-600	3.55	1.82	1.60	4.22	
601-700	3.53	1.85	1.64	4.29	
701-800	3.53	1.87	1.68	4.39	
801-900	3.52	1.89	1.69	4.41	
901-1000	3.52	1.89	1.69	4.36	
k	T1 - T2	T2 - T3	T3 - T4	T4 - T5	
501-600	0.704	1.376	1.562	0.592	
601-700	0.708	1.348	1.520	0.583	
701-800	0.709	1.335	1.489	0.570	
801-900	0.711	1.324	1.477	0.567	
901-1000	0.711	1.323	1.483	0.573	
min	0.704	1.323	1.477	0.567	
max	0.711	1.376	1.562	0.592	
Average	1.033				
St. Dev	0.398				

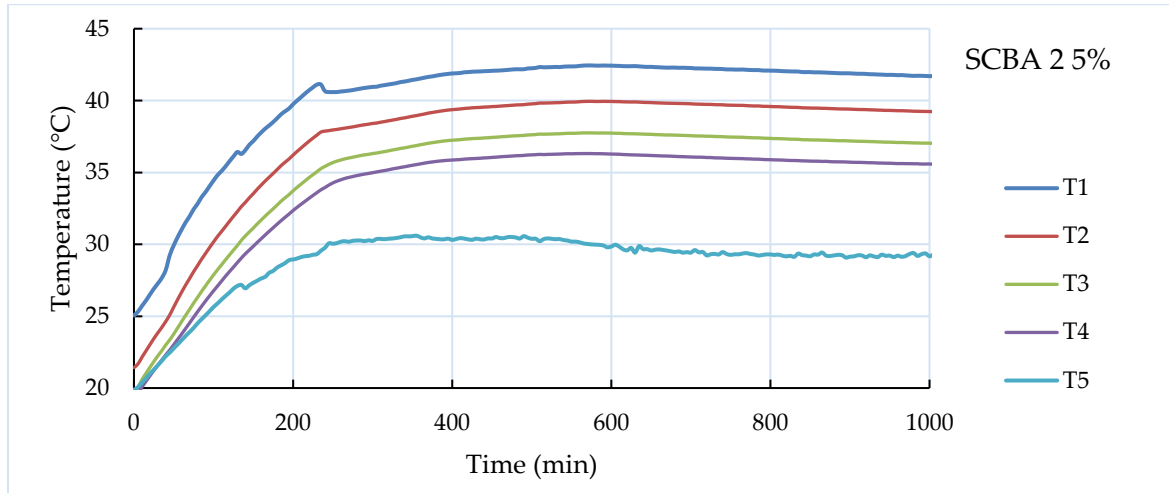


Figure A - 2: Heat flow for thermal conductivity test – SCBA 2 5%.

Table A - 2: Thermal conductivity measurements – SCBA 2 5% mortar.

SCBA 2 - 5%					
Time (min)	T1	T2	T3	T4	T5
501-600	42.37	39.88	37.71	36.28	30.18
601-700	42.35	39.86	37.65	36.18	29.63
701-800	42.17	39.69	37.47	35.99	29.34
801-900	41.99	39.49	37.28	35.80	29.24
901-1000	41.79	39.32	37.11	35.64	29.21
Δt	T1 - T2	T2 - T3	T3 - T4	T4 - T5	
501-600	2.49	2.18	1.42	6.10	
601-700	2.48	2.21	1.47	6.55	
701-800	2.49	2.22	1.48	6.64	
801-900	2.49	2.22	1.48	6.56	
901-1000	2.48	2.21	1.47	6.43	
k	T1 - T2	T2 - T3	T3 - T4	T4 - T5	
501-600	0.643	0.735	1.124	0.262	
601-700	0.644	0.724	1.090	0.244	
701-800	0.643	0.722	1.079	0.241	
801-900	0.642	0.722	1.083	0.244	
901-1000	0.646	0.724	1.092	0.249	
min	0.642	0.722	1.079	0.241	
max	0.646	0.735	1.124	0.262	
Average	0.678				
St. Dev	0.301				

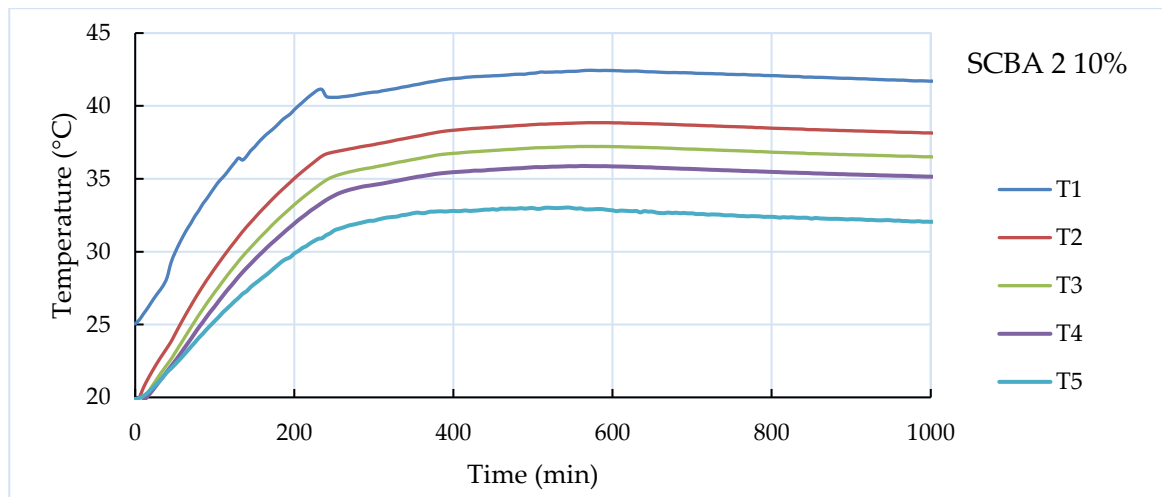


Figure A - 3: Heat flow for thermal conductivity test – SCBA 2 10%.

Table A - 3: Thermal conductivity measurements – SCBA 2 10% mortar.

SCBA 2 - 10%					
Time (min)	T1	T2	T3	T4	T5
501-600	42.37	38.81	37.19	35.85	32.96
601-700	42.35	38.78	37.14	35.77	32.72
701-800	42.17	38.59	36.94	35.58	32.50
801-900	41.99	38.39	36.74	35.39	32.30
901-1000	41.79	38.22	36.58	35.23	32.14
Δt	T1 - T2	T2 - T3	T3 - T4	T4 - T5	
501-600	3.57	1.62	1.34	2.89	
601-700	3.57	1.64	1.36	3.05	
701-800	3.59	1.65	1.37	3.08	
801-900	3.60	1.65	1.35	3.08	
901-1000	3.57	1.64	1.36	3.09	
k	T1 - T2	T2 - T3	T3 - T4	T4 - T5	
501-600	0.449	0.988	1.195	0.554	
601-700	0.448	0.976	1.175	0.525	
701-800	0.446	0.972	1.172	0.519	
801-900	0.445	0.971	1.182	0.519	
901-1000	0.448	0.975	1.179	0.519	
min	0.445	0.971	1.172	0.519	
max	0.449	0.988	1.195	0.554	
Average	0.783				
St. Dev	0.306				

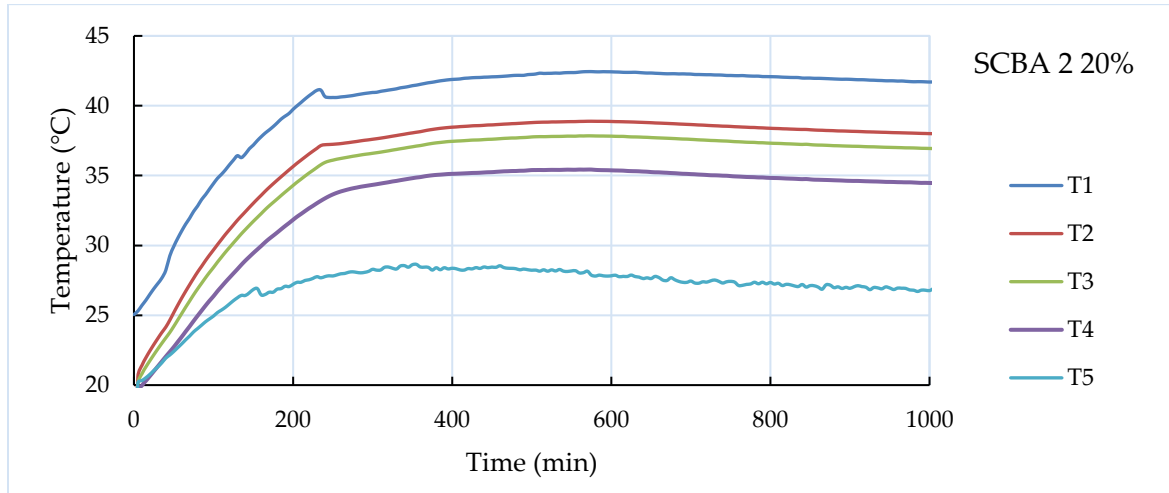


Figure A - 4: Heat flow for thermal conductivity test – SCBA 2 20%.

Table A - 4: Thermal conductivity measurements – SCBA 2 20% mortar.

SCBA 2 - 20%					
Time (min)	T1	T2	T3	T4	T5
501-600	42.37	38.86	37.82	35.41	28.09
601-700	42.35	38.78	37.72	35.26	27.66
701-800	42.17	38.52	37.46	34.97	27.34
801-900	41.99	38.28	37.22	34.73	27.11
901-1000	41.79	38.09	37.03	34.55	26.92
Δt	T1 - T2	T2 - T3	T3 - T4	T4 - T5	
501-600	3.52	1.04	2.41	7.32	
601-700	3.56	1.06	2.46	7.60	
701-800	3.65	1.07	2.49	7.64	
801-900	3.70	1.07	2.48	7.63	
901-1000	3.70	1.06	2.47	7.63	
k	T1 - T2	T2 - T3	T3 - T4	T4 - T5	
501-600	0.455	1.538	0.665	0.219	
601-700	0.449	1.510	0.649	0.210	
701-800	0.438	1.502	0.643	0.210	
801-900	0.432	1.501	0.644	0.210	
901-1000	0.432	1.503	0.647	0.210	
min	0.432	1.501	0.643	0.210	
max	0.455	1.538	0.665	0.219	
Average	0.703				
St. Dev	0.491				

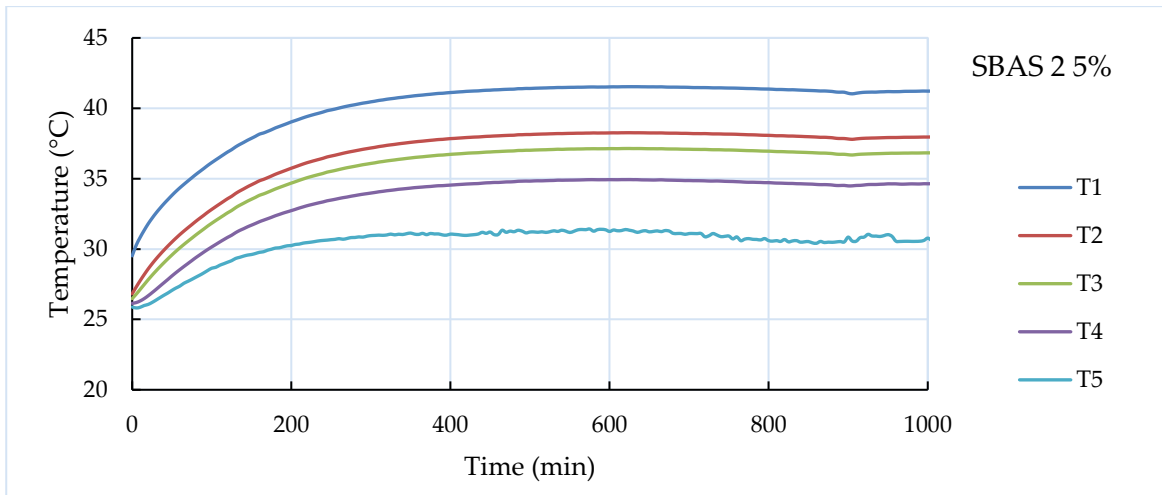


Figure A - 5: Heat flow for thermal conductivity test – SBAS 2 5%.

Table A - 5: Thermal conductivity measurements – SBAS 2 5% mortar.

SBAS 2 - 5%					
Time (min)	T1	T2	T3	T4	T5
501-600	41.48	38.21	37.09	34.89	31.29
601-700	41.52	38.25	37.13	34.91	31.25
701-800	41.44	38.16	37.03	34.80	30.87
801-900	41.27	37.98	36.85	34.62	30.53
901-1000	41.16	37.90	36.78	34.59	30.74
Δt	T1 - T2	T2 - T3	T3 - T4	T4 - T5	
501-600	3.27	1.12	2.20	3.60	
601-700	3.27	1.12	2.21	3.66	
701-800	3.28	1.13	2.23	3.93	
801-900	3.29	1.13	2.24	4.09	
901-1000	3.26	1.12	2.19	3.85	
k	T1 - T2	T2 - T3	T3 - T4	T4 - T5	
501-600	0.489	1.431	0.728	0.444	
601-700	0.489	1.426	0.722	0.437	
701-800	0.488	1.422	0.717	0.407	
801-900	0.487	1.422	0.716	0.391	
901-1000	0.491	1.428	0.730	0.415	
min	0.487	1.422	0.716	0.391	
max	0.491	1.431	0.730	0.444	
Average	0.764				
St. Dev	0.398				

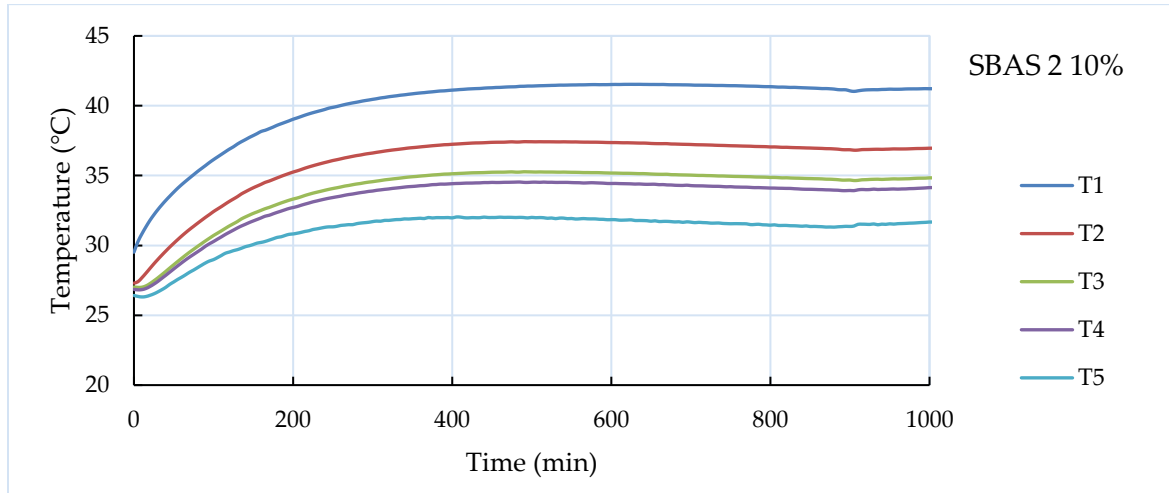


Figure A - 6: Heat flow for thermal conductivity test – SBAS 2 10%.

Table A - 6: Thermal conductivity measurements – SBAS 2 10% mortar.

SBAS 2 - 10%					
Time (min)	T1	T2	T3	T4	T5
501-600	41.48	37.41	35.23	34.50	31.93
601-700	41.52	37.31	35.12	34.37	31.76
701-800	41.44	37.15	34.96	34.20	31.57
801-900	41.27	36.97	34.78	34.02	31.38
901-1000	41.16	36.89	34.74	34.03	31.54
Δt	T1 - T2	T2 - T3	T3 - T4	T4 - T5	
501-600	4.07	2.17	0.74	2.57	
601-700	4.21	2.19	0.75	2.61	
701-800	4.29	2.19	0.75	2.63	
801-900	4.30	2.18	0.76	2.64	
901-1000	4.27	2.15	0.72	2.49	
k	T1 - T2	T2 - T3	T3 - T4	T4 - T5	
501-600	0.393	0.737	2.174	0.622	
601-700	0.380	0.731	2.145	0.612	
701-800	0.373	0.731	2.119	0.608	
801-900	0.372	0.733	2.100	0.605	
901-1000	0.375	0.745	2.231	0.642	
min	0.372	0.731	2.100	0.605	
max	0.393	0.745	2.231	0.642	
Average	0.971				
St. Dev	0.695				

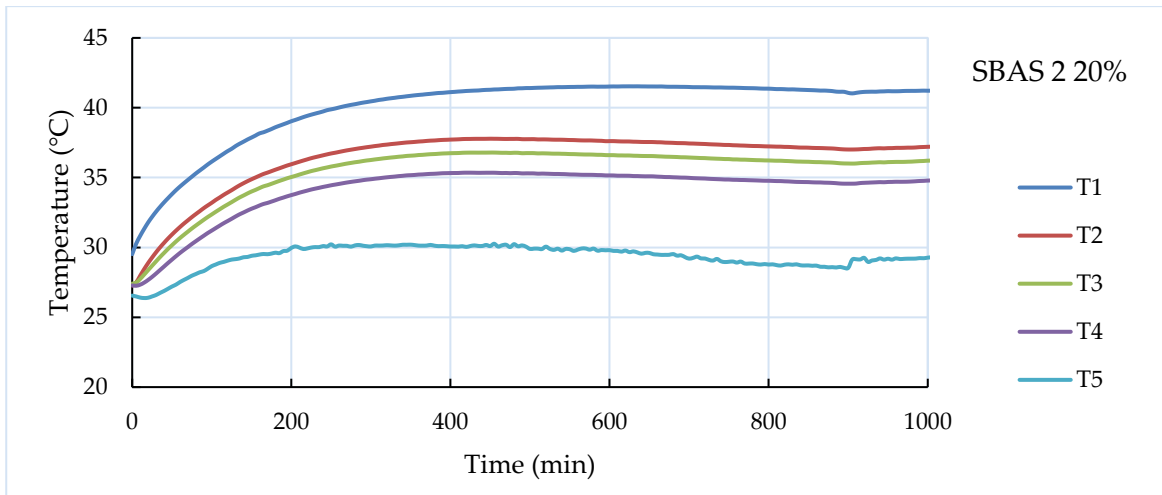


Figure A - 7: Heat flow for thermal conductivity test – SBAS 2 20%.

Table A - 7: Thermal conductivity measurements – SBAS 2 20% mortar.

SBAS 2 - 20%					
Time (min)	T1	T2	T3	T4	T5
501-600	41.48	37.69	36.69	35.23	29.87
601-700	41.52	37.54	36.54	35.08	29.58
701-800	41.44	37.34	36.33	34.87	29.02
801-900	41.27	37.14	36.13	34.68	28.69
901-1000	41.16	37.10	36.10	34.67	29.13
Δt	T1 - T2	T2 - T3	T3 - T4	T4 - T5	
501-600	3.79	1.00	1.45	5.36	
601-700	3.98	1.01	1.45	5.50	
701-800	4.10	1.01	1.46	5.85	
801-900	4.12	1.01	1.45	5.99	
901-1000	4.06	1.00	1.43	5.54	
k	T1 - T2	T2 - T3	T3 - T4	T4 - T5	
501-600	0.423	1.596	1.100	0.298	
601-700	0.402	1.591	1.101	0.291	
701-800	0.391	1.584	1.096	0.273	
801-900	0.388	1.584	1.100	0.267	
901-1000	0.394	1.598	1.122	0.289	
min	0.388	1.584	1.096	0.267	
max	0.423	1.598	1.122	0.298	
Average	0.844				
St. Dev	0.533				

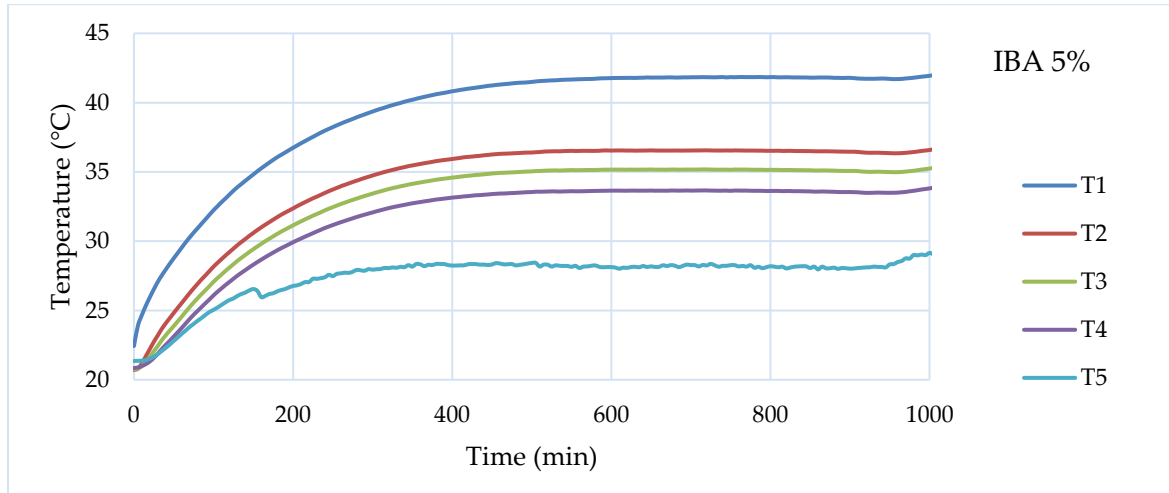


Figure A - 8: Heat flow for thermal conductivity test – IBA 2 5%.

Table A - 8: Thermal conductivity measurements – IBA 2 5% mortar.

IBA 2 - 5%					
Time (min)	T1	T2	T3	T4	T5
501-600	41.64	36.50	35.12	33.60	28.22
601-700	41.80	36.54	35.17	33.65	28.16
701-800	41.84	36.54	35.17	33.65	28.21
801-900	41.82	36.50	35.12	33.59	28.11
901-1000	41.75	36.41	35.05	33.56	28.41
Δt	T1 - T2	T2 - T3	T3 - T4	T4 - T5	
501-600	5.14	1.38	1.51	5.38	
601-700	5.26	1.38	1.52	5.49	
701-800	5.29	1.38	1.52	5.43	
801-900	5.32	1.38	1.52	5.49	
901-1000	5.34	1.37	1.49	5.14	
k	T1 - T2	T2 - T3	T3 - T4	T4 - T5	
501-600	0.311	1.159	1.056	0.297	
601-700	0.304	1.162	1.055	0.292	
701-800	0.302	1.160	1.055	0.294	
801-900	0.301	1.158	1.050	0.292	
901-1000	0.300	1.171	1.074	0.311	
min	0.300	1.158	1.050	0.292	
max	0.311	1.171	1.074	0.311	
Average	0.705				
St. Dev	0.406				

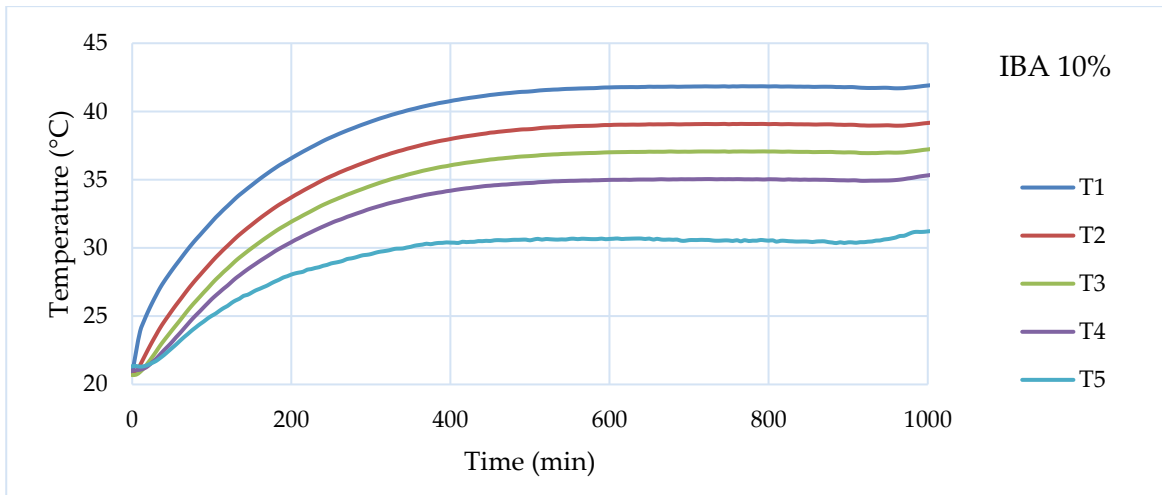


Figure A - 9: Heat flow for thermal conductivity test – IBA 2 10%.

Table A - 9: Thermal conductivity measurements – IBA 2 10% mortar.

IBA 2 - 10%					
Time (min)	T1	T2	T3	T4	T5
501-600	41.64	38.88	36.89	34.90	30.64
601-700	41.80	39.05	37.04	35.01	30.64
701-800	41.84	39.08	37.07	35.04	30.55
801-900	41.82	39.06	37.04	35.00	30.47
901-1000	41.75	39.00	37.01	35.01	30.71
Δt	T1 - T2	T2 - T3	T3 - T4	T4 - T5	
501-600	2.75	2.00	1.99	4.25	
601-700	2.75	2.00	2.03	4.37	
701-800	2.76	2.01	2.03	4.48	
801-900	2.76	2.02	2.04	4.53	
901-1000	2.75	1.99	2.00	4.30	
k	T1 - T2	T2 - T3	T3 - T4	T4 - T5	
501-600	0.581	0.802	0.803	0.376	
601-700	0.581	0.798	0.789	0.366	
701-800	0.580	0.794	0.788	0.357	
801-900	0.580	0.793	0.785	0.353	
901-1000	0.582	0.804	0.800	0.372	
min	0.580	0.793	0.785	0.353	
max	0.582	0.804	0.803	0.376	
Average	0.634				
St. Dev	0.179				

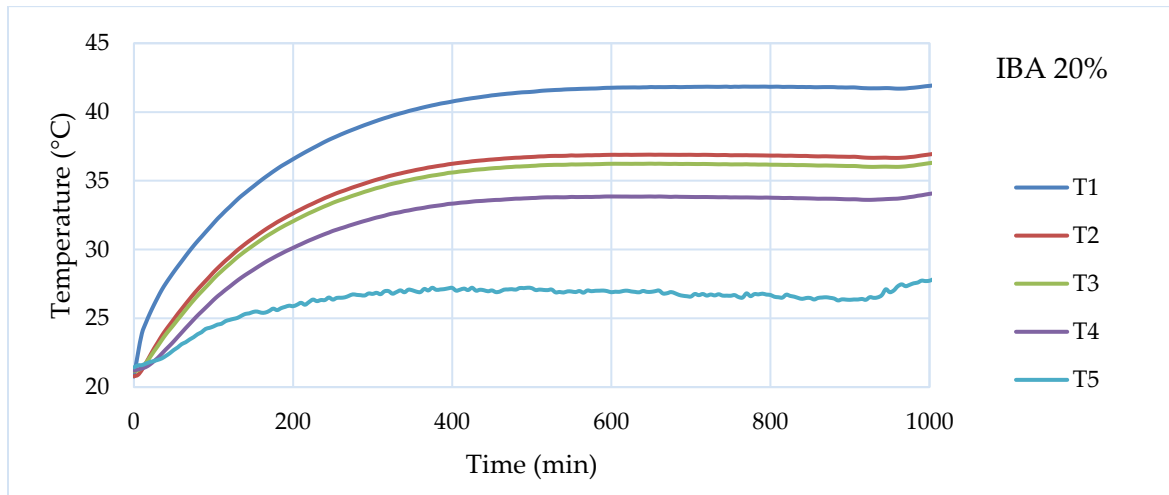


Figure A - 10: Heat flow for thermal conductivity test – IBA 2 20%.

Table A - 10: Thermal conductivity measurements – IBA 2 20% mortar.

IBA 2 - 20%					
Time (min)	T1	T2	T3	T4	T5
501-600	41.64	36.82	36.17	33.81	27.00
601-700	41.80	36.89	36.23	33.85	26.88
701-800	41.84	36.87	36.20	33.80	26.69
801-900	41.82	36.80	36.13	33.72	26.50
901-1000	41.75	36.72	36.06	33.72	26.96
Δt	T1 - T2	T2 - T3	T3 - T4	T4 - T5	
501-600	4.82	0.65	2.36	6.81	
601-700	4.91	0.66	2.39	6.96	
701-800	4.97	0.66	2.40	7.11	
801-900	5.02	0.67	2.41	7.22	
901-1000	5.04	0.65	2.34	6.76	
k	T1 - T2	T2 - T3	T3 - T4	T4 - T5	
501-600	0.332	2.460	0.677	0.235	
601-700	0.326	2.437	0.671	0.230	
701-800	0.322	2.406	0.666	0.225	
801-900	0.319	2.400	0.664	0.222	
901-1000	0.318	2.454	0.684	0.237	
min	0.318	2.400	0.664	0.222	
max	0.332	2.460	0.684	0.237	
Average	0.914				
St. Dev	0.892				

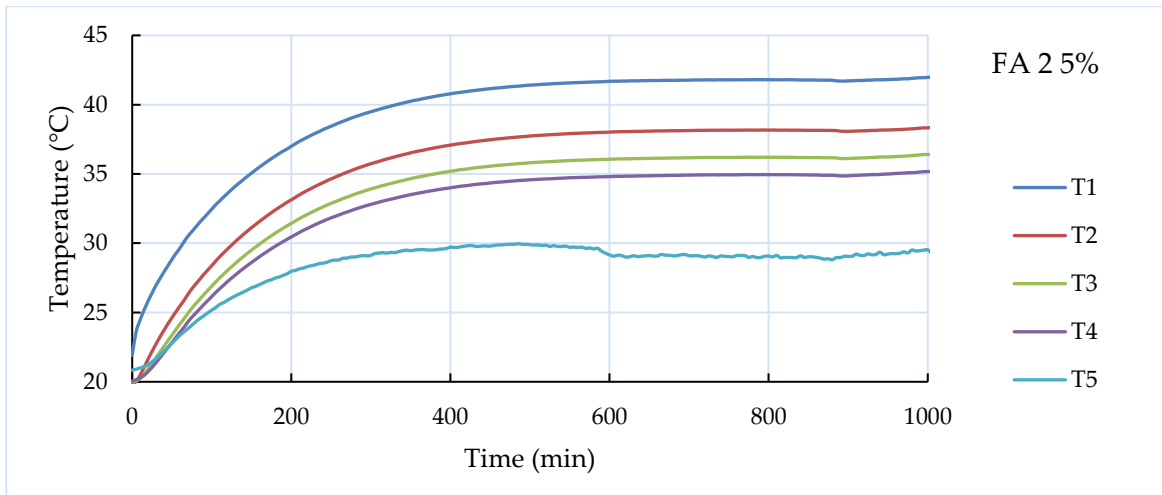


Figure A - 11: Heat flow for thermal conductivity test – FA 2.5%.

Table A - 11: Thermal conductivity measurements – FA 2.5% mortar.

FA 2 - 5%					
Time (min)	T1	T2	T3	T4	T5
501-600	41.54	37.89	35.94	34.70	29.71
601-700	41.72	38.08	36.12	34.86	29.10
701-800	41.79	38.15	36.19	34.94	29.05
801-900	41.78	38.14	36.18	34.92	28.98
901-1000	41.81	38.18	36.24	35.00	29.26
Δt	T1 - T2	T2 - T3	T3 - T4	T4 - T5	
501-600	3.65	1.94	1.24	4.99	
601-700	3.64	1.96	1.26	5.76	
701-800	3.63	1.96	1.25	5.89	
801-900	3.63	1.97	1.26	5.94	
901-1000	3.63	1.94	1.24	5.74	
k	T1 - T2	T2 - T3	T3 - T4	T4 - T5	
501-600	0.438	0.823	1.289	0.321	
601-700	0.439	0.815	1.275	0.278	
701-800	0.440	0.815	1.276	0.272	
801-900	0.440	0.814	1.273	0.269	
901-1000	0.441	0.824	1.294	0.279	
min	0.438	0.814	1.273	0.269	
max	0.441	0.824	1.294	0.321	
Average	0.706				
St. Dev	0.385				

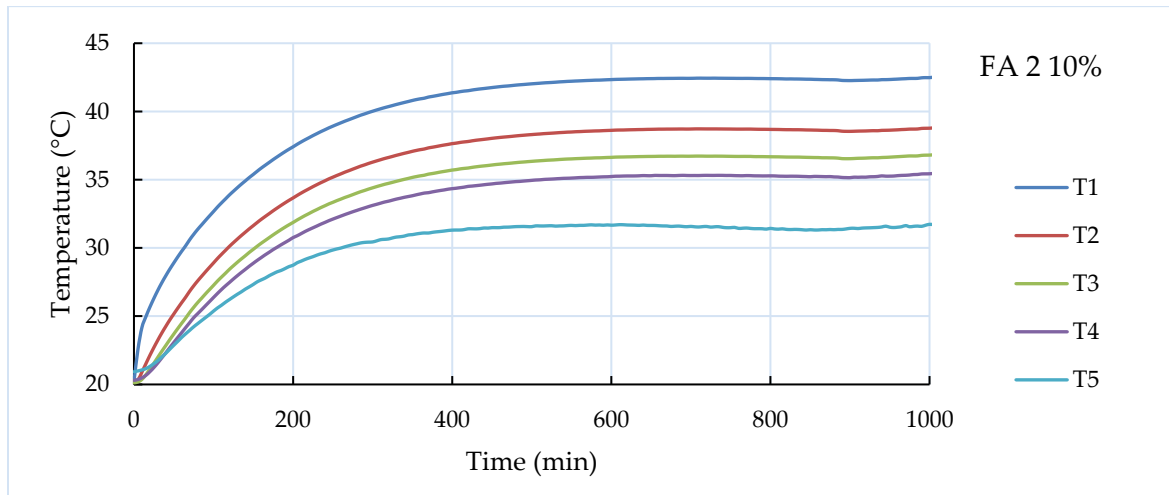


Figure A - 12: Heat flow for thermal conductivity test – FA 2 10%.

Table A - 12: Thermal conductivity measurements – FA 2 10% mortar.

FA 2 - 10%					
Time (min)	T1	T2	T3	T4	T5
501-600	42.20	38.48	36.51	35.11	31.64
601-700	42.40	38.68	36.70	35.29	31.64
701-800	42.43	38.71	36.71	35.30	31.49
801-900	42.36	38.64	36.63	35.23	31.36
901-1000	42.35	38.64	36.66	35.28	31.53
Δt	T1 - T2	T2 - T3	T3 - T4	T4 - T5	
501-600	3.72	1.97	1.40	3.47	
601-700	3.72	1.98	1.41	3.65	
701-800	3.72	2.00	1.41	3.81	
801-900	3.72	2.01	1.40	3.88	
901-1000	3.71	1.98	1.38	3.75	
k	T1 - T2	T2 - T3	T3 - T4	T4 - T5	
501-600	0.430	0.812	1.142	0.462	
601-700	0.431	0.806	1.138	0.438	
701-800	0.431	0.800	1.134	0.420	
801-900	0.430	0.797	1.146	0.413	
901-1000	0.431	0.808	1.159	0.427	
min	0.430	0.797	1.134	0.413	
max	0.431	0.812	1.159	0.462	
Average	0.703				
St. Dev	0.297				

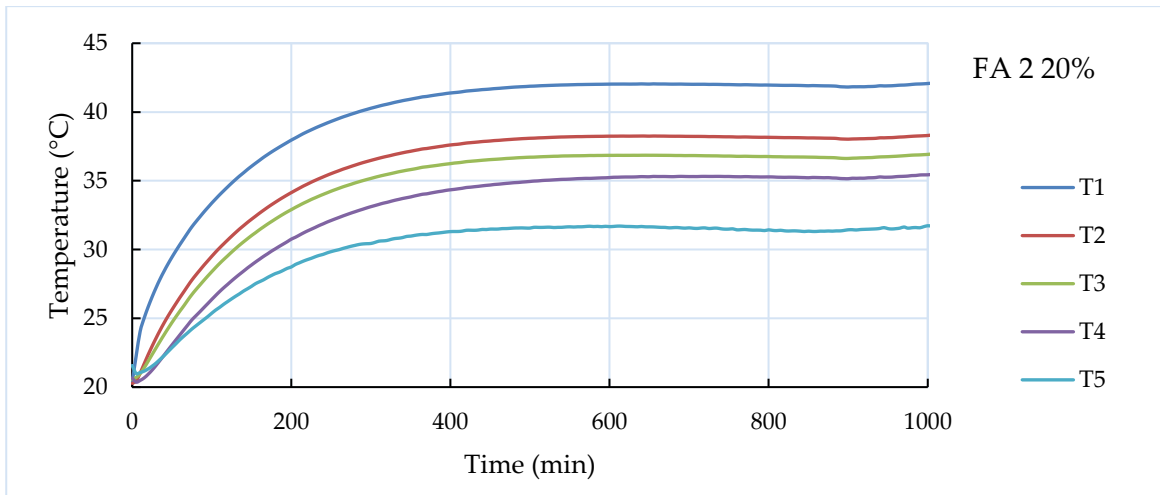


Figure A - 13: Heat flow for thermal conductivity test – FA 2 20%.

Table A - 13: Thermal conductivity measurements – FA 2 20% mortar.

FA 2 - 20%					
Time (min)	T1	T2	T3	T4	T5
501-600	41.97	38.18	36.80	35.11	31.64
601-700	42.03	38.25	36.85	35.29	31.64
701-800	41.99	38.20	36.80	35.30	31.49
801-900	41.92	38.12	36.71	35.23	31.36
901-1000	41.92	38.14	36.76	35.28	31.53
Δt	T1 - T2	T2 - T3	T3 - T4	T4 - T5	
501-600	3.78	1.39	1.69	3.47	
601-700	3.79	1.40	1.56	3.65	
701-800	3.80	1.40	1.49	3.81	
801-900	3.80	1.40	1.48	3.88	
901-1000	3.78	1.38	1.48	3.75	
k	T1 - T2	T2 - T3	T3 - T4	T4 - T5	
501-600	0.423	1.155	0.947	0.462	
601-700	0.422	1.146	1.027	0.438	
701-800	0.421	1.143	1.071	0.420	
801-900	0.421	1.140	1.082	0.413	
901-1000	0.423	1.158	1.082	0.427	
min	0.421	1.140	0.947	0.413	
max	0.423	1.158	1.082	0.462	
Average	0.761				
St. Dev	0.337				

Table A - 14: Determination of Specific Heat of samples.

Sample		Masses (g)		Initial temperatures (°C)		Equilibrium temperature (°C)	Changes in temperature (°C)		Q (J)	C specimen (J/g.°C)	Mean value (J/g.°C)	
		specimen	water	specimen	water		Δt specimen	Δt water				
Ref	0	a	52.55	364.50	80.10	20.10	22.90	-57.20	2.80	4270190.40	1420.622	1445.711
		b	44.73	262.03	80.10	19.10	22.60	-57.50	3.50	3837167.32	1491.915	
		c	40.68	292.41	98.20	18.60	22.20	-76.00	3.60	4404396.38	1424.596	
SCBA 1	5	a	48.28	216.57	99.80	17.00	21.90	-77.90	4.90	4440031.51	1180.542	1188.262
		b	48.88	222.07	99.90	17.50	22.30	-77.60	4.80	4459876.22	1175.790	
		c	51.46	223.58	99.80	17.90	23.00	-76.80	5.10	4770839.47	1207.157	
		d	56.79	223.99	99.80	18.00	23.50	-76.30	5.50	5154457.88	1189.561	
	10	a	45.40	222.48	99.90	18.10	22.50	-77.40	4.40	4095767.80	1165.570	1149.314
		b	49.77	214.68	100.00	17.90	22.80	-77.20	4.90	4401283.48	1145.498	
		c	47.06	223.23	99.90	18.00	22.50	-77.40	4.50	4202974.44	1153.889	
		d	49.70	226.02	100.00	18.10	22.70	-77.30	4.60	4350071.32	1132.297	
	20	a	48.54	227.35	100.00	18.30	22.80	-77.20	4.50	4280545.80	1142.305	1099.368
		b	51.28	230.45	99.90	18.40	22.80	-77.10	4.40	4242492.32	1073.047	
		c	52.77	234.32	100.00	18.50	23.00	-77.00	4.50	4411776.96	1085.765	
		d	54.23	232.20	100.00	18.50	23.20	-76.80	4.70	4566166.56	1096.354	
SCBA 2	5	a	39.63	218.28	100.00	18.50	22.80	-77.20	4.30	3927119.13	1283.609	1249.327
		b	43.85	249.87	99.80	19.10	23.10	-76.70	4.00	4181824.32	1243.371	
		c	48.00	235.31	99.90	19.50	24.00	-75.90	4.50	4430416.68	1216.078	
		d	48.62	234.75	99.90	19.50	24.20	-75.70	4.70	4616311.80	1254.251	
	10	a	45.70	231.98	99.90	19.60	23.80	-76.10	4.20	4076538.14	1172.170	1216.746
		b	49.40	239.68	99.90	19.30	23.90	-76.00	4.60	4612977.15	1228.686	
		c	43.31	223.69	100.00	19.60	23.90	-76.10	4.30	4024451.52	1221.051	
		d	42.97	237.34	100.00	19.80	23.90	-76.10	4.10	4071425.29	1245.078	
	20	a	39.38	230.18	99.90	20.90	24.80	-75.10	3.90	3755985.16	1270.013	1244.705
		b	40.72	241.66	100.00	21.20	25.00	-75.00	3.80	3842200.67	1258.088	

Sample	Masses (g)		Initial temperatures (°C)		Equilibrium temperature (°C)	Changes in temperature (°C)		Q (J)	C specimen (J/g.°C)	Mean value (J/g.°C)	
	specimen	water	specimen	water		Δt specimen	Δt water				
	c	44.94	238.95	99.80	21.30	25.40	-74.40	4.10	4099043.88	1225.961	
	d	41.69	222.94	99.90	20.90	25.00	-74.90	4.10	3824401.93	1224.757	
SBAS 1	5	a	46.07	229.80	99.90	18.40	22.60	-77.30	4.20	4038229.44	1133.948
		b	46.42	219.93	99.90	18.10	22.60	-77.30	4.50	4140842.04	1153.995
		c	48.47	243.24	99.90	18.10	22.40	-77.50	4.30	4376179.48	1164.985
		d	45.36	214.97	99.90	18.10	22.60	-77.30	4.50	4047455.16	1154.329
	10	a	44.13	228.86	99.90	18.00	22.10	-77.80	4.10	3925955.98	1143.489
		b	44.87	210.20	99.90	18.00	22.50	-77.40	4.50	3957645.60	1139.567
		c	45.64	212.67	99.90	18.00	22.60	-77.30	4.60	4093131.88	1160.194
		d	44.09	223.75	99.90	18.00	22.30	-77.60	4.30	4025531.00	1176.580
	20	a	50.52	222.90	99.90	18.10	22.80	-77.10	4.70	4383283.92	1125.335
		b	47.40	228.11	99.90	18.10	22.50	-77.40	4.40	4199413.85	1144.641
		c	18.29	236.70	99.90	18.10	19.80	-80.10	1.70	1683599.76	1149.192
		d	48.84	203.62	99.90	18.10	23.00	-76.90	4.90	4174535.79	1111.492
SBAS 2	5	a	42.97	229.41	99.90	18.10	22.00	-77.90	3.90	3743420.61	1118.319
		b	49.05	220.91	99.90	18.20	22.80	-77.10	4.60	4251722.22	1124.272
		c	49.58	235.95	99.80	18.30	22.60	-77.20	4.30	4245023.64	1109.063
		d	42.78	226.27	99.90	18.40	22.30	-77.60	3.90	3692183.35	1112.195
	10	a	44.82	219.42	99.90	18.40	22.70	-77.20	4.30	3947629.10	1140.899
		b	45.26	251.91	99.90	18.40	22.30	-77.60	3.90	4110566.61	1170.376
		c	53.85	221.95	99.90	18.40	23.50	-76.40	5.10	4736057.88	1151.166
		d	44.59	231.61	99.90	18.50	22.50	-77.40	4.00	3876224.96	1123.131
	20	a	80.32	235.79	99.90	18.50	25.10	-74.80	6.60	6511199.37	1083.766
		b	32.22	231.93	99.90	18.50	21.60	-78.30	3.10	3008224.87	1192.403
		c	45.82	237.24	99.90	18.50	22.60	-77.30	4.10	4069709.85	1149.023
		d	47.45	251.64	99.90	18.50	22.80	-77.10	4.30	4527305.56	1237.511

Sample		Masses (g)		Initial temperatures (°C)		Equilibrium temperature (°C)	Changes in temperature (°C)		Q (J)	C specimen (J/g·°C)	Mean value (J/g·°C)	
		specimen	water	specimen	water		Δt specimen	Δt water				
IBA 1	5	a	32.50	213.96	99.70	19.30	22.60	-77.10	3.30	2954188.51	1178.964	1143.488
		b	41.42	217.89	99.20	18.80	22.60	-76.60	3.80	3464276.68	1091.877	
		c	42.83	210.59	98.40	18.60	22.90	-75.50	4.30	3788766.80	1171.663	
		d	45.27	210.34	98.60	18.60	23.00	-75.60	4.40	3872275.26	1131.446	
	10	a	43.02	203.66	98.10	18.40	22.90	-75.20	4.50	3834510.48	1185.282	1175.189
		b	42.97	226.62	98.00	18.50	22.60	-75.40	4.10	3887530.12	1199.878	
		c	41.58	209.49	98.30	18.40	22.50	-75.80	4.10	3593675.25	1140.211	
		d	36.60	211.75	98.30	18.40	22.10	-76.20	3.70	3278059.40	1175.387	
	20	a	46.76	237.90	98.80	18.40	22.50	-76.30	4.10	4081031.76	1143.855	1160.553
		b	44.35	240.62	98.20	18.10	21.90	-76.30	3.80	3825665.50	1130.548	
		c	40.26	224.10	98.40	18.10	22.00	-76.40	3.90	3656774.16	1188.861	
		d	33.40	199.99	98.10	18.00	21.60	-76.50	3.60	3012329.37	1178.948	
IBA 2	5	a	45.33	214.07	99.90	18.10	22.60	-77.30	4.50	4030509.96	1150.257	1177.340
		b	44.98	207.16	99.90	18.20	22.80	-77.10	4.60	3987084.22	1149.692	
		c	54.23	231.98	99.90	18.30	23.20	-76.70	4.90	4755961.16	1143.414	
		d	44.62	231.32	100.00	18.40	22.90	-77.10	4.50	4355292.96	1265.999	
	10	a	42.50	221.92	99.90	18.60	22.70	-77.20	4.10	3806904.44	1160.288	1162.152
		b	50.34	234.48	100.00	18.80	23.30	-76.70	4.50	4414789.44	1143.409	
		c	45.64	234.41	100.00	18.80	23.00	-77.00	4.20	4119240.04	1172.143	
		d	54.23	247.09	100.00	18.90	23.60	-76.40	4.70	4858975.43	1172.767	
	20	a	79.85	254.62	99.90	19.10	25.00	-74.90	5.90	6285447.47	1050.944	1098.771
		b	56.33	248.91	99.90	19.10	23.60	-76.30	4.50	4686477.48	1090.391	
		c	48.32	246.83	99.80	21.00	25.20	-74.60	4.20	4337494.22	1203.298	
		d	53.80	243.13	99.90	22.00	26.10	-73.80	4.10	4170749.27	1050.450	
FA 1	5	a	43.66	236.04	100.00	16.00	20.20	-79.80	4.20	4147883.71	1190.529	1218.110
		b	42.65	233.99	100.00	16.20	20.40	-79.60	4.20	4111859.47	1211.173	

Sample	Masses (g)		Initial temperatures (°C)		Equilibrium temperature (°C)	Changes in temperature (°C)		Q (J)	C specimen (J/g.°C)	Mean value (J/g.°C)		
	specimen	water	specimen	water		Δt specimen	Δt water					
		c	43.91	238.66	100.00	16.30	20.50	-79.50	4.20	4193924.44	1201.407	
		d	48.28	235.25	100.00	16.40	21.30	-78.70	4.90	4823001.40	1269.332	
	10	a	47.15	243.32	100.00	16.50	21.10	-78.90	4.60	4683034.04	1258.834	
		b	43.65	236.88	100.00	16.50	20.80	-79.20	4.30	4261755.45	1232.762	
		c	39.44	235.33	100.00	16.70	20.70	-79.30	4.00	3938482.88	1259.270	
		d	44.54	239.41	100.00	16.80	21.10	-78.90	4.30	4307273.19	1225.675	
	20	a	42.17	234.53	100.00	16.90	21.10	-78.90	4.20	4121348.78	1238.679	
		b	40.55	230.13	100.00	16.90	21.00	-79.00	4.10	3947742.07	1232.341	
		c	40.44	233.64	100.00	17.00	21.20	-78.80	4.20	4105708.99	1288.400	
		d	48.62	249.16	100.00	17.00	21.60	-78.40	4.60	4795433.02	1258.047	
	FA 2	5	a	44.77	230.24	99.90	16.70	21.20	-78.70	4.50	4334958.72	1230.334
			b	43.20	231.51	99.80	16.80	21.00	-78.80	4.20	4068278.92	1195.090
c			47.70	220.89	99.80	16.70	21.40	-78.40	4.70	4343757.67	1161.532	
d			49.30	232.59	99.90	16.60	21.40	-78.50	4.80	4671151.48	1207.000	
10		a	42.96	215.16	99.90	16.30	21.30	-78.60	5.00	4501147.20	1333.019	
		b	49.30	232.00	100.00	16.30	21.30	-78.70	5.00	4853440.00	1250.916	
		c	45.65	231.54	100.00	16.50	21.30	-78.70	4.80	4650064.12	1294.325	
		d	38.97	227.64	99.90	16.70	20.90	-79.00	4.20	4000272.19	1299.368	
20		a	47.99	224.64	100.00	16.70	22.00	-78.00	5.30	4981436.92	1330.789	
		b	44.12	222.60	99.90	16.80	21.60	-78.30	4.80	4470520.32	1294.079	
		c	41.38	229.19	99.90	16.90	21.40	-78.50	4.50	4315189.32	1328.433	
		d	39.39	223.71	99.90	16.90	21.30	-78.60	4.40	4118411.61	1330.213	
FA 3	5	a	40.51	223.02	99.80	17.00	21.10	-78.70	4.10	3825774.28	1200.003	
		b	32.75	223.03	100.00	17.10	20.60	-79.40	3.50	3266051.32	1256.005	
		c	51.38	224.68	99.90	17.20	22.10	-77.80	4.90	4606299.48	1152.334	
		d	45.02	225.99	100.00	17.20	21.70	-78.30	4.50	4254939.72	1207.052	

Potential of waste materials as pozzolans and their influence on the quality of building materials

Sample		Masses (g)		Initial temperatures (°C)		Equilibrium temperature (°C)	Changes in temperature (°C)		Q (J)	C specimen (J/g·°C)	Mean value (J/g·°C)
		specimen	water	specimen	water		Δt specimen	Δt water			
10	a	40.29	226.58	100.00	17.20	21.10	-78.90	3.90	3697241.80	1163.064	1200.947
	b	37.42	215.11	100.00	17.20	21.20	-78.80	4.00	3600080.96	1220.906	
	c	46.65	218.09	100.00	17.30	22.10	-77.90	4.80	4379945.08	1205.257	
	d	41.42	203.88	100.00	17.40	22.00	-78.00	4.60	3923956.03	1214.561	
20	a	43.65	238.78	100.00	17.40	21.40	-78.60	4.00	3996222.08	1164.777	1212.044
	b	44.73	243.15	100.00	17.50	21.70	-78.30	4.20	4272826.32	1219.985	
	c	47.17	246.56	100.00	17.40	21.80	-78.20	4.40	4539070.97	1230.536	
	d	42.31	227.02	100.00	17.40	21.70	-78.30	4.30	4084362.22	1232.876	

Appendix B STANDARD FORCE VS STRAIN – MODULUS OF ELASTICITY

The series of tests were performed on specimens with dimensions of 160x40x40 mm. The results are presented as the arithmetic means of six determinations. In cases of a results varying more than $\pm 10\%$ from their mean, this result was discarded and the mean of the five remaining results are expressed, in accordance with EN 196-1 (2005).

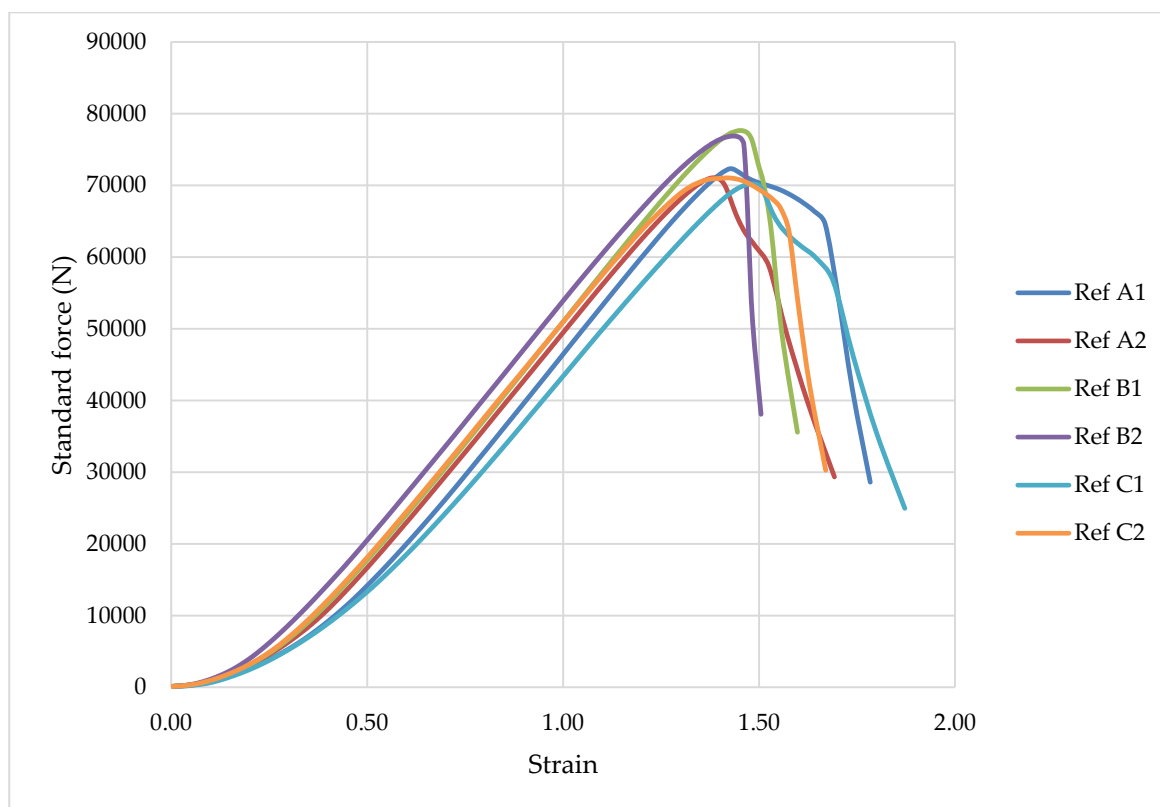


Figure B - 1: Compressive strength of reference mortar prisms.

Table B - 1: Compressive testing of reference mortar prisms.

Material	Force (N)	Strain	MOE (MPa)	
Reference	5 a1	72309.09	1.428	31.66
	5 a2	71043.55	1.385	32.06
	5 b1	77628.84	1.451	33.43
	5 b2	76859.91	1.435	33.48
	5 c1	70177.96	1.486	29.51
	5 c2	71021.76	1.417	31.33
Average	73173.52	1.43	31.91	
Std. Dev.	2953.16	0.031	1.35	

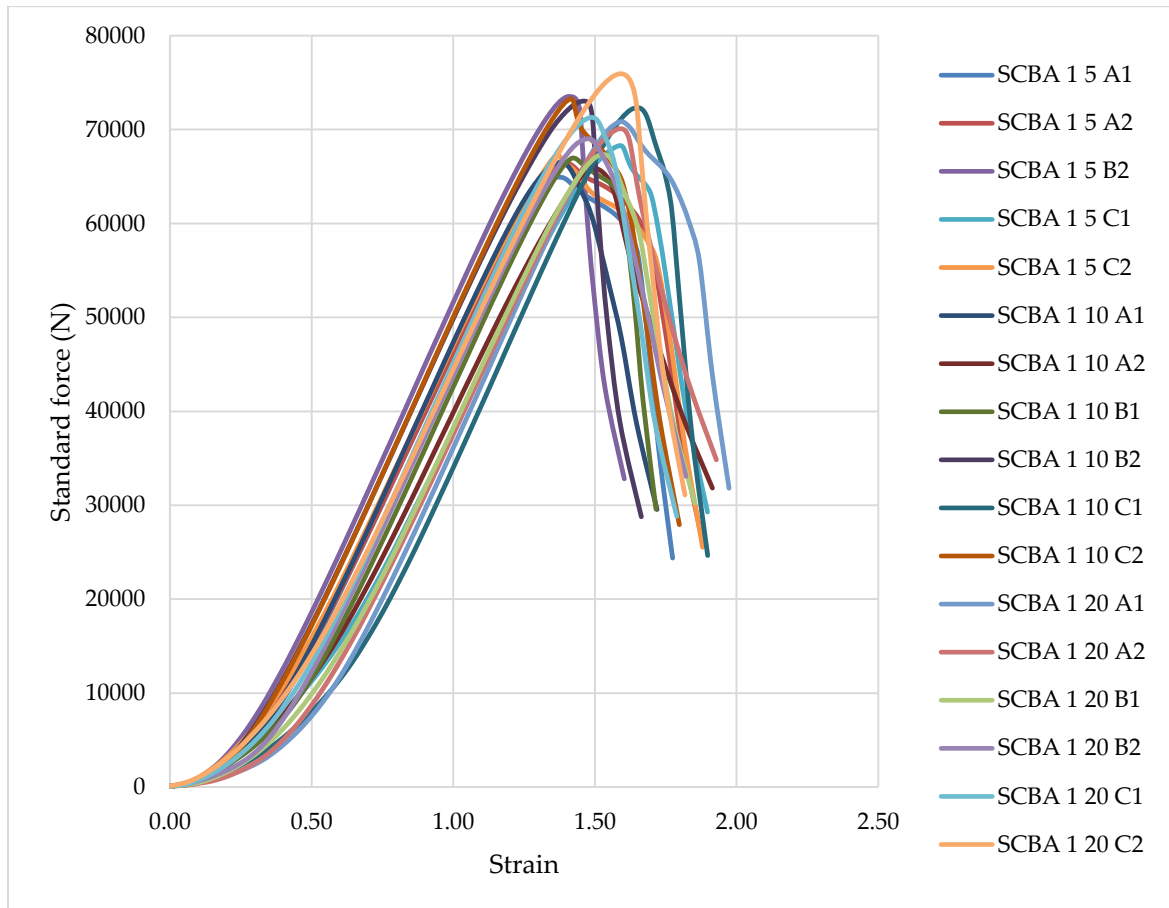


Figure B - 2: Compressive strength of SCBA 1 mortar prisms.

Table B - 2: Compressive testing of SCBA 1 mortar prisms.

Material	Sample	Force (N)	Strain	MOE (MPa)
SCBA 1 5%	5 a1	64939.23	1.372	29.59
	5 a2	66495.94	1.394	29.82
	5 b1	-	-	-
	5 b2	73525.40	1.410	32.58
	5 c1	68290.95	1.589	26.86
	5 c2	67277.05	1.369	30.73
	Average		68105.71	1.43
Std. Dev.		2922.74	0.083	1.86
SCBA 1 10%	10 a1	66498.73	1.377	30.18
	10 a2	65862.48	1.496	27.51
	10 b1	66976.41	1.423	29.42
	10 b2	73039.76	1.462	31.23
	10 c1	72325.19	1.651	27.38
	10 c2	73269.52	1.415	32.36
	Average		69662.02	1.47
Std. Dev.		3244.77	0.089	1.82
SCBA 1 20%	20 a1	70843.02	1.593	27.79
	20 a2	70092.33	1.591	27.54
	20 b1	67345.70	1.525	27.61
	20 b2	69030.45	1.478	29.19
	20 c1	71297.55	1.487	29.97
	20 c2	75945.33	1.589	29.87
	Average		70759.06	1.54
Std. Dev.		2654.50	0.049	1.05

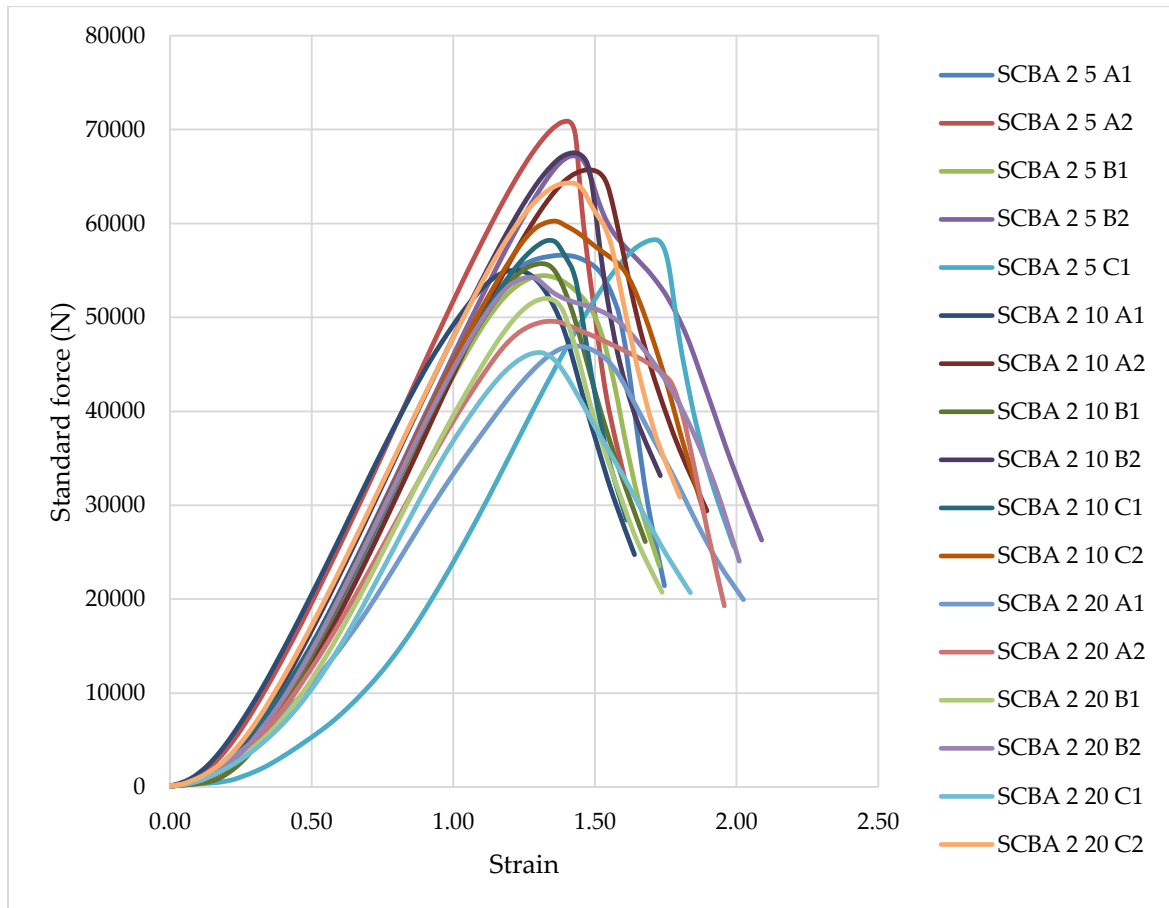


Figure B - 3: Compressive strength of SCBA 2 mortar prisms.

Table B - 3: Compressive testing of SCBA 2 mortar prisms.

	Sample	Force (N)	Strain	MOE (MPa)
SCBA 2 5%	5 a1	56623.19	1.378	25.68
	5 a2	70888.68	1.400	31.64
	5 b1	54450.82	1.316	25.85
	5 b2	67200.80	1.426	29.45
	5 c1	58277.12	1.711	21.29
	5 c2	-	-	-
	Average	61488.12	1.45	26.78
Std. Dev.	6395.42	0.137	3.55	
SCBA 2 10	10 a1	55027.03	1.222	28.14
	10 a2	65718.11	1.476	27.83
	10 b1	55724.29	1.309	26.61
	10 b2	67531.71	1.424	29.64
	10 c1	58208.29	1.341	27.13
	10 c2	60255.88	1.356	27.77
	Average	60410.89	1.35	27.85
Std. Dev.	4738.11	0.08	0.94	
SCBA 2 20%	20 a1	46958.18	1.431	20.51
	20 a2	49587.64	1.345	23.04
	20 b1	52014.55	1.328	24.48
	20 b2	54272.39	1.268	26.74
	20 c1	46263.00	1.302	22.22
	20 c2	64326.71	1.413	28.45
	Average	52237.08	1.35	24.24
Std. Dev.	6068.05	0.058	2.69	

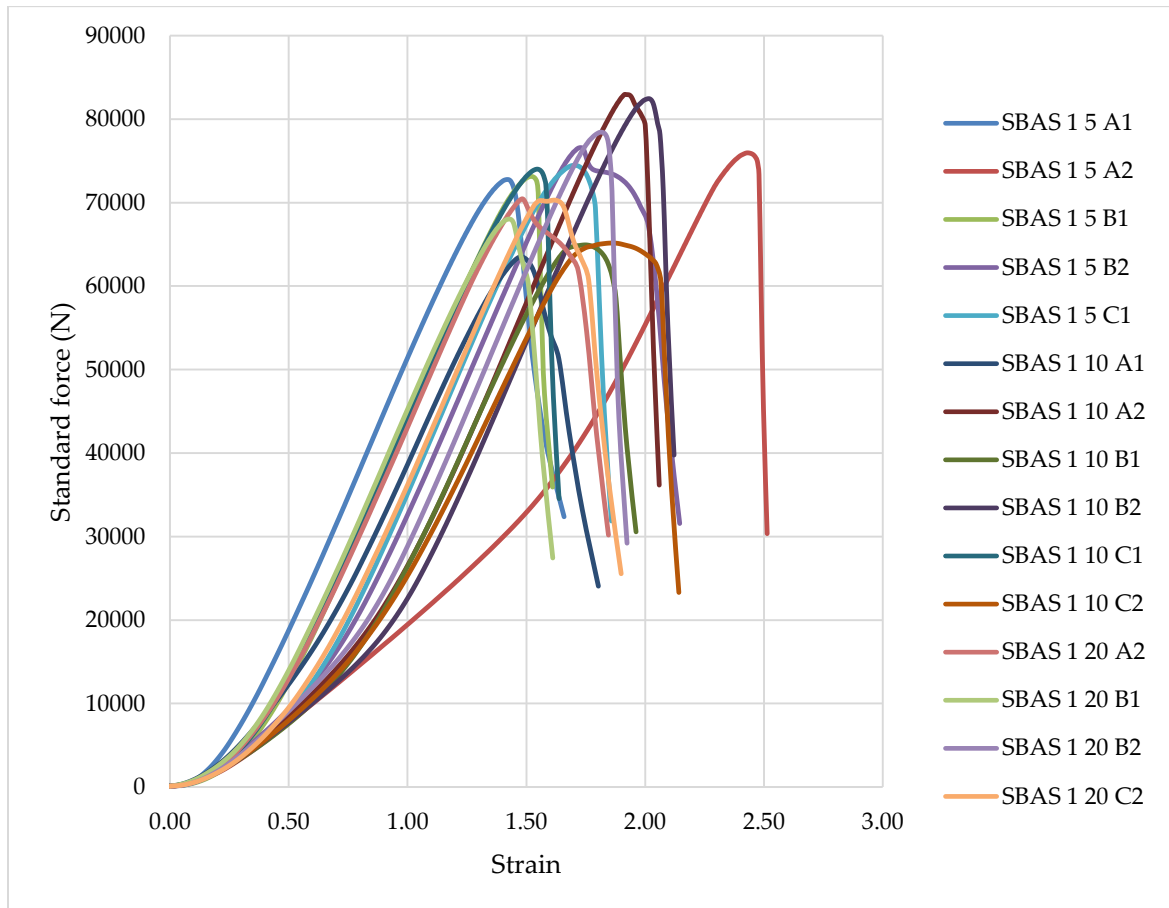


Figure B - 4: Compressive strength of SBAS 1 mortar prisms.

Table B - 4: Compressive testing of SBAS 1 mortar prisms.

	Sample	Force (N)	Strain	MOE (MPa)
SBAS 1 5%	5 a1	72771.10	1.421	32.00
	5 a2	75962.23	2.430	19.54
	5 b1	73138.24	1.520	30.07
	5 b2	76591.18	1.728	27.70
	5 c1	74474.20	1.703	27.34
	5 c2	-	-	-
	Average	74587.39	1.76	27.33
Std. Dev.	1504.47	0.354	4.25	
SBAS 1 10%	10 a1	63490.05	1.477	26.87
	10 a2	82967.63	1.916	27.07
	10 b1	64936.98	1.747	23.23
	10 b2	82454.30	2.014	25.59
	10 c1	74013.55	1.546	29.93
	10 c2	65159.96	1.864	21.85
	Average	72170.41	1.76	25.76
Std. Dev.	8190.98	0.194	2.65	
SBAS 1 20%	20 a1	-	-	-
	20 a2	70454.98	1.483	29.69
	20 b1	68032.74	1.427	29.79
	20 b2	78441.40	1.816	27.00
	20 c1	-	-	-
	20 c2	70300.80	1.616	27.20
	Average	71807.48	1.59	28.42
Std. Dev.	3948.32	0.149	1.32	

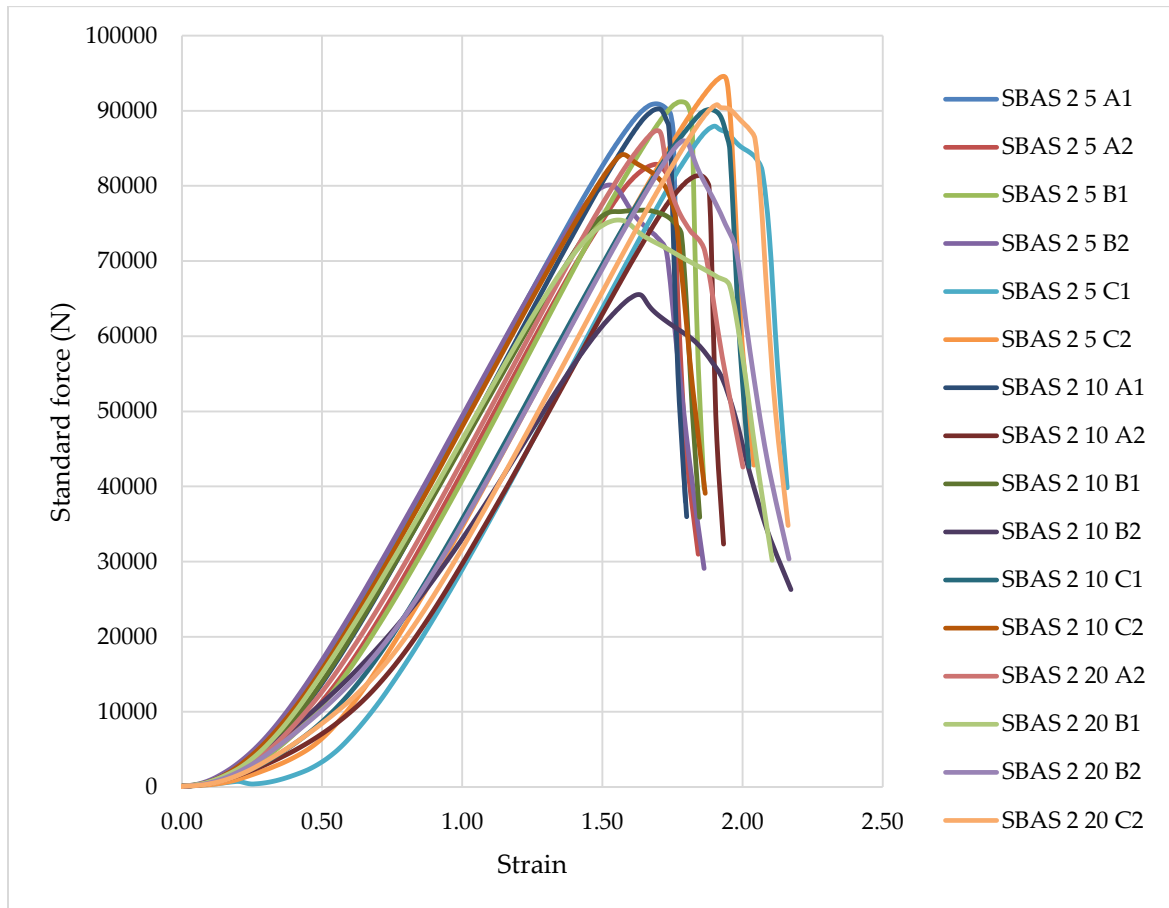


Figure B - 5: Compressive strength of SBAS 2 mortar prisms.

Table B - 5: Compressive testing of SBAS 2 mortar prisms.

	Sample	Force (N)	Strain	MOE (MPa)
SBAS 2 5%	5 a1	90933.66	1.691	33.61
	5 a2	82878.80	1.692	30.62
	5 b1	91201.55	1.781	32.01
	5 b2	80126.03	1.526	32.82
	5 c1	87951.54	1.901	28.92
	5 c2	-	-	-
	Average	86618.32	1.72	31.59
Std. Dev.	4416.77	0.123	1.66	
SBAS 2 10%	10 a1	90264.43	1.699	33.20
	10 a2	81391.54	1.847	27.55
	10 b1	76779.23	1.649	29.10
	10 b2	65543.49	1.629	25.14
	10 c1	90186.31	1.883	29.93
	10 c2	84180.25	1.574	33.42
	Average	81390.88	1.71	29.72
Std. Dev.	8527.28	0.11	2.94	
SBAS 2 20%	20 a1	-	-	-
	20 a2	87359.57	1.695	32.21
	20 b1	75462.73	1.555	30.33
	20 b2	86001.25	1.790	30.03
	20 c1	-	-	-
	20 c2	90811.12	1.909	29.73
	Average	84908.67	1.74	30.58
Std. Dev.	5728.55	0.130	0.97	

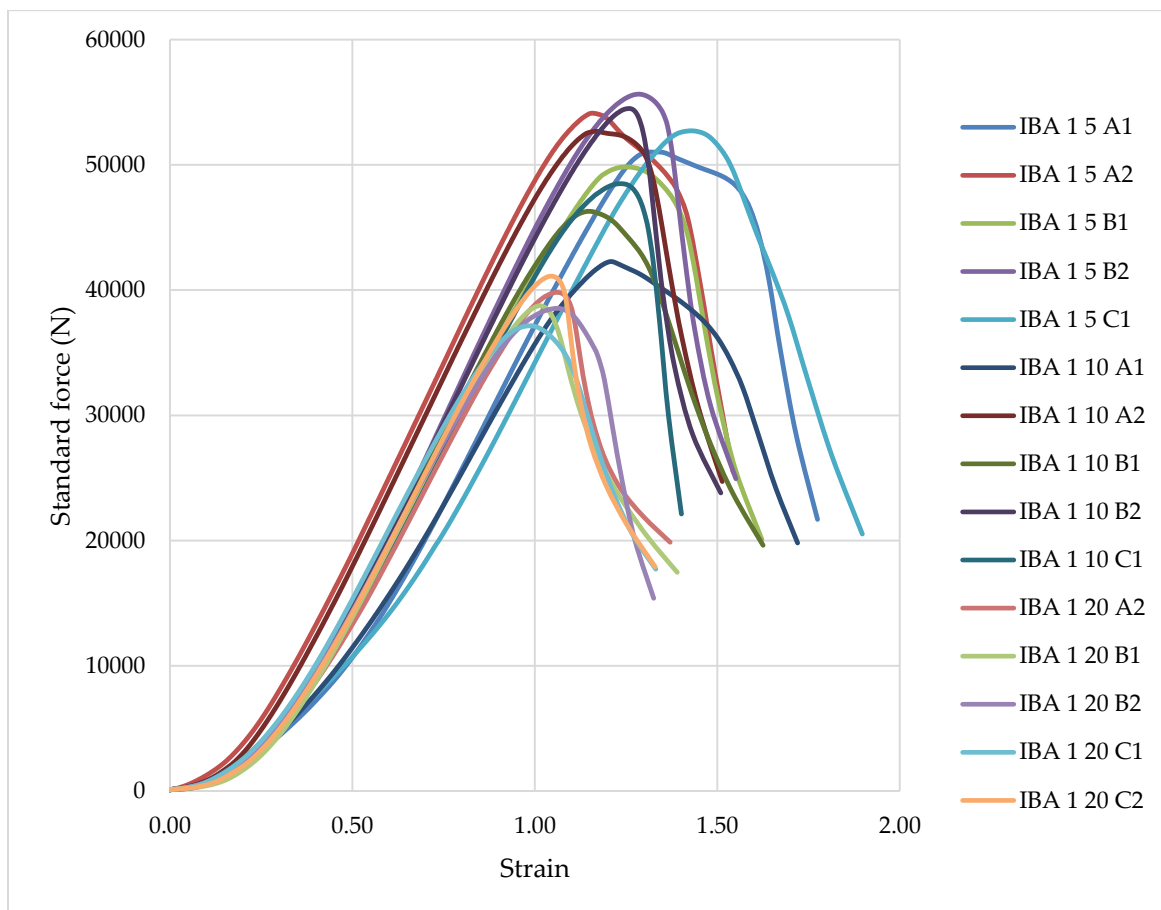


Figure B - 6: Compressive strength of IBA 1 mortar prisms.

Table B - 6: Compressive testing of IBA 1 mortar prisms.

	Sample	Force (N)	Strain	MOE (MPa)
IBA 1 5%	5 a1	51028.14	1.316	24.24
	5 a2	54128.89	1.158	29.22
	5 b1	49838.02	1.247	24.97
	5 b2	55649.27	1.285	27.07
	5 c1	52722.71	1.429	23.07
	5 c2	-	-	-
	Average	52673.41	1.29	25.71
Std. Dev.	2084.37	0.089	2.19	
IBA 1 10%	10 a1	42280.89	1.209	21.85
	10 a2	52685.45	1.166	28.24
	10 b1	46291.18	1.147	25.23
	10 b2	54501.47	1.257	27.09
	10 c1	48501.43	1.236	24.52
	10 c2	-	-	-
	Average	48852.08	1.20	25.39
Std. Dev.	4392.54	0.042	2.21	
IBA 1 20%	20 a1	-	-	-
	20 a2	39821.53	1.059	23.50
	20 b1	38750.48	1.014	23.89
	20 b2	38544.23	1.063	22.66
	20 c1	37152.24	0.987	23.52
	20 c2	41113.87	1.045	24.60
	Average	39076.47	1.03	23.63
Std. Dev.	1326.52	0.029	0.63	

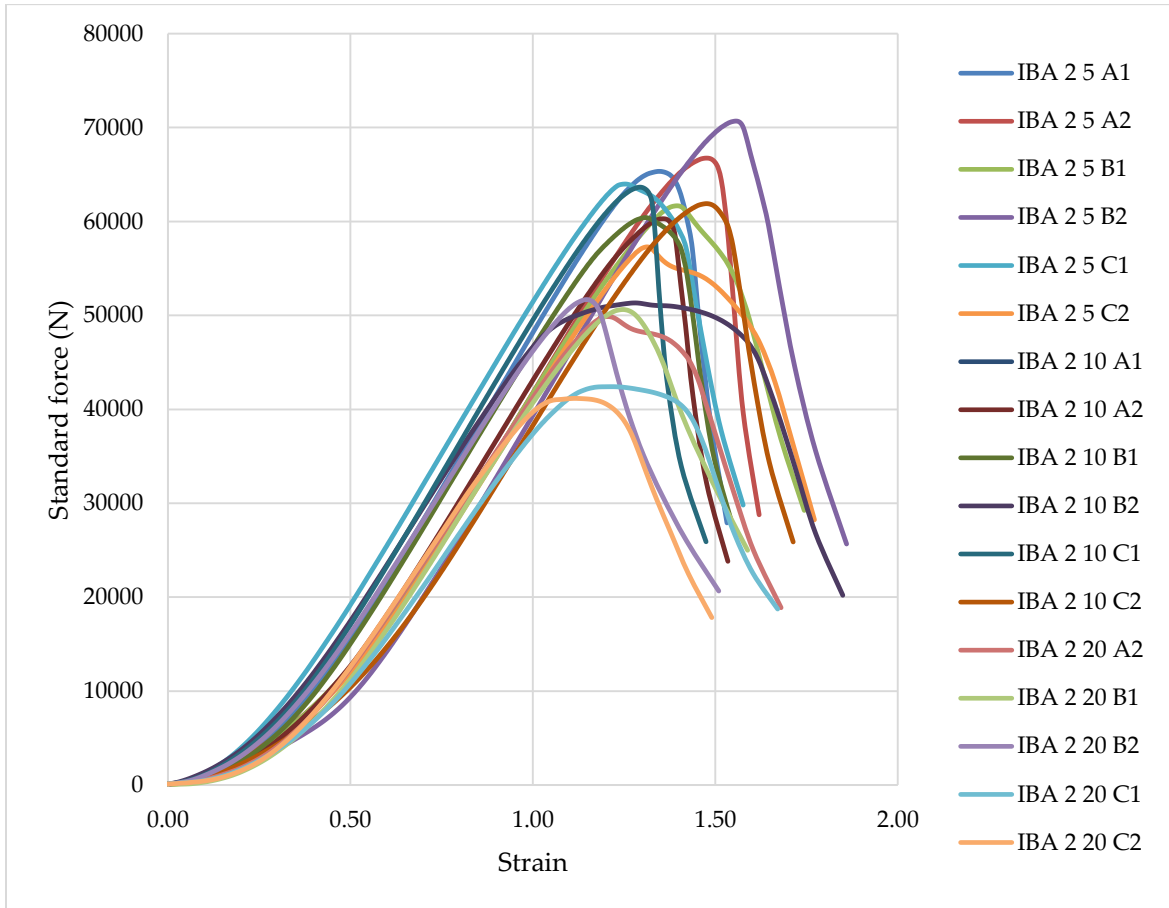


Figure B - 7: Compressive strength of IBA 2 mortar prisms.

Table B - 7: Compressive testing of IBA 2 mortar prisms.

	Sample	Force (N)	Strain	MOE (MPa)
IBA 2 5%	5 a1	65339.23	1.345	30.36
	5 a2	66750.65	1.476	28.26
	5 b1	61671.11	1.394	27.64
	5 b2	70693.59	1.556	28.39
	5 c1	63987.77	1.252	31.95
	5 c2	57295.14	1.31	27.30
	Average	64289.58	1.39	28.98
Std. Dev.	4164.13	0.102	1.64	
IBA 2 10%	10 a1	58783.68	1.316	27.92
	10 a2	60292.98	1.357	27.78
	10 b1	60419.41	1.308	28.87
	10 b2	51329.56	1.278	25.10
	10 c1	63656.13	1.294	30.74
	10 c2	61901.34	1.477	26.19
	Average	59397.18	1.34	27.77
Std. Dev.	3909.81	0.067	1.81	
IBA 2 20%	20 a1	-	-	-
	20 a2	49879.58	1.204	25.90
	20 b1	50628.01	1.246	25.40
	20 b2	51684.02	1.146	28.18
	20 c1	42412.17	1.216	21.79
	20 c2	41164.97	1.114	23.10
	Average	47153.75	1.19	24.87
Std. Dev.	4435.58	0.048	2.23	

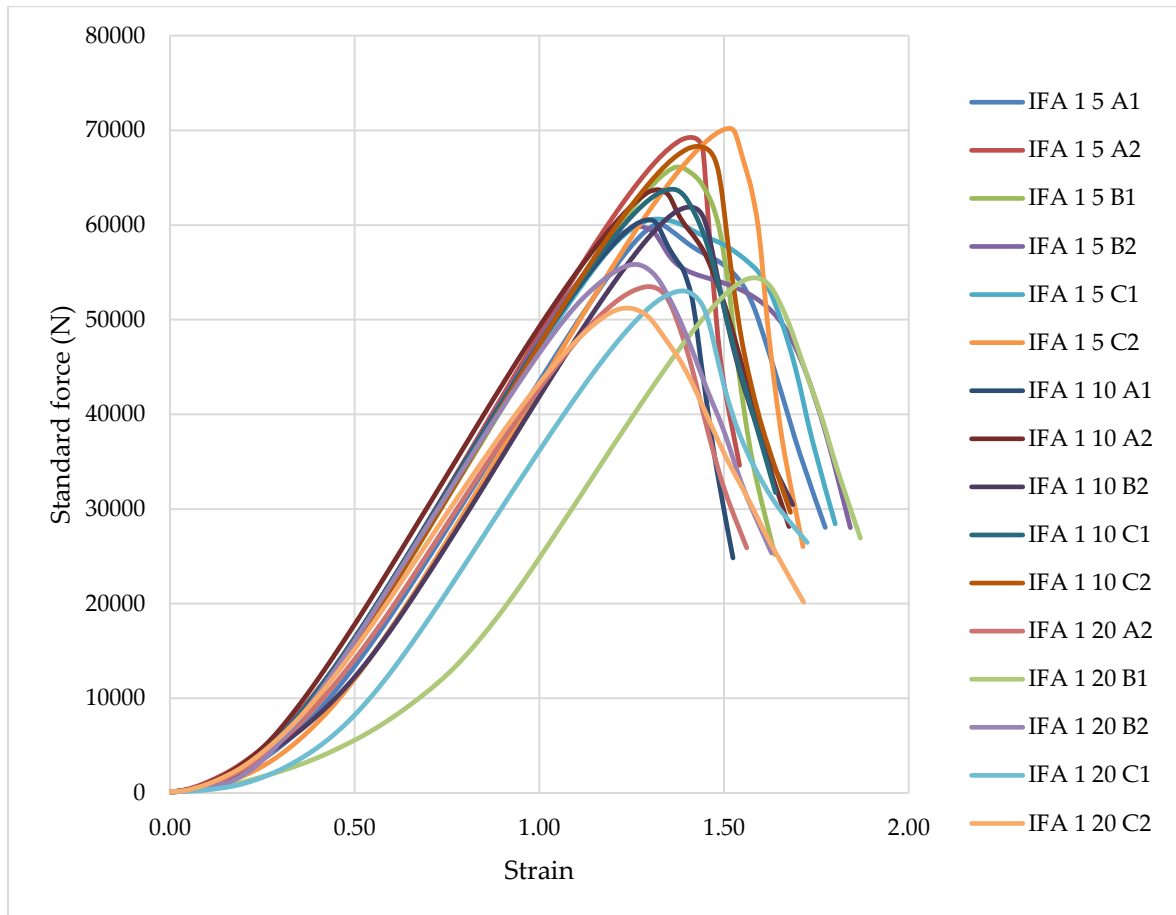


Figure B - 8: Compressive strength of FA 1 mortar prisms.

Table B - 8: Compressive testing of FA 1 mortar prisms.

	Sample	Force (N)	Strain	MOE
FA 1 5%	5 a1	60058.69	1.325	28.32
	5 a2	69249.01	1.410	30.69
	5 b1	66129.57	1.375	30.07
	5 b2	59853.22	1.272	29.42
	5 c1	60627.03	1.320	28.71
	5 c2	70194.02	1.515	28.96
		Average	64351.92	1.37
	Std. Dev.	4355.39	0.078	0.81
FA 1 10%	10 a1	60554.58	1.297	29.18
	10 a2	63731.11	1.318	30.21
	10 b1	-	-	-
	10 b2	61885.87	1.405	27.53
	10 c1	63774.95	1.361	29.28
	10 c2	68303.31	1.429	29.88
		Average	63649.96	1.36
	Std. Dev.	2621.80	0.050	0.93
FA 1 20%	20 a1	-	-	-
	20 a2	53490.76	1.298	25.76
	20 b1	54424.33	1.582	21.51
	20 b2	55836.34	1.260	27.69
	20 c1	53037.93	1.388	23.89
	20 c2	51225.06	1.237	25.87
		Average	53602.88	1.35
	Std. Dev.	1526.36	0.125	2.10

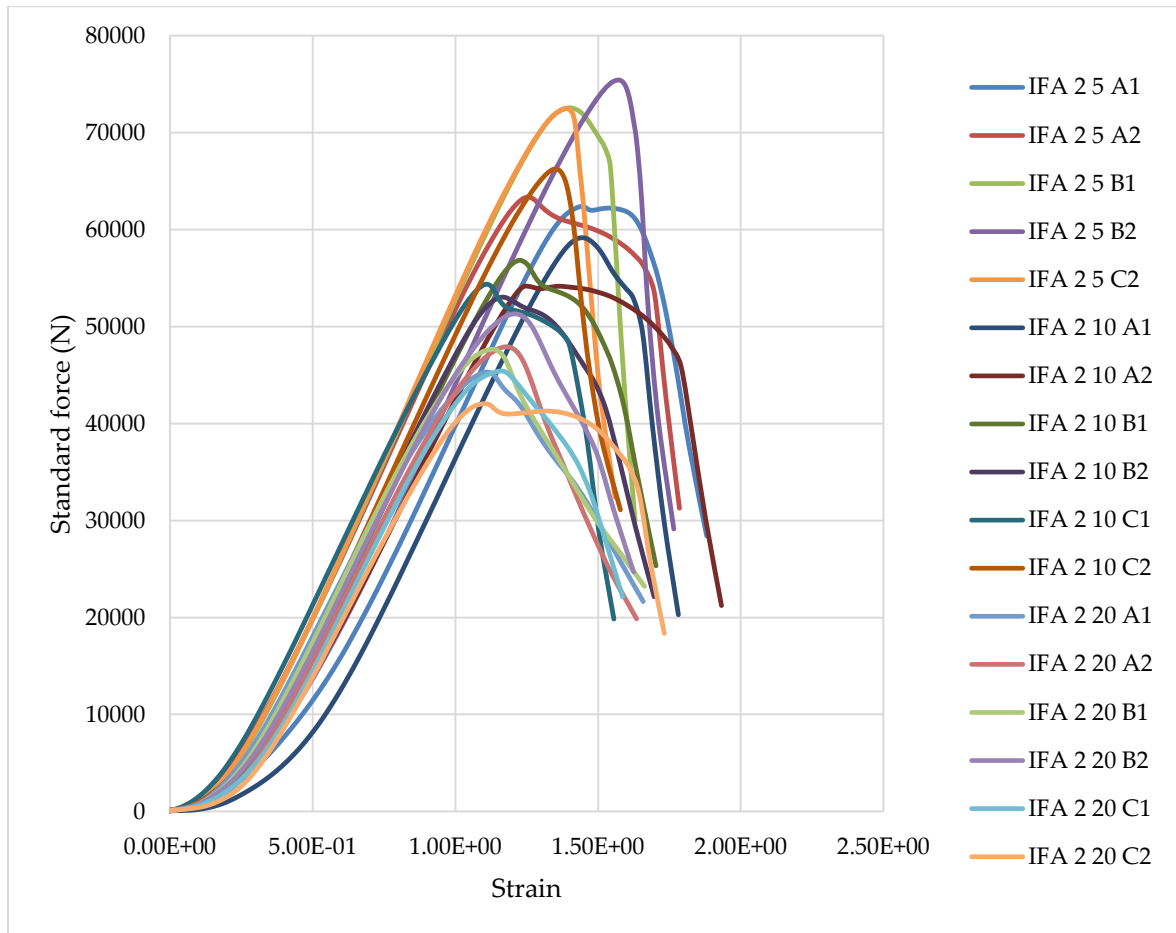


Figure B - 9: Compressive strength of FA 2 mortar prisms.

Table B - 9: Compressive testing of FA 2 mortar prisms.

	Sample	Force (N)	Strain	MOE
FA 2 5%	5 a1	62406.40	1.447	26.96
	5 a2	63345.91	1.256	31.53
	5 b1	72557.50	1.402	32.35
	5 b2	75427.86	1.570	30.03
	5 c1	-	-	-
	5 c2	72489.97	1.388	32.64
	Average	69245.53	1.41	30.70
Std. Dev.	5315.94	0.101	2.08	
FA 2 10%	10 a1	-	-	-
	10 a2	54178.51	1.247	27.15
	10 b1	56838.67	1.226	28.99
	10 b2	53036.24	1.168	28.38
	10 c1	54363.02	1.109	30.64
	10 c2	66247.67	1.350	30.68
	Average	56932.82	1.22	29.17
Std. Dev.	4819.72	0.081	1.35	
FA 2 20%	20 a1	45314.01	1.108	25.56
	20 a2	47917.19	1.179	25.40
	20 b1	47657.40	1.132	26.31
	20 b2	51309.09	1.208	26.54
	20 c1	45420.69	1.161	24.46
	20 c2	42038.13	1.105	23.77
	Average	46609.42	1.15	25.34
Std. Dev.	2854.33	0.037	0.97	

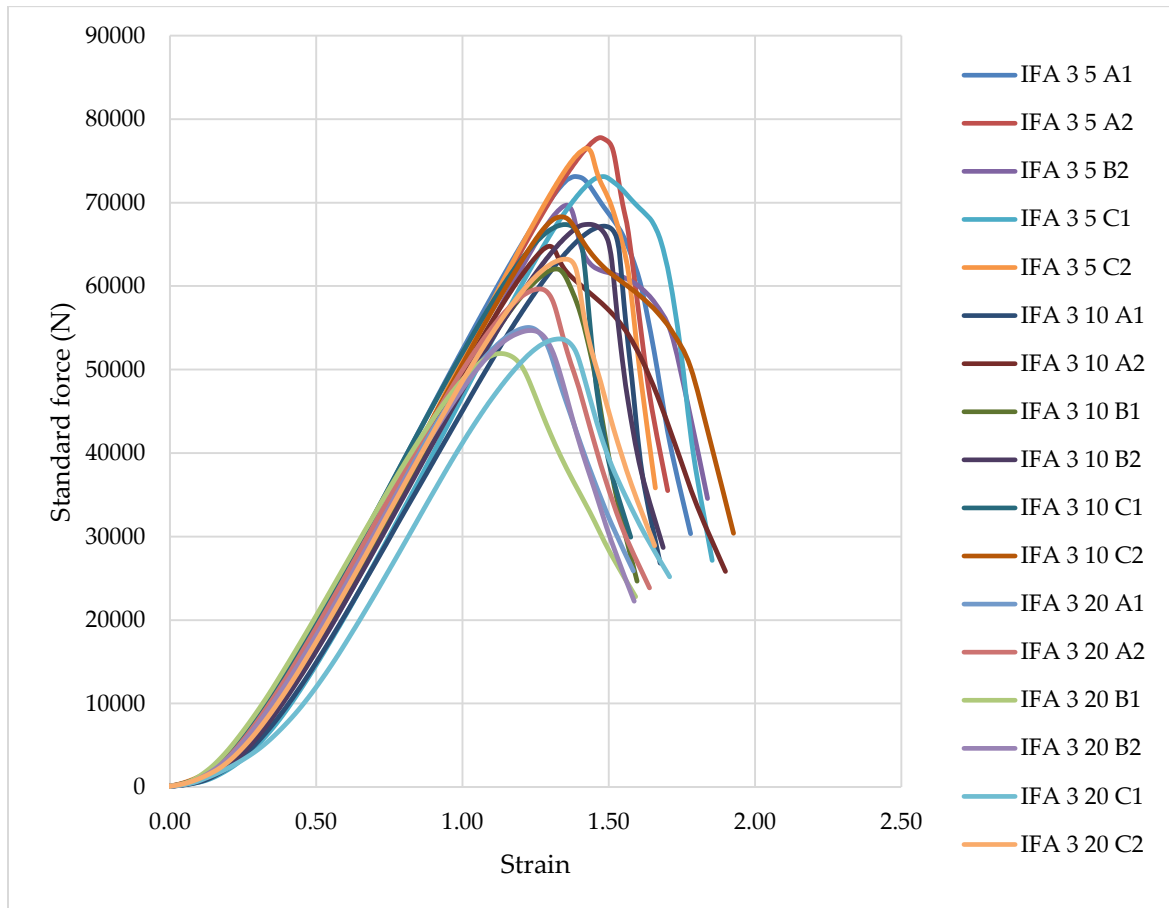


Figure B - 10: Compressive strength of FA 3 mortar prisms.

Table B - 10: Compressive testing of FA 3 mortar prisms.

	Sample	Force (N)	Strain	MOE (MPa)
FA 3 5%	5 a1	73129.27	1.385	33.00
	5 a2	77783.47	1.471	33.03
	5 b1	-	-	-
	5 b2	69696.10	1.355	32.13
	5 c1	73123.05	1.481	30.84
	5 c2	76497.70	1.424	33.57
	Average	74045.92	1.42	32.51
Std. Dev.	2849.33	0.048	0.95	
FA 3 10	10 a1	67179.66	1.485	28.28
	10 a2	64772.76	1.297	31.22
	10 b1	-	-	-
	10 b2	67399.10	1.432	29.42
	10 c1	67373.87	1.350	31.20
	10 c2	68296.40	1.340	31.87
	Average	67004.36	1.38	30.40
Std. Dev.	1180.89	0.068	1.34	
FA 3 20%	20 a1	-	-	-
	20 a2	59656.30	1.263	29.52
	20 b1	51926.87	1.132	28.66
	20 b2	54684.21	1.232	27.73
	20 c1	53670.89	1.333	25.16
	20 c2	63228.87	1.350	29.28
	Average	56633.43	1.26	28.07
Std. Dev.	4180.08	0.078	1.580	

Appendix C BEFORE AND AFTER OF SPECIMENS SUBJECTED TO SALT CRYSTALLISATION TEST

Reference

Table C - 1: Before and after of reference specimens subjected salt crystallisation.


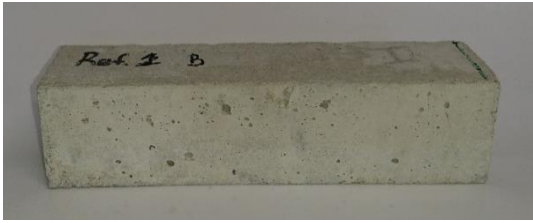



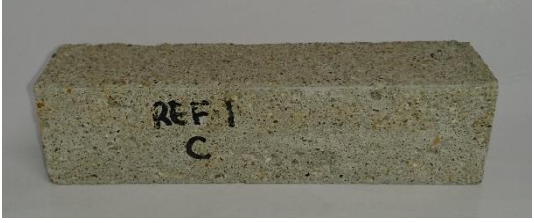
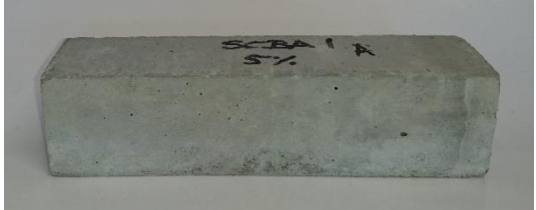
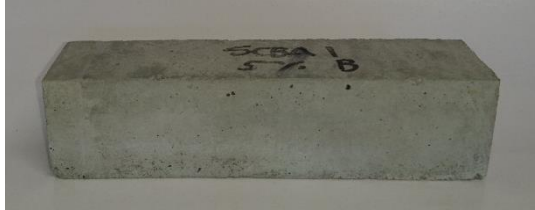
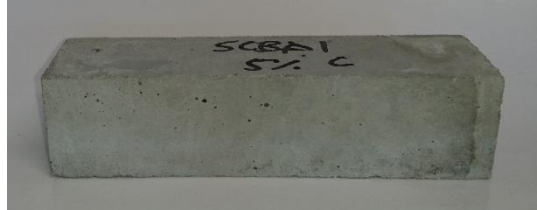



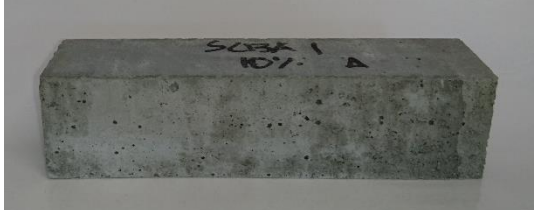
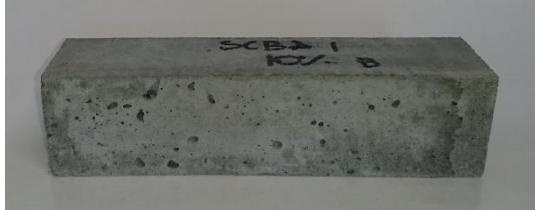
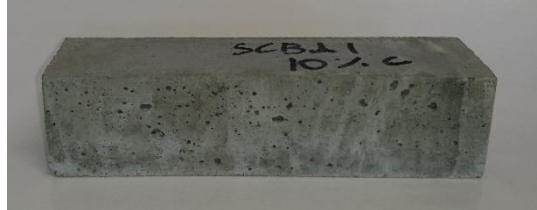
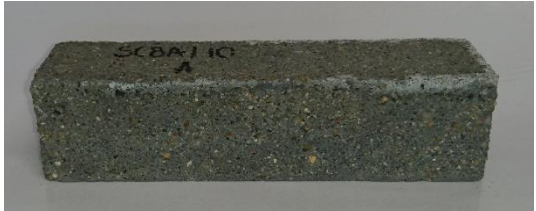


	A	B	C
Before	 A rectangular concrete specimen, light grey in color, with handwritten markings "Ref. 1 A" and "I" on its top surface.	 A rectangular concrete specimen, light grey in color, with handwritten markings "Ref. 1 B" on its top surface.	 A rectangular concrete specimen, light grey in color, with handwritten markings "Ref. 1 C" on its top surface.
After	 The same rectangular concrete specimen as before, but now heavily discolored with a dark, brownish-grey patina, indicating salt crystallisation. Handwritten markings "REF. 1 A" are visible on the top surface.	 The same rectangular concrete specimen as before, but now heavily discolored with a dark, brownish-grey patina, indicating salt crystallisation. Handwritten markings "REF. 1 B" are visible on the top surface.	 The same rectangular concrete specimen as before, but now heavily discolored with a dark, brownish-grey patina, indicating salt crystallisation. Handwritten markings "REF. 1 C" are visible on the top surface.

Table C - 2: Before and after of SCBA 1 mortar specimens subjected salt crystallisation.

%	SCBA 1 5 A	SCBA 1 5 B	SCBA 1 5 C
Before			
After			
%	SCBA 1 10 A	SCBA 1 10 B	SCBA 1 10 C
Before			
After			

Potential of waste materials as pozzolans and their influence on the quality of building materials






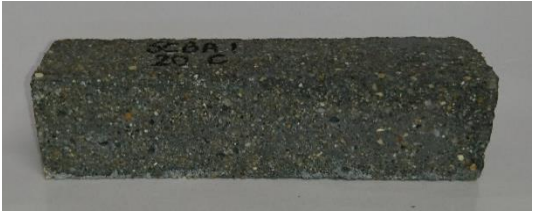
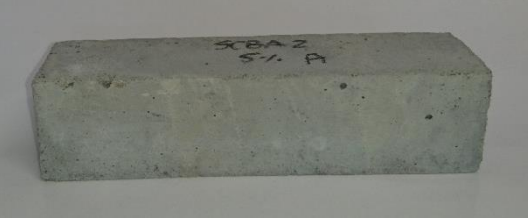

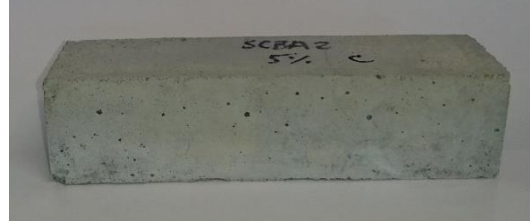




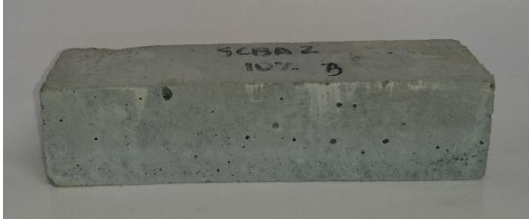
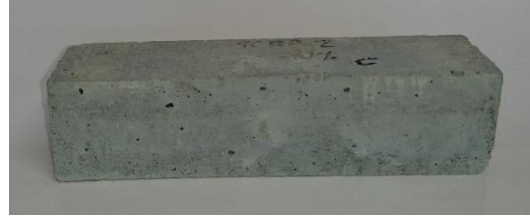
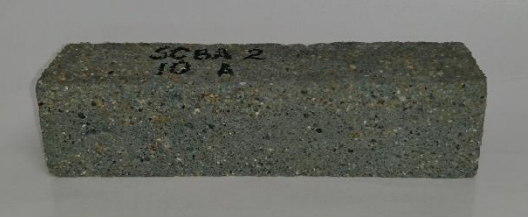
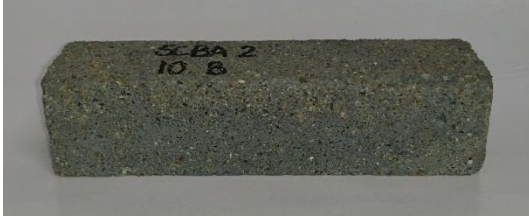
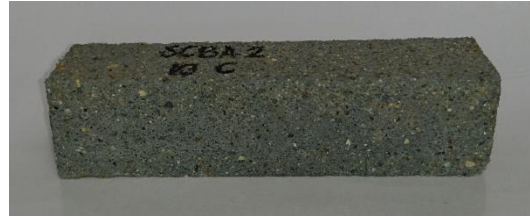
%	SCBA 1 20 A	SCBA 1 20 B	SCBA 1 20 C
Before	 A rectangular concrete block with a smooth, light grey surface. It has "SCBA 1 20 A" handwritten in black on top.	 A rectangular concrete block with a smooth, light grey surface. It has "SCBA 1 20 B" handwritten in black on top.	 A rectangular concrete block with a smooth, light grey surface. It has "SCBA 1 20 C" handwritten in black on top.
After	 The same rectangular concrete block as before, but now with a dark, granular, and porous surface texture. It has "SCBA 1 20 A" handwritten in black on top.	 The same rectangular concrete block as before, but now with a dark, granular, and porous surface texture. It has "SCBA 1 20 B" handwritten in black on top.	 The same rectangular concrete block as before, but now with a dark, granular, and porous surface texture. It has "SCBA 1 20 C" handwritten in black on top.

Table C - 3 Before and after of SCBA 2 mortar specimens subjected salt crystallisation.

%	SCBA 2 5 A	SCBA 2 5 B	SCBA 2 5 C
Before			
After			
%	SCBA 2 10 A	SCBA 2 10 B	SCBA 2 10 C
Before			
After			

Potential of waste materials as pozzolans and their influence on the quality of building materials


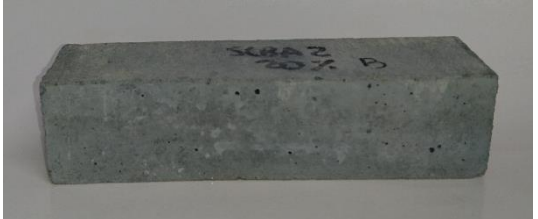
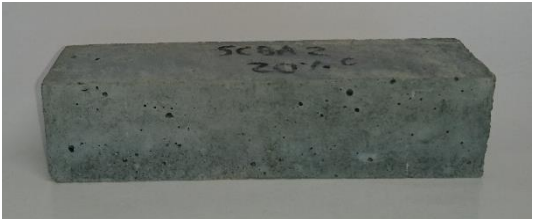




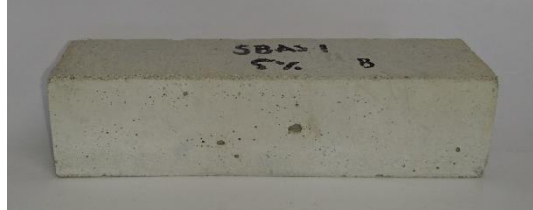





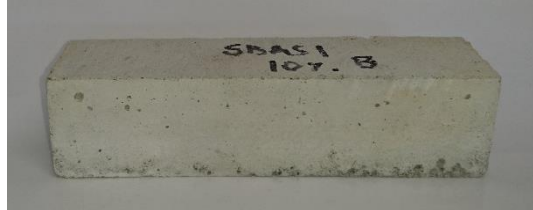


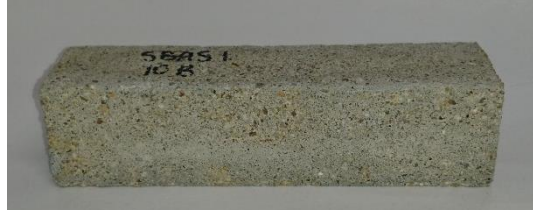

%	SCBA 2 20 A	SCBA 2 20 B	SCBA 2 20 C
Before	 A rectangular concrete specimen with a smooth, light grey surface. Handwritten markings on top read "SCBA 2 20 A".	 A rectangular concrete specimen with a smooth, light grey surface. Handwritten markings on top read "SCBA 2 20 B".	 A rectangular concrete specimen with a smooth, light grey surface. Handwritten markings on top read "SCBA 2 20 C".
After	 The same rectangular concrete specimen as before, but now with a dark, granular, and porous surface texture. Handwritten markings on top read "SCBA 2 20 A".	 The same rectangular concrete specimen as before, but now with a dark, granular, and porous surface texture. Handwritten markings on top read "SCBA 2 20 B".	 The same rectangular concrete specimen as before, but now with a dark, granular, and porous surface texture. Handwritten markings on top read "SCBA 2 20 C".






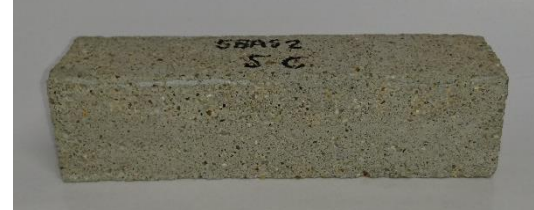

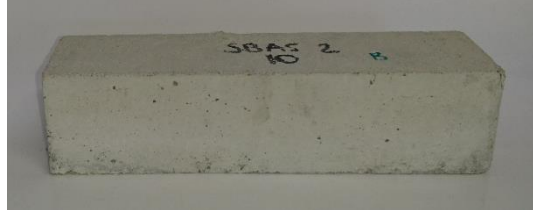


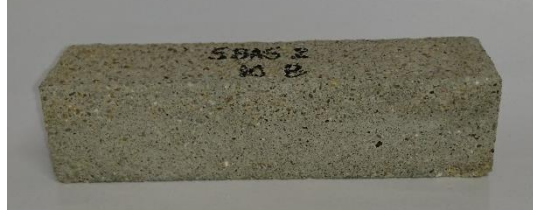

Table C - 4 Before and after of SBAS 1 mortar specimens subjected salt crystallisation.

%	SBAS 1 5 A	SBAS 1 5 B	SBAS 1 5 C
Before			
After			
%	SBAS 1 10 A	SBAS 1 10 B	SBAS 1 10 C
Before			
After			

Potential of waste materials as pozzolans and their influence on the quality of building materials

%	SBAS 1 20 A	SBAS 1 20 B	SBAS 1 20 C
Before	 A rectangular concrete specimen with a smooth, light-colored surface. Handwritten markings on top read "SBAS 1" and "20 A".	 A rectangular concrete specimen with a smooth, light-colored surface. Handwritten markings on top read "SBAS 1" and "20 B".	 A rectangular concrete specimen with a smooth, light-colored surface. Handwritten markings on top read "SBAS 1" and "20 C".
After	 The same specimen as before, but with a significantly rougher, more porous, and darker grey surface texture.	 The same specimen as before, but with a significantly rougher, more porous, and darker grey surface texture.	 The same specimen as before, but with a significantly rougher, more porous, and darker grey surface texture.

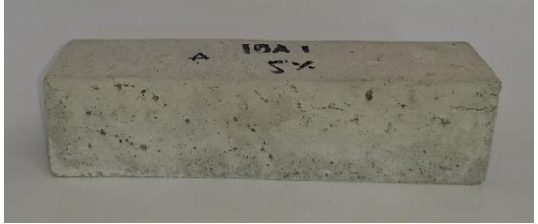


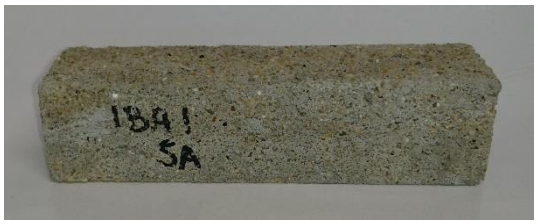
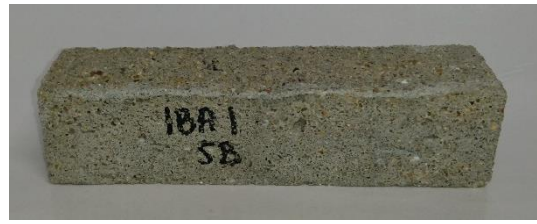
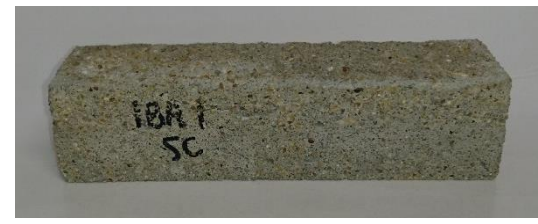





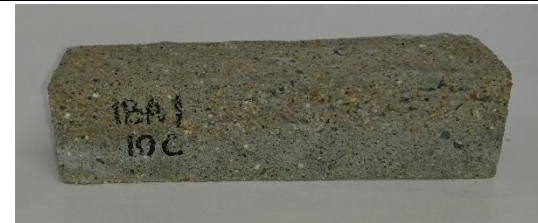
Table C - 5 Before and after of SBAS 2 mortar specimens subjected salt crystallisation.

%	SBAS 2 5 A	SBAS 2 5 B	SBAS 2 5 C
Before			
After			
%	SBAS 2 10 A	SBAS 2 10 B	SBAS 2 10 C
Before			
After			

Potential of waste materials as pozzolans and their influence on the quality of building materials

%	SBAS 2 20 A	SBAS 2 20 B	SBAS 2 20 C
Before	 A rectangular concrete specimen with a smooth, light grey surface. Handwritten markings on top read "SBAS 2 20 A".	 A rectangular concrete specimen with a smooth, light grey surface. Handwritten markings on top read "SBAS 2 20 B".	 A rectangular concrete specimen with a smooth, light grey surface. Handwritten markings on top read "SBAS 2 20 C".
After	 The same specimen as before, but now with a dark, porous, and textured surface. Handwritten markings on top read "SBAS 2 20 A".	 The same specimen as before, but now with a dark, porous, and textured surface. Handwritten markings on top read "SBAS 2 20 B".	 The same specimen as before, but now with a dark, porous, and textured surface. Handwritten markings on top read "SBAS 2 20 C".

Table C - 6 Before and after of IBA 1 mortar specimens subjected salt crystallisation.

%	IBA 1 5 A	IBA 1 5 B	IBA 1 5 C
Before			
After			
%	IBA 1 10 A	IBA 1 10 B	IBA 1 10 C
Before			
After			

Potential of waste materials as pozzolans and their influence on the quality of building materials






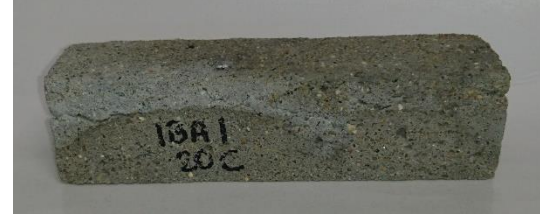
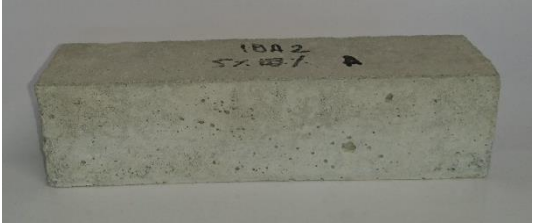

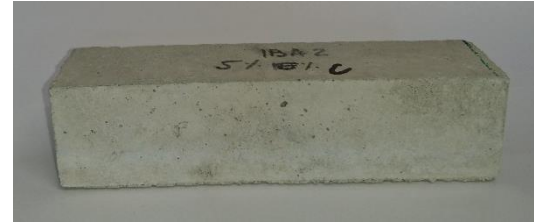

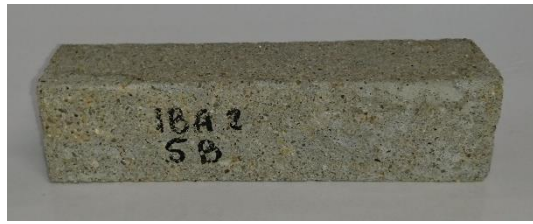


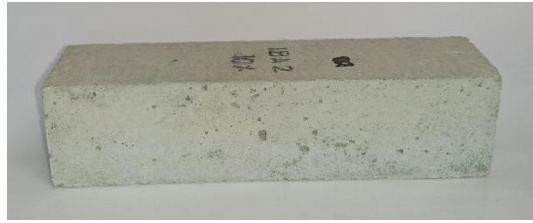
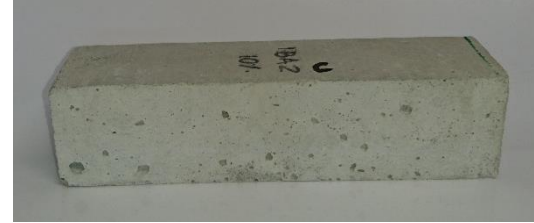

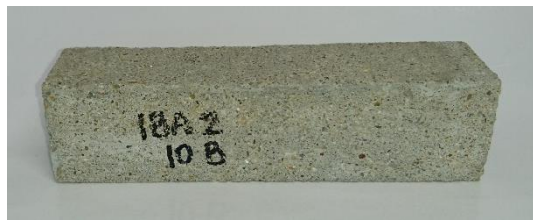
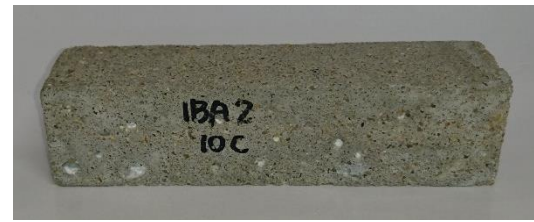
%	IBA 1 20 A	IBA 1 20 B	IBA 1 20 C
Before	 A rectangular concrete block with a light grey, slightly porous surface. It has handwritten markings "IBA 1 20 A" on its top surface.		
After	 The same rectangular concrete block as in the 'Before' row, but now with a significantly darker, more granular and textured surface, appearing almost blackish-grey. Handwritten markings "IBA 1 20 A" are visible on its side.		
		 A rectangular concrete block with a light grey, slightly porous surface. It has handwritten markings "IBA 1 20 B" on its top surface.	
		 The same rectangular concrete block as in the 'Before' row, but now with a significantly darker, more granular and textured surface, appearing almost blackish-grey. Handwritten markings "IBA 1 20 B" are visible on its side.	
		 A rectangular concrete block with a light grey, slightly porous surface. It has handwritten markings "IBA 1 20 C" on its top surface.	
		 The same rectangular concrete block as in the 'Before' row, but now with a significantly darker, more granular and textured surface, appearing almost blackish-grey. Handwritten markings "IBA 1 20 C" are visible on its side.	

Table C - 7: Before and after of IBA 2 mortar specimens subjected salt crystallisation.

%	IBA 2 5 A	IBA 2 5 B	IBA 2 5 C
Before			
After			
%	IBA 2 10 A	IBA 2 10 B	IBA 2 10 C
Before			
After			

Potential of waste materials as pozzolans and their influence on the quality of building materials







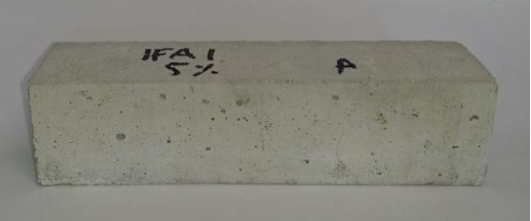
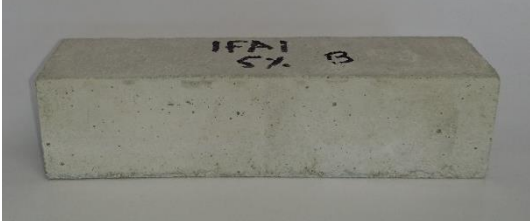
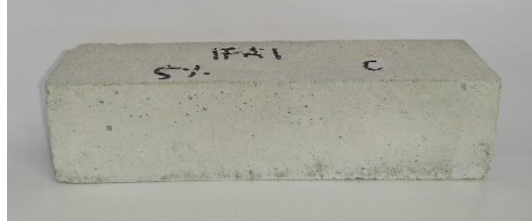



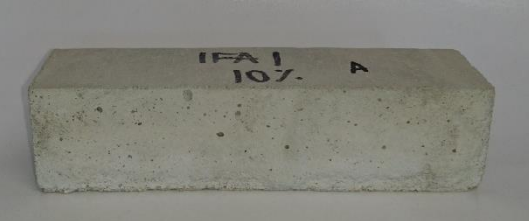




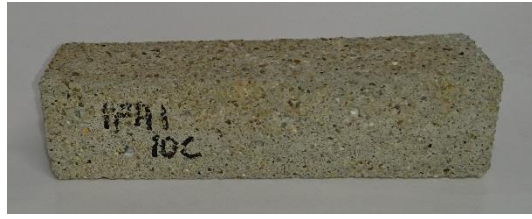
%	IBA 2 20 A	IBA 2 20 B	IBA 2 20 C
Before	 A rectangular concrete block with a smooth, light grey surface. It is marked with "IBA 2 20 A" in black ink on its top surface.	 A rectangular concrete block with a smooth, light grey surface. It is marked with "IBA 2 20 B" in black ink on its top surface.	 A rectangular concrete block with a smooth, light grey surface. It is marked with "IBA 2 20 C" in black ink on its top surface.
After	 The same rectangular concrete block as in the 'Before' row, but now with a rough, porous, and greyish-green surface texture. It is marked with "IBA 2 20 A" in black ink on its top surface.	 The same rectangular concrete block as in the 'Before' row, but now with a rough, porous, and greyish-green surface texture. It is marked with "IBA 2 20 B" in black ink on its top surface.	 The same rectangular concrete block as in the 'Before' row, but now with a rough, porous, and greyish-green surface texture. It is marked with "IBA 2 20 C" in black ink on its top surface.

Table C - 8: Before and after of FA 1 mortar specimens subjected salt crystallisation.

%	FA 15 A	FA 15 B	FA 15 C
Before			
After			
%	FA 110 A	FA 110 B	FA 110 C
Before			
After			

Potential of waste materials as pozzolans and their influence on the quality of building materials






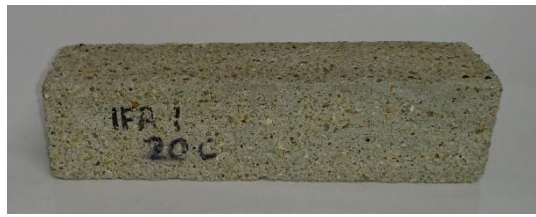


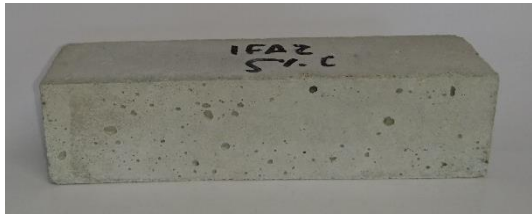






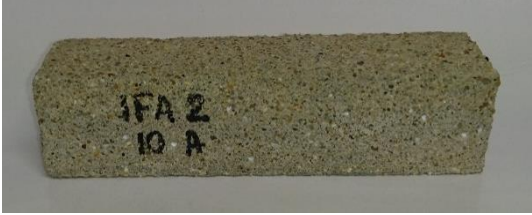


% FA 1 20 A	FA 1 20 A	FA 1 20 B	FA 1 20 C
Before	 A rectangular concrete block with a smooth, light-colored surface. It has black markings on top that read "IFA 1 20% A".	 A rectangular concrete block with a smooth, light-colored surface. It has black markings on top that read "IFA 1 20% B".	 A rectangular concrete block with a smooth, light-colored surface. It has black markings on top that read "IFA 1 20% C".
After	 The same rectangular concrete block as in the 'Before' row, but now with a rough, porous, and darker grey-green surface texture. It has black markings on top that read "IFA 1 20% A".	 The same rectangular concrete block as in the 'Before' row, but now with a rough, porous, and darker grey-green surface texture. It has black markings on top that read "IFA 1 20% B".	 The same rectangular concrete block as in the 'Before' row, but now with a rough, porous, and darker grey-green surface texture. It has black markings on top that read "IFA 1 20% C".

Table C - 9: Before and after of FA 2 mortar specimens subjected salt crystallisation.

%	FA 2 5 A	FA 2 5 B	FA 2 5 C
Before			
After			
%	FA 2 10 A	FA 2 10 B	FA 2 10 C
Before			
After			

Potential of waste materials as pozzolans and their influence on the quality of building materials

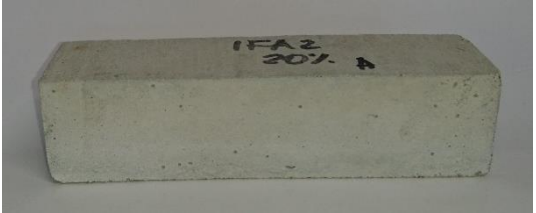


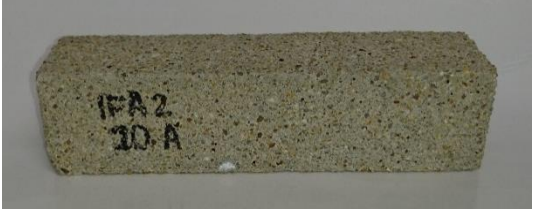







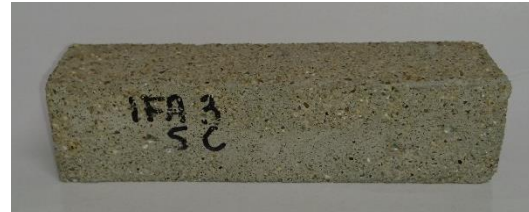




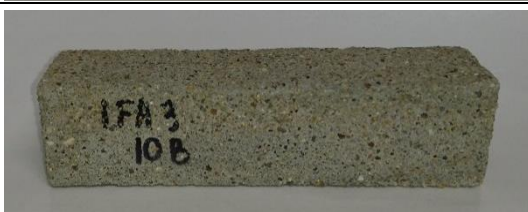


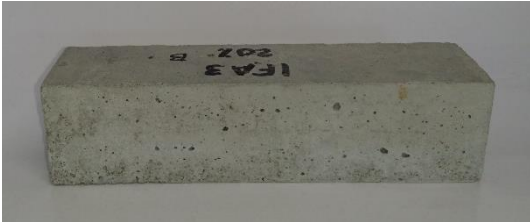
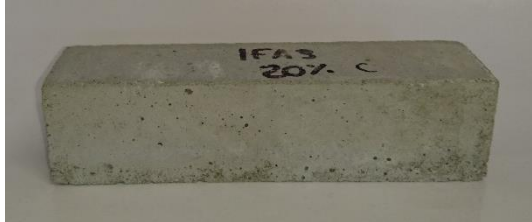


%	FA 2 20 A	FA 2 20 B	FA 2 20 C
Before			
After			

Table C - 10: Before and after of FA 3 mortar specimens subjected salt crystallisation.

%	FA 3 5 A	FA 3 5 B	FA 3 5 C
Before			
After			
%	FA 3 10 A	FA 3 10 B	FA 3 10 C
Before			
After			

Potential of waste materials as pozzolans and their influence on the quality of building materials

%	FA 3 20 A	FA 3 20 B	FA 3 20 C
Before			
After			

Appendix D CHANGE IN MASS FOR THE SELECTED TIME INTERVAL

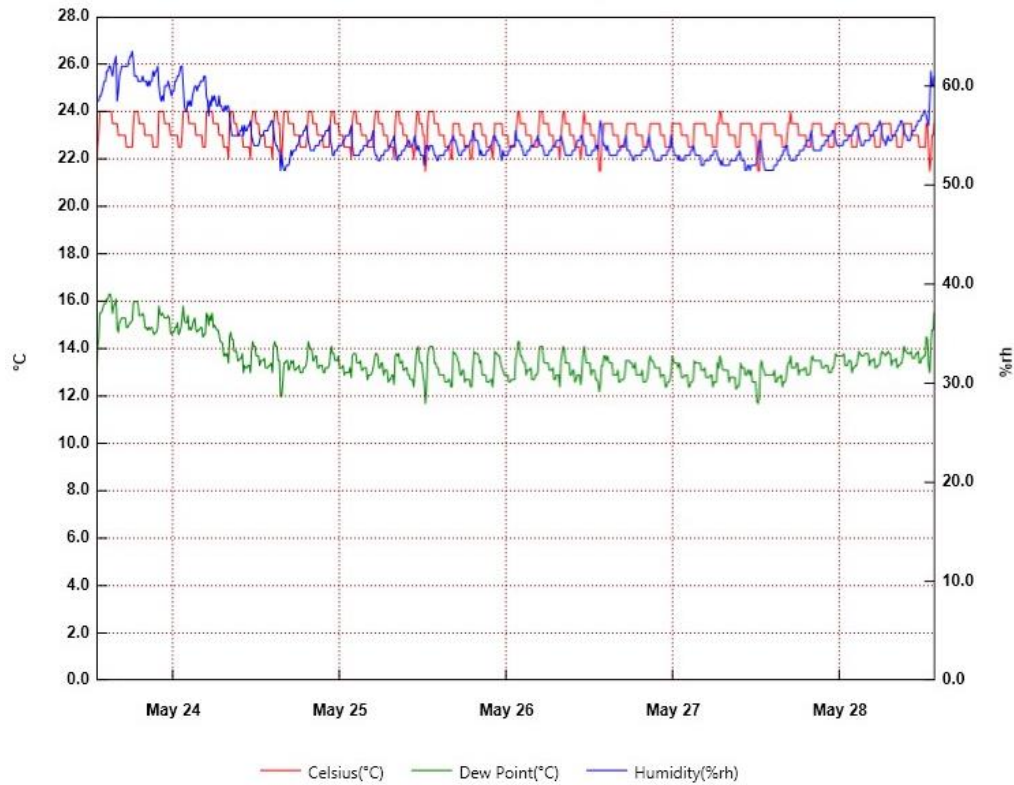


Figure D - 1: Chamber’s temperature and relative humidity conditions during test.

Table D - 1: Water vapour permeability test conditions and parameters.

Test condition	
Average Temperature (°C)	23.1
External Relative Humidity (%)	54.9
Internal Relative Humidity (%) – KNO ₃	94
A (m ²) – exposed area	0.0091205
Δp (Pa) – water vapour pressure difference	1210

Table D - 2: Vapour Permeability Test - SCBA 1 and SCBA 2.

Ash	SCBA 1			SCBA 2		
Replacement	5%	10%	20%	5%	10%	20%
Time (s)	Weight (kg)					
0	1,00983	1,00733	1,00152	1,01226	1,01913	1,00993
86400	1,00980	1,00720	1,00153	1,01206	1,0189	1,00963
172800	1,00977	1,00717	1,00148	1,01191	1,0189	1,0096
259200	1,00977	1,00718	1,00153	1,01170	1,0188	1,0095
345600	1,00953	1,00702	1,00140	1,01156	1,0187	1,00936
432000	1,00923	1,00680	1,00117	1,01148	1,01866	1,00929
G (kg/s)	1.389E-09	1.235E-09	0.810E-09	1.806E-09	1.080E-09	1.489E-09

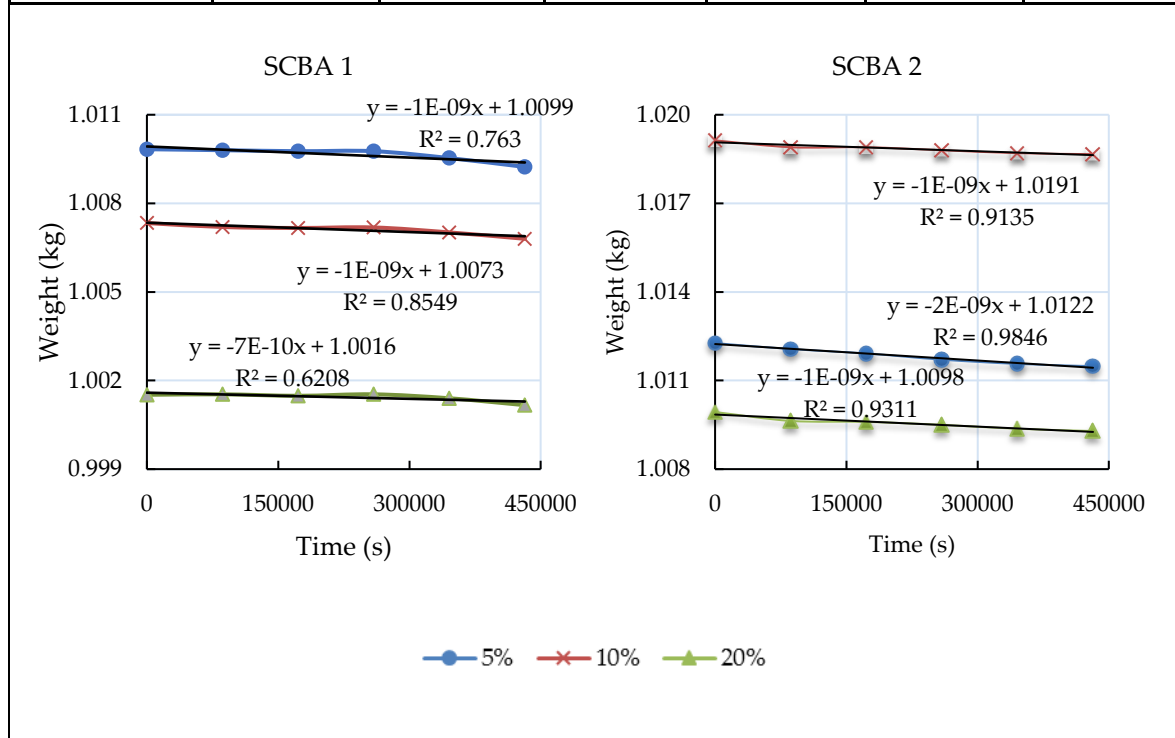


Table D - 3: Vapour Permeability Test - SBAS 1 and SBAS 2.

Ash	SBAS 1			SBAS 2		
Replacement	5%	10%	20%	5%	10%	20%
Time (s)	Weight (kg)					
0	1.01693	1.02555	1.01053	1.02393	1.0155	1.0165
86400	1.01686	1.02543	1.01048	1.02383	1.01536	1.01623
172800	1.01663	1.02521	1.0102	1.0237	1.0152	1.0161
259200	1.01643	1.02508	1.01013	1.0235	1.01506	1.01593
345600	1.0163	1.02486	1.00968	1.02328	1.01486	1.01581
432000	1.016153	1.02463	1.00956	1.0231	1.01473	1.01571
G (kg/s)	1.806E-09	2.122E-09	2.238E-09	1.929E-09	1.775E-09	1.813E-09

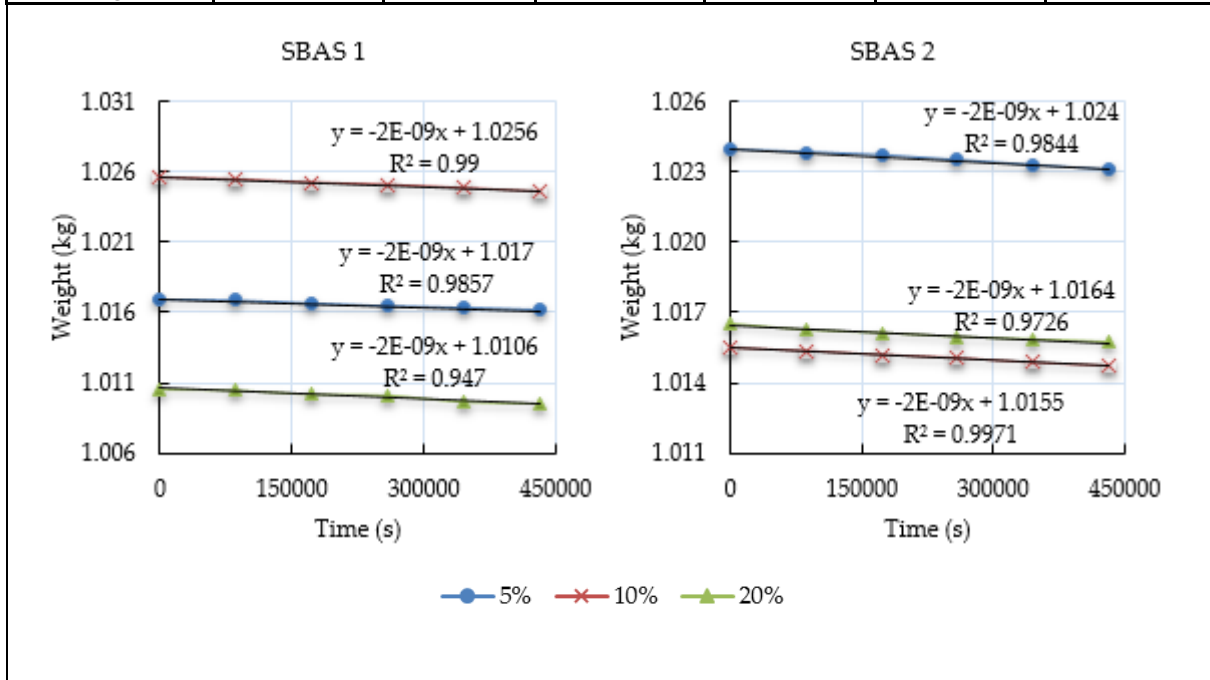


Table D - 4: Vapour Permeability Test - IBA 1 and IBA 2.

Ash	IBA 1			IBA 2		
	5%	10%	20%	5%	10%	20%
Replacement	5%	10%	20%	5%	10%	20%
Time (s)	Weight (kg)					
0	1.00133	1.01643	1.0062	0.99563	1.00353	0.9984
86400	1.00106	1.01616	1.0058	0.9953	1.0032	0.9979
172800	1.00086	1.01583	1.00556	0.99493	1.00286	0.9976
259200	1.0006	1.01546	1.005	0.9947	1.00263	0.9973
345600	1.00026	1.01516	1.0048	0.9943	1.00223	0.99685
432000	1.00003	1.01506	1.00466	0.99393	1.00186	0.99655
G (kg/s)	3.009E-09	3.164E-09	3.549E-09	3.935E-09	3.858E-09	4.282E-09

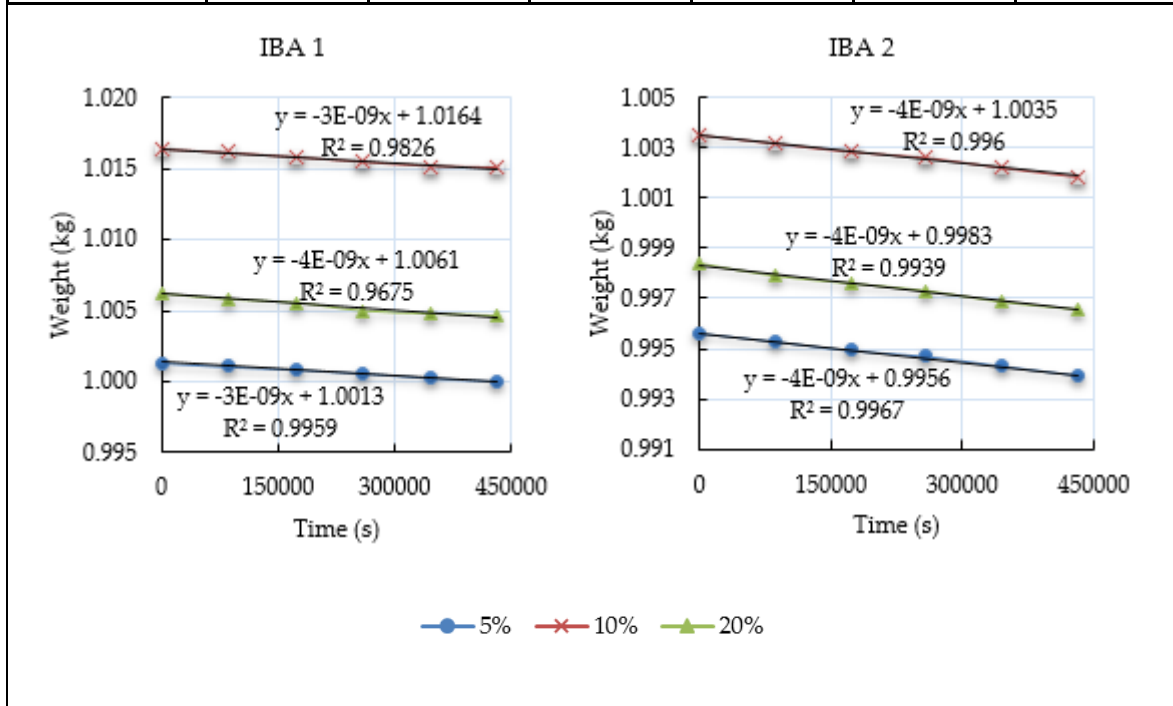
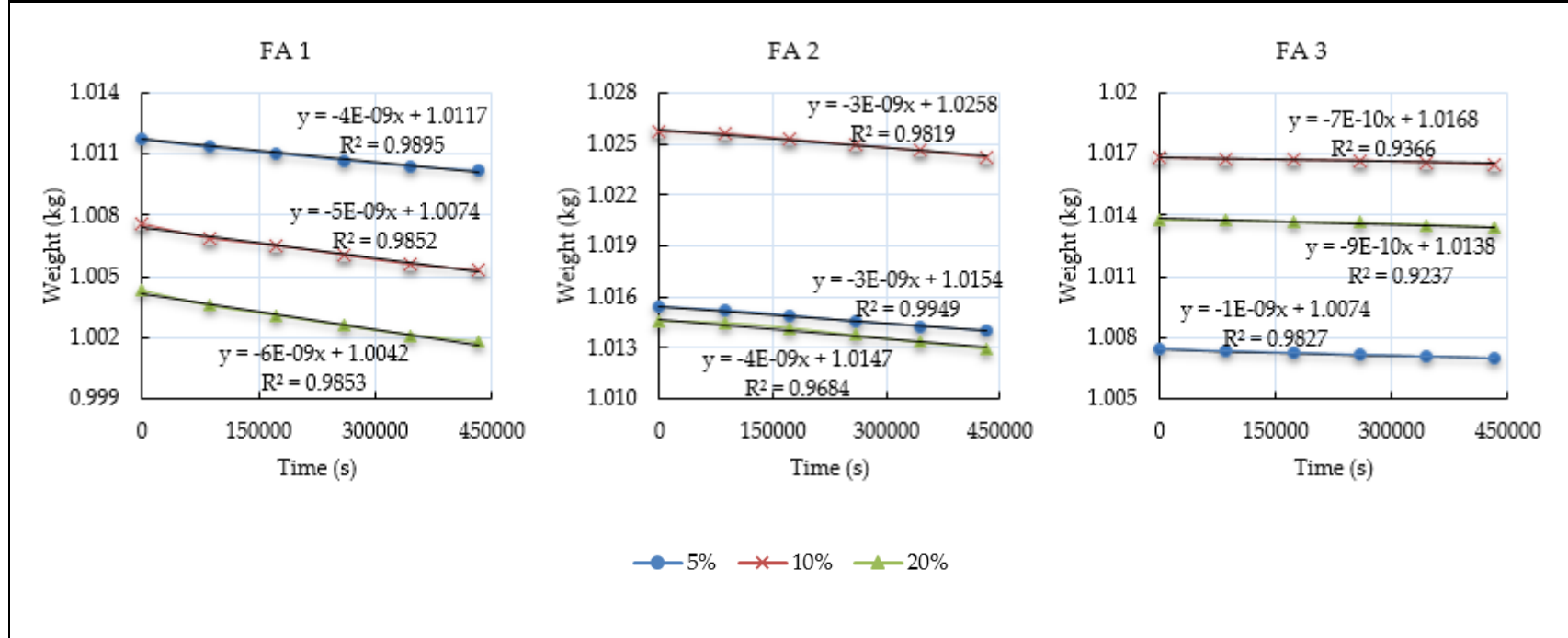


Table D - 5: Vapour Permeability Test – FA 1, FA 2 and FA 3.

Ash	FA 1			FA 2			FA 3		
	5%	10%	20%	5%	10%	20%	5%	10%	20%
Replacement	5%	10%	20%	5%	10%	20%	5%	10%	20%
Time (s)	Weight (kg)								
0	1.01176	1.00756	1.00433	1.0154	1.02566	1.01453	1.00743	1.0168	1.01376
86400	1.01133	1.00686	1.00356	1.01520	1.02556	1.01446	1.0073	1.01673	1.01376
172800	1.01103	1.0065	1.00308	1.0149	1.02523	1.01416	1.00723	1.0167	1.01366
259200	1.01066	1.00603	1.00256	1.01453	1.02491	1.01373	1.00713	1.01667	1.01362
345600	1.01036	1.00556	1.0021	1.01426	1.0246	1.01333	1.00708	1.01659	1.01352
432000	1.01016	1.0053	1.00176	1.014	1.02421	1.01295	1.007	1.01647	1.01336
G (kg/s)	3.704E-09	5.247E-09	5.941E-09	3.241E-09	3.356E-09	3.657E-09	1.003E-09	7.485E-10	9.259E-10



Appendix E HYDRATED LIME DATA SHEET



Hydrated Lime

Calcium Hydroxide

Revision Date: June 2010

Chemical Analysis		Typical Analysis	Specification
Calcium Hydroxide	Ca(OH) ₂	92%	>90%
Calcium Carbonate	CaCO ₃	1.5%	<9%
Magnesium Oxide	MgO	0.4%	< 5%
Silica	SiO ₂	1.4%	
Aluminium Oxide	Al ₂ O ₃	0.3%	
Ferric Oxide	Fe ₂ O ₃	0.2%	
Sulphur Trioxide	SO ₃	0.5%	< 2%
Physical Analysis			
Moisture Content	H ₂ O	0.3%	
<i>Grading</i>			
Passing 0.6mm		99.95%	
Passing 0.2mm		1.5%	< 2%
Passing 0.09mm		5%	< 7%
Bulk Density		300-600kg / m ³	

Additional Information

All results are given at 95% confidence levels and on a dry basis

Store away from air and moisture

Consult Hydrated Lime MSDS prior to use

All products are REACH compliant

The information contained in this data sheet is to the best of our knowledge true and accurate. The typical analysis values given are subject to variation as the raw material (limestone) is naturally occurring

White Rhino Hydrated Lime conforms to IS E.N. 459

Appendix F PORTLAND CEMENT DATA SHEET

Portland Limestone Cement CEM II/A-L 32,5N

I.S. EN 197-1:2011

Bagged Normal Cement

Normal Cement is a high quality general purpose bagged cement and is suitable for all general concreting, block laying and plastering applications.

The product has been specifically designed to reduce the carbon intensity of cement production and to provide enhanced workability in block laying and plastering applications.

The quality of all Normal Cement produced by Irish Cement is guaranteed to meet, in full, the requirements of Irish Standard I.S. EN 197-1 'Cement Part 1: Composition, Specifications and Conformity Criteria for Common Cements', and the product is independently certified by the National Standards Authority of Ireland and is CE marked.

Normal Cement is produced by grinding a combination of cement clinker and selected limestone and grinding aids, along with a small quantity of gypsum, to produce the final fine grey powder. Cement clinker is made by fusing together, at high temperatures, a precisely controlled blend of very finely ground limestone and shale. Normal Cement is manufactured in modern dry process works at Castlemungret, Co Limerick and Platin, Co Meath and is supplied in 25kg bags.



Setting time: I.S. EN 197-1 requires a minimum initial setting time of 75 minutes. Initial set for Normal Cement typically exceeds 100 minutes.

Strength: Minimum compressive strengths for standard mortar prisms of 16 N/mm² at 7 days and 32.5 N/mm² at 28 days are stipulated in I.S. EN 197-1 for class 32.5N cement in accordance with particular compliance rules.

Typical mortar prism strengths of Normal Cement are in the range 30-38 N/mm² at 7 days and 40-50 N/mm² at 28 days.

Concrete and mortar strength is significantly affected by mix constituents and proportions, ambient temperature and curing conditions. A durable concrete requires an adequate cement content and a low water/cement ratio. The correct mix ratio of cement:sand and the use of suitable mortar admixtures or lime is necessary to provide good durability in mortars or plasters. Guidance is available in Irish Standards for suitable concrete and mortar mixes for various exposure conditions.



APPLICATIONS

Normal Cement is suitable for a wide range of applications where no special or unusual considerations arise. Typical applications include use in site-mixed concrete for foundations, paths, etc., in small precast elements and in mortars, renders and grouts. Mortar mixes should have improved workability properties, compared with traditional cement based only on cement clinker, resulting in a more cohesive mortar or render mix, with better handling and finish characteristics.



PRODUCT DATA

Regular information is available on the performance aspects of Normal Cement, which are of direct interest to specifiers and users.

The requirements of I.S. EN 197-1 for CEM II/A-L class 32.5N cement are compared hereafter to typical performance data for Normal Cement.



Irish Cement Ltd.
Platin, Drogheda, Co. Louth

T: 041 987 6000 (Office hours)
E: info@irishcement.ie

www.irishcement.ie

BAGGED NORMAL CEMENT

Chemical Composition: Cement clinker consists predominantly of compounds formed from Calcium, Silica, Alumina and Iron. Calcium sulfate in the form of gypsum is added to cement to control the setting time. Limestone (Calcium Carbonate), complying with specified requirements in I.S. EN 197-1, is present in the range 6% - 20% in CEM II/A-L Normal Cement, as stipulated in I.S. EN 197-1.

Specific data on chemical and compound composition of Normal Cement is available on request.



TEST CERTIFICATES

Routine product test data covering the key physical and chemical parameters is made available on a weekly basis on request.



QUALITY ASSURANCE AND CERTIFICATION

In addition to the company's own guarantee, Normal Cement is CE marked in accordance with the requirements of the EU Construction Products Directive. The CE mark has been awarded by the National Standards Authority of Ireland (NSAI).

Irish Cement Ltd holds Quality Systems Certification to I.S. EN ISO 9001: 2008 and Environmental System Certification to I.S. EN ISO 14001: 2004 from NSAI.

Irish Cement has been awarded BES 6001 certification for the responsible sourcing of its CEM II 32,5 N products.



STORAGE

Cement should be stored dry, otherwise its quality will deteriorate through premature hydration and carbonation. Moisture from the air can be as harmful as direct moisture. The product is supplied in moisture resistant paper bags to give improved storage life.



HEALTH & SAFETY

Irritating to eyes, respiratory system and skin. Keep out of the reach of children. Avoid contact with the skin and eyes. In case of contact with eyes, rinse immediately with plenty of water and seek medical advice. After contact with skin, wash immediately with plenty of water. Wear suitable protective clothing. Chromium VI reducing agent added and effective for 3 months from date of packing (marked on bag) if stored in dry conditions (DIR 2003/53 /EC). A detail Safety Data Sheet is available from Irish Cement Limited. Tel: 041 987 6000. The Safety Guidance and Material Safety Data Sheet is available for download from www.irishcement.ie



ADVICE AND INFORMATION

As part of its ongoing commitment to the quality of design and construction in concrete, Irish Cement provides a comprehensive technical advisory service on the use of cement and concrete.

This technical support is provided by civil engineers, with wide experience of cement and concrete technology, who are available to answer queries and give advice.

They can be contacted at: Technical Marketing Department, Irish Cement Ltd, Platin, Drogheda, Co Louth.

Tel: 041 987 6000 Fax: 041 987 6400
Email: info@irishcement.ie Web: www.irishcement.ie

OTHER PRODUCTS

Irish Cement Limited also manufactures Normal Cement (Bulk), Rapid Hardening Portland Cement, Sulfate Resisting Portland Cement and Ground Granulated Blastfurnace Slag. Similar data sheets on each of these products are available on request.



Irish Cement Ltd.
Platin, Drogheda, Co. Louth

T: 041 987 6000 (Office hours)
E: info@irishcement.ie

www.irishcement.ie

Potential of waste materials as pozzolans and their influence on the quality of building materials

IBA 1 5	3	2248.02	13.92	(2231.45, 2264.58)
IBA 2 10	3	2303.0	23.6	(2286.5, 2319.6)
IBA 2 20	3	2284.9	19.8	(2268.3, 2301.4)
IBA 2 5	3	2326.87	10.66	(2310.30, 2343.43)
Ref	3	2380.06	9.90	(2363.49, 2396.63)
SBAS 1 10	3	2231.33	14.71	(2214.76, 2247.90)
SBAS 1 20	3	2221.62	11.29	(2205.05, 2238.18)
SBAS 1 5	3	2237.3	21.7	(2220.7, 2253.8)
SBAS 2 10	3	2331.7	18.4	(2315.2, 2348.3)
SBAS 2 20	3	2343.92	11.84	(2327.35, 2360.49)
SBAS 2 5	3	2344.38	10.54	(2327.81, 2360.95)
SCBA 1 10	3	2349.58	14.03	(2333.01, 2366.15)
SCBA 1 20	3	2344.79	5.71	(2328.22, 2361.36)
SCBA 1 5	3	2350.09	8.25	(2333.52, 2366.66)
SCBA 2 10	3	2301.82	6.52	(2285.26, 2318.39)
SCBA 2 20	3	2282.20	13.69	(2265.64, 2298.77)
SCBA 2 5	3	2299.96	13.80	(2283.39, 2316.53)

Pooled StDev = 14.3258

Dunnnett Multiple Comparisons with a Control

Grouping Information Using the Dunnnett Method and 95% Confidence

Sample	N	Mean	Grouping
Ref (control)	3	2380.06	A

FA 2 5	3	2377.07	A
FA 2 20	3	2370.44	A
SCBA 1 5	3	2350.09	A
SCBA 1 10	3	2349.58	A
SCBA 1 20	3	2344.79	A
SBAS 2 5	3	2344.38	A
SBAS 2 20	3	2343.92	A
FA 2 10	3	2337.4	
SBAS 2 10	3	2331.7	
FA 1 10	3	2327.11	
IBA 2 5	3	2326.87	
FA 1 5	3	2326.44	
FA 1 20	3	2321.4	
FA 3 5	3	2319.00	
IBA 2 10	3	2303.0	
SCBA 2 10	3	2301.82	
SCBA 2 5	3	2299.96	
FA 3 10	3	2295.6	
FA 3 20	3	2290.91	
IBA 2 20	3	2284.9	
SCBA 2 20	3	2282.20	
IBA 1 10	3	2273.87	
IBA 1 5	3	2248.02	
SBAS 1 5	3	2237.3	
SBAS 1 10	3	2231.33	
SBAS 1 20	3	2221.62	
IBA 1 20	3	2217.13	

Means not labeled with the letter A are significantly different from the control level mean.

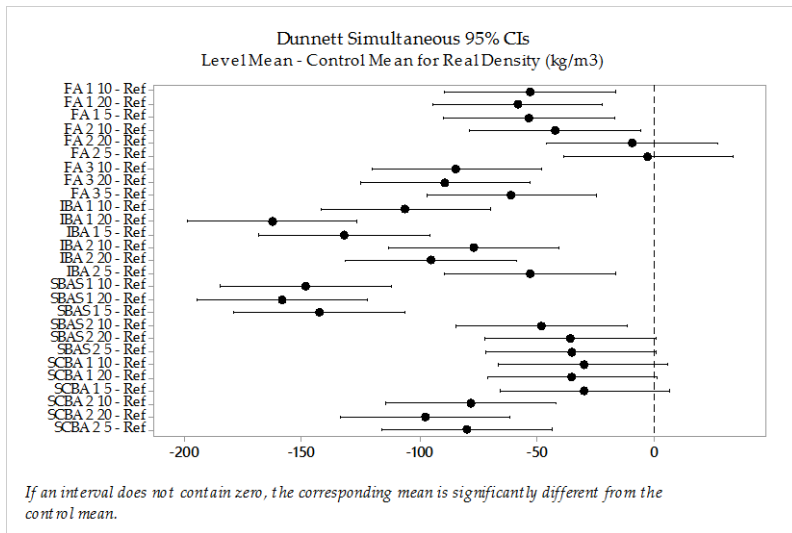
Dunnett Simultaneous Tests for Level Mean - Control Mean

Difference of Adjusted Levels	P-Value	Difference of Means	Difference	95% CI	SE of T-
FA 1 10 - Ref	0.001	-53.0	11.7	(-89.2, -16.7)	-
FA 1 20 - Ref	0.000	-58.6	11.7	(-94.8, -22.4)	-
FA 1 5 - Ref	0.001	-53.6	11.7	(-89.8, -17.4)	-
FA 2 10 - Ref	0.011	-42.6	11.7	(-78.8, -6.4)	-
FA 2 20 - Ref	1.000	-9.6	11.7	(-45.8, 26.6)	-
FA 2 5 - Ref	1.000	-3.0	11.7	(-39.2, 33.2)	-
FA 3 10 - Ref	0.000	-84.5	11.7	(-120.7, -48.3)	-
FA 3 20 - Ref	0.000	-89.1	11.7	(-125.4, -52.9)	-
FA 3 5 - Ref	0.000	-61.1	11.7	(-97.3, -24.9)	-
IBA 1 10 - Ref	0.000	-106.2	11.7	(-142.4, -70.0)	-
IBA 1 20 - Ref	0.000	-162.9	11.7	(-199.1, -126.7)	-

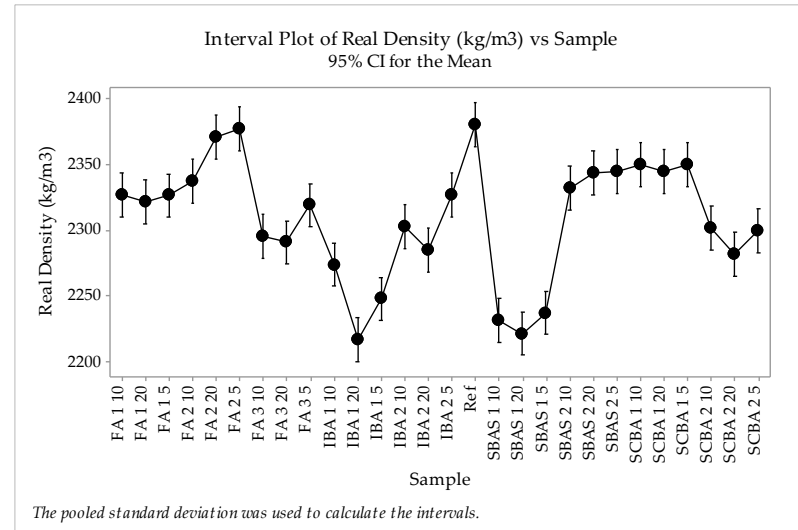
IBA 1 5 - Ref	0.000	-132.0	11.7	(-168.2, -95.8)	-
IBA 2 10 - Ref	0.000	-77.0	11.7	(-113.2, -40.8)	-
IBA 2 20 - Ref	0.000	-95.2	11.7	(-131.4, -59.0)	-
IBA 2 5 - Ref	0.001	-53.2	11.7	(-89.4, -17.0)	-
SBAS 1 10 - Ref	0.000	-148.7	11.7	(-184.9, -112.5)	-
SBAS 1 20 - Ref	0.000	-158.4	11.7	(-194.6, -122.2)	-
SBAS 1 5 - Ref	0.000	-142.8	11.7	(-179.0, -106.6)	-
SBAS 2 10 - Ref	0.003	-48.3	11.7	(-84.5, -12.1)	-
SBAS 2 20 - Ref	0.051	-36.1	11.7	(-72.3, 0.1)	-
SBAS 2 5 - Ref	0.056	-35.7	11.7	(-71.9, 0.5)	-
SCBA 1 10 - Ref	0.156	-30.5	11.7	(-66.7, 5.7)	-
SCBA 1 20 - Ref	0.061	-35.3	11.7	(-71.5, 0.9)	-
SCBA 1 5 - Ref	0.171	-30.0	11.7	(-66.2, 6.2)	-
SCBA 2 10 - Ref	0.000	-78.2	11.7	(-114.4, -42.0)	-
SCBA 2 20 - Ref	0.000	-97.9	11.7	(-134.1, -61.6)	-
SCBA 2 5 - Ref	0.000	-80.1	11.7	(-116.3, -43.9)	-

Individual confidence level = 99.69%

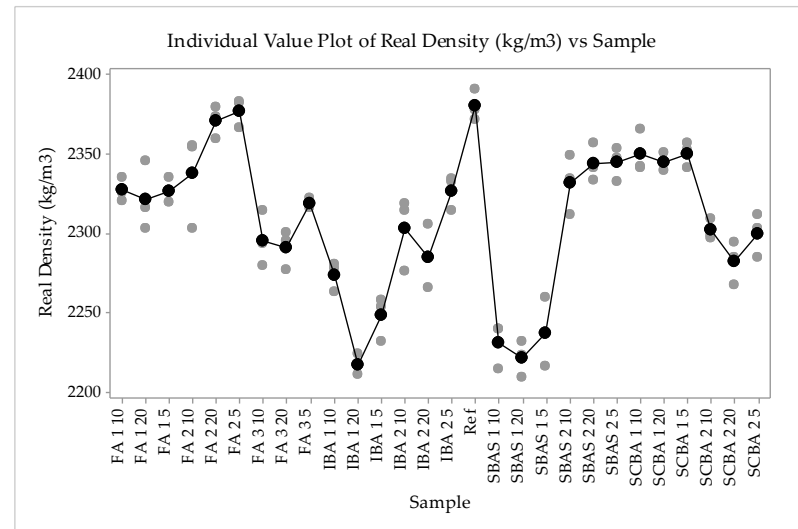
Dunnett Simultaneous 95% CIs



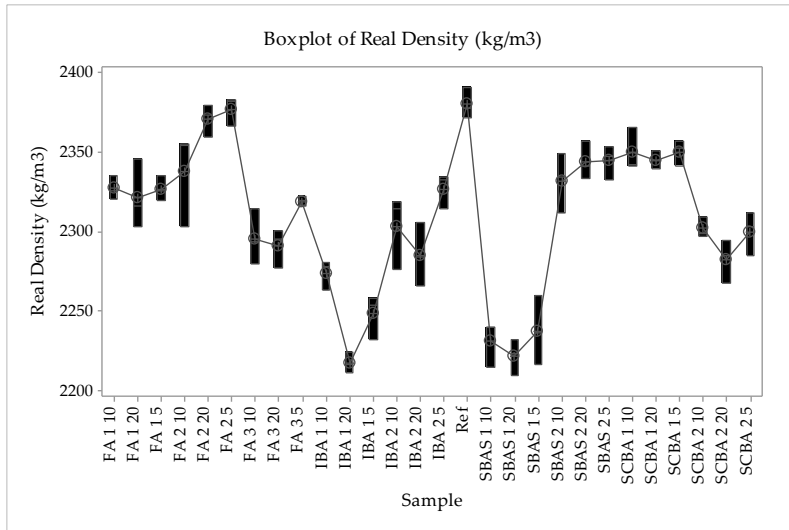
Interval Plot of Real Density (kg/m³) vs Sample



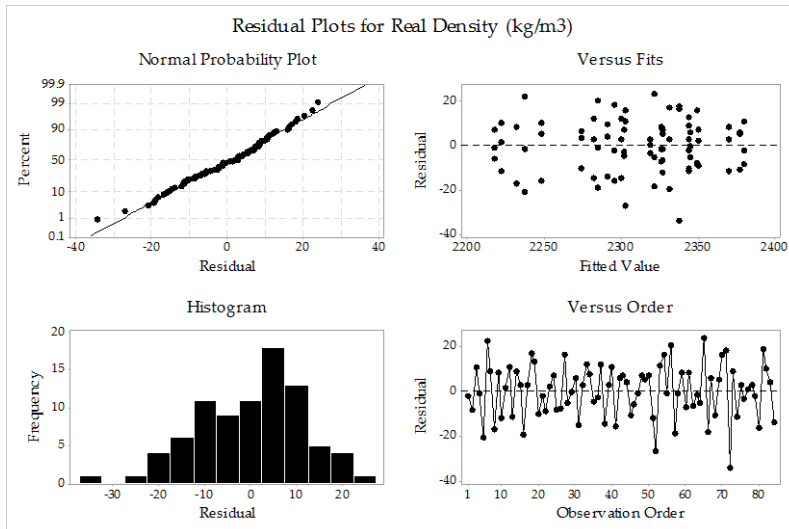
Individual Value Plot of Real Density (kg/m³) vs Sample



Boxplot of Real Density (kg/m³)



Residual Plots for Real Density (kg/m³)



One-way ANOVA: Bulk Density (kg/m³) versus Sample

Method

Null hypothesis All means are equal
 Alternative hypothesis At least one mean is different
 Significance level $\alpha = 0.05$

Equal variances were assumed for the analysis.

Factor Information

Factor Levels Values

Sample 28 FA 1 10, FA 1 20, FA 1 5, FA 2 10, FA 2 20, FA 2 5, FA 3 10, FA 3 20, FA 3 5,
 IBA 1 10, IBA 1 20, IBA 1 5, IBA 2 10, IBA 2 20, IBA 2 5, Ref, SBAS 1 10,
 SBAS 1 20, SBAS 1 5, SBAS 2 10, SBAS 2 20, SBAS 2 5, SCBA 1 10, SCBA 1 20,
 SCBA 1 5, SCBA 2 10, SCBA 2 20, SCBA 2 5

Analysis of Variance

Source	DF	Adj SS	Adj MS	F-Value	P-Value
Sample	27	322900	11959.3	48.13	0.000
Error	56	13914	248.5		
Total	83	336814			

Potential of waste materials as pozzolans and their influence on the quality of building materials

Model Summary

S	R-sq	R-sq(adj)	R-sq(pred)
15.7628	95.87%	93.88%	90.71%

Means

Sample	N	Mean	StDev	95% CI
FA 1 10	3	2006.09	15.13	(1987.86, 2024.32)
FA 1 20	3	1968.8	32.4	(1950.6, 1987.1)
FA 1 5	3	2038.11	2.62	(2019.88, 2056.34)
FA 2 10	3	1983.4	26.4	(1965.2, 2001.6)
FA 2 20	3	1965.0	21.8	(1946.7, 1983.2)
FA 2 5	3	2059.46	8.04	(2041.23, 2077.69)
FA 3 10	3	2103.27	16.03	(2085.04, 2121.51)
FA 3 20	3	2083.62	1.53	(2065.39, 2101.85)
FA 3 5	3	2090.96	10.78	(2072.73, 2109.19)
IBA 1 10	3	1951.5	23.3	(1933.3, 1969.7)
IBA 1 20	3	1900.39	2.25	(1882.16, 1918.63)
IBA 1 5	3	1984.29	17.02	(1966.06, 2002.52)
IBA 2 10	3	1981.2	31.8	(1963.0, 1999.4)
IBA 2 20	3	1929.59	16.97	(1911.36, 1947.83)
IBA 2 5	3	2007.53	11.76	(1989.30, 2025.76)
Ref	3	2054.66	2.69	(2036.43, 2072.89)
SBAS 1 10	3	2107.04	15.99	(2088.81, 2125.27)
SBAS 1 20	3	2080.35	7.95	(2062.12, 2098.58)

SBAS 1 5	3	2098.36	14.70	(2080.13, 2116.59)
SBAS 2 10	3	2087.9	20.6	(2069.7, 2106.1)
SBAS 2 20	3	2120.30	5.37	(2102.07, 2138.53)
SBAS 2 5	3	2097.89	12.47	(2079.66, 2116.12)
SCBA 1 10	3	2059.40	13.87	(2041.17, 2077.63)
SCBA 1 20	3	2080.31	13.96	(2062.08, 2098.54)
SCBA 1 5	3	2080.57	5.73	(2062.34, 2098.80)
SCBA 2 10	3	2109.84	11.79	(2091.61, 2128.07)
SCBA 2 20	3	2085.56	3.22	(2067.33, 2103.79)
SCBA 2 5	3	2107.12	7.82	(2088.89, 2125.36)

Pooled StDev = 15.7628

Dunnett Multiple Comparisons with a Control

Grouping Information Using the Dunnett Method and 95% Confidence

Sample	N	Mean	Grouping
Ref (control)	3	2054.66	A
SBAS 2 20	3	2120.30	
SCBA 2 10	3	2109.84	
SCBA 2 5	3	2107.12	
SBAS 1 10	3	2107.04	
FA 3 10	3	2103.27	
SBAS 1 5	3	2098.36	
SBAS 2 5	3	2097.89	

Appendix G Statistical Analysis

Radson Lima Figueiredo

					Levels	of Means	Difference	95% CI	T-
					Value				
					P-Value				
FA 3 5	3	2090.96	A						
SBAS 2 10	3	2087.9	A						
SCBA 2 20	3	2085.56	A	FA 1 10 - Ref	3.77	-48.6	12.9	(-88.4, -8.7)	-
FA 3 20	3	2083.62	A	FA 1 20 - Ref	6.67	-85.8	12.9	(-125.7, -46.0)	-
SCBA 1 5	3	2080.57	A	FA 1 5 - Ref	1.29	-16.5	12.9	(-56.4, 23.3)	-
SBAS 1 20	3	2080.35	A		0.943				
SCBA 1 20	3	2080.31	A	FA 2 10 - Ref	5.54	-71.3	12.9	(-111.1, -31.4)	-
FA 2 5	3	2059.46	A		0.000				
SCBA 1 10	3	2059.40	A	FA 2 20 - Ref	6.97	-89.7	12.9	(-129.5, -49.9)	-
FA 1 5	3	2038.11	A						
IBA 2 5	3	2007.53		FA 2 5 - Ref	0.37	4.8	12.9	(-35.0, 44.6)	
FA 1 10	3	2006.09			1.000				
IBA 1 5	3	1984.29		FA 3 10 - Ref	3.78	48.6	12.9	(8.8, 88.5)	
FA 2 10	3	1983.4							
IBA 2 10	3	1981.2		FA 3 20 - Ref	2.25	29.0	12.9	(-10.9, 68.8)	
FA 1 20	3	1968.8			0.311				
FA 2 20	3	1965.0		FA 3 5 - Ref	2.82	36.3	12.9	(-3.5, 76.1)	
IBA 1 10	3	1951.5			0.097				
IBA 2 20	3	1929.59		IBA 1 10 - Ref	8.02	-103.2	12.9	(-143.0, -63.3)	-
IBA 1 20	3	1900.39			0.000				
				IBA 1 20 - Ref	11.99	-154.3	12.9	(-194.1, -114.4)	-
					0.000				
				IBA 1 5 - Ref	5.47	-70.4	12.9	(-110.2, -30.5)	-
					0.000				
				IBA 2 10 - Ref	5.71	-73.5	12.9	(-113.3, -33.6)	-
					0.000				
				IBA 2 20 - Ref	9.72	-125.1	12.9	(-164.9, -85.2)	-
					0.000				
				IBA 2 5 - Ref	3.66	-47.1	12.9	(-87.0, -7.3)	-
					0.011				
				SBAS 1 10 - Ref	4.07	52.4	12.9	(12.5, 92.2)	
					0.003				

Means not labeled with the letter A are significantly different from the control level mean.

Dunnett Simultaneous Tests for Level Mean - Control Mean

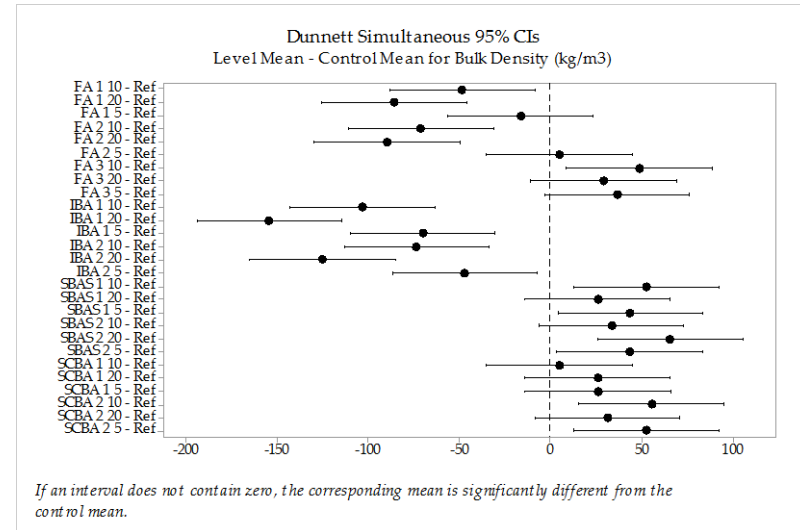
Difference of Adjusted Difference SE of

Potential of waste materials as pozzolans and their influence on the quality of building materials

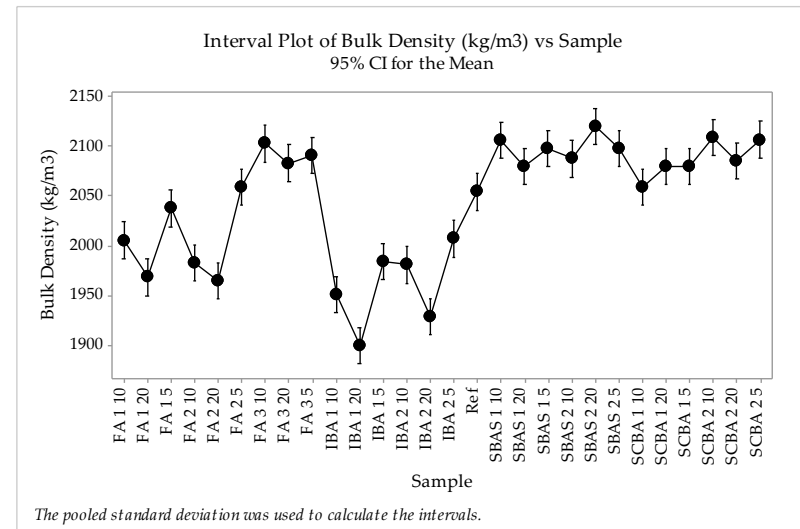
SBAS 1 20 - Ref	25.7	12.9	(-14.1, 65.5)
2.00 0.472			
SBAS 1 5 - Ref	43.7	12.9	(3.9, 83.5)
3.40 0.023			
SBAS 2 10 - Ref	33.3	12.9	(-6.6, 73.1)
2.58 0.163			
SBAS 2 20 - Ref	65.6	12.9	(25.8, 105.5)
5.10 0.000			
SBAS 2 5 - Ref	43.2	12.9	(3.4, 83.1)
3.36 0.025			
SCBA 1 10 - Ref	4.7	12.9	(-35.1, 44.6)
0.37 1.000			
SCBA 1 20 - Ref	25.7	12.9	(-14.2, 65.5)
1.99 0.474			
SCBA 1 5 - Ref	25.9	12.9	(-13.9, 65.7)
2.01 0.460			
SCBA 2 10 - Ref	55.2	12.9	(15.3, 95.0)
4.29 0.002			
SCBA 2 20 - Ref	30.9	12.9	(-8.9, 70.7)
2.40 0.235			
SCBA 2 5 - Ref	52.5	12.9	(12.6, 92.3)
4.08 0.003			

Individual confidence level = 99.69%

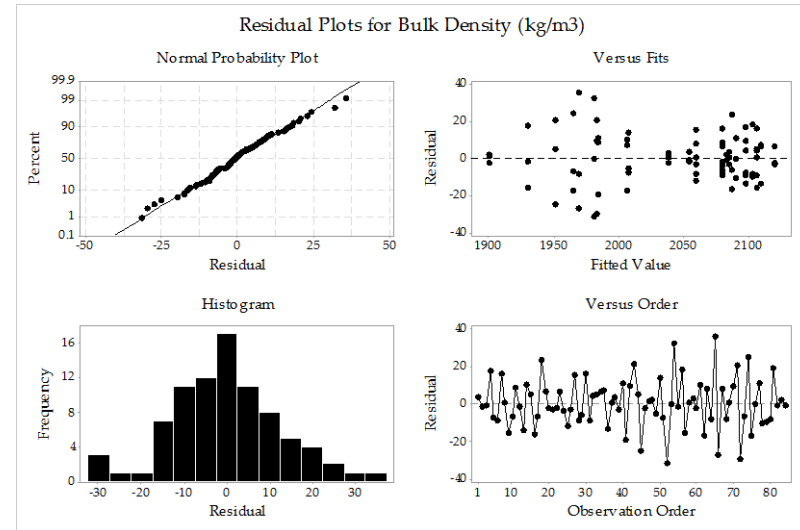
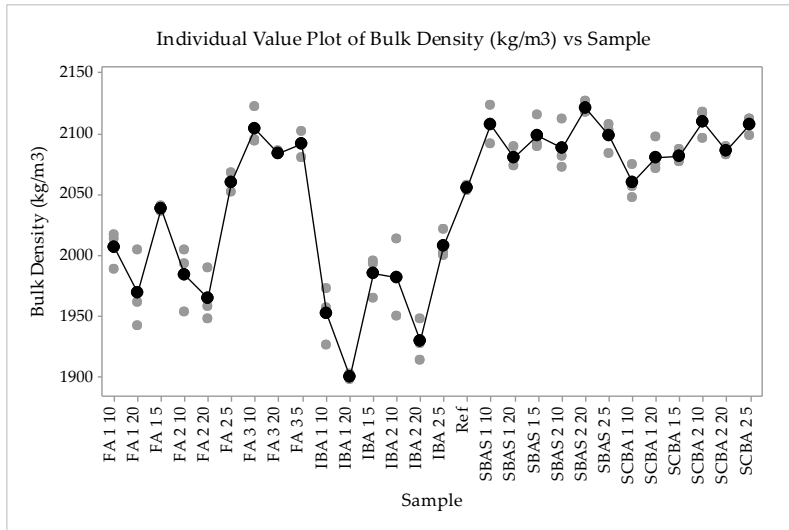
Dunnett Simultaneous 95% CIs



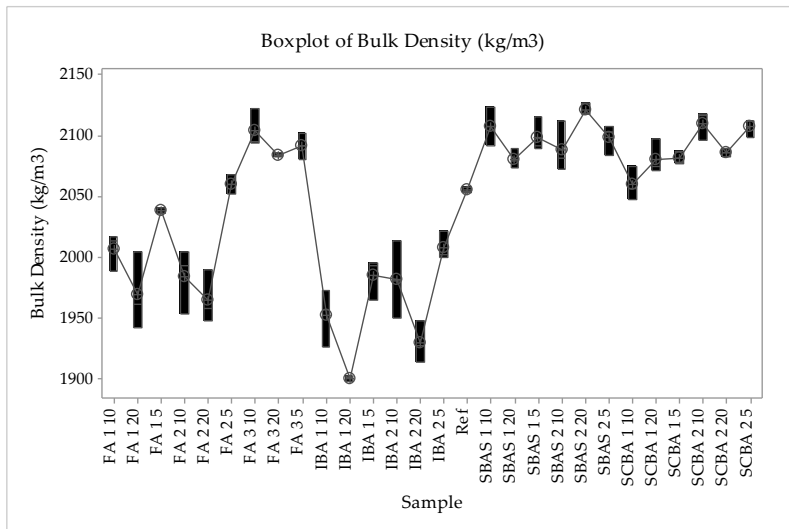
Interval Plot of Bulk Density (kg/m³) vs Sample



Individual Value Plot of Bulk Density (kg/m³) vs Sample



Boxplot of Bulk Density (kg/m³)



One-way ANOVA: Open Porosity (%) versus Sample

Method

Null hypothesis All means are equal
 Alternative hypothesis At least one mean is different
 Significance level $\alpha = 0.05$

Equal variances were assumed for the analysis.

Factor Information

Factor Levels Values

Residual Plots for Bulk Density (kg/m³)

Potential of waste materials as pozzolans and their influence on the quality of building materials

Sample 28 FA 1 10, FA 1 20, FA 1 5, FA 2 10, FA 2 20, FA 2 5, FA 3 10, FA 3 20, FA 3 5,
 IBA 1 10, IBA 1 20, IBA 1 5, IBA 2 10, IBA 2 20, IBA 2 5, Ref, SBAS 1 10,
 SBAS 1 20, SBAS 1 5, SBAS 2 10, SBAS 2 20, SBAS 2 5, SCBA 1 10, SCBA 1 20,
 SCBA 1 5, SCBA 2 10, SCBA 2 20, SCBA 2 5

FA 2 10	3	15.147	0.205	(14.534, 15.761)
FA 2 20	3	17.102	1.247	(16.489, 17.716)
FA 2 5	3	13.3613	0.1515	(12.7478, 13.9749)
FA 3 10	3	8.377	0.312	(7.763, 8.990)
FA 3 20	3	9.047	0.472	(8.433, 9.660)
FA 3 5	3	9.833	0.520	(9.220, 10.447)
IBA 1 10	3	14.179	0.682	(13.565, 14.792)
IBA 1 20	3	14.286	0.175	(13.672, 14.899)
IBA 1 5	3	11.732	0.225	(11.119, 12.346)
IBA 2 10	3	13.977	0.689	(13.364, 14.591)
IBA 2 20	3	15.5491	0.0380	(14.9355, 16.1626)
IBA 2 5	3	13.724	0.398	(13.110, 14.337)
Ref	3	13.671	0.375	(13.057, 14.285)
SBAS 1 10	3	5.568	0.946	(4.954, 6.181)
SBAS 1 20	3	6.358	0.451	(5.744, 6.971)
SBAS 1 5	3	6.202	1.173	(5.589, 6.816)
SBAS 2 10	3	10.457	0.364	(9.843, 11.070)
SBAS 2 20	3	9.540	0.264	(8.926, 10.153)
SBAS 2 5	3	10.5145	0.1356	(9.9010, 11.1281)
SCBA 1 10	3	12.350	0.180	(11.737, 12.964)
SCBA 1 20	3	11.280	0.399	(10.666, 11.894)
SCBA 1 5	3	11.468	0.383	(10.854, 12.081)
SCBA 2 10	3	8.341	0.487	(7.727, 8.954)
SCBA 2 20	3	8.614	0.644	(8.000, 9.227)
SCBA 2 5	3	8.384	0.241	(7.770, 8.997)

Analysis of Variance

Source	DF	Adj SS	Adj MS	F-Value	P-Value
Sample	27	773.72	28.6564	101.83	0.000
Error	56	15.76	0.2814		
Total	83	789.48			

Model Summary

S	R-sq	R-sq(adj)	R-sq(pred)
0.530496	98.00%	97.04%	95.51%

Means

Sample	N	Mean	StDev	95% CI
FA 1 10	3	13.795	0.452	(13.182, 14.409)
FA 1 20	3	15.193	0.606	(14.580, 15.807)
FA 1 5	3	12.393	0.182	(11.780, 13.007)

Pooled StDev = 0.530496

Dunnett Multiple Comparisons with a Control

Grouping Information Using the Dunnett Method and 95% Confidence

Sample	N	Mean	Grouping
Ref (control)	3	13.671	A
FA 2 20	3	17.102	
IBA 2 20	3	15.5491	
FA 1 20	3	15.193	
FA 2 10	3	15.147	
IBA 1 20	3	14.286	A
IBA 1 10	3	14.179	A
IBA 2 10	3	13.977	A
FA 1 10	3	13.795	A
IBA 2 5	3	13.724	A
FA 2 5	3	13.3613	A
FA 1 5	3	12.393	A
SCBA 1 10	3	12.350	A
IBA 1 5	3	11.732	
SCBA 1 5	3	11.468	
SCBA 1 20	3	11.280	
SBAS 2 5	3	10.5145	
SBAS 2 10	3	10.457	
FA 3 5	3	9.833	
SBAS 2 20	3	9.540	
FA 3 20	3	9.047	

SCBA 2 20	3	8.614
SCBA 2 5	3	8.384
FA 3 10	3	8.377
SCBA 2 10	3	8.341
SBAS 1 20	3	6.358
SBAS 1 5	3	6.202
SBAS 1 10	3	5.568

Means not labeled with the letter A are significantly different from the control level mean.

Dunnett Simultaneous Tests for Level Mean - Control Mean

Difference of Adjusted Levels Value	P-Value	Difference of Means	Difference	95% CI	SE of T-
FA 1 10 - Ref	0.29	0.124	0.433	(-1.217, 1.465)	
FA 1 20 - Ref	3.51	1.522	0.433	(0.181, 2.863)	
FA 1 5 - Ref	2.95	-1.278	0.433	(-2.618, 0.063)	-
FA 2 10 - Ref	3.41	1.476	0.433	(0.136, 2.817)	
FA 2 20 - Ref	7.92	3.431	0.433	(2.091, 4.772)	
FA 2 5 - Ref	0.71	-0.310	0.433	(-1.650, 1.031)	-
FA 3 10 - Ref	12.22	-5.294	0.433	(-6.635, -3.954)	-

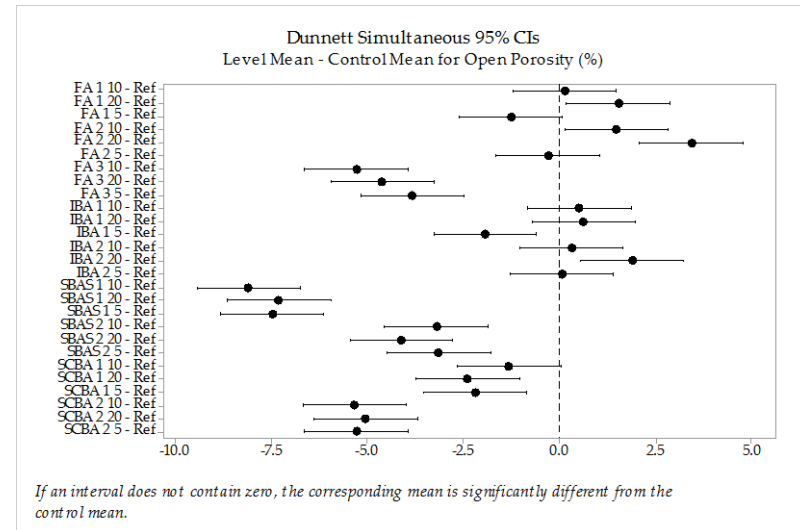
Potential of waste materials as pozzolans and their influence on the quality of building materials

FA 3 20 - Ref	-4.624	0.433	(-5.965, -3.284)	-
10.68	0.000			
FA 3 5 - Ref	-3.838	0.433	(-5.178, -2.497)	-
8.86	0.000			
IBA 1 10 - Ref	0.508	0.433	(-0.833, 1.848)	
1.17	0.975			
IBA 1 20 - Ref	0.615	0.433	(-0.726, 1.955)	
1.42	0.884			
IBA 1 5 - Ref	-1.939	0.433	(-3.279, -0.598)	-
4.48	0.001			
IBA 2 10 - Ref	0.306	0.433	(-1.034, 1.647)	
0.71	1.000			
IBA 2 20 - Ref	1.878	0.433	(0.537, 3.219)	
4.34	0.001			
IBA 2 5 - Ref	0.053	0.433	(-1.288, 1.393)	
0.12	1.000			
SBAS 1 10 - Ref	-8.103	0.433	(-9.444, -6.763)	-
18.71	0.000			
SBAS 1 20 - Ref	-7.313	0.433	(-8.654, -5.973)	-
16.88	0.000			
SBAS 1 5 - Ref	-7.469	0.433	(-8.809, -6.128)	-
17.24	0.000			
SBAS 2 10 - Ref	-3.214	0.433	(-4.555, -1.873)	-
7.42	0.000			
SBAS 2 20 - Ref	-4.131	0.433	(-5.472, -2.791)	-
9.54	0.000			
SBAS 2 5 - Ref	-3.156	0.433	(-4.497, -1.816)	-
7.29	0.000			
SCBA 1 10 - Ref	-1.320	0.433	(-2.661, 0.020)	-
3.05	0.056			
SCBA 1 20 - Ref	-2.391	0.433	(-3.732, -1.050)	-
5.52	0.000			
SCBA 1 5 - Ref	-2.203	0.433	(-3.544, -0.862)	-
5.09	0.000			

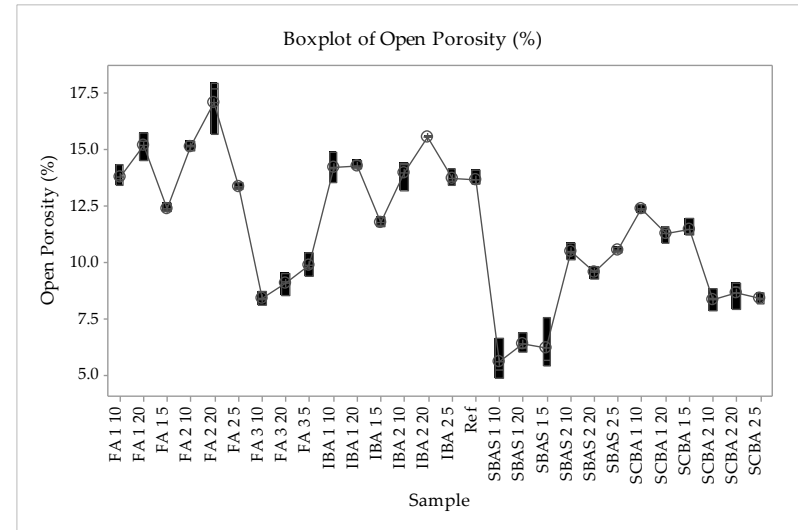
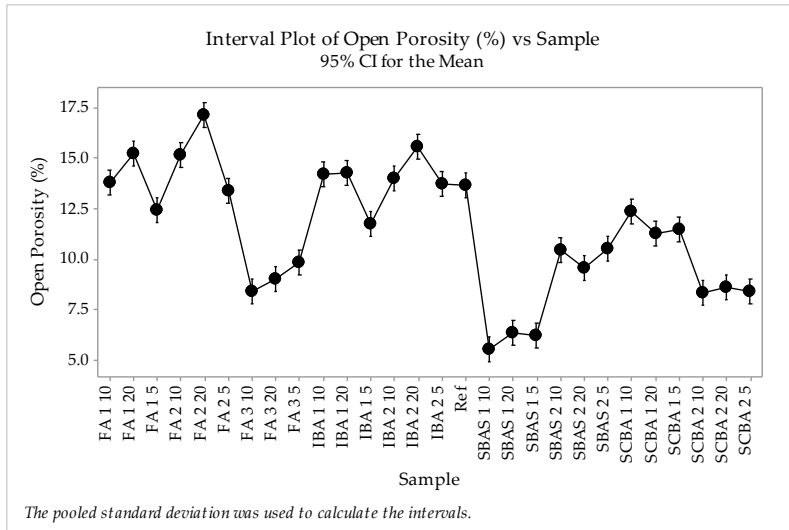
SCBA 2 10 - Ref	-5.330	0.433	(-6.671, -3.990)	-
12.31	0.000			
SCBA 2 20 - Ref	-5.057	0.433	(-6.398, -3.716)	-
11.68	0.000			
SCBA 2 5 - Ref	-5.287	0.433	(-6.628, -3.947)	-
12.21	0.000			

Individual confidence level = 99.69%

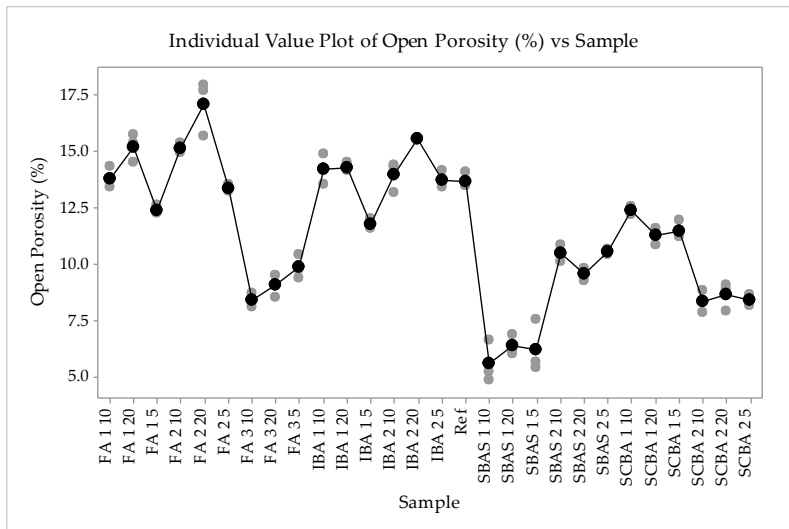
Dunnett Simultaneous 95% CIs



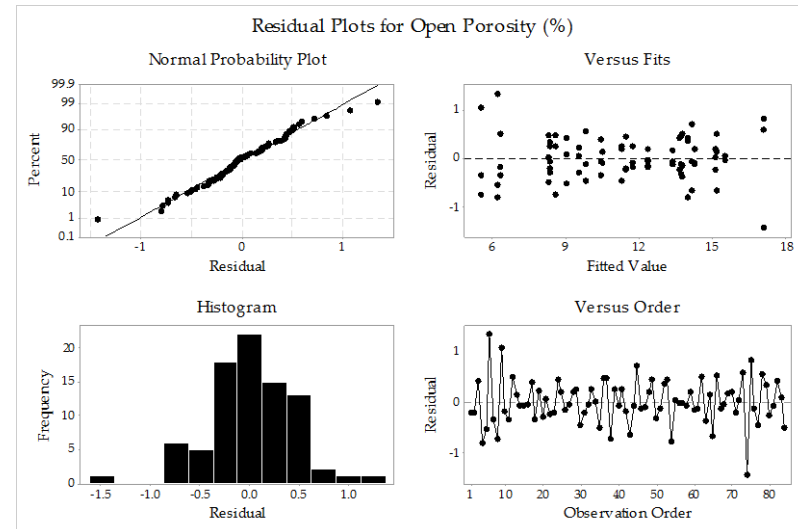
Interval Plot of Open Porosity (%) vs Sample



Individual Value Plot of Open Porosity (%) vs Sample



Residual Plots for Open Porosity (%)



Boxplot of Open Porosity (%)

One-way ANOVA: Capillary Action (kg/m2.min) versus Sample

Error	56	0.02190	0.000391
Total	83	0.34384	

Method

Null hypothesis All means are equal
 Alternative hypothesis At least one mean is different
 Significance level $\alpha = 0.05$

Model Summary

S	R-sq	R-sq(adj)	R-sq(pred)
0.0197758	93.63%	90.56%	85.67%

Equal variances were assumed for the analysis.

Means

Factor Information

Factor Levels Values

Sample 28 FA 1 10, FA 1 20, FA 1 5, FA 2 10, FA 2 20, FA 2 5, FA 3 10, FA 3 20, FA 3 5,
 IBA 1 10, IBA 1 20, IBA 1 5, IBA 2 10, IBA 2 20, IBA 2 5, Ref, SBAS 1 10,
 SBAS 1 20, SBAS 1 5, SBAS 2 10, SBAS 2 20, SBAS 2 5, SCBA 1 10, SCBA 1 20,
 SCBA 1 5, SCBA 2 10, SCBA 2 20, SCBA 2 5

Sample	N	Mean	StDev	95% CI
FA 1 10	3	0.2500	0.0173	(0.2271, 0.2729)
FA 1 20	3	0.27633	0.01415	(0.25346, 0.29921)
FA 1 5	3	0.22667	0.01528	(0.20379, 0.24954)
FA 2 10	3	0.3183	0.0369	(0.2955, 0.3412)
FA 2 20	3	0.3800	0.0200	(0.3571, 0.4029)
FA 2 5	3	0.2373	0.0237	(0.2145, 0.2602)
FA 3 10	3	0.14100	0.00656	(0.11813, 0.16387)
FA 3 20	3	0.17333	0.01258	(0.15046, 0.19621)
FA 3 5	3	0.1560	0.0226	(0.1331, 0.1789)
IBA 1 10	3	0.18467	0.01301	(0.16179, 0.20754)
IBA 1 20	3	0.19800	0.01054	(0.17513, 0.22087)
IBA 1 5	3	0.2007	0.0303	(0.1778, 0.2235)
IBA 2 10	3	0.11100	0.01015	(0.08813, 0.13387)
IBA 2 20	3	0.12233	0.01079	(0.09946, 0.14521)
IBA 2 5	3	0.12667	0.00577	(0.10379, 0.14954)

Analysis of Variance

Source	DF	Adj SS	Adj MS	F-Value	P-Value
Sample	27	0.32194	0.011924	30.49	0.000

Ref	3	0.2500	0.0173	(0.2271, 0.2729)
SBAS 1 10	3	0.12333	0.00981	(0.10046, 0.14621)
SBAS 1 20	3	0.1353	0.0334	(0.1125, 0.1582)
SBAS 1 5	3	0.12233	0.00651	(0.09946, 0.14521)
SBAS 2 10	3	0.14333	0.00751	(0.12046, 0.16621)
SBAS 2 20	3	0.1790	0.0301	(0.1561, 0.2019)
SBAS 2 5	3	0.15233	0.00702	(0.12946, 0.17521)
SCBA 1 10	3	0.20833	0.01258	(0.18546, 0.23121)
SCBA 1 20	3	0.17333	0.01528	(0.15046, 0.19621)
SCBA 1 5	3	0.1933	0.0451	(0.1705, 0.2162)
SCBA 2 10	3	0.20533	0.00635	(0.18246, 0.22821)
SCBA 2 20	3	0.1580	0.0202	(0.1351, 0.1809)
SCBA 2 5	3	0.19633	0.01710	(0.17346, 0.21921)

Pooled StDev = 0.0197758

Dunnett Multiple Comparisons with a Control

Grouping Information Using the Dunnett Method and 95% Confidence

Sample	N	Mean	Grouping
Ref (control)	3	0.2500	A
FA 2 20	3	0.3800	
FA 2 10	3	0.3183	
FA 1 20	3	0.27633	A
FA 1 10	3	0.2500	A

FA 2 5	3	0.2373	A
FA 1 5	3	0.22667	A
SCBA 1 10	3	0.20833	A
SCBA 2 10	3	0.20533	A
IBA 1 5	3	0.2007	A
IBA 1 20	3	0.19800	
SCBA 2 5	3	0.19633	
SCBA 1 5	3	0.1933	
IBA 1 10	3	0.18467	
SBAS 2 20	3	0.1790	
SCBA 1 20	3	0.17333	
FA 3 20	3	0.17333	
SCBA 2 20	3	0.1580	
FA 3 5	3	0.1560	
SBAS 2 5	3	0.15233	
SBAS 2 10	3	0.14333	
FA 3 10	3	0.14100	
SBAS 1 20	3	0.1353	
IBA 2 5	3	0.12667	
SBAS 1 10	3	0.12333	
SBAS 1 5	3	0.12233	
IBA 2 20	3	0.12233	
IBA 2 10	3	0.11100	

Means not labeled with the letter A are significantly different from the control level mean.

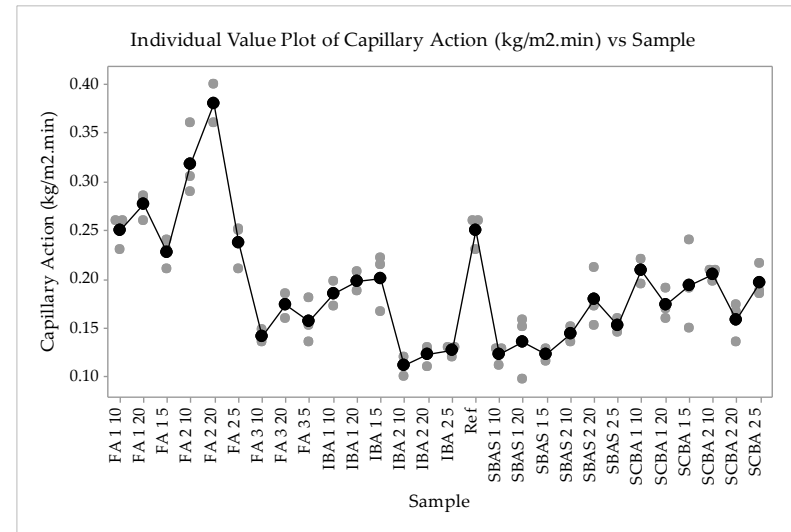
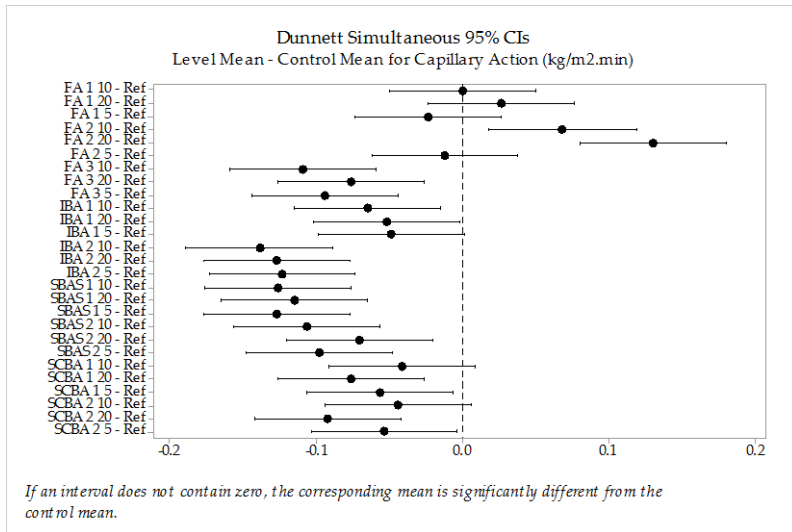
Potential of waste materials as pozzolans and their influence on the quality of building materials

Dunnett Simultaneous Tests for Level Mean - Control Mean

Difference of Adjusted Levels Value	P-Value	Difference of Means	Difference	95% CI	SE of T-			
FA 1 10 - Ref 0.00	1.000	0.0000	0.0161	(-0.0500, 0.0500)		IBA 2 5 - Ref -7.64	0.000	-0.1233 0.0161 (-0.1733, -0.0734)
FA 1 20 - Ref 1.63	0.746	0.0263	0.0161	(-0.0236, 0.0763)		SBAS 1 10 - Ref -7.84	0.000	-0.1267 0.0161 (-0.1766, -0.0767)
FA 1 5 - Ref -1.45	0.869	-0.0233	0.0161	(-0.0733, 0.0266)		SBAS 1 20 - Ref -7.10	0.000	-0.1147 0.0161 (-0.1646, -0.0647)
FA 2 10 - Ref 4.23	0.002	0.0683	0.0161	(0.0184, 0.1183)		SBAS 1 5 - Ref -7.91	0.000	-0.1277 0.0161 (-0.1776, -0.0777)
FA 2 20 - Ref 8.05	0.000	0.1300	0.0161	(0.0800, 0.1800)		SBAS 2 10 - Ref -6.61	0.000	-0.1067 0.0161 (-0.1566, -0.0567)
FA 2 5 - Ref -0.78	1.000	-0.0127	0.0161	(-0.0626, 0.0373)		SBAS 2 20 - Ref -4.40	0.001	-0.0710 0.0161 (-0.1210, -0.0210)
FA 3 10 - Ref -6.75	0.000	-0.1090	0.0161	(-0.1590, -0.0590)		SBAS 2 5 - Ref -6.05	0.000	-0.0977 0.0161 (-0.1476, -0.0477)
FA 3 20 - Ref -4.75	0.000	-0.0767	0.0161	(-0.1266, -0.0267)		SCBA 1 10 - Ref -2.58	0.164	-0.0417 0.0161 (-0.0916, 0.0083)
FA 3 5 - Ref -5.82	0.000	-0.0940	0.0161	(-0.1440, -0.0440)		SCBA 1 20 - Ref -4.75	0.000	-0.0767 0.0161 (-0.1266, -0.0267)
IBA 1 10 - Ref -4.05	0.003	-0.0653	0.0161	(-0.1153, -0.0154)		SCBA 1 5 - Ref -3.51	0.017	-0.0567 0.0161 (-0.1066, -0.0067)
IBA 1 20 - Ref -3.22	0.036	-0.0520	0.0161	(-0.1020, -0.0020)		SCBA 2 10 - Ref -2.77	0.110	-0.0447 0.0161 (-0.0946, 0.0053)
IBA 1 5 - Ref -3.06	0.055	-0.0493	0.0161	(-0.0993, 0.0006)		SCBA 2 20 - Ref -5.70	0.000	-0.0920 0.0161 (-0.1420, -0.0420)
IBA 2 10 - Ref -8.61	0.000	-0.1390	0.0161	(-0.1890, -0.0890)		SCBA 2 5 - Ref -3.32	0.028	-0.0537 0.0161 (-0.1036, -0.0037)
IBA 2 20 - Ref -7.91	0.000	-0.1277	0.0161	(-0.1776, -0.0777)				

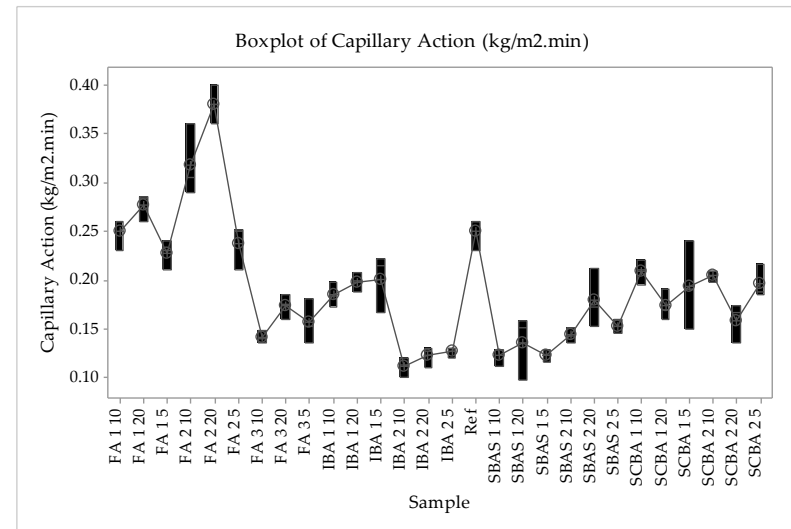
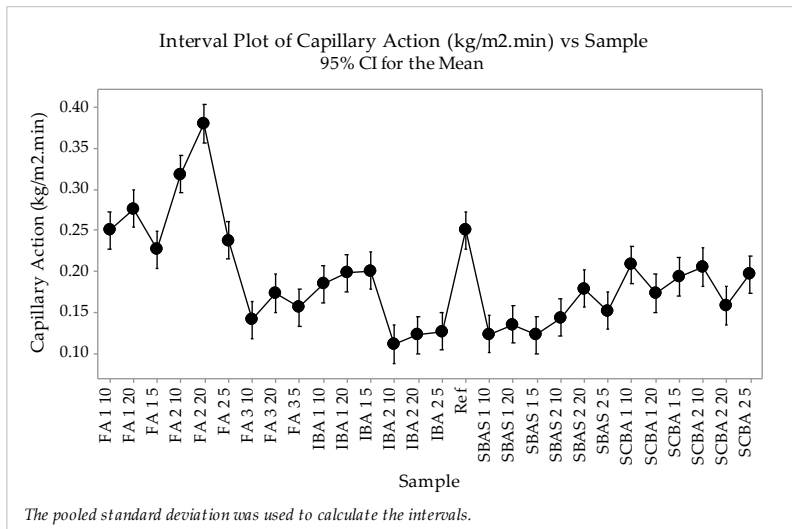
Individual confidence level = 99.69%

Dunnett Simultaneous 95% CIs



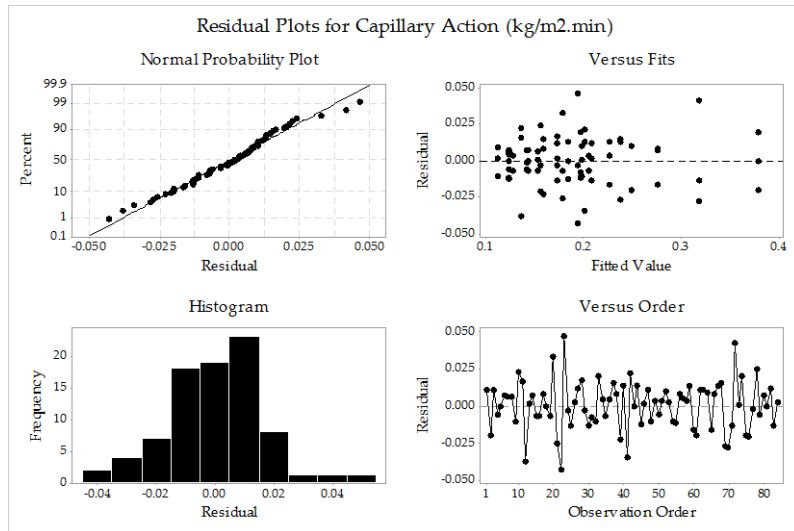
Interval Plot of Capillary Action (kg/m².min) vs Sample

Boxplot of Capillary Action (kg/m².min)



Individual Value Plot of Capillary Action (kg/m².min) vs Sample

Residual Plots for Capillary Action (kg/m².min)



```

Factor      Levels  Values
Sample_1    28    FA 1 10, FA 1 20, FA 1 5, FA 2 10, FA 2 20,
FA 2 5, FA 3 10, FA 3 20, FA 3
                    5, IBA 1 10, IBA 1 20, IBA 1 5, IBA 2 10,
IBA 2 20, IBA 2 5, Ref, SBAS 1
                    10, SBAS 1 20, SBAS 1 5, SBAS 2 10, SBAS 2
20, SBAS 2 5, SCBA 1 10, SCBA 1
                    20, SCBA 1 5, SCBA 2 10, SCBA 2 20, SCBA 2 5
    
```

Analysis of Variance

Source	DF	Adj SS	Adj MS	F-Value	P-Value
Sample_1	27	0.51455	0.019057	17.56	0.000
Error	83	0.09010	0.001086		
Total	110	0.60465			

One-way ANOVA: Specific Heat (J/g°C) versus Sample_1

Method

Null hypothesis All means are equal
 Alternative hypothesis At least one mean is different
 Significance level $\alpha = 0.05$

Equal variances were assumed for the analysis.

Factor Information

Model Summary

S	R-sq	R-sq(adj)	R-sq(pred)
0.0329471	85.10%	80.25%	73.26%

Means

Sample_1	N	Mean	StDev	95% CI
FA 1 10	4	1.24414	0.01747	(1.21137, 1.27690)
FA 1 20	4	1.2544	0.0252	(1.2216, 1.2871)

FA 1 5	4	1.2181	0.0352	(1.1853, 1.2509)
FA 2 10	4	1.2944	0.0337	(1.2616, 1.3272)
FA 2 20	4	1.32088	0.01789	(1.28811, 1.35364)
FA 2 5	4	1.1985	0.0287	(1.1657, 1.2313)
FA 3 10	4	1.2009	0.0261	(1.1682, 1.2337)
FA 3 20	4	1.2120	0.0320	(1.1793, 1.2448)
FA 3 5	4	1.2038	0.0424	(1.1711, 1.2366)
IBA 1 10	4	1.1752	0.0254	(1.1424, 1.2080)
IBA 1 20	4	1.1606	0.0278	(1.1278, 1.1933)
IBA 1 5	4	1.1435	0.0403	(1.1107, 1.1763)
IBA 2 10	4	1.16215	0.01375	(1.12939, 1.19492)
IBA 2 20	4	1.0988	0.0722	(1.0660, 1.1315)
IBA 2 5	4	1.1773	0.0592	(1.1446, 1.2101)
Ref	3	1.4457	0.0401	(1.4079, 1.4835)
SBAS 1 10	4	1.15496	0.01696	(1.12219, 1.18772)
SBAS 1 20	4	1.13267	0.01750	(1.09990, 1.16543)
SBAS 1 5	4	1.15181	0.01296	(1.11905, 1.18458)
SBAS 2 10	4	1.14639	0.01974	(1.11363, 1.17916)
SBAS 2 20	4	1.1657	0.0655	(1.1329, 1.1984)
SBAS 2 5	4	1.11596	0.00674	(1.08320, 1.14873)
SCBA 1 10	4	1.14931	0.01402	(1.11655, 1.18208)
SCBA 1 20	4	1.0994	0.0302	(1.0666, 1.1321)
SCBA 1 5	4	1.18826	0.01383	(1.15550, 1.22103)
SCBA 2 10	4	1.2167	0.0314	(1.1840, 1.2495)
SCBA 2 20	4	1.2447	0.0229	(1.2119, 1.2775)
SCBA 2 5	4	1.2493	0.0279	(1.2166, 1.2821)

Pooled StDev = 0.0329471

Dunnett Multiple Comparisons with a Control

Grouping Information Using the Dunnett Method and 95% Confidence

Sample_1	N	Mean	Grouping
Ref (control)	3	1.4457	A
FA 2 20	4	1.32088	
FA 2 10	4	1.2944	
FA 1 20	4	1.2544	
SCBA 2 5	4	1.2493	
SCBA 2 20	4	1.2447	
FA 1 10	4	1.24414	
FA 1 5	4	1.2181	
SCBA 2 10	4	1.2167	
FA 3 20	4	1.2120	
FA 3 5	4	1.2038	
FA 3 10	4	1.2009	
FA 2 5	4	1.1985	
SCBA 1 5	4	1.18826	
IBA 2 5	4	1.1773	
IBA 1 10	4	1.1752	
SBAS 2 20	4	1.1657	
IBA 2 10	4	1.16215	
IBA 1 20	4	1.1606	
SBAS 1 10	4	1.15496	

Potential of waste materials as pozzolans and their influence on the quality of building materials

SBAS 1 5	4	1.15181			FA 3 10 - Ref	-0.2448	0.0252	(-0.3205, -0.1691)	
SCBA 1 10	4	1.14931			-9.73	0.000			
SBAS 2 10	4	1.14639			FA 3 20 - Ref	-0.2337	0.0252	(-0.3094, -0.1580)	
IBA 1 5	4	1.1435			-9.29	0.000			
SBAS 1 20	4	1.13267			FA 3 5 - Ref	-0.2419	0.0252	(-0.3176, -0.1661)	
SBAS 2 5	4	1.11596			-9.61	0.000			
SCBA 1 20	4	1.0994			IBA 1 10 - Ref	-0.2705	0.0252	(-0.3462, -0.1948)	-
IBA 2 20	4	1.0988			10.75	0.000			
					IBA 1 20 - Ref	-0.2852	0.0252	(-0.3609, -0.2094)	-
					11.33	0.000			
					IBA 1 5 - Ref	-0.3022	0.0252	(-0.3779, -0.2265)	
					-12.01	0.000			
					IBA 2 10 - Ref	-0.2836	0.0252	(-0.3593, -0.2078)	-
					11.27	0.000			
					IBA 2 20 - Ref	-0.3469	0.0252	(-0.4227, -0.2712)	-
					13.79	0.000			
					IBA 2 5 - Ref	-0.2684	0.0252	(-0.3441, -0.1927)	
					-10.66	0.000			
					SBAS 1 10 - Ref	-0.2908	0.0252	(-0.3665, -0.2150)	-
					11.55	0.000			
					SBAS 1 20 - Ref	-0.3130	0.0252	(-0.3888, -0.2373)	-
					12.44	0.000			
					SBAS 1 5 - Ref	-0.2939	0.0252	(-0.3696, -0.2182)	-
					11.68	0.000			
					SBAS 2 10 - Ref	-0.2993	0.0252	(-0.3750, -0.2236)	-
					11.89	0.000			
					SBAS 2 20 - Ref	-0.2800	0.0252	(-0.3557, -0.2043)	-
					11.13	0.000			
					SBAS 2 5 - Ref	-0.3297	0.0252	(-0.4055, -0.2540)	-
					13.10	0.000			
					SCBA 1 10 - Ref	-0.2964	0.0252	(-0.3721, -0.2207)	-
					11.78	0.000			
					SCBA 1 20 - Ref	-0.3463	0.0252	(-0.4221, -0.2706)	-
					13.76	0.000			

Means not labeled with the letter A are significantly different from the control level mean.

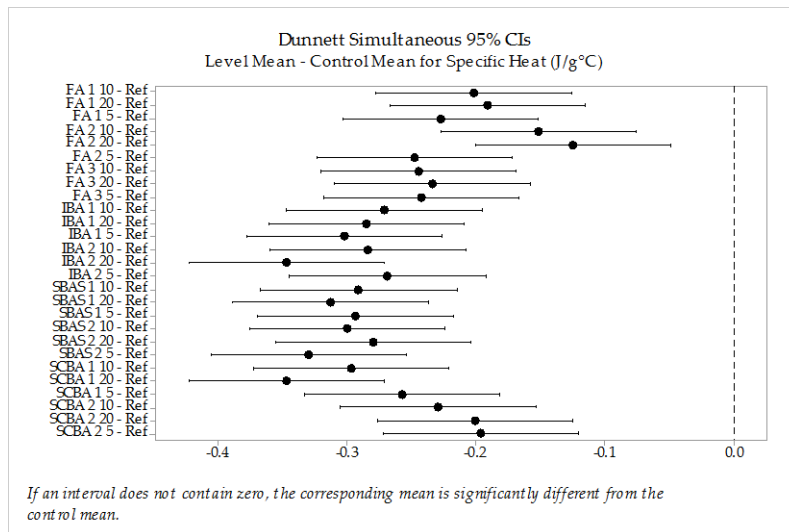
Dunnett Simultaneous Tests for Level Mean - Control Mean

Difference of Adjusted Levels Value	P-Value	Difference of Means	Difference	95% CI	SE of T-
FA 1 10 - Ref	-8.01	0.000	-0.2016	0.0252	(-0.2773, -0.1259)
FA 1 20 - Ref	-7.60	0.000	-0.1913	0.0252	(-0.2671, -0.1156)
FA 1 5 - Ref	-9.04	0.000	-0.2276	0.0252	(-0.3033, -0.1519)
FA 2 10 - Ref	-6.01	0.000	-0.1513	0.0252	(-0.2270, -0.0756)
FA 2 20 - Ref	-4.96	0.000	-0.1248	0.0252	(-0.2005, -0.0491)
FA 2 5 - Ref	-9.82	0.000	-0.2472	0.0252	(-0.3229, -0.1715)

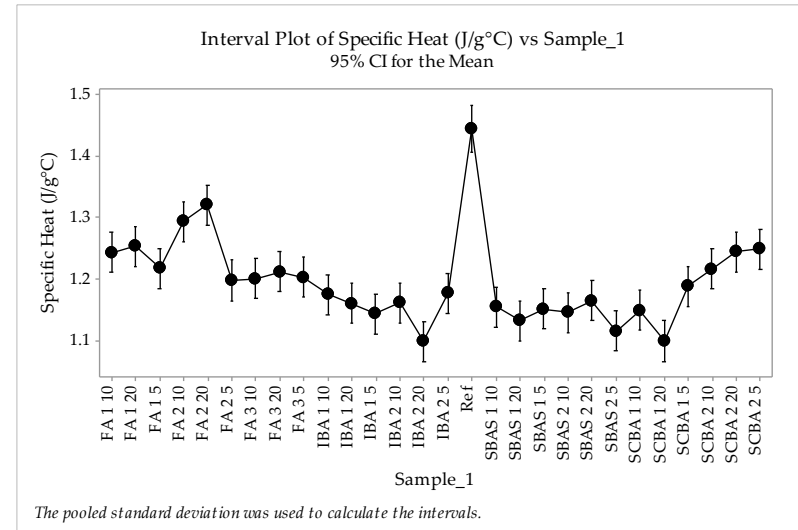
SCBA 1 5 - Ref	-0.2574	0.0252	(-0.3332, -0.1817)	-
10.23	0.000			
SCBA 2 10 - Ref	-0.2290	0.0252	(-0.3047, -0.1533)	
-9.10	0.000			
SCBA 2 20 - Ref	-0.2010	0.0252	(-0.2767, -0.1253)	
-7.99	0.000			
SCBA 2 5 - Ref	-0.1964	0.0252	(-0.2721, -0.1207)	
-7.80	0.000			

Individual confidence level = 99.65%

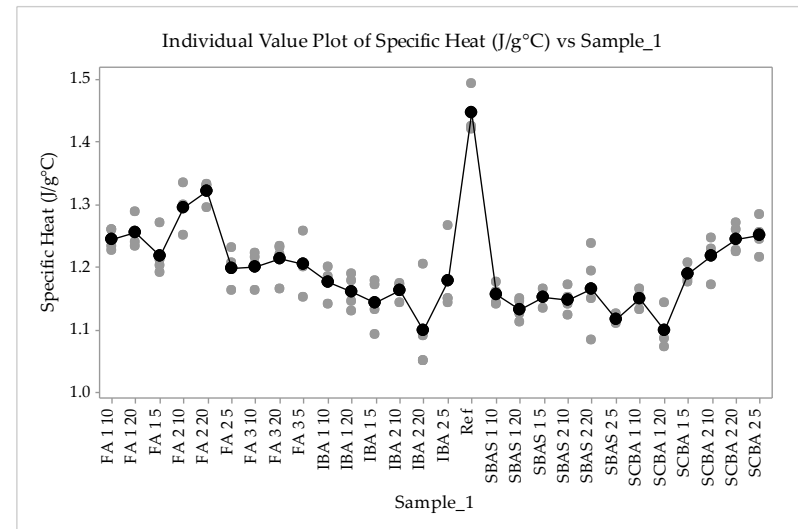
Dunnett Simultaneous 95% CIs



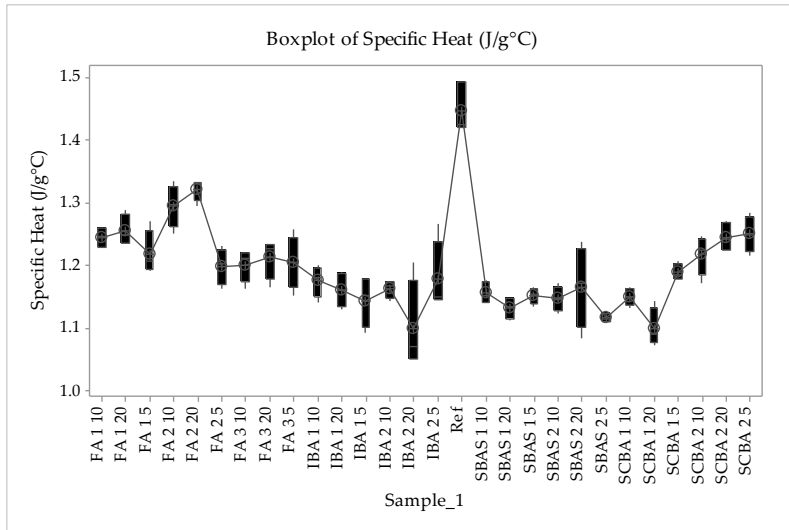
Interval Plot of Specific Heat (J/g°C) vs Sample_1



Individual Value Plot of Specific Heat (J/g°C) vs Sample_1



Boxplot of Specific Heat (J/g°C)



Method

Null hypothesis All means are equal
 Alternative hypothesis At least one mean is different
 Significance level $\alpha = 0.05$

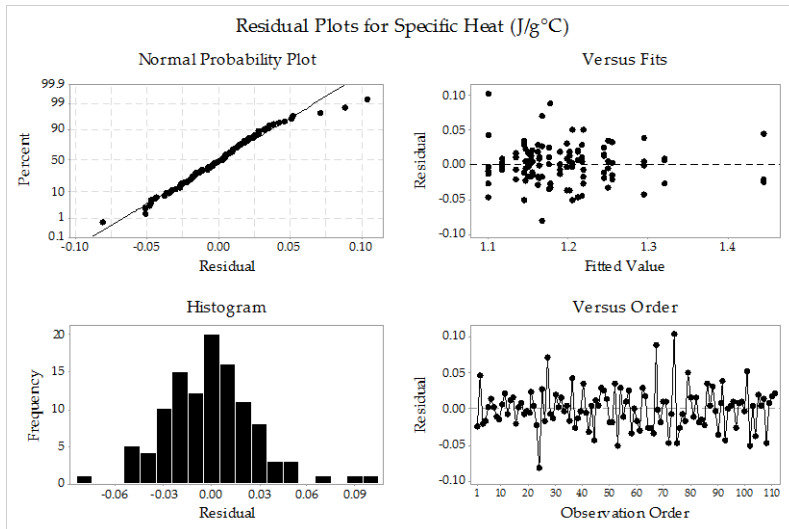
Equal variances were assumed for the analysis.

Factor Information

Factor Levels Values

Sample 28 FA 1 10, FA 1 20, FA 1 5, FA 2 10, FA 2 20, FA 2 5, FA 3 10, FA 3 20, FA 3 5,
 IBA 1 10, IBA 1 20, IBA 1 5, IBA 2 10, IBA 2 20, IBA 2 5, Ref, SBAS 1 10,
 SBAS 1 20, SBAS 1 5, SBAS 2 10, SBAS 2 20, SBAS 2 5, SCBA 1 10, SCBA 1 20,
 SCBA 1 5, SCBA 2 10, SCBA 2 20, SCBA 2 5

Residual Plots for Specific Heat (J/g°C)



Analysis of Variance

Source	DF	Adj SS	Adj MS	F-Value	P-Value
Sample	27	128.47	4.7582	11.05	0.000
Error	56	24.11	0.4306		
Total	83	152.58			

One-way ANOVA: Flexural Strength (MPa) versus Sample

Model Summary

S	R-sq	R-sq(adj)	R-sq(pred)
0.656190	84.20%	76.58%	64.44%

Means

Sample	N	Mean	StDev	95% CI
FA 1 10	3	7.697	0.793	(6.938, 8.456)
FA 1 20	3	6.784	0.440	(6.025, 7.543)
FA 1 5	3	7.953	0.441	(7.194, 8.712)
FA 2 10	3	6.9612	0.1325	(6.2023, 7.7201)
FA 2 20	3	5.447	0.379	(4.688, 6.206)
FA 2 5	3	8.022	0.272	(7.263, 8.781)
FA 3 10	3	7.0519	0.0480	(6.2930, 7.8108)
FA 3 20	3	6.1680	0.0655	(5.4091, 6.9269)
FA 3 5	3	8.331	0.478	(7.572, 9.090)
IBA 1 10	3	6.8440	0.1725	(6.0851, 7.6029)
IBA 1 20	3	4.620	0.667	(3.861, 5.379)
IBA 1 5	3	6.438	0.192	(5.679, 7.197)
IBA 2 10	3	7.710	1.300	(6.951, 8.469)
IBA 2 20	3	6.916	0.362	(6.157, 7.675)
IBA 2 5	3	8.156	0.557	(7.397, 8.915)
Ref	3	9.8844	0.1688	(9.1255, 10.6433)
SBAS 1 10	3	6.946	0.787	(6.187, 7.705)
SBAS 1 20	3	7.439	0.273	(6.680, 8.198)

SBAS 1 5	3	7.25	1.93	(6.50, 8.01)
SBAS 2 10	3	6.654	0.899	(5.895, 7.413)
SBAS 2 20	3	9.314	0.266	(8.555, 10.073)
SBAS 2 5	3	10.022	0.444	(9.263, 10.781)
SCBA 1 10	3	7.360	0.653	(6.602, 8.119)
SCBA 1 20	3	6.379	0.827	(5.620, 7.138)
SCBA 1 5	3	6.630	1.064	(5.871, 7.389)
SCBA 2 10	3	6.002	0.388	(5.243, 6.761)
SCBA 2 20	3	5.3660	0.0769	(4.6071, 6.1249)
SCBA 2 5	3	6.1011	0.1323	(5.3422, 6.8600)

Pooled StDev = 0.656190

Dunnnett Multiple Comparisons with a Control

Grouping Information Using the Dunnnett Method and 95% Confidence

Sample	N	Mean	Grouping
Ref (control)	3	9.8844	A
SBAS 2 5	3	10.022	A
SBAS 2 20	3	9.314	A
FA 3 5	3	8.331	A
IBA 2 5	3	8.156	
FA 2 5	3	8.022	
FA 1 5	3	7.953	
IBA 2 10	3	7.710	

Potential of waste materials as pozzolans and their influence on the quality of building materials

				Levels	of Means	Difference	95% CI	T-
				Value	P-Value			
FA 1 10	3	7.697						
SBAS 1 20	3	7.439						
SCBA 1 10	3	7.360		FA 1 10 - Ref	-2.188	0.536	(-3.846, -0.529)	-
SBAS 1 5	3	7.25		4.08	0.003			
FA 3 10	3	7.0519		FA 1 20 - Ref	-3.100	0.536	(-4.758, -1.442)	-
FA 2 10	3	6.9612		5.79	0.000			
SBAS 1 10	3	6.946		FA 1 5 - Ref	-1.932	0.536	(-3.590, -0.273)	-
IBA 2 20	3	6.916		3.61	0.013			
IBA 1 10	3	6.8440		FA 2 10 - Ref	-2.923	0.536	(-4.582, -1.265)	-
FA 1 20	3	6.784		5.46	0.000			
SBAS 2 10	3	6.654		FA 2 20 - Ref	-4.437	0.536	(-6.096, -2.779)	-
SCBA 1 5	3	6.630		8.28	0.000			
IBA 1 5	3	6.438		FA 2 5 - Ref	-1.863	0.536	(-3.521, -0.204)	-
SCBA 1 20	3	6.379		3.48	0.018			
FA 3 20	3	6.1680		FA 3 10 - Ref	-2.833	0.536	(-4.491, -1.174)	-
SCBA 2 5	3	6.1011		5.29	0.000			
SCBA 2 10	3	6.002		FA 3 20 - Ref	-3.716	0.536	(-5.375, -2.058)	-
FA 2 20	3	5.447		6.94	0.000			
SCBA 2 20	3	5.3660		FA 3 5 - Ref	-1.553	0.536	(-3.212, 0.105)	-
IBA 1 20	3	4.620		2.90	0.081			
				IBA 1 10 - Ref	-3.040	0.536	(-4.699, -1.382)	-
				5.67	0.000			
				IBA 1 20 - Ref	-5.264	0.536	(-6.923, -3.606)	-
				9.83	0.000			
				IBA 1 5 - Ref	-3.446	0.536	(-5.105, -1.788)	-
				6.43	0.000			
				IBA 2 10 - Ref	-2.174	0.536	(-3.833, -0.516)	-
				4.06	0.003			
				IBA 2 20 - Ref	-2.969	0.536	(-4.627, -1.310)	-
				5.54	0.000			
				IBA 2 5 - Ref	-1.728	0.536	(-3.387, -0.070)	-
				3.23	0.036			
				SBAS 1 10 - Ref	-2.939	0.536	(-4.597, -1.280)	-
				5.48	0.000			
Difference of Adjusted		Difference	SE of					

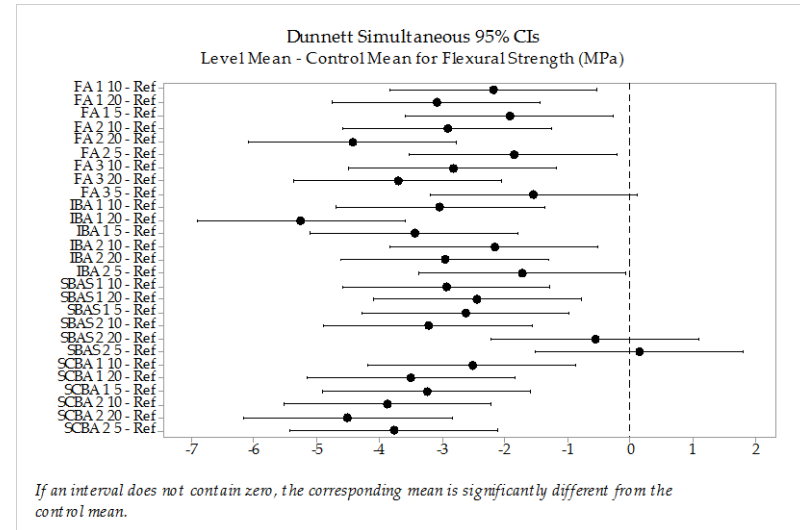
Means not labeled with the letter A are significantly different from the control level mean.

Dunnett Simultaneous Tests for Level Mean - Control Mean

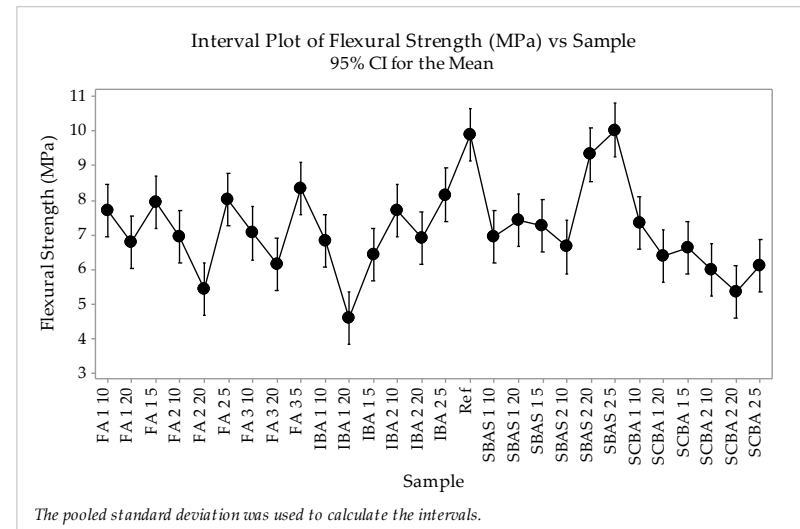
SBAS 1 20 - Ref	-2.445	0.536	(-4.104, -0.787)	-
4.56	0.001			
SBAS 1 5 - Ref	-2.630	0.536	(-4.289, -0.972)	-
4.91	0.000			
SBAS 2 10 - Ref	-3.230	0.536	(-4.889, -1.572)	-
6.03	0.000			
SBAS 2 20 - Ref	-0.570	0.536	(-2.228, 1.088)	-
1.06	0.991			
SBAS 2 5 - Ref	0.137	0.536	(-1.521, 1.796)	-
0.26	1.000			
SCBA 1 10 - Ref	-2.524	0.536	(-4.182, -0.866)	-
4.71	0.000			
SCBA 1 20 - Ref	-3.506	0.536	(-5.164, -1.847)	-
6.54	0.000			
SCBA 1 5 - Ref	-3.255	0.536	(-4.913, -1.596)	-
6.07	0.000			
SCBA 2 10 - Ref	-3.883	0.536	(-5.541, -2.224)	-
7.25	0.000			
SCBA 2 20 - Ref	-4.518	0.536	(-6.177, -2.860)	-
8.43	0.000			
SCBA 2 5 - Ref	-3.783	0.536	(-5.442, -2.125)	-
7.06	0.000			

Individual confidence level = 99.69%

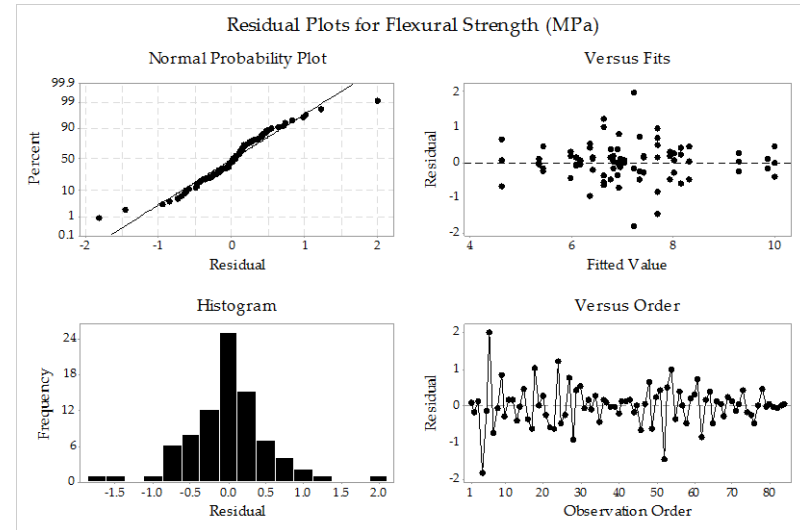
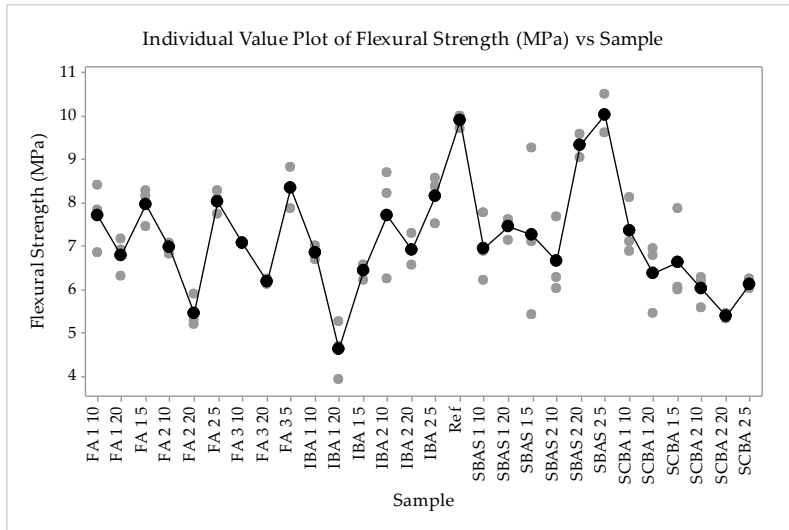
Dunnett Simultaneous 95% CIs



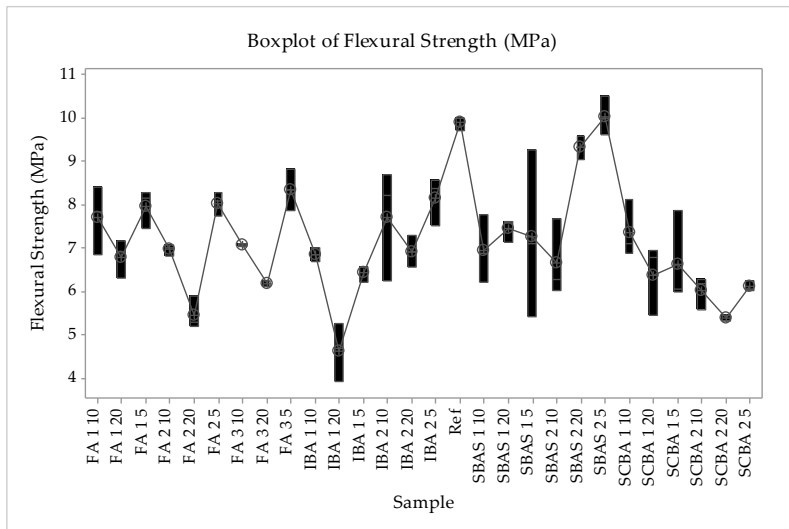
Interval Plot of Flexural Strength (MPa) vs Sample



Individual Value Plot of Flexural Strength (MPa) vs Sample



Boxplot of Flexural Strength (MPa)



One-way ANOVA: Compressive Strength (MPa) versus Sample_2

Method

Null hypothesis All means are equal
 Alternative hypothesis At least one mean is different
 Significance level $\alpha = 0.05$
 Rows unused 11

Equal variances were assumed for the analysis.

Residual Plots for Flexural Strength (MPa)

Factor Information

Factor Levels Values

Sample_2 28 FA 1 10, FA 1 20, FA 1 5, FA 2 10, FA 2 20, FA 2 5, FA 3 10, FA 3 20, FA 3 5, IBA 1 10, IBA 1 20, IBA 1 5, IBA 2 10, IBA 2 20, IBA 2 5, Ref, SBAS 1 10, SBAS 1 20, SBAS 1 5, SBAS 2 10, SBAS 2 20, SBAS 2 5, SCBA 1 10, SCBA 1 20, SCBA 1 5, SCBA 2 10, SCBA 2 20, SCBA 2 5

FA 1 10	6	38.93	2.66	(36.39, 41.46)
FA 1 20	6	32.38	2.92	(29.84, 34.91)
FA 1 5	6	40.22	2.98	(37.69, 42.75)
FA 2 10	6	35.81	3.07	(33.28, 38.35)
FA 2 20	6	29.131	1.954	(26.598, 31.664)
FA 2 5	6	42.10	4.40	(39.57, 44.63)
FA 3 10	6	41.362	1.463	(38.829, 43.895)
FA 3 20	6	35.23	2.64	(32.70, 37.76)
FA 3 5	6	45.34	2.91	(42.81, 47.87)
IBA 1 10	6	29.68	3.45	(27.14, 32.21)
IBA 1 20	6	23.855	1.619	(21.322, 26.388)
IBA 1 5	6	32.226	2.144	(29.693, 34.758)
IBA 2 10	6	37.12	2.68	(34.59, 39.66)
IBA 2 20	6	27.80	4.94	(25.27, 30.34)
IBA 2 5	6	40.18	2.85	(37.65, 42.71)
Ref	6	45.733	2.022	(43.201, 48.266)
SBAS 1 10	5	46.19	5.52	(43.42, 48.97)
SBAS 1 20	4	43.608	0.726	(40.506, 46.710)
SBAS 1 5	5	46.617	1.051	(43.843, 49.392)
SBAS 2 10	5	52.19	4.53	(49.42, 54.97)
SBAS 2 20	4	53.07	4.13	(49.97, 56.17)
SBAS 2 5	5	56.13	4.17	(53.36, 58.90)
SCBA 1 10	6	43.539	2.222	(41.006, 46.071)
SCBA 1 20	6	44.224	1.817	(41.692, 46.757)
SCBA 1 5	5	42.566	2.042	(39.792, 45.341)
SCBA 2 10	6	37.76	3.24	(35.22, 40.29)
SCBA 2 20	5	33.39	4.17	(30.62, 36.17)
SCBA 2 5	5	40.37	4.17	(37.59, 43.14)

Analysis of Variance

Source	DF	Adj SS	Adj MS	F-Value	P-Value
Sample_2	27	8823	326.779	33.24	0.000
Error	129	1268	9.832		
Total	156	10091			

Model Summary

S	R-sq	R-sq(adj)	R-sq(pred)
3.13563	87.43%	84.80%	81.20%

Means

Sample_2	N	Mean	StDev	95% CI
----------	---	------	-------	--------

Potential of waste materials as pozzolans and their influence on the quality of building materials

Pooled StDev = 3.13563

Dunnnett Multiple Comparisons with a Control

Grouping Information Using the Dunnnett Method and 95% Confidence

Sample_2	N	Mean	Grouping
Ref (control)	6	45.733	A
SBAS 2 5	5	56.13	
SBAS 2 20	4	53.07	
SBAS 2 10	5	52.19	
SBAS 1 5	5	46.617	A
SBAS 1 10	5	46.19	A
FA 3 5	6	45.34	A
SCBA 1 20	6	44.224	A
SBAS 1 20	4	43.608	A
SCBA 1 10	6	43.539	A
SCBA 1 5	5	42.566	A
FA 2 5	6	42.10	A
FA 3 10	6	41.362	A
SCBA 2 5	5	40.37	A
FA 1 5	6	40.22	
IBA 2 5	6	40.18	
FA 1 10	6	38.93	
SCBA 2 10	6	37.76	

IBA 2 10	6	37.12
FA 2 10	6	35.81
FA 3 20	6	35.23
SCBA 2 20	5	33.39
FA 1 20	6	32.38
IBA 1 5	6	32.226
IBA 1 10	6	29.68
FA 2 20	6	29.131
IBA 2 20	6	27.80
IBA 1 20	6	23.855

Means not labeled with the letter A are significantly different from the control level mean.

Dunnnett Simultaneous Tests for Level Mean - Control Mean

Difference of Adjusted Levels	P-Value	Difference of Means	Difference	95% CI	SE of Difference	T-
FA 1 10 - Ref	3.76	0.006	-6.81	1.81	(-12.31, -1.30)	-
FA 1 20 - Ref	7.38	0.000	-13.36	1.81	(-18.87, -7.85)	-
FA 1 5 - Ref	3.05	0.050	-5.51	1.81	(-11.02, -0.01)	-
FA 2 10 - Ref	5.48	0.000	-9.92	1.81	(-15.43, -4.41)	-
FA 2 20 - Ref	9.17	0.000	-16.60	1.81	(-22.11, -11.09)	-

Appendix G Statistical Analysis

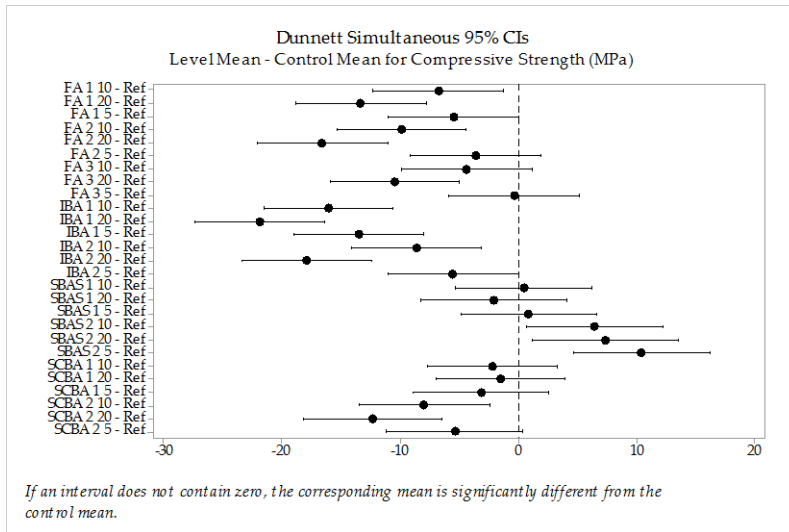
Radson Lima Figueiredo

FA 2 5 - Ref 2.01 0.469	-3.64	1.81	(-9.14, 1.87)	-
FA 3 10 - Ref 2.41 0.224	-4.37	1.81	(-9.88, 1.14)	-
FA 3 20 - Ref 5.80 0.000	-10.50	1.81	(-16.01, -5.00)	-
FA 3 5 - Ref 0.22 1.000	-0.39	1.81	(-5.90, 5.12)	-
IBA 1 10 - Ref 8.87 0.000	-16.06	1.81	(-21.56, -10.55)	-
IBA 1 20 - Ref 12.09 0.000	-21.88	1.81	(-27.39, -16.37)	-
IBA 1 5 - Ref 7.46 0.000	-13.51	1.81	(-19.02, -8.00)	-
IBA 2 10 - Ref 4.76 0.000	-8.61	1.81	(-14.12, -3.10)	-
IBA 2 20 - Ref 9.90 0.000	-17.93	1.81	(-23.44, -12.42)	-
IBA 2 5 - Ref 3.07 0.047	-5.55	1.81	(-11.06, -0.04)	-
SBAS 1 10 - Ref 0.24 1.000	0.46	1.90	(-5.32, 6.23)	-
SBAS 1 20 - Ref 1.05 0.995	-2.13	2.02	(-8.28, 4.03)	-
SBAS 1 5 - Ref 0.47 1.000	0.88	1.90	(-4.89, 6.66)	-
SBAS 2 10 - Ref 3.40 0.018	6.46	1.90	(0.68, 12.24)	-
SBAS 2 20 - Ref 3.62 0.009	7.33	2.02	(1.18, 13.49)	-
SBAS 2 5 - Ref 5.48 0.000	10.40	1.90	(4.62, 16.17)	-
SCBA 1 10 - Ref 1.21 0.974	-2.19	1.81	(-7.70, 3.31)	-

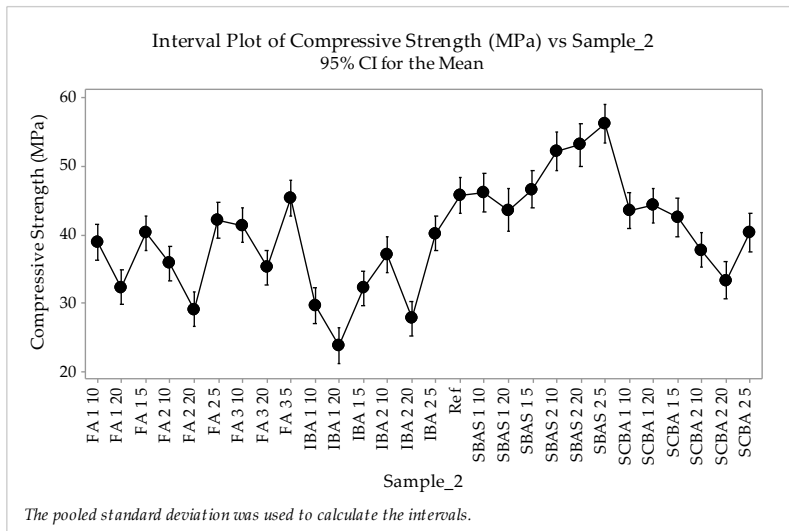
SCBA 1 20 - Ref 0.83 1.000	-1.51	1.81	(-7.02, 4.00)	-
SCBA 1 5 - Ref 1.67 0.735	-3.17	1.90	(-8.94, 2.61)	-
SCBA 2 10 - Ref 4.41 0.001	-7.98	1.81	(-13.48, -2.47)	-
SCBA 2 20 - Ref 6.50 0.000	-12.34	1.90	(-18.12, -6.56)	-
SCBA 2 5 - Ref 2.83 0.088	-5.37	1.90	(-11.14, 0.41)	-

Individual confidence level = 99.72%

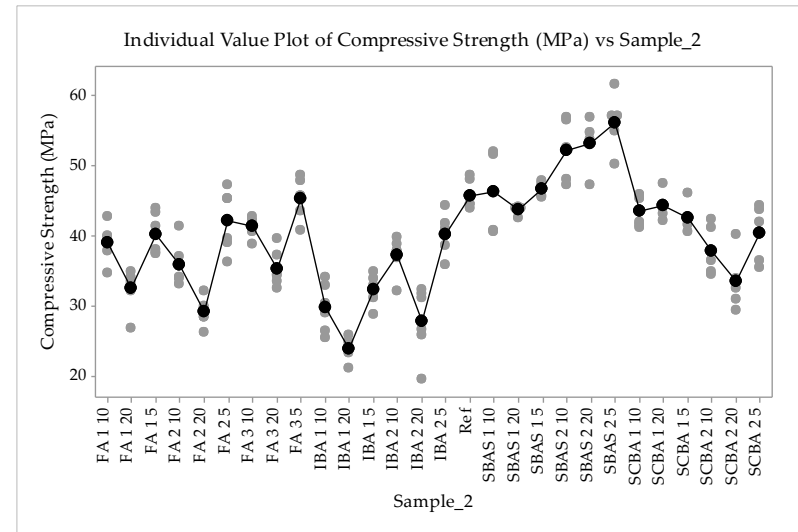
Dunnett Simultaneous 95% CIs



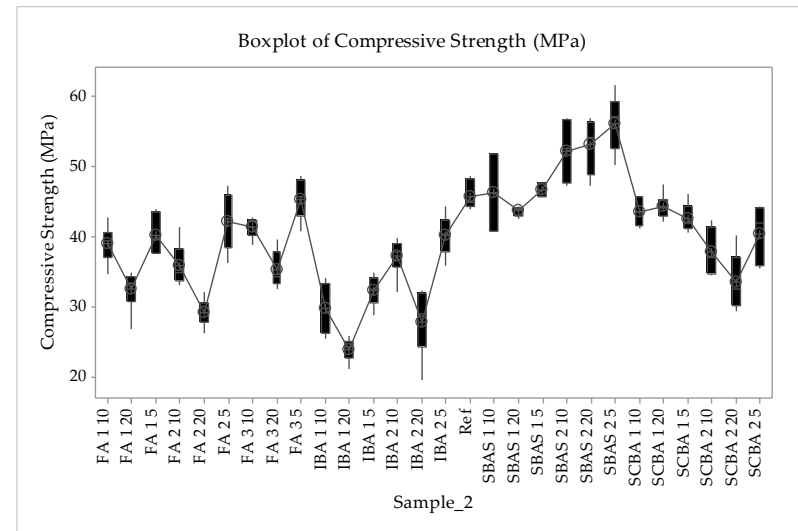
Interval Plot of Compressive Strength (MPa) vs Sample_2



Individual Value Plot of Compressive Strength (MPa) vs Sample_2



Boxplot of Compressive Strength (MPa)



Residual Plots for Compressive Strength (MPa)

